THE LIGATING VERSATILITY OF HALIDES AND PSEUDOHALIDES IN COPPER(II) COMPLEXES- MONOMERS, DIMERS AND CHAINS

Thesis submitted to the

COCHIN UNIVERSITY OF SCIENCE AND TECHNOLOGY

In partial fulfillment of the requirements for the degree of

DOCTOR OF PHILOSOPHY

Under the Faculty of Science

By

ROJI J. KUNNATH

DEPARTMENT OF APPLIED CHEMISTRY

COCHIN UNIVERSITY OF SCIENCE AND TECHNOLOGY

KOCHI-682 022

August 2013

Phone Off : 0484-2862423
0484-2575804
Phone Res : 0484-2576904
Fax : 0484-2577595
Email : mrp@cusat.ac.in
mrp_k@yahoo.com

DEPARTMENT OF APPLIED CHEMISTRY
COCHIN UNIVERSITY OF SCIENCE AND TECHNOLOGY
KOCHI - 682 022, INDIA

Prof. M.R. Prathapachandra Kurup
Professor

5th August 2013

Certificate

This is to certify that the thesis entitled **"The ligating versatility of halides and pseudohalides in copper(II) complexes- monomers, dimers and chains"** submitted by Mr. Roji J. Kunnath, in partial fulfillment of the requirements for the degree of Doctor of Philosophy, to the Cochin University of Science and Technology, Kochi-22, is an authentic record of the original research work carried out by him under my guidance and supervision. The results embodied in this thesis, in full or in part, have not been submitted for the award of any other degree.

M. R. Prathapachandra Kurup

(Supervisor)

Declaration

I hereby declare that the work presented in this thesis entitled **"The ligating versatility of halides and pseudohalides in copper(II) complexes-monomers, dimers and chains"** is entirely original and was carried out independently under the supervision of Dr. M. R. Prathapachandra Kurup, Department of Applied Chemistry, Cochin University of Science and Technology and has not been included in any other thesis submitted previously for the award of any other degree.

05-08-13 **Roji J. Kunnath**

Kochi-22

ACKNOWLEDGEMENT

With humbleness I acknowledge my indebtedness……

First of all I kneel down before the Lord Jesus Christ for the blessings and mercies He showers unto me always and without His grace this project would not have been possible.

I consider it as a great privilege to work under the guidance of Prof. (Dr.) M.R. Prathapachandra Kurup, his vast experiences in research, his dedication to the work his passion for perfection and constructive criticism, have encouraged me to carry out my work more efficiently at the Department of Applied Chemistry, CUSAT. I owe sincere gratitude and thanks to him for his whole hearted support and inspiration throughout the study.

I express my sincere thanks to Prof. K.K. Mohammed Yusuff (Doctoral Committee member and former HOD) and Dr. N. Manoj (Head of the Department) for their kind consideration and continuous encouragement. I am grateful to Prof. (Dr.) K. Sreekumar (Former Head of the Department) and Prof. (Dr.) K. Girish Kumar for their valuable suggestions and cooperation during the period of the work. I am thankful to Prof. (Dr.) Seik Weng Ng (Department of Chemistry, University of Malaya, Kuala Lumpur, Malaysia for crystal refinements of some compounds.

I acknowledge all faculty members of the Department of Applied Chemistry for their support and advice. I also acknowledge all the non-teaching staff of the Department in taking care of all issues regarding the administration of my academic programme.

I am indebted to all the staff of SAIF, Kochi and IIT Bombay. I place my special thanks to Dr. Shibu, SAIF, Kochi for the kind help and consideration extended to me through the entire course of work.

I am thankful to the U.G.C. for the financial support in the form of Research Fellowship.

I owe to my senior researchers Dr. E.B. Seena, Dr. E. Manoj, Dr Leji, Dr. Sheeja, Dr. Reena, Dr. Nancy, Dr. Neema, Dr. Laly, Dr. Renjusha, Dr. Jessy, Dr. Jayakumar and Dr. Annie for their boundless support.

I am extremely grateful to Dr. M. Sithambaresan, my colleague, for guiding, caring, encouraging and helping me in every way, I can think of. I wish to express special thanks to all my lab mates, Aiswarya, Ambili, Sreejith, Bibitha, Jinsa, Nisha, Vineetha, Reshma, Mridula, Nithya, Sajitha, Rakhi, Fousia, and Anila for their great support and help during the period of my research work. You all changed our working environment to a more curious and pleasant one and also helped a lot to develop helping attitude among our lab mates.

Words fail to express my thanks to my dear better half, Sumi Zacharias who is the driving force in bringing this thesis in the present form. Sumi, your patience, love, assistance and encouragement have upheld me when I needed it the most. I also express my deep sense of love to my little daughter Joanna Theresa, who missed our care and attention during the course of this investigation.

I am grateful to my Pappa (Jacob K.L.), Mummy (Anice Jacob), Appachai (P.J. Scaria) and Ammachi (Elsy Scaria) for their understanding and forbearance through all the ups and downs of my work. Their prayers and blessings have always guided me to carry out this endeavor.

Lastly, it is imperative to point out that all may not be mentioned none are forgotten.

Roji J. Kunnath

PREFACE

The work embodied in this thesis was carried out by the author in the Department of Applied Chemistry, CUSAT, Kochi, during the period 2008-2013. The thesis brings to light, our attempts to evaluate the coordination behavior of some compounds of interest. The biological activities of semicarbazones and their metal complexes have been an active area of research during the past years because of their significant role in naturally occurring biological systems. Tridentate NNO and ONO semicarbazone systems formed from heterocyclic and aromatic carbonyl compounds and their transition metal complexes are well-authenticated compounds in this field and their synthesis, crystal structures and spectral studies are well desirable. Hence, we decided to develop a research program aimed at the syntheses, crystal structures and spectral studies of copper complexes with halides and pseudohalides. In addition to single crystal X-ray diffraction studies, various physico-chemical methods of analysis were also used for the characterization of the complexes.

The thesis has been divided into seven chapters carrying a detailed account of copper(II) complexes with semicarbazones, thiosemicarbazones and Schiff bases as ligands and halides and pseudohalides as coligands. Chapter 1 describes the survey of applications and recent developments in the field of semicarbazones, thiosemicarbazones, Schiff bases and their metal complexes. Chapter 2 deals with the syntheses and characterization of copper(II) complexes containing thiocyanate as coligand. Chapter 3 explains the syntheses and spectral studies of azide linked copper(II) complexes. Two of the synthesised complexes are trans-$\mu_{1,1}$-azido bridged 1D coordination polymers. In both of them, each monomeric unit is related to its adjacent ones by a 2-fold screw axis, leading to a helical propagation. Chapter 4 comprises the syntheses and spectral studies of copper(II) complexes containing cyanate as coligand. Packing polymorphism exhibited by these binuclear complexes have been explained here in detail. Along with the synthesis and spectral studies, the mesohelical nature of copper(II) complex containing dicyanamide anion is discussed in Chapter 5. Chapter 6 deals with the syntheses and spectral studies of copper(II) complexes containing chloride as coligand. The chloride bridged 1D chains of Cu(II) complexes crystallizes in centrosymmetric space group *Pbca* of orthorhombic crystal system. Syntheses and spectral studies of copper(II) complexes containing bromide as coligand are discussed in Chapter 7. The influence of non covalent interactions on the directional nature of crystal packing has been well studied through our work. Summary of the thesis is also given at the end.

Contents

Chapter 1

Copper(II) complexes with halides and pseudohalides: A brief introduction

Contents

1.1. Introduction

Copper is widely distributed in nature as metal, in sulphides, arsenides, chlorides, carbonates and so on [1]. Copper is one of the transition elements frequently found at the active site of proteins. The copper containing enzymes and proteins constitute an important class of biologically active compounds [2]. The biological functions of copper proteins/enzymes include electron transfer, dioxygen transport, oxygenation, oxidation, reduction, and disproportionation [3,4]. The common oxidation states of copper are I (d^{10}), II (d^{9}), and III (d^{8}). Cu(I) forms mononuclear and polynuclear complexes having linear, planar, tetrahedral and distorted planar geometries. The most common oxidation state of Cu is +2, and Cu(II) complexes have been extensively studied. These complexes have trigonal planar, tetrahedral, octahedral, distorted octahedral, square planar and pentagonal bipyramidal geometries. Thiosemicarbazones and semicarbazones are molecules of great interest due to their potential pharmacological properties and a wide variation in their modes of bonding and stereochemistry. Semicarbazones are also reported to possess versatile structural features [5] and have very good antifungal and antibacterial properties [6,7]. A variety of semicarbazones and their metal complexes possess anti-protozoa and anti-convulsant activity also [8]. Copper(II) complexes are interesting due to their biological applications and interesting stereochemistries. Recently there has been considerable amount of interest in the studies of semicarbazones due to their unusual coordination modes when bound to metals, high pharmacological potentiality and good chelating property [9].

Copper is a bioelement and is an active site in several metalloenzymes and proteins [10,11]. Among all the transition metal complexes, copper(II) Schiff base

complexes with pseudohalogens are well known for their preparational accessibilities, exhibiting the flexibility of the coordination geometry around the metal center azide-copper(II) complexes are also of great interest for bioinorganic chemists to explore the structure and role of active sites in copper proteins such as metalazido hemocyanins and tyrosinases [12,13]. The chemistry of copper(II)-azido complexes has also received great deal of attention to enhance the fundamental knowledge about the magnetic interactions between the paramagnetic centers and for developing new functional molecule-based materials [14]. Examples of Cu(II)-azide systems with bidentate coligands are numerous and their structures are much diverse and more sensitive to the coligands used. Hence a variety of mononuclear, binuclear and polymeric complexes have been obtained, not only due to the coordination diversity of the azide ion, but also due to the coordination flexibility of the Cu(II) ion.

Even though thiocyanate is not as good a mediator of magnetic exchange between metal centers as the azide ion, still many copper complexes have been reported with thiocyanate and Schiff bases with ferromagnetic as well as antiferromagnetic interactions. Also the thiocyanate-bridged metal-coordination complexes have deserved special attention because they exhibit interesting electrochemical, zeolitic, magnetic, and photomagnetic properties [15]. The tetranuclear copper(II) chain complexes designed using the dipyridylmethanediol ligand has been found to promote ferromagnetic couplings between the copper(II) centers, thus opening a new avenue for the synthesis of molecular magnets [16].

1.2. Stereochemistry

The Cu(II) ion with $3d^9$ outer electron configuration lacks cubic symmetry and hence yields distorted forms of the basic stereochemistries such as tetrahedral, square planar, square pyramidal and octahedral [17]. Coordination numbers four, five and six predominate, but variations of each structure occur through bond length or bond angle distortions. The four coordinate complexes may be tetrahedral, square planar or a distorted mixture thereof, and the five coordinate complexes, square pyramidal, trigonal bipyramidal or a mixed version thereof. Jahn Teller effect plays a major role in deciding the distortion effect on stereochemistries of Cu(II) complexes. The typical distortion involved in octahedral geometry is elongated structures with the odd electron residing in the $d_{x^2-y^2}$ orbital resulting in four short Cu–L bonds and two *trans* long bonds, which are

usually more energetically favorable than the compressed structures, consistent with their more frequent occurrence. In the six coordinate species, the structures vary from compressed tetragonal through regular octahedral to elongated tetragonal but also include examples where the bond angles are clearly not 90^{o}.

1.3. Outline of proligands used in the present study

1.3.1. Semicarbazones

Semicarbazones are usually obtained by the condenzation of semicarbazides with suitable aldehydes and ketones. An interesting fact is that the semicarbazones exist predominantly in the amido form in the solid state, whereas due to the interaction of the solvent molecules they can exhibit a amido-iminol tautomerism in solution state. Amido form acts as a neutral ligand and the iminol form can deprotonate and serve as anionic ligand in metal complexes. Thus semicarbazones are versatile ligands in both neutral and anionic forms. Both tautomeric forms have an efficient electron delocalization along the semicarbazone moiety. Aromatic substituents on the semicarbazone skeleton can further enhance the delocalization of electron charge density. These classes of compounds usually react with metallic cations giving complexes in which the semicarbazones behave as chelating ligands. Upon coordination to a metal center, the delocalization is further increased through the metal chelate rings. The coordination possibilities are further increased if the substituent has additional donor atoms. The following three semicarbazone ligands were synthesized by varying the carbonyl compuonds.

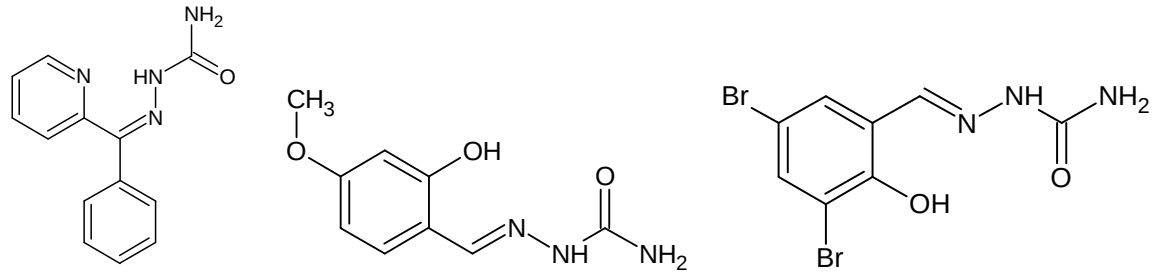

Hbpsc **H_2mssc** **H_2dbssc**

Fig. 1.1. Structures of the three semicarbazone ligands.

1.3.2. Thiosemicarbazones

Thiosemicarbazones are compounds obtained by the reaction of thiosemicarbazides or substituted thiosemicarbazides with aldehydes and ketones. The –C=S group provides the

possibility for the electron delocalization within the thiosemicarbazone moiety and also, increases the denticity of these compounds. The thioamide sulfur and azomethine nitrogen are the available donor sites present in the thiosemicarbazone compounds. Further, the number of coordination sites can be increased by the suitable substitution on the thiosemicarbazone framework. If heterocyclic rings are attached to the thiosemicarbazone moiety, the hetero atoms can act as the donor sites. An interesting attribute of the thiosemicarbazones is that in the solid state, they predominantly exist in the thioamido form, whereas in solution they exist both in thioamido and in thioiminol forms. The thioiminol form predominates in the solution state and can effectively coordinate to a metal atom. The following two thiosemicarbazone ligands were prepared by varying the ketones.

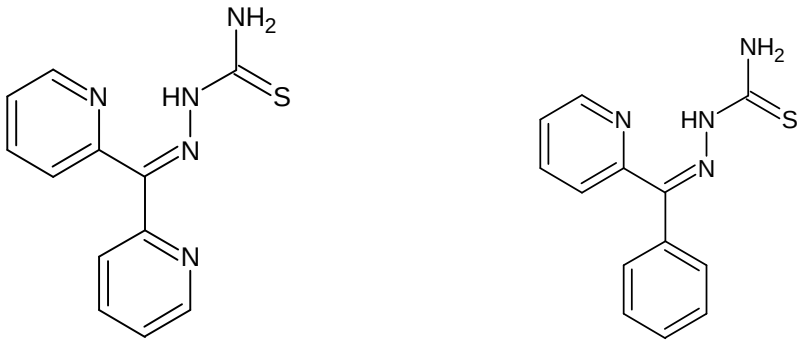

Hdpktsc **Hbptsc**

Fig. 1.2. Structures of the two thiosemicarbazone ligands.

1.3.3. Schiff bases

The condenzation of primary amines with carbonyl compounds yields Schiff bases that are regarded as one of the most potential groups of chelators for the facile preparations of metallo-organic hybrid materials [18]. The exceptional qualities of Schiff bases such as facile syntheses, easily tunable steric, electronic properties and good solubility in common solvents have led to their extensive study [19]. In the past two decades, the synthesis, structure and properties of Schiff base complexes have stimulated much interest for their noteworthy contributions in the development of single molecule magnets, material science [20,21], catalysis of many reactions like carbonylation, hydroformylation, reduction, oxidation, epoxidation, hydrolysis etc [22]. This is due to the fact that Schiff bases offer opportunities for inducing substrate chirality, tuning the metal centered electronic factor, enhancing the solubility and stability of either homogeneous or heterogeneous catalysts. The flexibility of disposition of different donor sites is the secret behind their successful performance in mimicking peculiar geometries

around the metal centers, leading to very interesting spectroscopic properties with varied magnetic activities [23]. Schiff bases also display biological activity and play an important role in biological systems [24]. Additionally the Schiff bases are found to have wide applications in field such as antibacterial, antiviral, antifungal agents [25].

In view of the above observation, the following five Schiff base ligands were synthesized by varying the aldehyde/ketone and the amine/hydrazide.

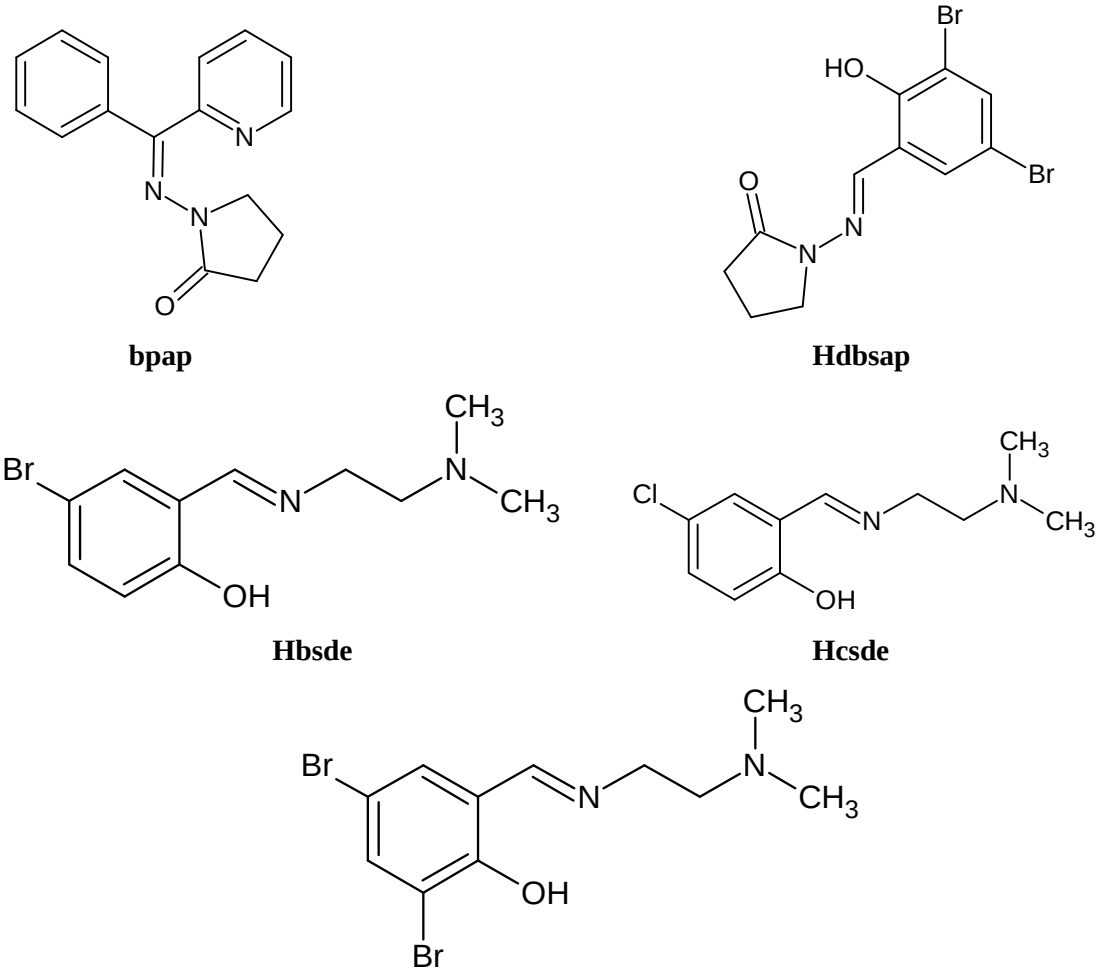

bpap **Hdbsap**

Hbsde **Hcsde**

Hdbsde

Fig. 1.3. Structures of the five Schiff base ligands.

Copper complexes containing pseudohalogens like azide or thiocyanate ions have been extensively investigated due to their excellent magnetic properties [26]. The use of Schiff bases as coligands in such metal-pseudohalogen complexes lead to interesting results [27]. This is because even a very small change in the coligands can lead to astonishing variation in the structure and magnetism of the resulting complexes. The stereochemical properties of the coligands certainly influence the structural diversity of the metal complexes [28]. The metal-pseudohalogeno systems containing Schiff base coligands are not as investigated as the systems without Schiff bases.

1.4. Classification of copper(II) complexes based on nuclearity

1.4.1. Mononuclear complexes: These are divided into three types. (i) Four coordinated complexes in which the copper ion has square planar geometry. (ii) Five coordinated complexes in which the copper ion has square pyramidal geometry. The tridentate Schiff base ligand coordinates the Cu(II) atom in equatorial mode and the axial position is occupied by an anionic ligand. (iii) Six coordinated complexes have distorted octahedral geometry and the tridentate ligand binds the Cu(II) atom in the equatorial mode and axial positions are occupied by anionic ligands.

1.4.2. Dinuclear complexes: The coordination mode flexibility of the coligands enabled the bridging of the entities leading to dinuclear complexes.

1.4.3. Polymers: Depending upon the crystallization conditions, the [Cu(L)X] complexes may sometimes build *trans*-$\mu_{1,3}$ bridged 1D-polymeric chains along the Jahn-Teller axis. In these complexes the tridentate ligand coordinates in the equatorial mode, and the axial positions are occupied by X.

1.4.4. Weak interactions: Aggregation of mononuclear complexes into dimers and networks *via* H-bonding involving coordinated or lattice solvent molecules have been reported.

1.5. Objectives of the present work:

1. To synthesize mononuclear to multinuclear copper coordination complexes with pseudohalides and halides as coligands and their molecular structural determination.
2. To explore the various intermolecular interactions present in them.
3. To study the packing modes, in the context of these interactions.
4. To study the versatility in coordination modes of Cu(II) complexes with halides and pseudohalides as coligands.
5. Magnetostructural corelation of copper complexes based on its stereochemistry and the coordination mode of coligands.

REFERENCES

1. F.A. Cotton, G. Wilkinson, C.A. Murillo, M. Bochmann, Advanced Inorganic Chemistry, 6th Ed., Wiley, New York, 1999.
2. R.N. Mukherjee, Indian J. Chem., 2003, 42A, 2175.
3. R.N. Mukherjee, Comprehensive Coordination Chemistry-II: From Biology to Nanotechnology, 2003, 5.
4. R.H. Holm, P. Kennepohl, E.I. Solomon, Chem. Rev., 1996, 96.
5. M. Akkurt, S. Ozfuric, S. Ide, Anal. Sci., 2000, 16, 667.
6. J.R. Dimmock, R.N. Puthucode, J.M. Smith, M. Hetherington, J.W. Quil, U. Pugazhenthi, J. Med. Chem., 1996, 39, 3984.
7. J.R. Dimmock, K.K. Sidhu, S.D. Thumber, S.K. Basran, M. Chen, J.W. Quil, Eur. J. Chem., 1995, 30, 287.
8. H. Beraldo, D. Gambino, Mini Rev. Med. Chem., 2004, 4, 31.
9. L.A. Saryan, E. Ankel, C. Krishnamurthi, D.H. Petering, H. Elford, J. Med. Chem., 1979, 22, 1218.
10. R.R. Gay, R.S. Himmelwright, N.C. Eickman, V.A. Norris, H.C. Freeman, E.I. Solomon, J. Am. Chem. Soc., 1981, 103, 4382.
11. E.I. Solomon, K.W. Penfield, D.E. Wilcox, Struct. Bonding, 1983, 53, 1.
12. V. Mckee, M. Zvagulis, J.V. Dagdigian, M.G. Patch, C.A. Reed, J. Am. Chem. Soc., 1984, 106, 4765.
13. V. Mckee, J.V. Dagdigian, R. Bau, C.A. Reed, J. Am. Chem. Soc., 1981, 103, 7000.
14. E.-Q. Gao, Y.-F. Yue, S.-Q. Bai, Z. He, C.-H. Yan, Cryst. Growth Des., 2005, 5, 1119.
15. Z.E. Serna, R. Cortés, M.K. Urtiaga, M.G. Barandika, L. Lezama, M.I. Arriortua, T. Rojo, Eur. J. Inorg. Chem., 2001, 865.
16. S.R. Breeze, S. Wang, J.E. Greedan, N.P. Raju, Inorg. Chem., 1996, 35, 6944.
17. B.J. Hathaway, G. Wilkinson, R.D. Gillard, J.A. McCleverty, In Comprehensive Coordination Chemistry, 1987, 5, 558.
18. U. Casellato, P.A. Vigato, Coord. Chem. Rev., 1977, 23, 31.
19. Q. Shi, L. Xu, J. Ji, Y. Li, R. Wang, Z. Zhou, R. Cao, M. Hong, A. S. C. Chan, Inorg. Chem. Commun., 2004, 7, 1254.
20. I. Ramade, O. Kahn, Y. Jeannin, F. Robert, Inorg. Chem., 1977, 36, 930.

21. H. Miyasaka, H. Ieda, N. Matsumoto, R. Crescenzi, C. Floriani, Inorg. Chem., 1998, 37, 255.

22. (a) M.M.T. Khan, S. Shukla, J. Shark, J. Mol. Catal., 1990, 57, 301. (b) E. Fujita, B.S. Brunschwig, T. Ogata, S. Yanagida, Coord. Chem. Rev., 1994, 132, 195. (c) E. Kimura, S. Wada, M. Shiyonoya, Y. Okazaki, Inorg. Chem., 1994, 33, 770. (d) B. De Clercq, F. Verpoort, Macromolecules, 2002, 35, 8943. (e) T. Opstal, F. Verpoort, Angew. Chem. Int. Ed., 2003, 42, 2876. (f) B. De Clercq, F. Lefebvre, F. Verpoort, Appl. Catal., 2003, A247, 345.

23. D.E. Fenton, Chem. Soc. Rev., 1999, 28, 159.

24. (a) V. Razakantoanina, P.P. Nguyen Kim, G. Jaureguiberry, Parasitol Res., 2000, 86, 665. (b) R.E. Royer, L.M. Deck, T.J.V. Jagt, F.J. Martinez, R.G. Mills, S. Young, A.D.L.V. Jagt, J. Med. Chem., 1995, 38, 2427. (c) M.R. Flack, R.G. Pyle, N. Mullen, M.B. Lorenzo, Y.W. Wu, R.A. Knazek, B.C. Nusule, M.M. Reidenberg, J. Clin. Endocrinol Metab., 1993, 76, 1019. (d) R. Baumgrass, M. Weiwad, F. Edmann, J. Biol. Chem., 2001, 276, 47914. (e) P.J.E. Quintana, A. Peyster de, S. Klatzke, H. Park, J. Toxicol Lett., 2000, 117, 85.

25. S. Chandra, X. Sangeetika, Spectrochim. Acta, Part A, 2004, 60, 147.

26. K. Vrieze, G.V. Katong, G. Wilkinson, R.D. Gillard, J.A. McCleverty, In Comprehensive Coordination Chemistry, (Eds.), Pergamon Press : Oxford, England, 1987, 2, 225.

27. (a) P.S. Mukherjee, T.K. Maji, A. Escuer, R. Vicente, J. Ribas, G. Rosair, F.A. Mautner, N.R. Chaudhuri, Eur. J. Inorg. Chem., 2002, 943. (b) S. Deoghoria, S. Sain, B. Moulton, M.J. Zaworotko, S.K. Bera, S.K. Chandra, Polyhedron, 2002, 21, 2457. (c) E.-Q. Gao, S.-Q. Bai, Y.-F. Yue, Z.-M. Wang, C.-H. Yan, Inorg. Chem., 2003, 42, 3642. (d) M.S. Ray, A. Ghosh, S. Chaudhuri, M.G.B. Drew, J. Ribas, Eur. J. Inorg. Chem., 2004, 3110. (e) S. Chattopadhyay, M.S. Ray, M.G.B. Drew, A. Figuerola, C. Diaz, A. Ghosh, Polyhedron, 2006, 25, 2241.

28. C. Adhikary, D. Mal, K.-I. Okamoto, S. Chaudhuri, S. Koner, Polyhedron, 2006, 25, 2191.

Chapter 2

Copper(II) complexes containing thiocyanate as coligand

Contents

2.1. Introduction

During the past few decades the design and synthesis of metallo-organic superstructures based on strong covalent bonds and multiple weak non-covalent forces has become one of the most active fields in coordination chemistry and crystal engineering. Coordination polymers have been employed in catalysis, molecular adsorption, molecular magnetism, nonlinear optics, luminescence or model bioinorganic chemistry [1,2,3]. Intensive magnetostructural investigations of homo- and heteropolynuclear complexes have contributed to the understanding of the factors governing the sign and the magnitude of the intramolecular exchange interactions between either identical or different paramagnetic centers [4]. Generally, the type and topology of the coordination polymers depend on the metal element, valences and geometry needs of the metal ion and functionality of the ligand. However, the fine tuning of the framework is difficult to realize, and a subtle modification of ligands may lead to the formation of drastically different structures [5]. Various interesting topologies have yielded in one-pot synthesis using appropriate molar ratios of metal ions, organic ligands, counter ions and thiocyanate ions as bridging units. Thiocyanate $(SCN)^-$ is a highly versatile ambidentate ligand with a polarizable π system and two different donor atoms, which can coordinate to metals through either the nitrogen or the sulfur atom, or both. Different bridging modes of the thiocyanato ligand can generate various types of supramolecular structures with particular properties. The thiocyanate ligand may act as an efficient mediator for the magnetic interaction between the paramagnetic transition metal centers [6]. Most of the extended networks are related to the end-to-end coordination modes, leading either to

one-dimensional compounds [7,8], two-dimensional compounds [9] or three dimensional compounds [10].

One of the most attractive metal ion template in the molecular recognition process in extended materials is copper(II). The attractiveness of copper ions in the synthesis of polymeric compounds results mainly from their attractive magnetic properties, mixed valence oxidation-state pairs, photoluminescence, structural features and biological relevance involving the binuclear site in cytochrome oxidases and related model compounds [11].

The chalcogenocyanate ion, XCN^-, where X=S (thiocyanate), Se (selenocyanate), or Te (tellurocyanate), is a linear triatomic pseudohalide. Thiocyanate is a highly versatile ambidentate ligand with two donor atoms. It can coordinate through either the nitrogen or the sulfur atom, or both, giving rise to linkage isomers or polymers. The resonance structures are:

$$^{-}S–C\equiv N \leftrightarrow S=C=N^{-} \leftrightarrow {}^{+}S\equiv C–N^{2-}$$

(A) **(B)** **(C)**

Scheme 2.1. Resonance structures of Thiocyanate ion.

The relative importance of the resonance structures follows the trend A>B≫C. There are two types of terminal coordination of SCN^- ligand: S-coordinated SCN^- (M–SCN) which is termed thiocyanate and N-coordinated SCN^-(M–NCS) which is called isothiocyanate. Metal thiocyanates, M–S–C≡N, are usually bent with M–S–C angle of 100° (ranging from 80 to 110°) whereas in metal isothiocyanates, M–N≡C–S, the M–N–C angles are variable, though commonly with M–N–C angle of around 150° (with a range of 110–180°). In either case, the S–C–N ligand is inevitably linear. While the M–N or M–S bond length depends on the nature and the electronic configuration of the metal (M), the C–N and C–S distances are close to 1.16 and 1.62 Å respectively [12]. Stereoisomers arising from N *vs*. S coordinated SCN^- (or any other ambidentate) ligands are termed linkage isomers.

The modes of metal coordination of chalcogenocyanates in general, and the thiocyanates in particular, are best understood in terms of the hard-soft acid-base concept developed by Pearson, Basolo, and Burmeister [13]. In accordance with the

hard-soft acid-base concept, the S atom of the SCN^- ligand, being a soft base, preferentially coordinates to the soft acid whereas the N atom, being a hard base, preferentially coordinates to the hard acid. However, there are limitations to the hard-soft acid-base concept. Generally speaking, regardless of oxidation state or geometry, all of the metals in the first transition series, and all of the lanthanides and actinides exhibit only N-coordination. The first half of the second and third transition series also tend to be N-coordinated whereas at Rh(III) and Ir(III), there is a switch to S-coordination. The tetrahedral Hg(II) complexes are almost always S-bonded. Cd(II), in-between, becomes 'schizophrenic'[14], exhibiting both (S and N) bonding modes.

An account of metal thiocyanate complexes has been reported which shows versatile coordinate structural diversity [15]. Thiocyanate can act as a terminal or bridging ligand. Except for two types of terminal coordinate modes, Teo and co-workers have depicted that there are theoretically 13 multidentate bridging modes, ranging from bi- to hexadentate as simplified in Fig. 2.1. However, not all of these coordinate modes have been observed. The most commonly observed modes are the uni-, bi-, and tridentate coordination. The ambidentate nature and the highly versatile bridging modes of the thiocyanate ligand also allow the formation of a wide variety of 1-D, 2-D, and 3-D polymeric metal-thiocyanate coordinate structures.

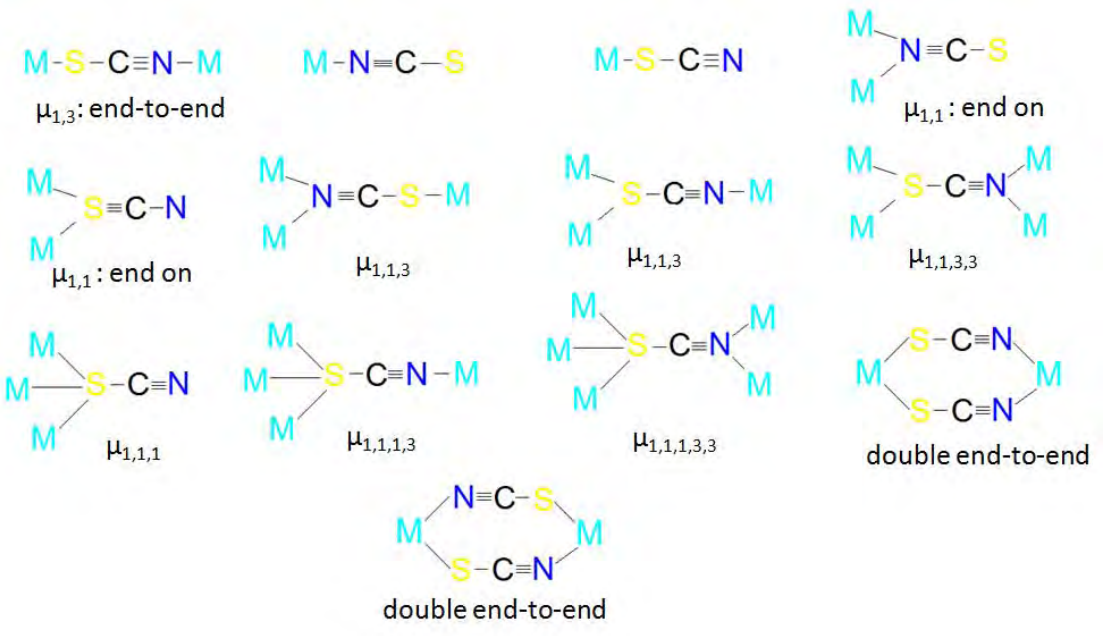

Fig. 2.1. Different binding modes of thiocyanate ion.

The $\mu_{1,1,1}$, $\mu_{1,1,1,3}$ and $\mu_{1,1,1,3,3}$-thiocyanate coordinate modes have not been observed [16]. The study of polynuclear complexes of Cu(II) with pseudohalogen bridges has received considerable attention in the recent years. Many doubly thiocyanato bridged copper(II) compounds have been characterized. However, single thiocyanato bridged copper(II) compounds are comparatively rare. Thiocyanato (SCN^-), with extraordinary varieties in the binding of complexes, has great potential in building coordination network. It can adopt the end-to-end and end-on fashions *via* the nitrogen and sulfur atoms to build coordination networks [17] as well as interlink the 1-D or 2-D molecules into frameworks *via* the non-covalent interactions [18].

It is well known that the thiocyanate anions usually bridge different metal atoms through the end-to-end and end-on modes [19,20,21]. For the copper(II) complexes, examples of the end-on bridging mode of the thiocyanate anions are very few [22]. The thiocyanate ligand may act as an efficient mediator for the magnetic interaction between the paramagnetic copper(II) centers. The literature available for magnetostructural studies on copper(II) complexes containing bridging thiocyanate groups is scarce, as this ligand is less versatile and less efficient as a transmitter of magnetic interactions than azide.

Thiocyanate with the end-to-end mode of coordination has been found able to transmit weak ferro- [19**]** or antiferro-magnetic [23] interactions depending on the geometry and the bridging mode in the Cu–NCS–Cu entity: the equatorial-axial disposition (EA) of the thiocyanate bridging leads to very weak or zero overlap between the involved magnetic orbitals and consequently weak magnetic interaction (ferro- or antiferro-magnetic) is observed [24,25]. However, the equatorial-equatorial (EE) disposition enables significant overlap of the orbitals of the bridging entities with the magnetic orbitals of the metal atoms and so strong antiferromagnetic interaction takes place [26]. Theoretically, the EA disposition leads to the accidental orthogonality of the MO arising from the e_g metallic orbitals, minimising the antiferromagnetic component of the global *J* constant.

From the Goodenough-Kanamory rules the dinuclear end-to-end thiocyanato bridged copper(II) compounds should present ferromagnetic coupling [27,28].

2.2. Experimental

2.2.1. Synthesis of the complexes

All chemicals used for synthesis were of Analar grade. The ligands were formed *in situ*.

2.2.1.1. Synthesis of $[Cu(bpsc)(NCS)]_n$ (1)

2-Benzoylpyridine semicarbazone (Hbpsc) was synthesized *in situ* from 2-benzoylpyridine (0.183 g, 1 mmol) and semicarbazide hydrochloride (0.112 g, 1 mmol) by heating the reactants in methanol for 2 h. Copper acetate monohydrate (0.199 g, 1 mmol) and potassium thiocyanate (0.099 g, 1 mmol) was added to it and the mixture was heated for 3 h. The dark green solid was collected and recrystallized from methanol. Yield: 79%.

2.2.1.2. Synthesis of $[Cu(Hbpsc)(NCS)_2]$ (2)

2-Benzoylpyridine semicarbazone (Hbpsc) was synthesized *in situ* from 2-benzoylpyridine (0.183 g, 1 mmol) and semicarbazide hydrochloride (0.112 g, 1 mmol) by heating the reactants in methanol for 2 h. Copper sulfate pentahydrate (0.250 g, 1 mmol) and potassium thiocyanate (0.198 g, 2 mmol) was added to it and the mixture heated for 3 h. The dark green solid was collected and recrystallized from methanol. Yield: 77%.

2.2.1.3. Synthesis of $[Cu(Hbpsc)\mu^2(S)NCS]_2 \cdot S$ (3)

2-Benzoylpyridine semicarbazone was synthesized *in situ* from 2-benzoylpyridine (0.183 g, 1 mmol) and semicarbazide hydrochloride (0.112 g, 1 mmol) by heating the reactants in methanol for 2 h. Copper sulfate pentahydrate (0.250 g, 1 mmol) and potassium thiocyanate (0.099 g, 1 mmol) was added to it and mixture was heated for 3 h. The dark green solid was collected and recrystallized from methanol. Yield: 9%.

2.2.1.4. Synthesis of $[Cu(bpap)(NCS)_2]$ (4)

1-[(E)-[Phenyl(pyridin-2-yl)methylidene]amino]pyrrolidine-2-one (bpap) was synthesized *in situ* from 2-benzoylpyridine (0.183 g, 1 mmol) and 1-aminopyrrolidin-2-one (0.100 g, 1 mmol) by heating the reactants in methanol for 2 h. Copper(II) chloride dihydrate (0.170 g, 1 mmol) was added to it and the mixture was heated for 2 h. Sodium thiocyanate (0.194 g, 2 mmol) was added to this mixture and it was

heated for another one hour. The resulting pale green solid was collected and recrystallized from alcohol. Yield: 65%.

2.2.1.5. Synthesis of [Cu(dbsde)(NCS)] (5)

The Schiff base (Hdbsde) was synthesized *in situ* from 3,5-dibromosalicylaldehyde (0.280 g, 1 mmol) and N,N-dimethylethylenediamine (0.088 g, 1 mmol) by heating the reactants in methanol for 2 h. Copper(II) chloride dihydrate (0.170 g, 1 mmol) was added to it and the mixture was heated for 2 h. Sodium thiocyanate (0.194 g, 2 mmol) was added to it and the reaction mixture was heated for another one hour. The resulting pale green solid was collected and recrystallized from alcohol. Yield: 68%.

2.2.1.6. Synthesis of $[Cu(msc)_2(NCS)_2]$ (6)

A methanol solution of N-methylsemicarbazide (0.089 g, 1 mmol), copper acetate monohydrate (0.199 g, 1 mmol) and potassium thiocyanate (0.198 g, 2 mmol) was heated for 5 h. The dark green solid was collected and recrystallized from methanol. Yield: 27%.

2.2.2. Physical measurements

Carbon, hydrogen and nitrogen analyses were carried out using a Vario EL III CHNS analyzer at the SAIF, Kochi, India. Infrared spectra were recorded on a JASCO FT-IR-5300 Spectrometer in the range 4000-400 cm^{-1} using KBr pellets. Electronic spectra were recorded on Ocean Optics USB 4000 UV-Vis Fiber Optic Spectrometer in the 200-850 nm range using solutions in methanol. The molar conductivities of the complexes in DMF solutions (10^{-3} M) at room temperature were measured using a Systronic model 303 direct reading conductivity meter at the Department of Applied Chemistry, CUSAT, Kochi, India. Magnetic susceptibility measurements of the complexes were carried out on a Vibrating Sample Magnetometer using $Hg[Co(SCN)_4]$ as a calibrant at the SAIF, Indian Institute of Technology, Madras. The EPR spectra of the complexes in the solid state at 298 K and in DMF/DMSO at 77 K were recorded on a Varian E-112 spectrometer using TCNE as the standard, with 100 kHz modulation frequency, 2 G modulation amplitude and 9.1 GHz microwave frequency at SAIF, IIT Bombay, India.

2.2.3. X-ray crystallography

Single crystals of compounds $[Cu(bpsc)(NCS)]_n$ (**1**), $[Cu(Hbpsc)(NCS)_2]$ (**2**), $[Cu(Hbpsc)\mu^2(S)NCS]_2 \cdot S$ (**3**), $[Cu(bpap)(NCS)_2]$ (**4**), [Cu(dbsde)(NCS)] (**5**), and $[Cu(msc)_2(NCS)_2]$ (**6**) suitable for X-ray diffraction studies were grown from their methanolic solution by slow evaporation at room temperature. Single crystals were selected and mounted on a Bruker SMART APEX diffractometer, equipped with a graphite crystal, incident-beam monochromator, and a fine focus sealed tube with Mo Kα (λ = 0.71073 Å) as the X-ray source. The crystallographic data along with details of structure solution refinements are given in Tables 2.1a and 2.1b. The unit cell dimensions were measured and the data collection was performed at 293(2) K. Bruker SMART software was used for data acquisition and Bruker SAINT software for data integration [29]. Absorption corrections were carried out using SADABS based on Laue symmetry using equivalent reflections [30]. The structures were solved by direct methods and refined by full-matrix least-squares calculations with the WinGX software package [31]. The molecular and crystal structures were plotted using DIAMOND version 3.2g [32]. All non-hydrogen atoms were refined anisotropically, and all H atoms on C and N were placed in calculated positions, guided by difference maps and refined isotropically, with C–H and N–H bond distances of 0.93 Å and 0.86 Å respectively. In the $[Cu(bpsc)(NCS)]_n$ (**1**), $[Cu(Hbpsc)(NCS)_2]$ (**2**), $[Cu(Hbpsc)\mu^2(S)NCS]_2 \cdot S$ (**3**) the hydrogen atoms of the NH_2 group were located from a difference Fourier map and restrained using DFIX and DANG instructions. In $[Cu(Hbpsc)(NCS)_2]$ (**2**) and $[Cu(Hbpsc)\mu^2(S)NCS]_2 \cdot S$ (**3**), N–H hydrogen atoms were located from Fourier maps and restrained to a distance of 0.88±0.01. In the refinement of $[Cu(bpap)(NCS)_2]$ (**4**), carbon-bound H-atoms were placed in calculated positions (C–H 0.93–0.97 Å) and were included in the refinement in the riding model approximation, with U(H) set to 1.2U(C). Two of the methylene carbons in the pyrrolidine ring of compound (**4**) are disordered; the disorder was regarded as a 1:1 type of disorder. In the refinement of [Cu(dbsde)(NCS)] (**5**), carbon-bound H-atoms were placed in calculated positions (C–H 0.93–0.97 Å) and were included in the refinement in the riding model approximation.

Table 2.1a. Crystallographic data and structure refinement for **1**, **2** and **3**

Parameters	$[Cu(bpsc)(NCS)]_n$ (**1**)	$[Cu(Hbpsc)(NCS)_2]$ (**2**)	$[Cu(Hbpsc)\mu^2(S)NCS]_2 \cdot S$ (**3**)
Empirical formula	$C_{14}H_{11}CuN_5OS$	$C_{15}H_{12}CuN_6OS_2$	$C_{28}H_{24}Cu_2N_{10}O_2S_4$
Formula weight	360.90	420.00	787.95
Color	Dark Green	Dark Green	Green
Temperature (T) K	296(2)	296(2)	296(2)
Wavelength (Mo Kα) (Å)	0.71073	0.71073	0.71073
Crystal system	Monoclinic	Triclinic	Monoclinic
Space group	$P2_1/n$	$P\bar{1}$	$C2/c$
Cell parameters			
a	5.5620(4) Å	8.8945(5) Å	20.0065(9) Å
b	14.5617(12) Å	8.8997(5) Å	7.7422(3) Å
c	18.2360(15) Å	12.6009(7) Å	20.8934(6) Å
α	90°	99.298(2)°	90°
β	97.052(3)°	108.795(2)°	92.878(2)°
γ	90°	106.796(2)°	90°
Volume V ($Å^3$)	1465.8(2)	867.57(8)	3232.2(2)
Z	4	2	4
Calculated density (ρ) (Mg m^{-3})	1.635	1.608	1.619
Absorption coefficient, μ (mm^{-1})	1.640	1.516	1.619
F(000)	732.0	426	1600.0
Crystal size (mm^3)	0.40 x 0.25 x 0.20	0.35 x 0.30 x 0.25	0.30 x 0.25 x 0.25
θ range for data collection	2.25 to 25.00°	2.49 to 25.00°	2.89 to 26.00
Limiting indices	-6≤h≤6, -17≤k≤17, -21≤l≤21	-10≤h≤10, -10≤k≤10, -14≤l≤14	-24≤h≤24, -9≤k≤9, -25≤l≤25
Reflections collected	20941	12594	24415
Unique Reflections (R_{int})	2589 [R(int) = 0.0490]	3063 [R(int) = 0.0615]	3189 [R(int) = 0.0469]
Completeness to θ	25.00 (100.0 %)	25.00 (100.0 %)	26.00 (99.8 %)
Absorption correction	Semi-empirical from equivalents	Semi-empirical from equivalents	Semi-empirical from equivalents
Maximum and minimum transmission	0.720 and 0.618	0.685 and 0.594	0.666 and 0.620
Refinement method	Full-matrix least-squares on F^2	Full-matrix least-squares on F^2	Full-matrix least-squares on F^2
Data / restraints / parameters	2588 / 2 / 207	3062 / 3 / 239	3183 / 0 / 210
Goodness-of-fit on F^2	1.173	1.062	1.048
Final R indices [I > 2σ (I)]	R_1 = 0.0261, wR_2 = 0.0634	R_1 = 0.0311, wR_2 = 0.0876	R_1 = 0.0375, wR_2 = 0.0999
R indices (all data)	R_1 = 0.0385, wR_2 = 0.0756	R_1 = 0.0325, wR_2 = 0.0892	R_1 = 0.0520, wR_2 = 0.1102
Largest difference peak and hole (e $Å^{-3}$)	0.301 and -0.280	0.322 and -0.417	0.626 and -0.620

$R_1 = \Sigma||F_o| - |F_c|| / \Sigma|F_o|$ $\quad$ $wR_2 = [\Sigma w(F_o^2-F_c^2)^2 / \Sigma w(F_o^2)^2]^{1/2}$

Table 2.1b. Crystallographic data and structure refinement for **4**, **5** and **6**

Parameters	$[Cu(bpap)(NCS)_2]$ (**4**)	$[Cu(dbsde)(NCS)]$ (**5**)	$[Cu(msc)_2(NCS)_2]$ (**6**)
Empirical formula	$C_{18}H_{15}CuS_2N_5O$	$C_{12}H_{13}Br_2CuN_3OS$	$C_6H_{14}CuN_8O_2S_2$
Formula weight	445.01	470.67	357.94
Color	Green	Green	Green
Temperature (T) K	296(2)	296(2)	296(2)
Wavelength (Mo Kα) (Å)	0.71073	0.71073	0.71073
Crystal system	Monoclinic	Monoclinic	Monoclinic
Space group	*C*2/c	$P2_1/n$	$P2_1/n$
Cell parameters			
a	11.8883(3) Å	7.1653(18) Å	7.8780(4) Å
b	13.3578(3) Å	19.222(6) Å	10.5881(5) Å
c	23.9669(6) Å	11.239(4) Å	17.6362(9) Å
α	90°	90°	90°
β	98.596(1)°	90.910(9)°	101.971(2)°
γ	90°	90°	90°
Volume V ($Å^3$)	3763.23(16)	1547.8(8)	1439.10(12)
Z	8	4	4
Calculated density (ρ) ($Mg\ m^{-3}$)	1.571	2.020	1.652
Absorption coefficient, μ(mm^{-1})	1.40	6.706	1.819
F(000)	1816	916	732.0
Crystal size (mm^3)	0.4 × 0.3 × 0.2	0.40 x 0.25 x 0.20	0.30 x 0.25 x 0.20
θ range for data collection	2.3 to 28.2°	2.10 to 25.10 °	2.66 to 25.00
Limiting indices	-10≤h≤15, -17≤k≤16, -28≤l≤31	-8≤h≤8, -22≤k≤22, -10≤l≤13	-9≤h≤9, -12≤k≤12, -20≤l≤19
Reflections collected	8181	9088	10482
Unique Reflections (R_{int})	4493 [R(int) = 0.0335]	2744 [R(int) = 0.0480]	2541 [R(int) = 0.0630]
Completeness to θ	28.28 (96.3 %)	25.10 (99.5 %)	25.00 (99.9%)
Absorption correction	Semi-empirical from equivalents	Semi-empirical from equivalents	Semi-empirical from equivalents
Maximum and minimum transmission	0.7668 and 0.6039	0.3473 and 0.1745	0.694 and 0.584
Refinement method	Full-matrix least-squares on F^2	Full-matrix least-squares on F^2	Full-matrix least-squares on F^2
Data / restraints / parameters	4493 / 0 / 239	2744 / 0 / 183	2539 / 8 / 198
Goodness-of-fit on F^2	1.127	1.111	1.049
Final R indices [I > 2σ (I)]	R_1 = 0.0849, wR_2 = 0.2135	R_1 = 0.0963, wR_2 = 0.2876	R_1 = 0.0523, wR_2 = 0.1596
R indices (all data)	R_1 = 0.1038, wR_2 = 0.2238	R_1 = 0.1174, wR_2 = 0.3054	R_1 = 0.0546, wR_2 = 0.1630
Largest difference peak and hole (e $Å^{-3}$)	1.782 and -1.525	2.029 and -1.520	0.799 and -0.916

$R_1 = \Sigma||F_o| - |F_c|| / \Sigma|F_o|$ $\qquad$ $wR_2 = [\Sigma w(F_o^2-F_c^2)^2 / \Sigma w(F_o^2)^2]^{1/2}$

2.3. Results and discussion

2.3.1. Analytical measurements

The analytical data of all the complexes are listed in Table 2.2. The CHNS obtained showed that all the complexes are analytically pure.

Table 2.2. Preliminary analytical data of Cu(II) thiocyanato complexes

Compounds	Observed (Calculated)%				λ_m	μ_{eff}(B.M.)
	C	H	N	S		
$[Cu(bpsc)(NCS)]_n$ **(1)**	46.12 (46.59)	3.01 (3.07)	19.20 (19.41)	8.95 (8.89)	27	1.709
$[Cu(Hbpsc)(NCS)_2]$ **(2)**	42.61 (42.90)	2.43 (2.88)	20.41 (20.01)	14.98 (15.27)	10	1.623
$[Cu(Hbpsc)\mu^2(S)NCS]_2 \cdot S$ **(3)**	46.12 (46.49)	3.44 (3.60)	16.50 (16.68)	9.47 (9.55)	07	1.512
$[Cu(bpap)(NCS)_2]$ **(4)**	48.31 (48.58)	3.37 (3.40)	15.52 (15.74)	14. 63 (14.41)	03	1.704
[Cu(dbsde)(NCS)] **(5)**	30.54 (30.62)	2.63 (2.78)	8.80 (8.93)	6.73 (6.81)	15	1.751
$[Cu(msc)_2(NCS)_2]$ **(6)**	20.36 (20.14)	3.77 (3.94)	31.02 (31.31)	17.80 (17.92)	09	1.806

The complexes are soluble in organic polar solvents. The conductivity measurements were made in methanol solutions and all complexes are found to be non-electrolytes [33].

Polymeric 1-D thiocyanato copper(II) complex **1** containing $\mu_{1,3}$-NCS bridge with a N(basal)-S(apical) disposition of the bridge exhibit either very low values of J or a paramagnetic behavior [34].

But the room temperature magnetic moments of complexes formulated with one metal centre almost have the values very close to expected spin only value of 1.73 B.M. for a d^9 copper system.

2.3.2. Crystal structure of complex $[Cu(bpsc)(NCS)]_n$ (1)

The asymmetric unit of complex **1** is shown in Fig. 2.2. A summary of crystal data for the complexes is listed in Table 2.1a. The structure of $[Cu(bpsc)(NCS)]_n$ (**1**) (Fig. 2.3) consists of an infinite 1D polymeric chain of Cu(II) with 2-benzoylpyridine semicarbazone ligand. Each thiocyanate function as a *cis*-$\mu_{1,3}$ bridge, resulting in a one dimensional polymer. Each monomeric unit is related to its adjacent ones by a

twofold screw axis, leading to zig-zag propagation along the crystallographic 'c' axis. The overall coordination geometry of each copper(II) ion is thus distorted square pyramidal. The bidentate SCN^- ligand links adjacent units into a one dimensional chain running along the [001] axis.

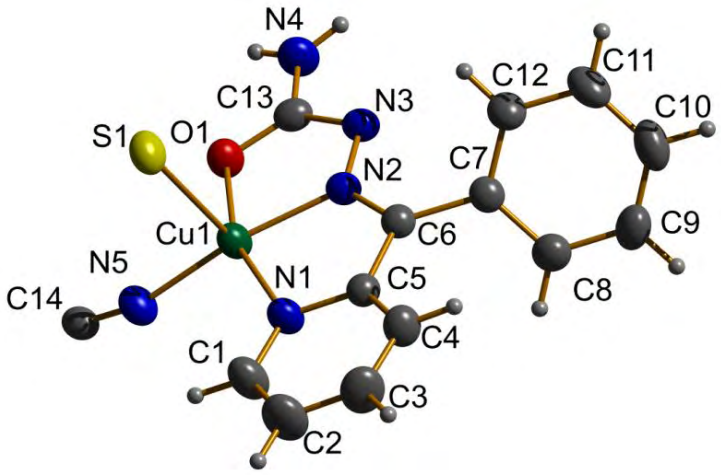

Fig. 2.2. Asymmetric unit of $[Cu(bpsc)(NCS)]_n$ (**1**) polymeric chain with atom numbering scheme.

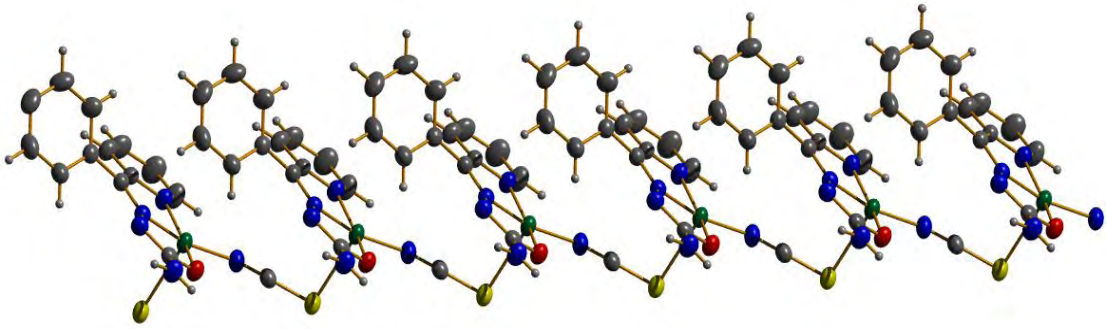

Fig. 2.3. Single chain Cu(II) thiocyanato bridged complex **1**.

The bond dimensions of the complex are included in Table 2.3. The structure is made up of infinite chains, in which Cu(II) centres are connected by single end-to-end thiocyanate bridges. The copper(II) pentacoordination sphere comprises the NNO donor atoms from the tridentate deprotonated semicarbazone ligand, and a nitrogen and a sulfur atom from two molecules of bridging thiocyanate ligands. The basal plane is formed by the NNO donor atoms of the ligand and the nitrogen atom of a thiocyanate ligand. The bond dimensions around the Cu(II) ion are comparable to those in similar systems [8] The slight distortion of the square pyramidal coordination can be observed from the coordinate bond lengths and angles (Table 2.3). The intrachain copper-copper separation is 5.562 Å which is comparable to previously reported singly thiocyanate bridged copper complexes [35].

Table 2.3. Selected bond lengths [Å] and angles [°] for $[Cu(bpsc)(NCS)]_n$ (**1**)

Bond lengths (Å)	
Cu1–N2	1.926(2)
Cu1–N1	1.991(2)
Cu1–O1	1.949(18)
C13–O1	1.280(3)
C13–N3	1.347(3)
N2–N3	1.355(3)
Cu1–S1	2.7121(8)
Cu1–N5	1.935(2)
C6–N2	1.299(3)
Bond angles (°)	
N2–Cu1–N1	81.24(9)
N1–Cu1–N5	101.30(9)
O1–Cu1–S1	96.34(6)
O1–Cu1–N2	79.89(8)
S1–Cu1–N5	94.70(7)
N1–Cu1–S1	93.16(7)
N2–Cu1–N5	164.68(9)

The apical position is occupied by a sulfur S(1) atom from a bridging SCN^- (isothiocyanate) group with rather long bond length of 2.7121 Å. A 1-D hydrogen bonded ribbon constructed *via* $R_2^2(8)$ and $R_3^3(18)$ association between two parallel chains (Figs. 2.4, 2.5 and 2.6).

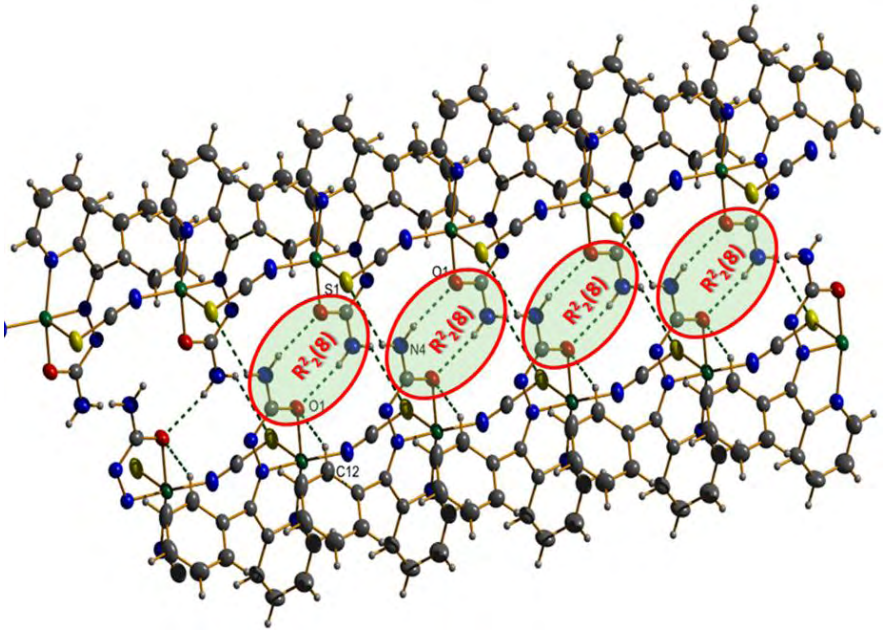

Fig. 2.4. A 1-D hydrogen bonded ribbon constructed *via* $R_2^2(8)$ association between two parallel chains.

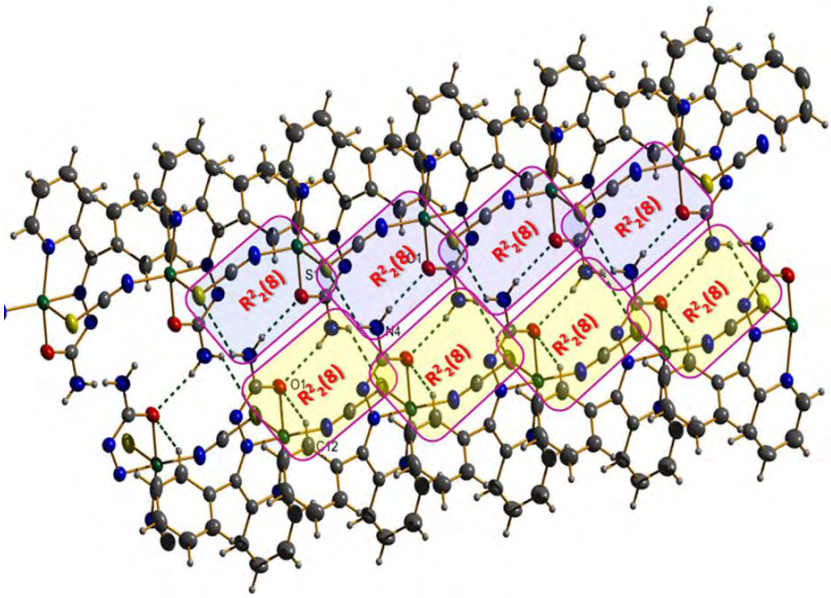

Fig. 2.5. A 1-D hydrogen bonded ribbon constructed *via* $R_2^2(8)$ association in antiparallel direction.

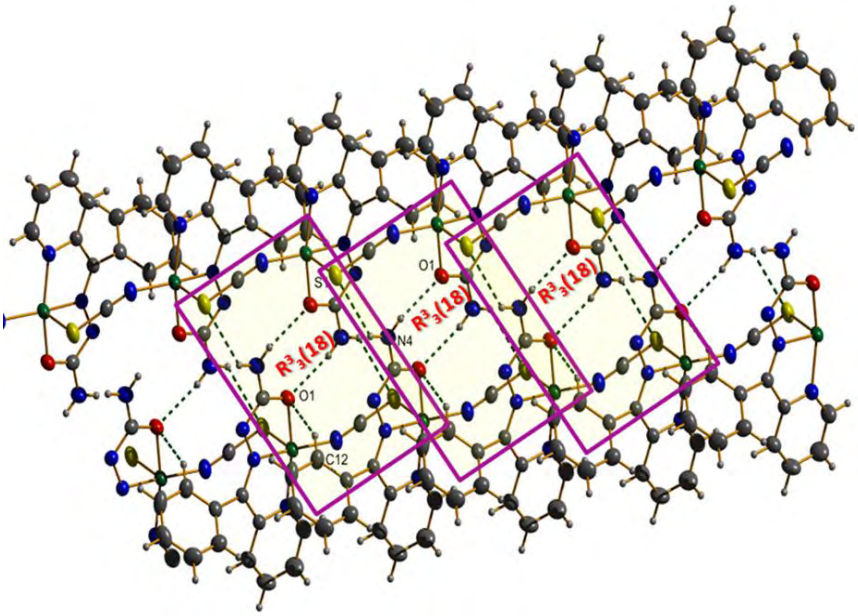

Fig. 2.6. A 1-D hydrogen bonded ribbon constructed *via* $R_3^3(18)$ association between two parallel chains.

The crystal packing of this complex shows layers made up of two parallel chains connected through double hydrogen bonds involving N(4)–H(4A)···O(1)[a] and N(4)–H(4B)···S(1)[b](a=2-x,1-y,-z; b=3-x,1-y,-z) (Fig. 2.7 and Table 2.4).

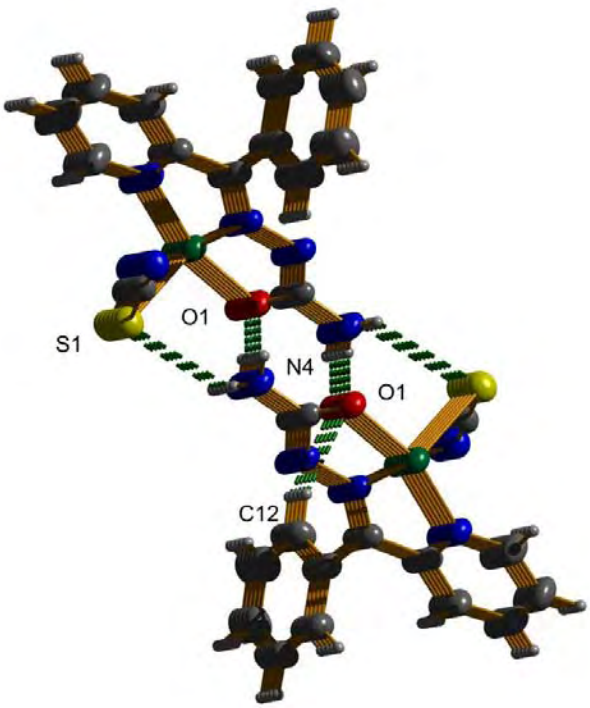

Fig. 2.7. Intermolecular and intramolecular hydrogen bonding interactions of $[Cu(bpsc)(NCS)]_n$ (**1**).

Table 2.4. Hydrogen bonding interaction of the complex $[Cu(bpsc)(NCS)]_n$ (**1**)

D–H···A	D–H (Å)	H···A (Å)	D···A (Å)	∠D–H···A(°)
N(4)–H(4A)···O(1)^a	0.82(3)	2.20(3)	3.003(3)	166(3)
N(4)–H(4B)···S(1)^b	0.84(3)	2.86(3)	3.496(3)	134(2)
C(12)–H(12)···O(1)^c	0.9294	2.5707	3.393(3)	147.73

Equivalent position codes: a=2-x,1-y,-z; b=3-x,1-y,-z

The N–H and C–H···π interactions (Fig. 2.8) mainly involve in the interconnection of the neighboring molecules with H···Cg distances of 3.31(3) and 2.597(8) Å (Table 2.5). The adjacent chains are linked by N–H···π and C–H···π interactions, by overlap of phenyl with pyridine rings, with adjacent chains, thus connecting the chains in a three-dimensional network.

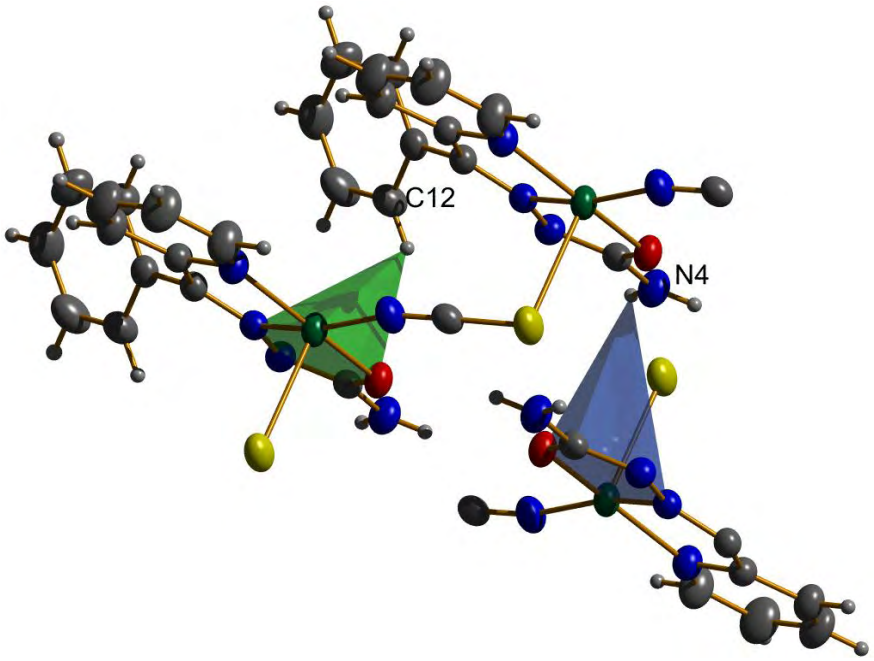

Fig. 2.8. N–H···π and C–H···π interactions in $[Cu(bpsc)(NCS)]_n$ (**1**).

Table 2.5. N–H ···π and C–H···π interactions in $[Cu(bpsc)(NCS)]_n$ (**1**)

X—H(I)···Cg(J)	H···Cg (Å)	X···Cg (Å)	∠X–H···Cg (°)
N(4)-H(4B)···Cg(3)^b	3.31(3)	3.510(3)	97(2)
C(12)-H(12)···Cg(3)^c	2.597(8	3.171(3)	120.41

Equivalent position codes: a=2-x,1-y,-z; b=3-x,1-y,-z; c=-1+x,y,z ; Cg(3) = Cu(1), O(1), C(13), N(3), N(2)

The arrangement of the molecules along 'c' axis is shown in Fig. 2.9.

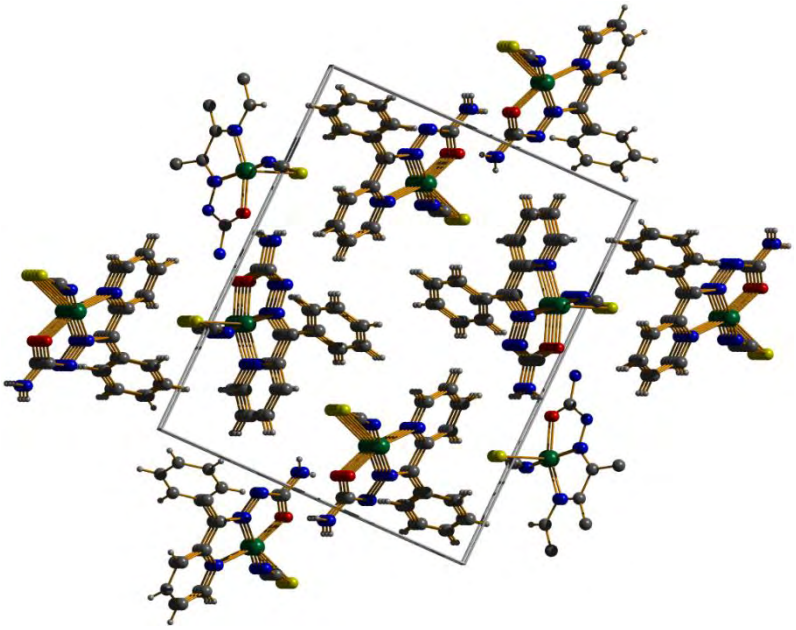

Fig. 2.9. Packing diagram of the complex $[Cu(bpsc)(NCS)]_n$ (**1**) along 'c' axis.

2.3.3. Crystal structure of complex [Cu(Hbpsc)(NCS)$_2$] (2)

The molecular structure of the mononuclear Cu(II) complex with the atom numbering scheme is shown in Fig. 2.10. The compound crystallizes in the triclinic space group $P\bar{1}$ and the coordination around the Cu(II) ion can be best described as a distorted square pyramidal (τ = 0.07). Metal atom is coordinated by azomethine nitrogen, oxygen atom, one pyridyl nitrogen from semicarbazone and two thiocyanate units. The oxygen atom of the semicarbazone ligand coordinates the metal atom in amido form, which is confirmed by the double bond nature of C13–O1 (1.245(3) Å) and single bond nature of N3–C13 (1.375(3) Å) bond lengths (Table 2.6) [35].

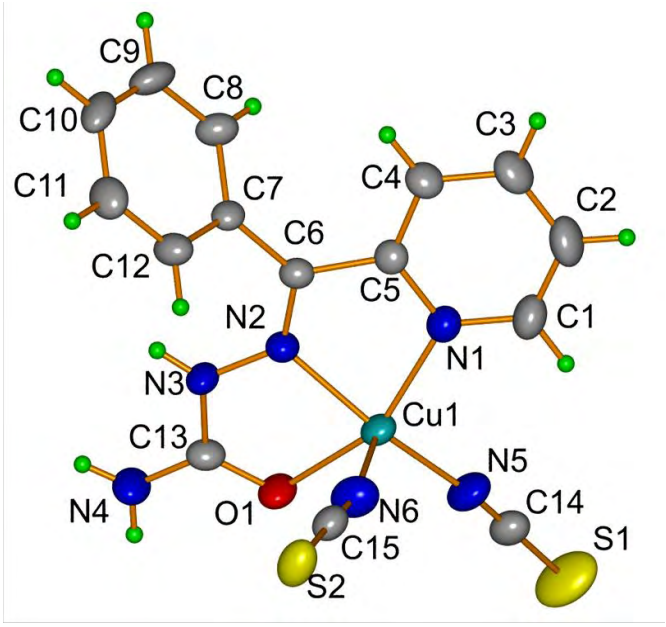

Fig. 2.10. Molecular structure and labelling diagram for [Cu(Hbpsc)(NCS)$_2$] (**2**).

Table 2.6. Selected bond lengths [Å] and angles [°] for [Cu(Hbpsc)(NCS)$_2$] (**2**)

Bond lengths (Å)	
Cu1–N2	1.9561(17)
Cu1–N1	2.0184(18)
Cu1–O1	2.0517(15)
C13–O1	1.245(3)
C13–N3	1.375(3)
N2–N3	1.353(2)
Bond angles (°)	
N2–Cu1–N1	79.15(7)
N1–Cu1–N5	101.45(8)
O1–Cu1–N6	93.57(8)
O1–Cu1–N2	78.08(6)
N6–Cu1–N5	107.51(9)

The zero dimensional monomeric units are building 1-D polymeric chains through intermolecular hydrogen bonding between N(4)–H(4A)···O(1)^{b} (b=-x,-y,-z) and hydrogen bonded ring motif $R_2^1(6)$ along 'a' direction (Fig. 2.11 and Table 2.7a).

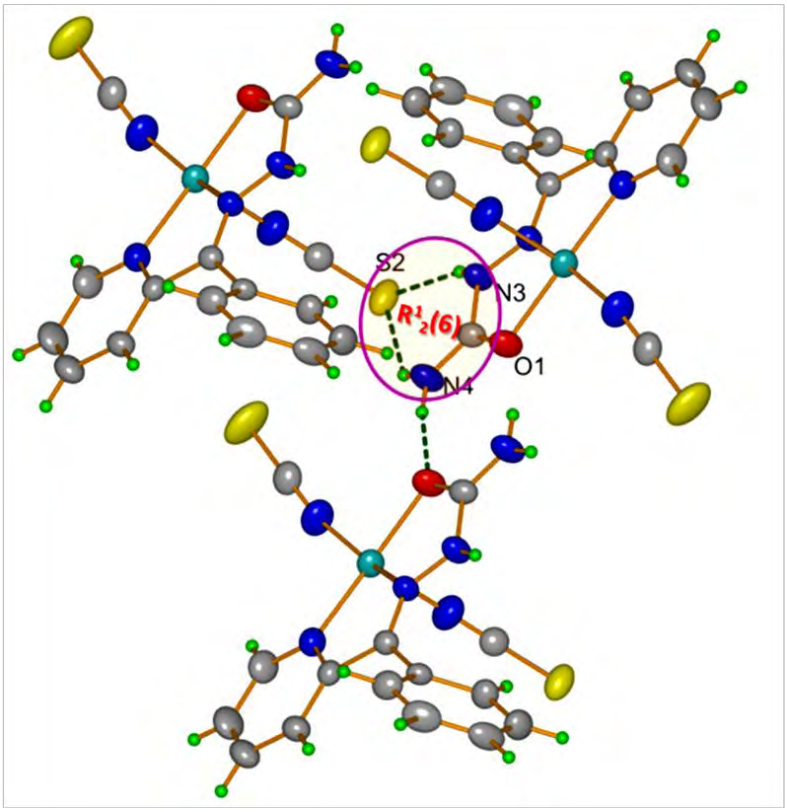

Fig. 2.11. Intermolecular hydrogen bonding in [Cu(Hbpsc)(NCS)$_2$] (**2**).

Table 2.7a. Hydrogen bonding interactions of [Cu(Hbpsc)(NCS)$_2$] (**2**).

D–H···A	D–H (Å)	H···A (Å)	D···A (Å)	∠D–H···A(°)
N(3)–H(3')···S(2)^{a}	0.82(3)	2.50(2)	3.2784(19)	158(2)
N(4)–H(4A)···O(1)^{b}	0.842(19)	2.18(2)	2.992(2)	162(2)
N(4)–H(4B)···S(2)^{a}	0.83(3)	2.76(4)	3.453(2)	142(2)

Equivalent position codes: a = -x,1-y,-z; b = -x,-y,-z.

C–H···π interactions are also present in this complex (Fig. 2.12 and Table 2.7b).

Table 2.7b. C–H···π interactions of [Cu(Hbpsc)(NCS)$_2$] (**2**)

X–H(I)···Cg(J)	H···Cg (Å)	X···Cg (Å)	∠X–H···Cg (°)
C(3)–H(3)···Cg(7)^{d}	2.7639	3.545(3)	142.12

Equivalent position codes : d = 1-x,2-y,1-z; Cg (7) = C(7), C(8), C(9), C(10), C(11), C(12); Cg : centroid

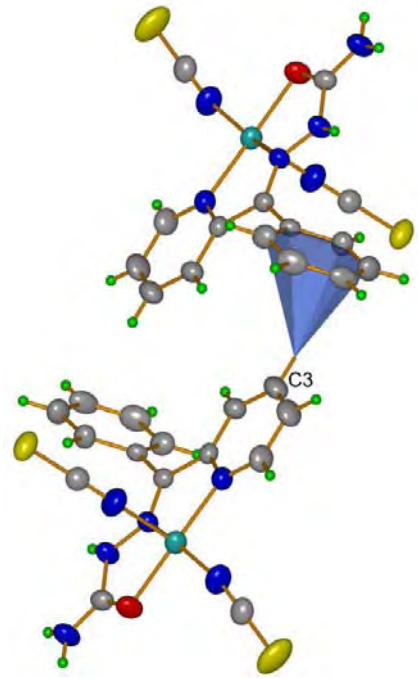

Fig. 2.12. Structure showing C–H···π interactions.

Weak π···π interactions are also present in the molecule and it increases the rigidity of the molecule (Fig. 2.13 and Table 2.7c).

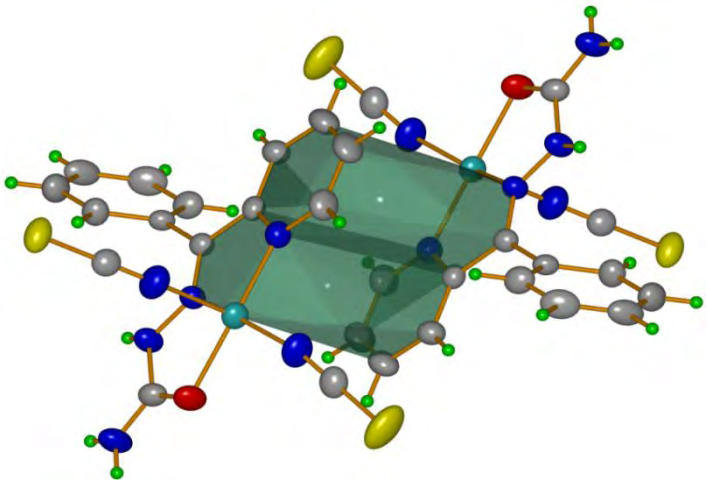

Fig. 2.13. Molecular structure showing π···π interactions.

Table 2.7c. π···π interactions of $[Cu(Hbpsc)(NCS)_2]$ (**2**)

Cg(I)···Cg(J)	Cg···Cg (Å)	α (°)	β (°)	γ(°)
Cg(4)···Cg(6)^{c}	3.8076(13)	0.59	24.39	24.84

Equivalent position codes: c = 1-x,1-y,1-z; Cg (4) = Cu(1), N(1), C(5), C(6), N(2); Cg (6) = N(1), C(1), C(2), C(3), C(4), C(5)

α : dihedral angles between planes I and J ; β : angle between Cg-Cg and Cg(J)_perp ; γ : angle between Cg-Cg and Cg(I)_perp.

The hydrogen bonded 1-D ribbon is packed parallel to each other *via* face to face $\pi\cdots\pi$ interactions between pyridine ring Cg(6) and chelate ring Cg(4) along bc plane (Fig. 2.14).

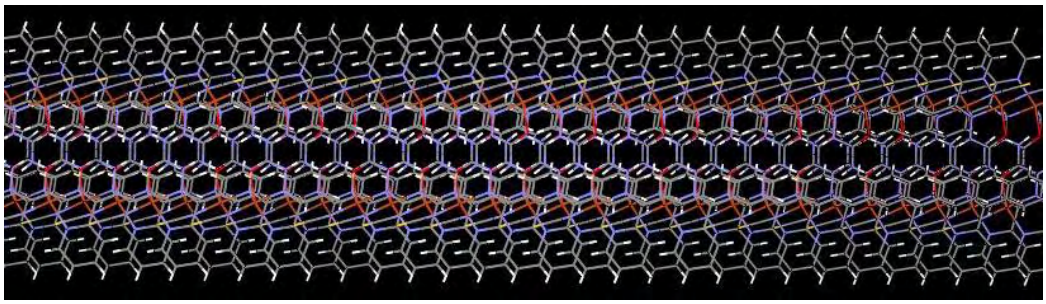

Fig. 2.14. The hydrogen bonded 1D ribbon [Cu(Hbpsc)$(NCS)_2$] (**2**).

The packing of the molecule in the crystal lattice (Fig. 2.15) is under the combined effect of hydrogen bonding, $\pi\cdots\pi$ and C–H$\cdots\pi$ interactions.

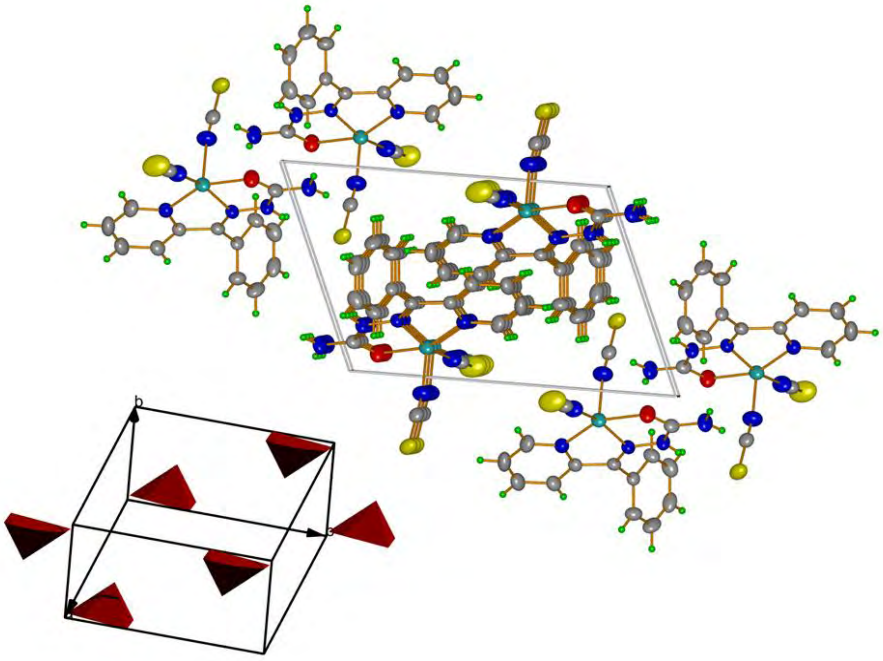

Fig 2.15. Packing diagram along 'b' axis.

2.3.4. Crystal structure of complex [Cu(Hbpsc)μ^2(S)NCS]$_2$·S (3)

Single crystal X-ray diffraction studies of compound show that it exists as a μ^2–S–bridged dimer. The centrosymmetric nature of the molecule is revealed by a C_2 axis perpendicular to the Cu(II) μ^2–S–Cu(II) plane. The lattice nature is monoclinic with space group *C*2/c. The semicarbazone ligand coordinates in a tridentate manner with the metal atom using its azomethine nitrogen, amido oxygen and pyridyl nitrogen resulting in two five membered chelate rings. The compound exhibits a distorted

square pyramidal geometry with the basal plane occupied by the semicarbazone ligand and thiocyanate nitrogen atom plunges into the axial position resulting in a dimer with a Cu–S–Cu separation of 5.264 Å approximately (Fig. 2.16).

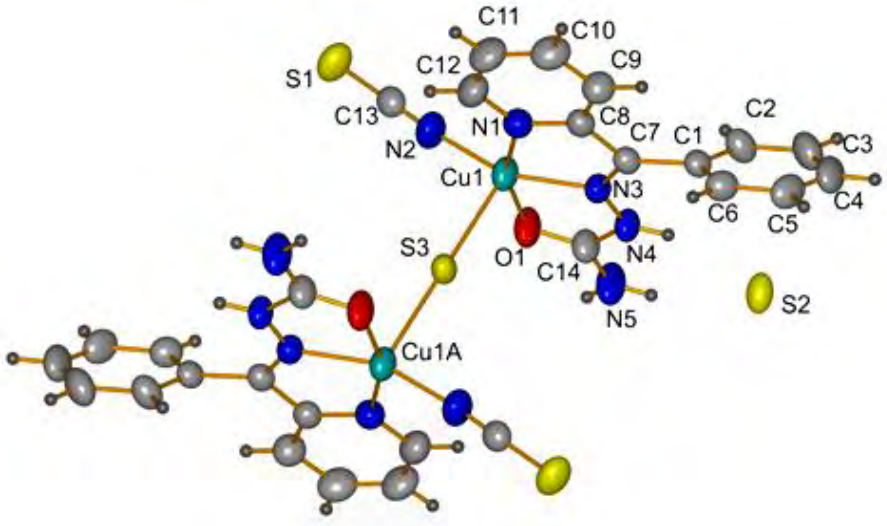

Fig. 2.16. Molecular structure of $[Cu(Hbpsc)\mu^2(S)NCS]_2 \cdot S$ (**3**).

The elemental sulfur atom present in the crystal lattice makes a 1D hydrogen bonded polymeric chain along the crystallographic 'b' axis (Fig. 2.17). Hydrogen bonding interactions are shown in Table 2.8.

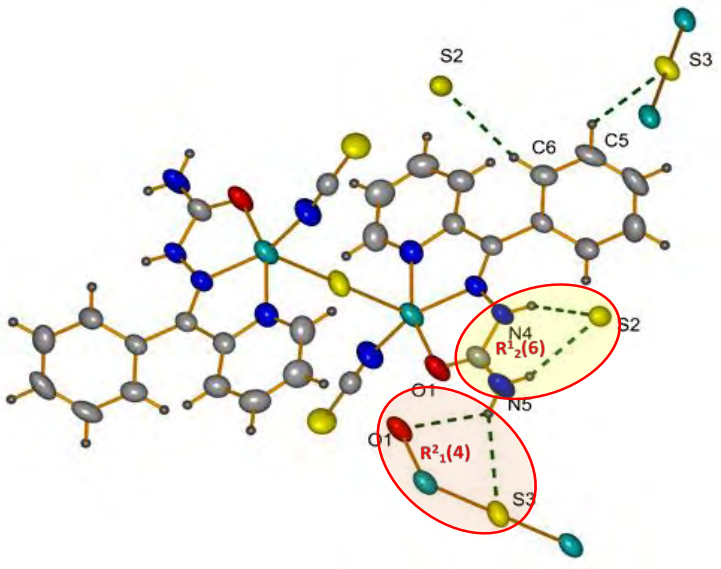

Fig. 2.17. Intermolecular hydrogen bonding network of $[Cu(Hbpsc)\mu^2(S)NCS]_2 \cdot S$ (**3**).

Table 2.8. Hydrogen bonding network of $[Cu(Hbpsc)\mu^2(S)NCS]_2 \cdot S$ (**3**)

D—H···A	D—H (Å)	H···A (Å)	D···A (Å)	∠D—H···A(°)
N(5)—H(3A)···S(2)[a]	0.8606	2.8056	3.589(3)	152.19
N(5)—H(3A)···O(1)[b]	0.8606	2.5310	3.114(4)	125.84
N(5)—H(3B)···S(3)	0.8603	2.4746	3.258(3)	151.78
C(6)—H(6)···S(3)[c]	0.9301	2.7918	3.698(4)	164.98
C(5)—H(7)···S(2)[d]	0.9300	2.8258	3.543(4)	134.75

The packing of this molecule involves a hydrogen bonding network supported by C–H···π interactions throughout the entire lattice (Fig. 2.18 and Table 2.9).

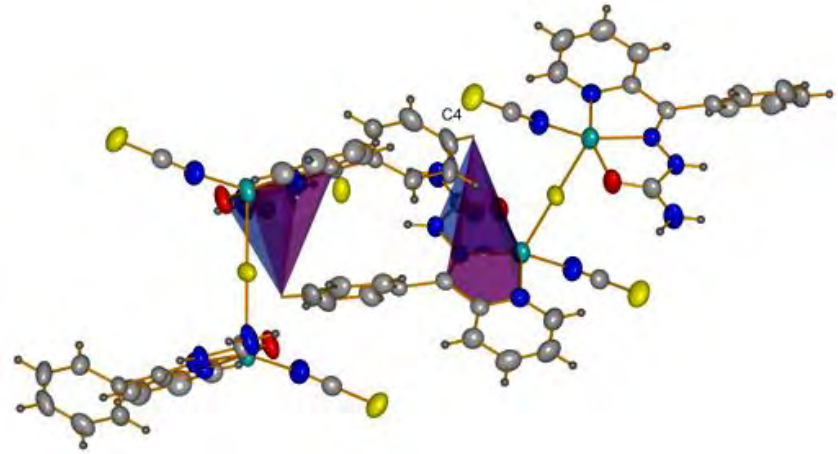

Fig. 2.18. Molecular structure of $[Cu(Hbpsc)\mu^2(S)NCS]_2 \cdot S$ (**3**) showing C—H···π interactions.

Table 2.9. C—H···π interactions of $[Cu(Hbpsc)\mu^2(S)NCS]_2 \cdot S$ (**3**)

X-H(I)···Cg(J)	H···Cg (Å)	X···Cg (Å)	∠X-H···Cg (°)
C(4)—H(4)···Cg(3)[d]	3.3649	3.612(4)	97.88

The arrangement of the molecules along 'b' axis is shown in Fig. 2.19.

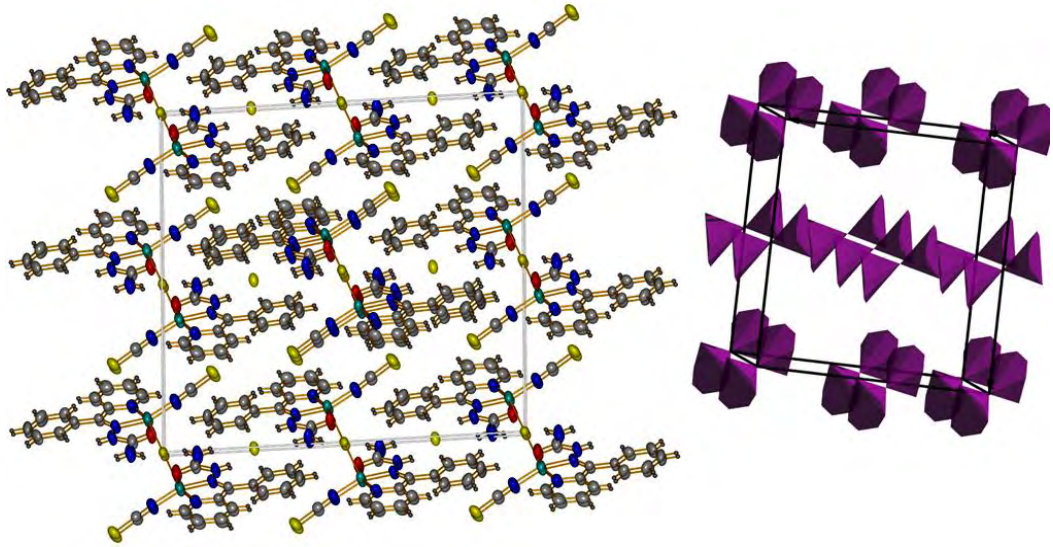

Fig. 2.19. The antiparallel arrangement of the coordination polyhedral in the consecutive chains in unit cell packing along the crystallographic 'b' axis.

2.3.5. Crystal structure of complex [Cu(bpap)(NCS)$_2$] (4)

The Cu(II) atom in this compound, is bonded to the N atoms of two thiocyanate ions, and is *N,N'* -chelated by the Schiff base ligand. The structural refinement parameters are given in Table 2.1b and the molecular structure of the complex is depicted in Fig. 2.20. The important bond lengths and bond angles are given in Table 2.10. In the present copper dithiocyanate adduct, the geometry is also a square pyramid but the apical O atom lies at 2.676 (4) Å whereas the geometry of the copper dichloride analog is an almost undistorted square pyramid [36]. The four N atoms surround the metal atom to form a distorted square; the square environment is distorted towards a square pyramid by a long Cu···O interaction. In the crystal, two C atoms of the pyrrolidin-2-one ring are disordered over two positions in a 1:1 ratio.

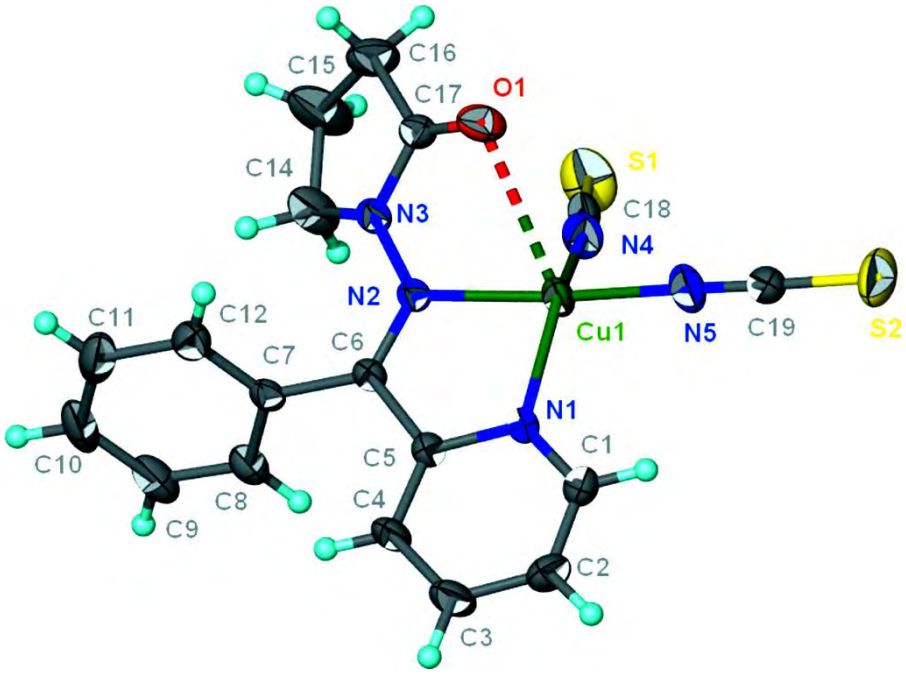

Fig. 2.20. Thermal ellipsoid plot of [Cu(bpap)(NCS)$_2$] (**4**) at the 50% probability level; hydrogen atoms are drawn as spheres of arbitrary radius. The disorder in the pyrrolidine ring is not shown.

Table 2.10. Selected bond lengths [Å] and angles [°] for [Cu(bpap)$(NCS)_2$] (**4**)

Bond lengths (Å)	
Cu1–N2	2.000 (3)
Cu1–N1	1.998 (4)
Cu1–O1	2.676 (4)
Cu1–N4	1.957 (4)
Cu1–N5	1.912 (4)
Bond angles (°)	
N5–Cu1–N4	98.09 (19)
N4–Cu1–N2	92.65 (16)
O1–Cu1–N4	77.12 (16)
O1–Cu1–N2	67.36 (13)
N1–Cu1–N5	98.49 (17)
N1–Cu1–N2	79.61 (14)

The crystal structure is devoid of any strong classical hydrogen bonds and other molecular interactions. The packing diagram of the compound viewed along the 'a' and 'b' axes are shown in Figs. 2.21 and 2.22 respectively. In the crystal, the molecules are arranged in a zig-zag manner.

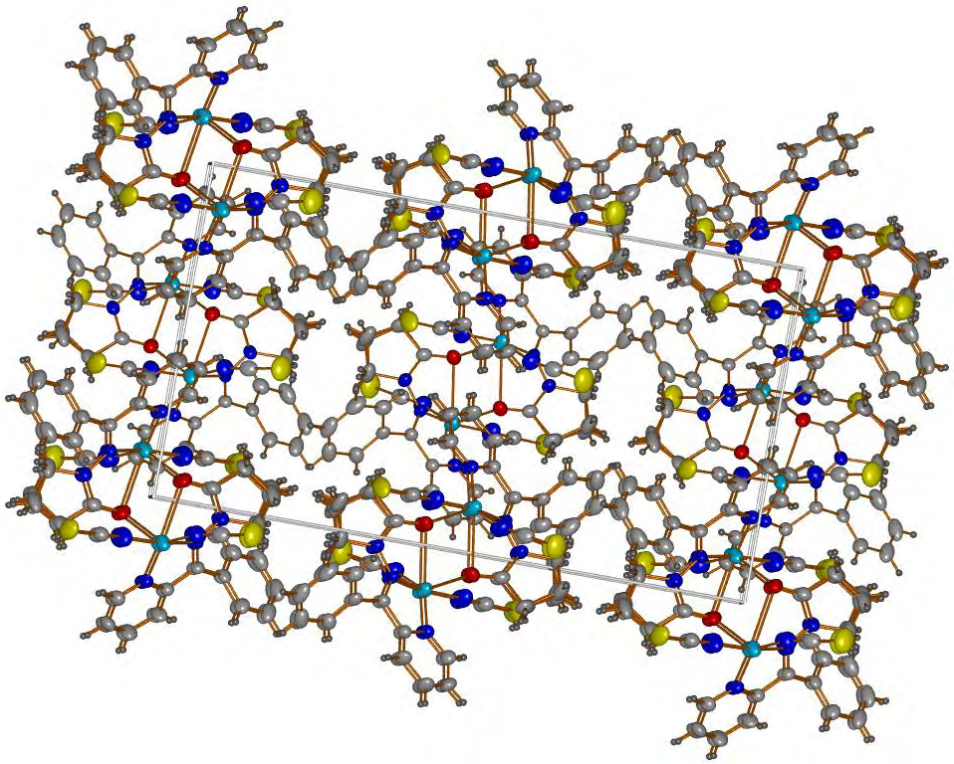

Fig. 2.21. Packing diagram of [Cu(bpap)$(NCS)_2$] (**4**) along 'a' axis.

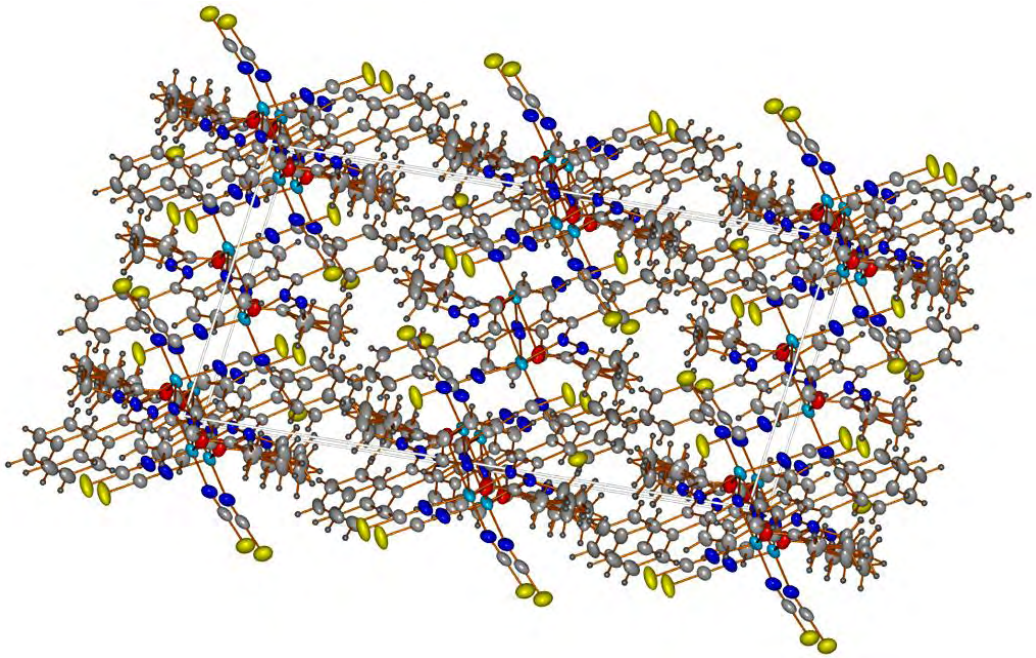

Fig. 2.22. Packing diagram of [Cu(bpap)$(NCS)_2$] (**4**) along 'b' axis.

2.3.6. Crystal structure of complex [Cu(dbsde)(NCS)] (5)

The complex is mononuclear and crystallographically characterized in the monoclinic space group $P2_1/c$ with four molecules present in the unit cell. The molecular structure is shown in Fig. 2.23. The copper ion occupies the central position of a distorted square planar arrangement. Out of its four coordination sites, three positions are occupied by the tridentate Schiff base through two nitrogen (amino and imino) atoms while the other one is occupied by deprotonated phenolate oxygen atom. The remaining (fourth) coordination is satisfied by an isothiocyanato ion.

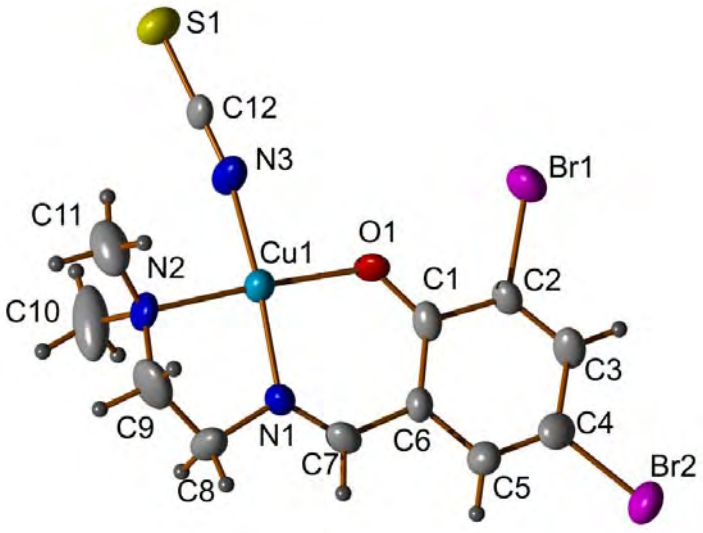

Fig. 2.23. The molecular structure of [Cu(dbsde)(NCS)] (**5**).

The Cu–N bond lengths are found to be Cu1–N1 = 1.940(14); Cu1–N2 = 2.070(14); Cu1–N3 = 1.947(16) Å while the Cu1–O1 bond length is 1.948(12) Å. The bond lengths and angles are gathered in Table 2.11. The distortion from the regular square planar structure is evident from the divergence of the bond angles around Cu(II) from 90º. Bond angle of N1–Cu1–N2 is less than 90º while the bond angles of O1–Cu1–N1, N3–Cu1–O1 and N3–Cu1–N2 are greater than 90º. The distortion may be due to the rigidity of the chelate rings formed [37]. All the bond lengths and bond angles are in good agreement with those reported in the mononuclear copper(II) complexes of Schiff bases [38].

Table 2.11. Selected bond lengths [Å] and angles [°] for [Cu(dbsde)(NCS)] (**5**)

Bond lengths (Å)	
Cu1–N2	2.070(14)
Cu1–N1	1.940(14)
Cu1–O1	1.948(12)
Cu1–N3	1.947(16)
Bond angles (°)	
N1–Cu1–O1	92.0(5)
N3–Cu1–O1	91.6(6)
N1–Cu1–N2	84.0(6)
N3–Cu1–N2	92.7(6)

The crystal is stabilized by hydrogen bonds (Fig. 2.24 and Table 2.12).

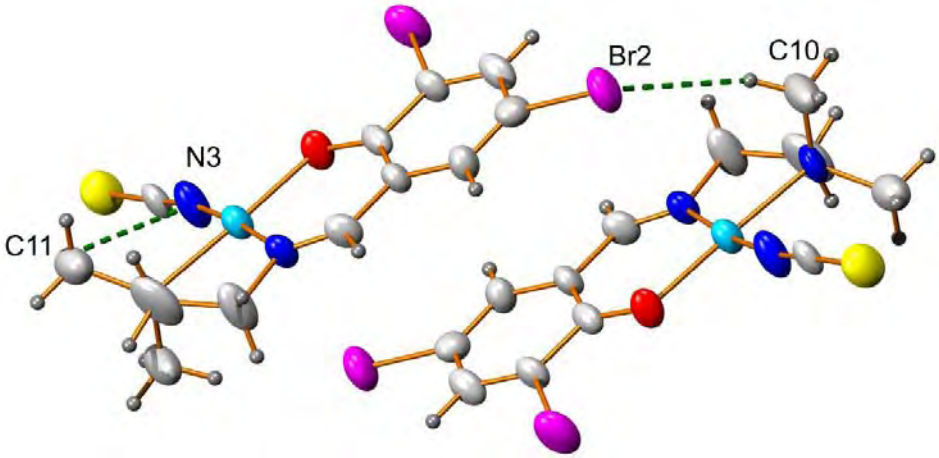

Fig. 2.24. Hydrogen bonding interactions for [Cu(dbsde)(NCS)] (**5**).

Table 2.12. Hydrogen bonding interactions for [Cu(dbsde)(NCS)] (**5**)

D–H···A	D–H (Å)	H···A (Å)	D···A (Å)	∠D–H···A(°)
C(10)–H(10A)···Br(2)^{a}	0.9574	2.7783	3.65(3)	151.65
C(11)–H(11A)···N(3)	0.9619	2.6299	3.13(3)	112.94

Equivalent position codes: a = -x,-y,-z.

The crystal structure is further stabilized by significant π···π interaction (Fig. 2.25 and Table 2.13).

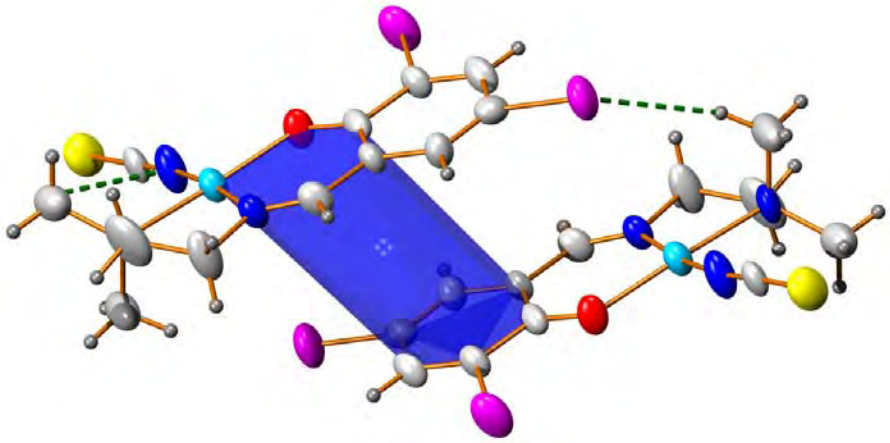

Fig. 2.25. π···π interaction for [Cu(dbsde)(NCS)] (**5**).

Table 2.13. The π···π interactions for [Cu(dbsde)(NCS)] (**5**)

Cg(I)···Cg(J)	Cg···Cg (Å)	α (°)	β (°)	γ(°)
Cg(2)···Cg(3)[b]	3.690(9)	2.89	20.05	18.23

Equivalent position codes: b = 1-x,-y,-z. Cg (2) = Cu(1, O(1), C(1), C(6), C(7), N(1); Cg (3) = C(1), C(2), C(3), C(4), C(5), C(6).

The packing of the molecule in the crystal lattice (Figs. 2.26 and 2.27) is under the combined effect of hydrogen bonding and π···π interactions.

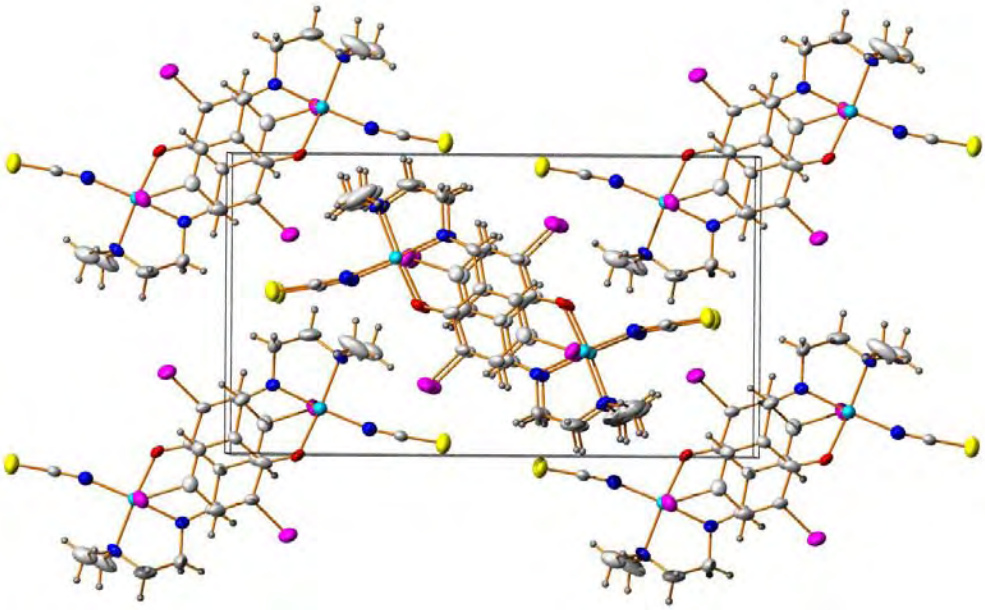

Fig. 2.26. The packing diagram of the molecule along 'a' axis.

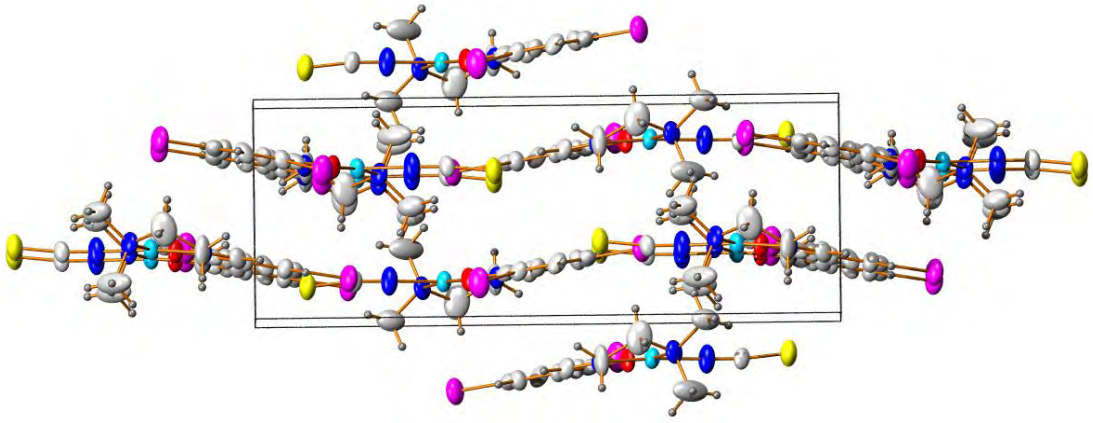

Fig. 2.27. The packing diagram of the molecule along 'c' axis.

2.3.7. Crystal structure of complex $[Cu(msc)_2(NCS)_2]$ (6)

Single crystal X-ray diffraction analysis reveals that this mononuclear complex has space group $P2_1/n$ and crystallizes in a monoclinic system. The molecular structure of the molecule is shown in Fig. 2.28. Coordination around copper is octahedral with CuN_4O_2 skeleton having slight distortion in all directions accommodating the oxygen atoms of both ligands in *cis* configuration and the two thiocyanate anions coordinating *via* N atom in *cis* configuration with respect to each other. A summary of the key crystallographic information is given in Table 2.1b. Selected bond lengths and bond angles are listed in Table 2.14.

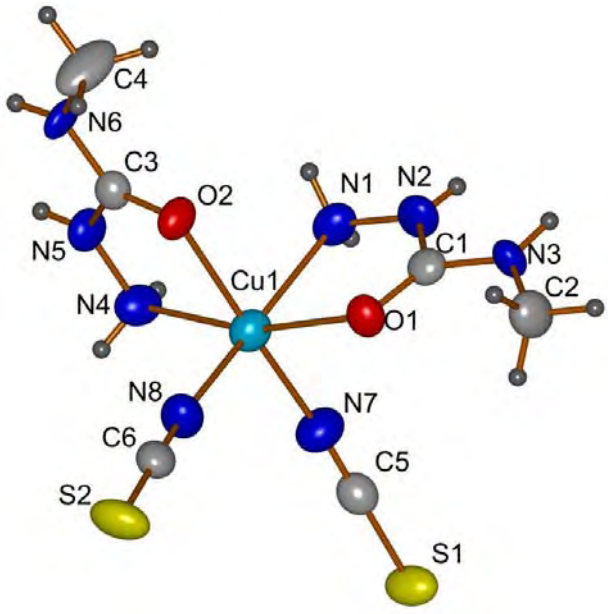

Fig. 2.28. Molecular structure of $[Cu(msc)_2(NCS)_2]$ (**6**).

Table 2.14. Selected bond lengths [Å] and angles [°] for $[Cu(msc)_2(NCS)_2]$ (**6**)

Bond lengths (Å)	
Cu1–N4	2.163(3)
Cu1–N1	2.176(3)
Cu1–O1	2.170(3)
Cu1–O2	2.164(3)
Cu1–N8	2.039(4)
Cu1–N7	2.049(4)
Bond angles (°)	
O2–Cu1–N4	76.59(11)
N4–Cu1–N8	97.71(15)
N8–Cu1–N7	96.92(16
O1–Cu1–N7	90.37(13)
N1–Cu1–O1	76.09(11)
N1–Cu1–O2	85.30(12)

The molecule is centrosymmetric and the structure consists of a neutral monomer in which the copper(II) ion is octahedrally coordinated by two semicarbazide ligands (through N1, N4, O1 and O2) and two terminal NCS^- ligands (through N7 and N8). The thiocyanate groups are coordinated to the Cu(II) ion through the nitrogen atoms [39].

In this compound packing is determined by the N–H···O and N–H···S hydrogen bonds which join the molecules together to form a two dimensional network (Table 2.15). A molecule in this system involves hydrogen bonding with two other molecules as shown in Fig. 2.29. The semicarbazide unit is planar and there are no significant differences in the bond distances between metal coordinated semicarbazide and N-methylsemicarbazide [40].

Table 2.15. Hydrogen bonding interactions of the compound $[Cu(msc)_2(NCS)_2]$ (**6**)

D–H···A	D–H (Å)	H···A (Å)	D···A (Å)	∠D–H···A (°)
N(1)–H(1A)···S(2)^a	0.85(3)	2.52(3)	3.368(4)	172(3)
N(1)–H(1B)···S(1)^b	0.86(4)	2.56(4)	3.372(3)	158(4)
N(2)–H(2)···S(1)^c	0.81(4)	2.57(4)	3.378(4)	170(4)
N(4)–H(4A)···O(2)^a	0.84(4)	2.35(3)	3.121(4)	153(5)
N(4)–H(4B)···S(2)^d	0.84(4)	2.65(4)	3.389(4)	149(4)
N(5)–H(5)···O(1)^a	0.83(3)	2.12(3)	2.876(4)	152(3)

Equivalent position codes: a = 1/2-x,1/2+y,1/2-z; b = -x,2-y,-z; c = 1+x,y,z; d = -1/2-x,1/2+y,1/2-z.

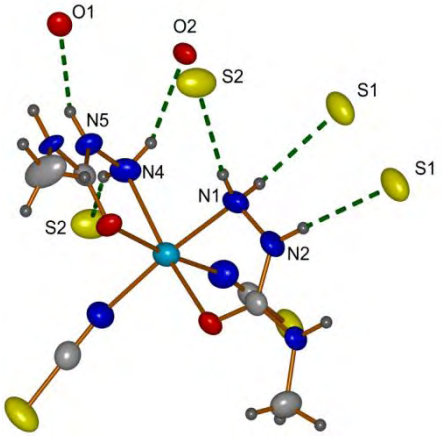

Fig. 2.29. Hydrogen bonding interactions of the compound $[Cu(msc)_2(NCS)_2]$ (**6**).

The packing of the molecules in the crystal lattice (Figs. 2.30 and 2.31) is in a head to tail manner.

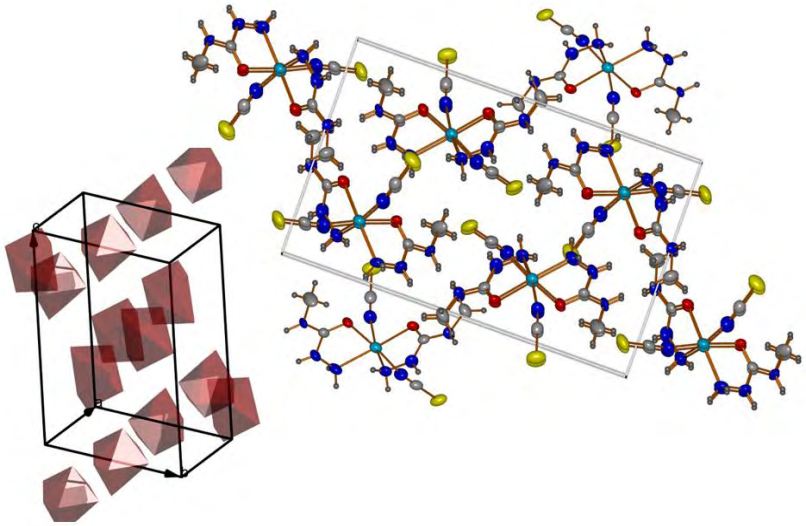

Fig. 2.30. Packing diagram of the compound $[Cu(msc)_2(NCS)_2]$ (**6**) along 'a' axis.

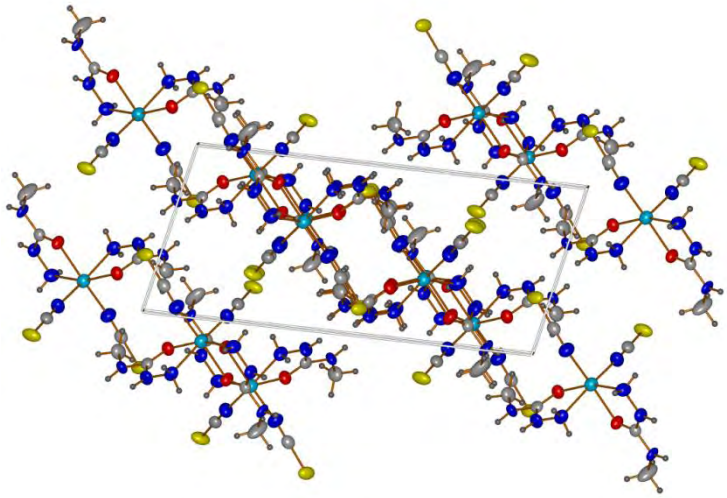

Fig. 2.31. Packing diagram of the compound $[Cu(msc)_2(NCS)_2]$ (**6**) along 'b' axis.

2.3.8. Infrared spectral studies

The tentative assignments for the IR spectral bands are most useful for determining the ligand's mode of coordination and it is listed in Table 2.16.

Table 2.16. IR spectral data of the Cu(II) thiocyanato complexes (cm^{-1})

Compounds	ν_a(NCS)	ν_s(NCS)	δ(NCS)	ν(C=N)	ν(C=O)	ν(N–N)
$[Cu(bpsc)(NCS)]_n$ **(1)**	2093	1411	632	1550	1622	1126
$[Cu(Hbpsc)(NCS)_2]$ **(2)**	2078	1333	604	1503	1662	1149
$[Cu(Hbpsc)\mu^2(S)NCS]_2 \cdot S$ **(3)**	2107	1333	614	1501	1663	1149
$[Cu(bpap)(NCS)_2]$ **(4)**	2089	1397	698	1594	-	-
[Cu(dbsde)(NCS)] **(5)**	2084	1316	703	1577	-	-
$[Cu(msc)_2(NCS)_2]$ **(6)**	2109	1315	615	-	-	-

A sharp band around 1600 cm^{-1} can be attributed to the characteristic >C=N group stretching frequency of semicarbazone/Schiff base ligand. This band shifts slightly (4-12 cm^{-1}) towards lower frequencies in the copper(II) complexes [41,42] indicating the coordination of azomethine nitrogen to copper. The increase in ν(N–N) values in the spectra of these complexes is due to the increase in double bond character, off-setting the loss of electron density *via* donation to the metal and is a confirmation of the coordination of the ligand through the azomethine nitrogen. The appearance of bands in the 1543-1579 cm^{-1} region in some complexes is due to asymmetric stretching vibration of the newly formed C=N bond as a result of enolization of the ligand. Disappearance of intense bands of C═O stretching vibrations of complex of semicarbazone in $[Cu(bpsc)(NCS)]_n$ (**1**) indicate the enolization of the semicarbazone during complexation. Appearance of new sharp intense bands at 2107, 2017, 2078, 2089, 2084 and 2109 cm^{-1} are due to the presence of NCS group in the complexes $[Cu(Hbpsc)(NCS)]_n$ (**1**), $[Cu(Hbpsc)(NCS)_2]$ (**2**), $[Cu(Hbpsc)\mu^2(S)NCS]_2 \cdot S$ (**3**), $[Cu(bpap)(NCS)_2]$ (**4**), [Cu(dbsde)(NCS)] (**5**) and $[Cu(msc)_2(NCS)_2]$ (**6**) respectively as shown in Figs. 2.32-2.37. The crystal structure of the complexes confirms the presence of thiocyanate and explains its mode of coordination.

The SCN group may coordinate to a metal through the nitrogen or sulfur or both sulfur and nitrogen. The CN stretching frequencies are generally lower in N-bonded complexes (near and below 2050 cm^{-1}) than in S-bonded complexes (near 2100 cm^{-1}) [43]

and the bridging [M–NCS–M′] complexes exhibits ν(CN) well above 2100 cm^{-1}. But deviations from this rule is frequently observed since ν(CN) bands are affected by many other factors as well [44]. The ν(CS) band for S-bonded complexes are found in the 720-690 cm^{-1} region [45,46]. The N-bonded complexes exhibit a single sharp δ(NCS) near 480 cm^{-1}, where as the S-bonded complexes show several weak bands near 421 cm^{-1} [47]. However these frequencies are very much sensitive to the overall structure of the complex, the nature of the central metal, nature of other ligands in the complex and steric consideration [48].

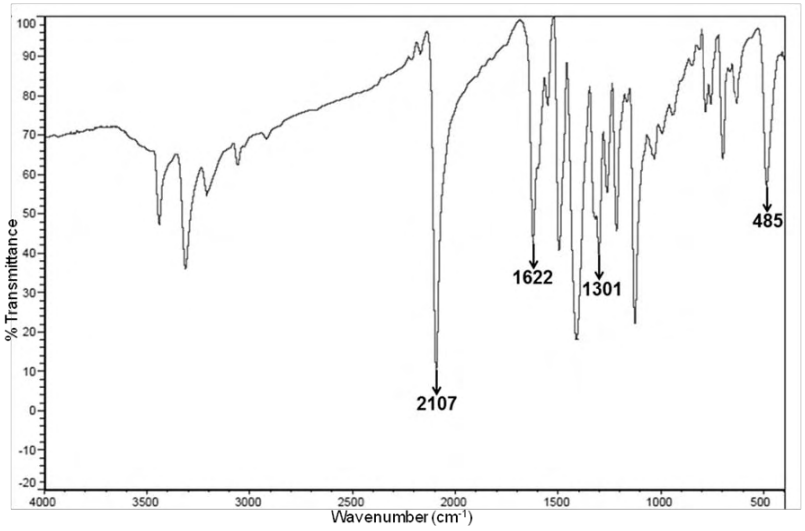

Fig. 2.32. IR spectrum of $[Cu(Hbpsc)(NCS)]_n$ (**1**).

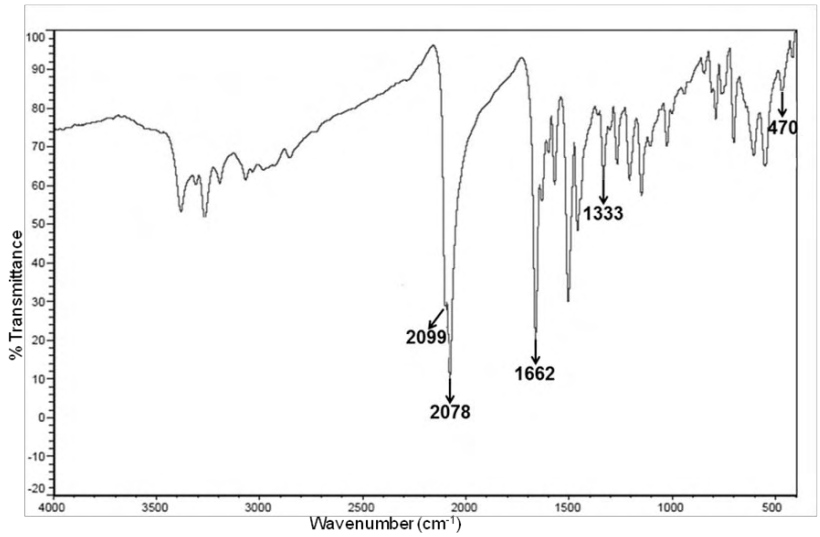

Fig. 2.33. IR spectrum of $[Cu(Hbpsc)(NCS)_2]$ (**2**).

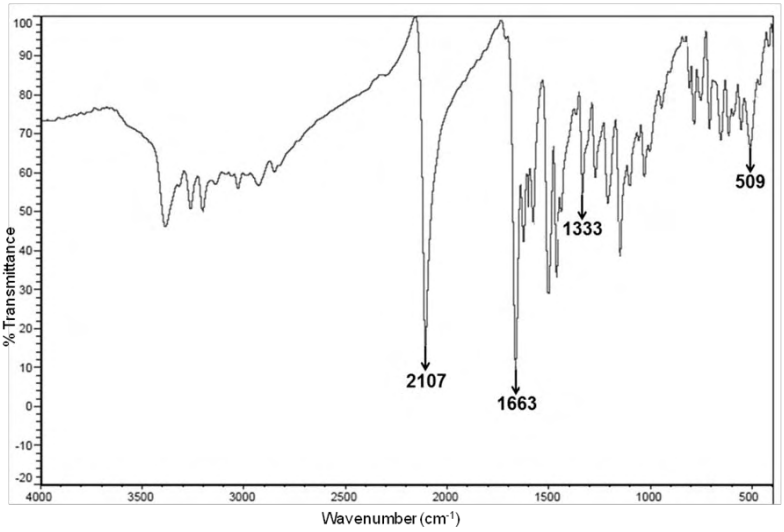

Fig. 2.34. IR spectrum of $[Cu(Hbpsc)\mu^2(S)NCS]_2 \cdot S$ (**3**).

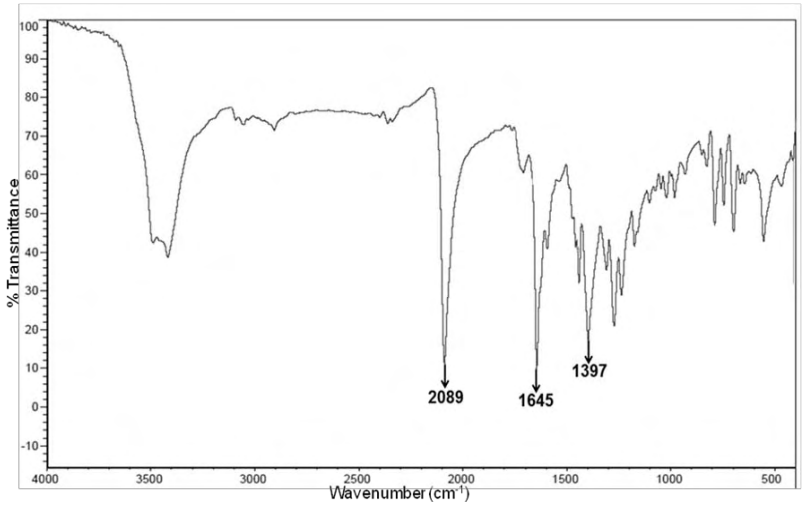

Fig. 2.35. IR spectrum of $[Cu(bpap)(NCS)_2]$ (**4**).

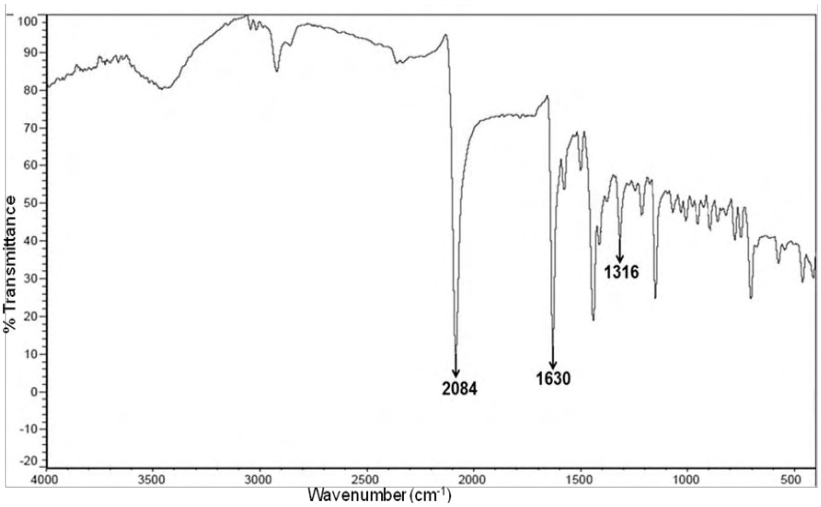

Fig. 2.36. IR spectrum of [Cu(dbsde)(NCS)] (**5**).

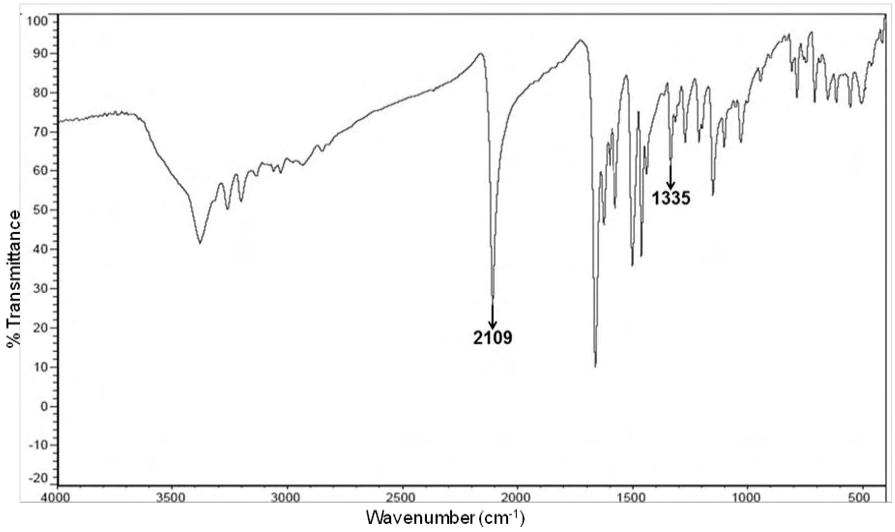

Fig. 2.37. IR spectrum of $[Cu(msc)_2(NCS)_2]$ (**6**).

2.3.9. Electronic spectral studies

The significant electronic absorption bands in the spectra of complexes recorded in methanol are presented in Table 2.16.

The semicarbazone-copper(II) complexes have two bands; one centered around 37290-45360 cm^{-1} region and the other around 30150-33170 cm^{-1} region. These bands are due to $\pi\rightarrow\pi^*$ and $n\rightarrow\pi^*$ transitions (Figs. 2.38-2.43) of phenyl rings and semicarbazide moiety [49]. The charge transfer bands were observed in the 24660-26150 cm^{-1} region and its broadness can be explained as due to the combination of O→Cu and N→Cu LMCT transitions [50].

Table 2.16. Electronic spectral assignments (cm^{-1}) of Cu(II) thiocyanato complexes

Compound	*d-d*	LMCT	$n\rightarrow\pi^*/\pi\rightarrow\pi^*$
$[Cu(bpsc)(NCS)]_n$ **(1)**	14750	26050	33850, 39560
$[Cu(Hbpsc)(NCS)_2]$ **(2)**	13250	26000	32950, 38150
$[Cu(Hbpsc)\mu^2(S)NCS]_2 \cdot S$ **(3)**	12100	26200	31860, 47700
$[Cu(bpap)(NCS)_2]$ **(4)**	13580	26730	38070, 47460
[Cu(dbsde)(NCS)] **(5)**	15150	25100	35650, 42800
$[Cu(msc)_2(NCS)_2]$ **(6)**	12970	25940	31550, 38200, 47600

All the complexes exhibit *d-d* bands around 12000-17500 cm^{-1}. For a square planar complex with $d_{x^2-y^2}$ ground state, three transitions are possible *viz*, $d_{x^2-y^2}\rightarrow d_{xy}$, $d_{x^2-y^2}\rightarrow d_{z^2}$ and $d_{x^2-y^2}\rightarrow d_{xz}$, d_{yz} ($^2B_{2g}\leftarrow {}^2B_{1g}$, $^2A_{1g}\leftarrow {}^2B_{1g}$, and $^2E_g\leftarrow {}^2B_{1g}$) and square pyramidal complexes have the transitions of $d_{x^2-y^2}\rightarrow d_{z^2}$, $d_{x^2-y^2}\rightarrow d_{xy}$ and $d_{x^2-y^2}\rightarrow d_{xz}$,

d_{yz} [51,52]. However, since the four *d* orbitals lie very close together, each transition cannot be expected to be distinguished by their energy in all complexes and hence it is very difficult to resolve the bands into separate components.

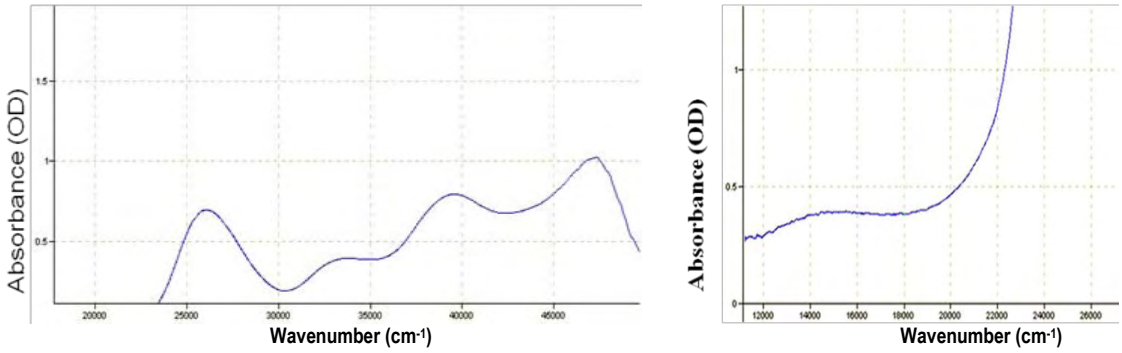

Fig. 2.38. Electronic spectra of complex $[Cu(Hbpsc)(NCS)]_n$ (**1**).

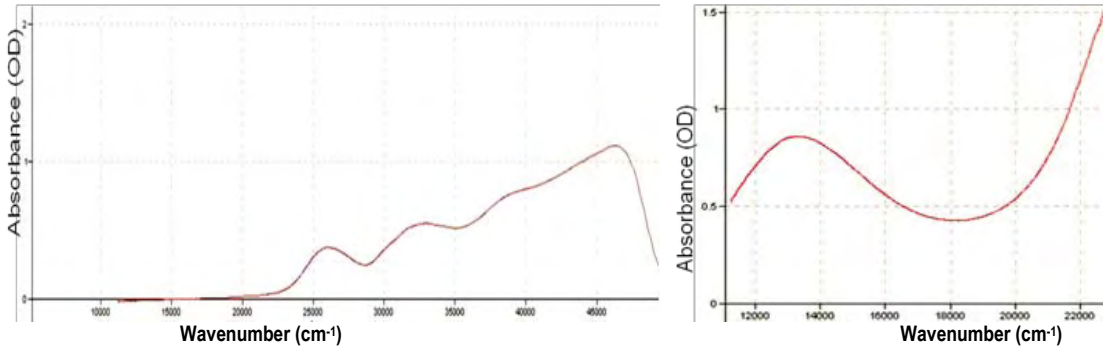

Fig. 2.39. Electronic spectra of complex $[Cu(Hbpsc)(NCS)_2]$ (**2**).

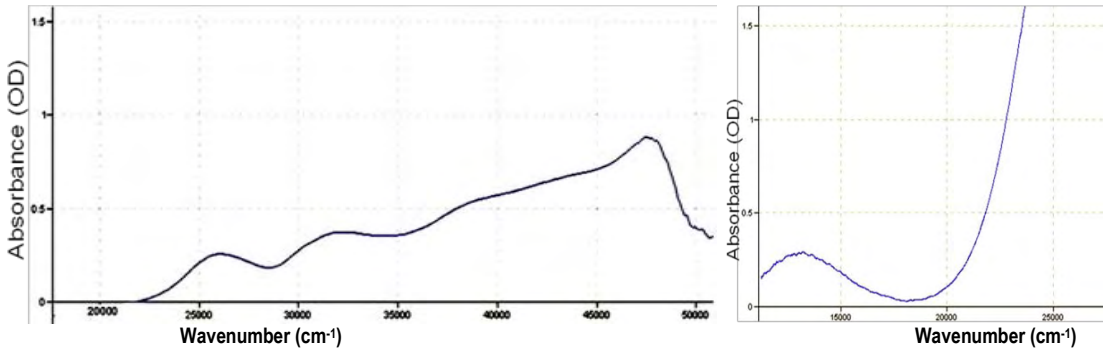

Fig. 2.40. Electronic spectra of complex $[Cu(Hbpsc)\mu^2(S)NCS]_2 \cdot S$ (**3**).

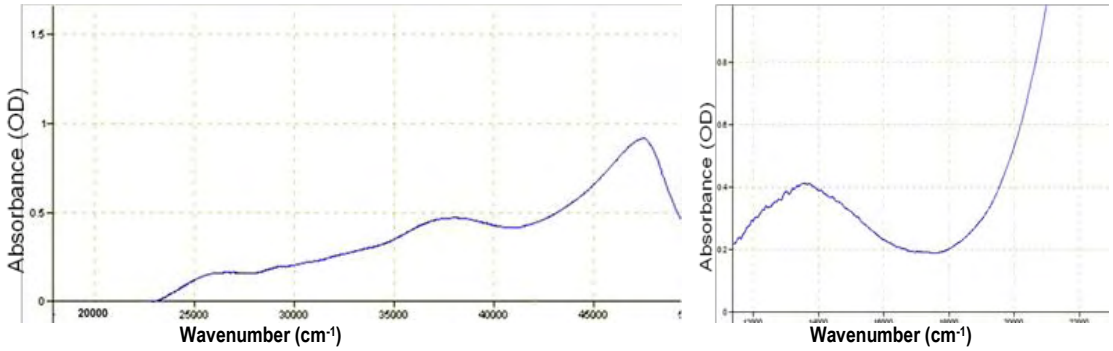

Fig. 2.41. Electronic spectra of complex $[Cu(bpap)(NCS)_2]$ (**4**).

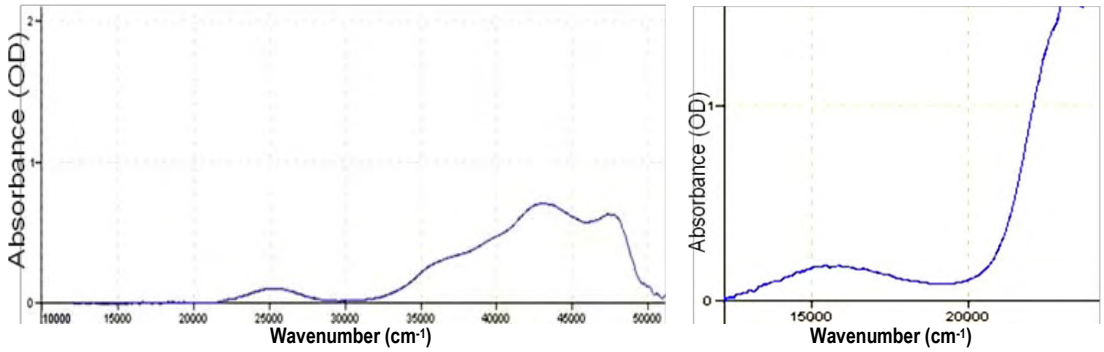

Fig. 2.42. Electronic spectra of complex [Cu(dbsde)(NCS)] (**5**).

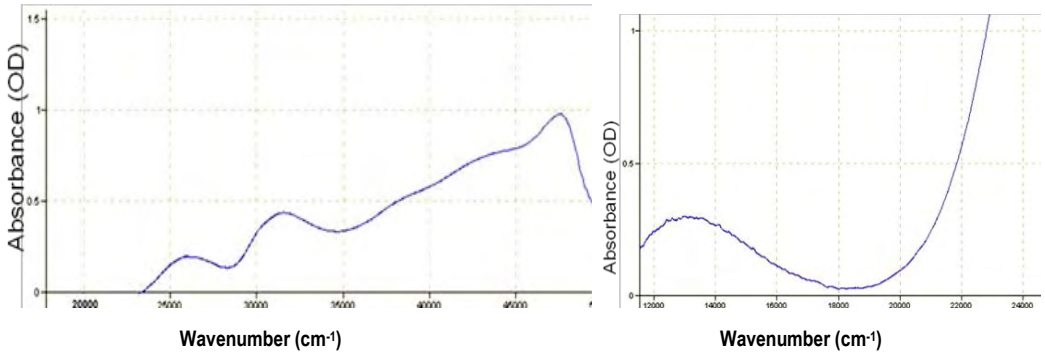

Fig. 2.43. Electronic spectra of complex $[Cu(msc)_2(NCS)_2]$ (**6**).

2.3.10. EPR spectral studies

The magnetic parameters measured in EPR study are related to the structure of the paramagnetic complex, the number of ligands, nature of bonding and spatial arrangements of the ligands around the central metal ion. The copper(II) ion, with a d^9 configuration, has an effective spin of $S = 1/2$ and is associated with a spin angular momentum, $m_s = \pm 1/2$, leading to a doubly degenerate spin state in the absence of a magnetic field. In a magnetic field the degeneracy is lifted between these states and

the energy difference between them is given by $\Delta E = h\nu = g\beta B$, where h is Planck's constant, ν is the microwave frequency for transition from $m_s = +½$ to $m_s = -½$, g is the Lande splitting factor (equal to 2.0023 for a free electron), β is the Bohr magneton and B is the magnetic field. For the case of a $3d^9$ copper(II) ion, the appropriate spin Hamiltonian assuming a B_{1g} ground state is given by:

$$\hat{H} = \beta[g_{\|}B_a S + g_{\perp}(B_x S_x + B_y S_y)] + A_{\|}I_z S_z + A_{\perp}(I_x S_x + I_y S_y)$$

The EPR spectra of the polycrystalline samples at 298 K, DMF solution at 298 and 77 K were recorded in the X-band, using 100-kHz modulaton; g factors were quoted relative to the standard marker TCNE (g = 2.00277). The EPR spectra of the complexes recorded in polycrystalline state at room temperature provide information about the coordination environment around copper(II) in these complexes.

The EPR parameters $g_{\|}$, $g_{\perp}$, $A_{\|}$(Cu) and the energies of *d-d* transitions were used to evaluate the bonding parameters α^2, β^2 and γ^2 which may be regarded as measures of the covalency in the in-plane σ-bonds, in-plane π-bonds and out-of-plane π-bonds. The value of in-plane σ-bonding parameter α^2 estimated from the expression,

$$\alpha^2 = -A_{\|} / 0.036 + (g_{\|} - 2.0023) + 3/7(g_{\perp} - 2.0023) + 0.04 \text{ [27]}.$$

The following simplified parameters were used to evaluate the bonding parameters [53],

$$K_{\|}^2 = (g_{\|} - 2.0023)\, E_{\text{d-d}} / 8\lambda_o$$

$$K_{\perp}^2 = (g_{\perp} - 2.0023)\, E_{\text{d-d}} / 2\lambda_o$$

Where $K_{\|}^2 = \alpha^2 \beta^2$ and $K_{\perp}^2 = \alpha^2 \gamma^2$, $K_{\|}$ and $K_{\perp}$ are orbital reduction factors and λ_o represents the one electron spin orbit coupling constant which equals -828 cm^{-1}.

The EPR parameters of the copper(II) complexes are presented in the Table 2.17.

Table 2.17. Spin Hamiltonian and bonding parameters of the complexes

	$[Cu(bpsc)(NCS)]_n$ **(1)**	$[Cu(Hbpsc)(NCS)_2]$ **(2)**	$[Cu(Hbpsc)\mu^2(S)NCS]_2 \cdot S$ **(3)**	$[Cu(bpap)(NCS)_2]$ **(4)**	[Cu(Hdbsde)(NCS)] **(5)**
	Polycrystalline state at 298 K				
$g_{\|\|}$	2.157	2.184	2.231	2.157	2.211
$g_\perp$	2.125	2.092	2.109	2.125	2.059
g_{isc}/g_{rv}	2.1357	2.123	2.150	2.124	2.110
G	1.261	2.026	2.142	3.807	3.677
	Solution state at 77 K				
$g_{\|\|}$	2.227	2.247	2.286	2.275	2.202
$g_\perp$	2.069	2.079	2.110	2.067	2.050
$A_{\|\|}$	20.5	19.33	17.33	24.8	0.0207
α^2	0.885	0.881	0.883	1.176	1.034
β^2	0.800	0.794	0.816	0.744	0.875
γ^2	0.871	0.889	1.005	0.543	0.639
$K_{\|\|}$	0.700	0.700	0.720	0.875	0.905
$K_\perp$	0.783	0.783	0.887	0.639	0.661

All these compounds, (Fig. 2.44-2.48) in polycrystalline state at 298 K showed axial spectra with well defined $g_{||}$ and $g_\perp$ features. The variation in the $g_{||}$ and $g_\perp$ values indicates that the geometry of the compounds in the solid state is affected by the nature of coordinating ligands. The geometric parameter G which is a measure of the exchange interaction between copper centers in the polycrystalline compound is calculated using the equation, $G = (g_{||}-2.0023)/ g_\perp-2.0023)$. If the G value is greater than 4, exchange interaction is negligible [54,55]

As $g_{||} > g_\perp$, a square pyramidal geometry can be assigned and rules out the possibility of a trigonal bipyramidal structure which would be expected to have $g_\perp > g_{||}$. The α^2, β^2 and γ^2 values of these complex are less than one indicate that complexes have strong in-plane π-bonding.

Hathaway [56] has pointed out that, for pure σ bonding, $K_{||} \approx K_\perp \approx 0.77$, and for in-plane π bonding, $K_{||} < K_\perp$, while for out-of-plane π bonding $K_\perp < K_{||}$. Here in compounds **1, 2** and **3** it is observed that $K_{||} < K_\perp$, *i.e.*, in-plane π bonding is significant. In complex **5**, $K_\perp < K_{||}$ indicates the presence of out-of-plane π bonding.

The metal-ligand bond is purely ionic, if the value of α^2 is unity and it is completely covalent, if α^2= 0.5 [57]. In frozen DMF at 77 K, we got an axial spectrum with hyperfine splitting into four lines in the parallel region of all the copper thiocyanato complexes **1-5.** The hyperfine splitting is due to the interaction of the electron spin with the copper nuclear spin (I = 3/2). The $g_{\|} > g_{\perp}$, suggests a distorted square pyramidal geometry for the complexes **1-5** which was already proved by the single crystal XRD results.

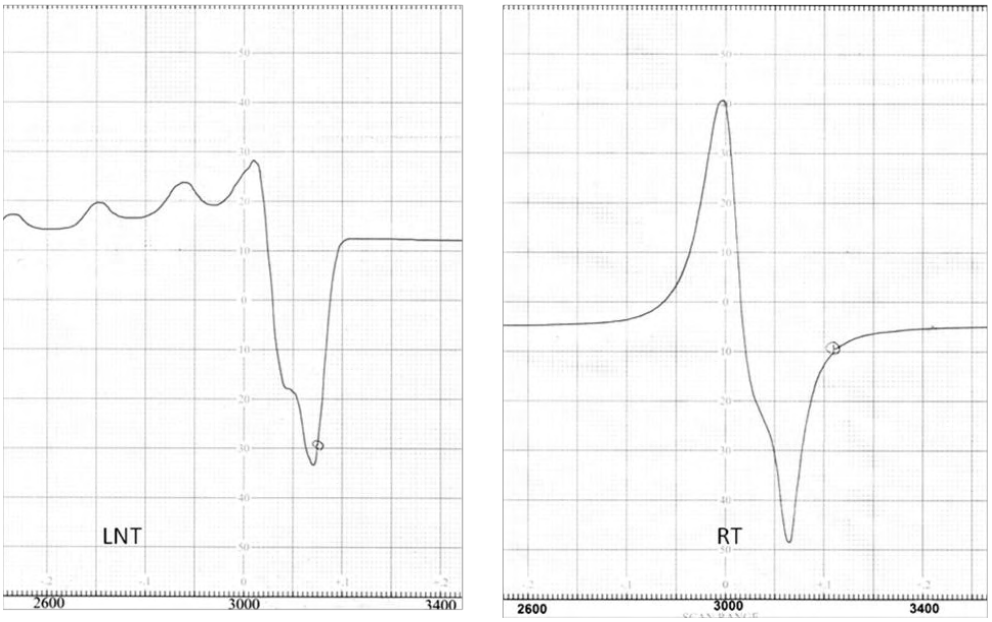

Fig. 2.44. EPR spectra of complex $[Cu(Hbpsc)(NCS)]_n$ (**1**).

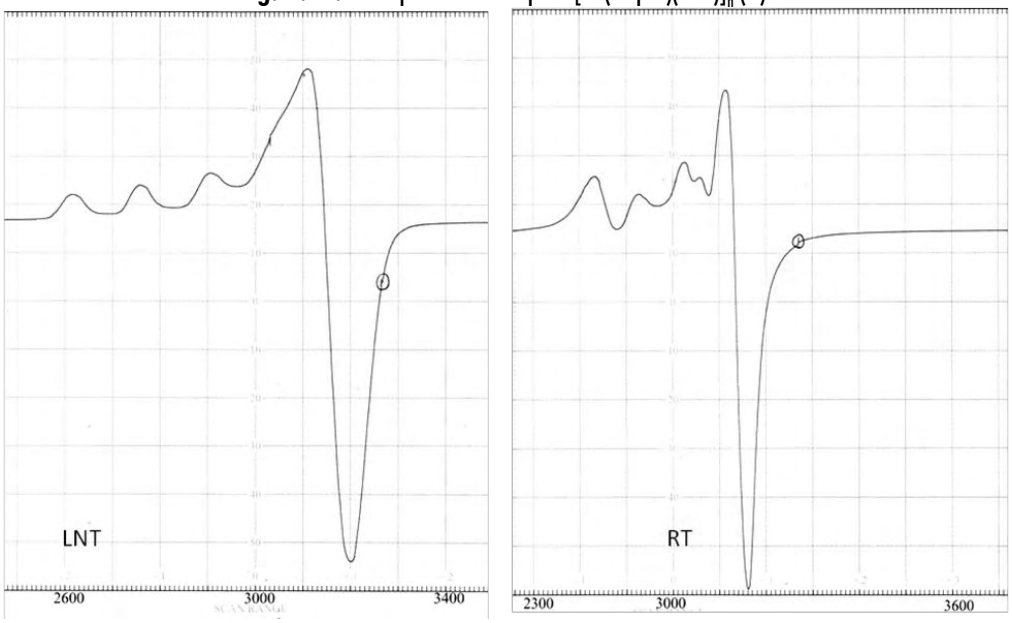

Fig. 2.45. EPR spectra of complex $[Cu(Hbpsc)(NCS)_2]$ (**2**).

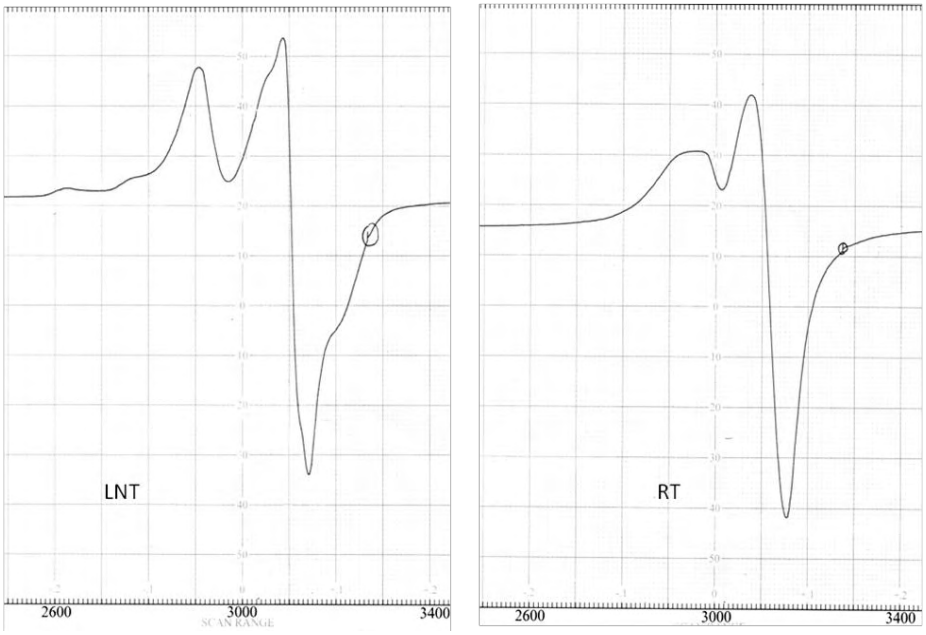

Fig. 2.46. EPR spectra of complex $[Cu(Hbpsc)\mu^2(S)NCS]_2 \cdot S$ (**3**).

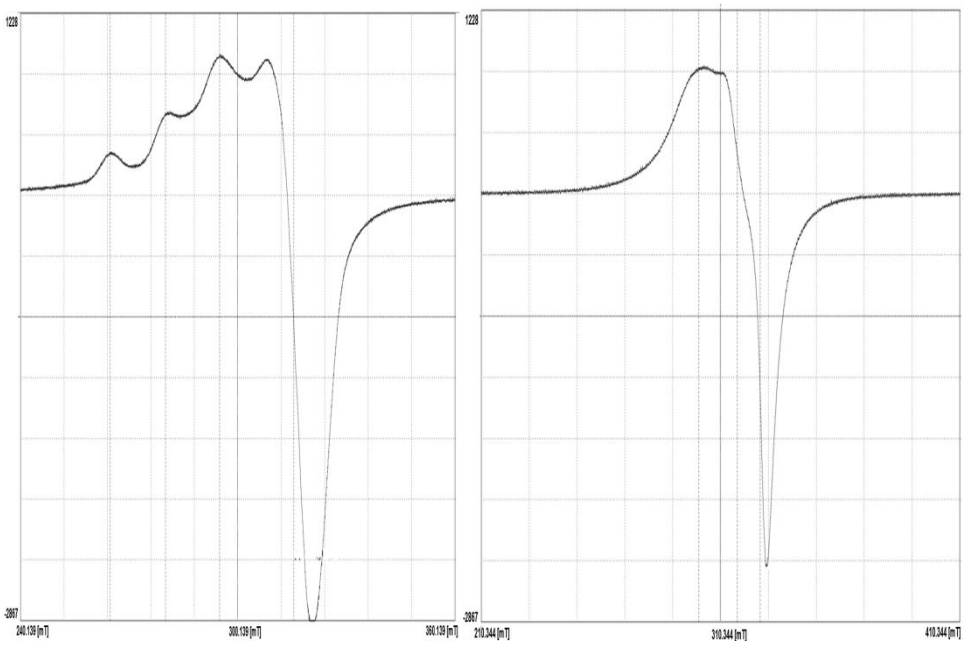

Fig. 2.47. EPR spectra of complex $[Cu(bpap)(NCS)_2]$ (**4**).

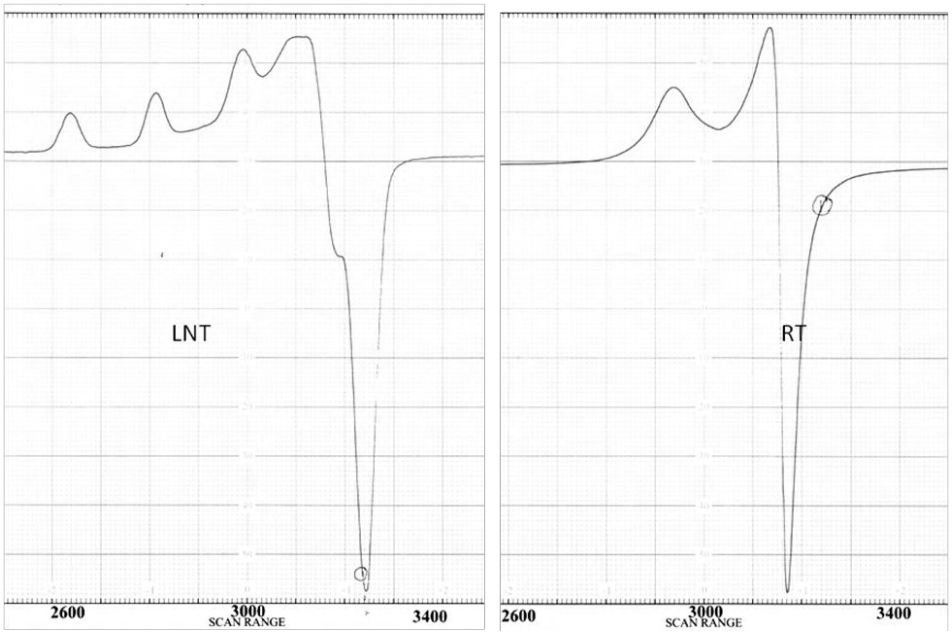

Fig. 2.48. EPR spectra of complex [Cu(dbsde)(NCS)] (**5**).

REFERENCES

1. S.A. Barnett, N.R. Champness, Coord. Chem. Rev., 2003, 246, 145.
2. A.Y. Robin, K.M. Fromm, Coord. Chem. Rev., 2006, 250, 2127.
3. W.K. Chan, Coord. Chem. Rev., 2007, 251, 2104.
4. O. Kahn, Adv. Inorg. Chem., 1995, 43, 179.
5. A.-Q. Wu, Y. Li, F.-K. Zheng, G.-C. Guo, J.-S. Huang, Cryst. Growth Des., 2006, 6, 444.
6. S.A. Barnett, A.J. Blake, N.R. Champness, C. Wilson, Chem. Commun., 2002, 1640.
7. Z.E. Serna, R. Cortes, M.K. Urtiaga, M.G. Barandika, L. Lezama, M.I. Arriortua, T. Rojo, Eur. J. Inorg. Chem., 2001, 865.
8. P. Talukder, A. Datta, S. Mitra, G. Rosair, M.S. El Fallah, J. Ribas, Dalton Trans., 2004, 4161.
9. S. Ferlay, G. Francese, H.W. Schmalle, S. Decurtins, Inorg. Chim. Acta, 1999, 286, 108.
10. H.Y. Bie, J.H. Yu, J.Q. Xu, J. Lu, Y. Li, X.-B. Cui, X. Zhang, Y.-H. Sun, L.-Y. Pan, J. Mol. Struct., 2003, 660, 107.
11. J.Y. Lu, Coord. Chem. Rev., 2003, 246, 1882.

12. A.M. Golub, H. Kohler, V.V. Skopenko (Eds.), Chemistry of Pseudohalides, Elsevier, Amsterdam, 1986.
13. (a) R.G. Pearson, J. Am. Chem. Soc., 1963, 85, 3533. (b) R.G. Pearson, Adv. Inorg. Chem. Radiochem., 1966, 8, 177. (c) F. Basolo, Coord. Chem. Rev., 1968, 3, 213. (d) J.L. Burmeister, Chem. Rev., 1968, 3, 225.
14. J.L. Burmeister, A.A. Newman (Ed.), Chemistry and Biochemistry of Thiocyanic Acid and its Derivatives, Academic Press, New York, 1975, Ch. 2, 68.
15. H. Zhang, X. M. Wang, K. C. Zhang, B. K. Teo, Coord. Chem. Rev., 1999, 183, 157.
16. M.-X. Li, H. Wang, S.-W. Liang, M. Shao, X. He, Z.-X. Wang. Cryst. Growth Des., 2009, 9, 11.
17. M.A.S. Goher, F.A. Mautner, A.K. Hafez, M.A.M. Abu-Youssef, C. Gspan, A.M.A. Badr, Polyhedron, 2003, 22, 975.
18. G. Yang, H.G. Zhu, B.H. Liang, X.M. Chen, J. Chem Soc, Dalton Trans., 2001, 580.
19. R. Vicente, A. Escuer, E. Peñalba, X. Solans, M. Font- Bardìa, Inorg. Chim. Acta, 1997, 255, 7.
20. H.-D. Bian, W. Gu, Q. Yu, S.-P. Yan, D.-Z. Liao, Z.-H. Jiang, Cheng, P. Polyhedron, 2005, 24, 2002.
21. O.A. Babich, V.N. Kokozay, V.A. Pavlenko, Polyhedron, 1996, 15, 2727.
22. Z.-L. You, H.-L. Zhu, Anorg. Allg. Chem., 2004, 630, 2754.
23. S. Ferlay, G. Francese, H.W. Schmalle, S. Decurtins, E. Greedan, R. J. Crutchley, J. Inorg. Chem., 1999, 38, 2548.
24. P. Gomez-Saiz, J. Garcia-Tojal, F.J. Arnaiz, M.A. Maestro, L. Lezama, T. Rojo, Inorg. Chem. Commun., 2003, 6, 558.
25. H. Grove, M. Julve, F. Lloret, P.E. Kruger, K.W. Tornroos, J. Sletten, Inorg. Chim. Acta, 2001, 325, 115.
26. J.A.R. Navarro, M.A. Romero, J.M. Salas, M. Quiros, E.R.T. Tiekink, Inorg. Chem., 1997, 36, 4988.
27. J. Ribas, C. Diaz, X. Solans, M. Font- Bardìa, Inorg. Chim. Acta, 1995, 231, 229.

28. A.P. Ginsberg, Inorg. Chim. Acta Rev., 1971, 5, 45.
29. SMART and SAINT, Area Detector Software Package and SAX Area Detector Integration Program, Bruker Analytical X-ray; Madison, WI, USA, 1997.
30. SADABS, Area Detector Absorption Correction Program; Bruker Analytical X-ray; Madison, WI, 1997.
31. L.J. Farrugia, J. Appl. Cryst., 2012, 45, 849.
32. K. Brandenburg, Diamond Version 3.2g, Crystal Impact GbR, Bonn, Germany, 2010.
33. W.J. Geary, Coord. Chem. Rev., 1971, 7, 81.
34. (a) M. Julve, M. Verdaguer, G.D. Munno, J.A. Real, G. Bruno, Inorg. Chem., 1993, 32, 795. (b) M.A.S. Goher, L.A. Al-Shatti, F.A. Mautner, Polyhedron, 1997, 16, 889. (c) S. Ferlay, G. Francese, H.W. Schmalle, S. Decurtins, Inorg. Chim. Acta, 1999, 286, 108.
35. A. Sreekanth, U.L. Kala, C.R. Nayar, M.R.P. Kurup, Polyhedron, 2004, 23, 41.
36. R.J. Kunnath, M.R.P. Kurup, S.W. Ng, Acta Cryst., 2012, E 68, m1181.
37. X.-W. Li, Y. Qiu, Acta Cryst., 2008, E64, m113.
38. (a) X.-F. Huang, Y.-B. Zhang, X.-L. Wang, J.-F. Tang, B.-F. Ruan. J. Coord. Chem., 2011, 64, 630. (b) Y. Song, Z. Xu, Q. Sun, B. Su, Q. Gao, H. Liu, J. Zhao. J. Coord. Chem., 2008, 61, 1212. (c) L. Chen, J.-L. Bai, H. Zhou, Z.-Q. Pan, Q.-M. Huang, Y. Song. J. Coord. Chem., 2008, 61, 1412. (d) C. Gao, X. Ma, J. Lu, Z. Wang, J. Tian, S. Yan. J. Coord. Chem., 2011, 64, 2157. (e) K.S. Banu, T. Ghosh, A. Guha, T. Chattopadhyay, D. Das, E. Zangrando. J. Coord. Chem., 2010, 63, 3714. (f) C.E. Xanthopoulos, C.C. Hadjikostas, G.A. Katsoulos, A. Terzis, M.P. Sigalas. J. Coord. Chem., 2002, 55, 717.
39. D. Chattopadhyay, S.K. Majumdar, P. Lowe, C.H. Schwalbe, S.K. Chattopadhyay, S. Ghosh, Dalton Trans., 1991, 2121.
40. M. Nardelli, G.F. Gasparri, P. Boldrini, G.G. Battistini, Acta Cryst., 1965, 19, 491.
41. G. Murphy, C.O. Sullivan, B. Murphy, B. Hathaway, Inorg. Chem., 1998, 37, 240.

42. U.L. Kala, S. Suma, M.R.P. Kurup, S. Krishnan, R.P. John, Polyhedron, 2007, 26, 1427.

43. P.C.H. Mitchell, R.J.P. Williams, J. Chem. Soc., 1960, 1912.

44. R.A. Bailey, S.L. Kozak, T.W. Michelsen, W.N. Mills, Coord. Chem. Rev., 1971, 6, 407.

45. A. Sabatini, I. Bertini, Inorg. Chem., 1965, 4, 959.

46. A. Turco, C. Pecile, Nature (London), 1961, 191, 66.

47. J. Lewis, R.S. Nyholm, P.W. Smith, J. Chem. Soc., 1961, 4590.

48. P.F. Rapheal, E. Manoj, M.R.P. Kurup, Polyhedron, 2006, 26, 818.

49. M.R.P Kurup, B. Varghese, M. Sithambaresan, S. Krishnan, S.R. Sheeja, E. Suresh, Polyhedron, 2010, 30, 70.

50. R. P. John, A. Sreekanth, V. Rajakannan, T.A. Ajith, M.R.P. Kurup, Polyhedron, 2004, 23, 2549.

51. A.B.P. Lever, Inorganic Electronic Spectroscopy, 2nd Ed., Elsevier, Amsterdam, 1984.

52. B.J. Hathaway, A.A.G. Tomlinson, Coord. Chem. Rev., 1970, 5, 24.

53. A.W. Addison, T.N. Rao, J. Reedijk, J. van Rijn, G.C. Vershoor, J. Chem. Soc. Dalton Trans., 1984, 1349.

54. J.A. De Bolfo, T.D. Smith, J.F. Boas, J.R. Pilbrow, J. Chem. Soc. Faraday II, 1976, 72, 481.

55. M.J. Bew, B.J. Hathaway, R.J. Faraday, J. Chem. Soc. Dalton Trans., 1972, 1229.

56. B.J. Hathaway, G. Wilkinson, R.D. Gillard, J.A. McCleverty, In Comprehensive Coordination Chemistry; Eds. Permagon: Oxford, 1987, 5, 533.

57. J. R. Wasson, C. Trapp. J. Phys. Chem., 1969, 73, 3763.

Chapter 3

Copper(II) complexes containing azide as coligand

Contents

3.1. Introduction

Supramolecular chemistry/crystal engineering and molecular magnetism of coordination compounds are two research areas of current age vast fascination. Design of suitable building blocks and utilization of coordinate bonds and noncovalent interactions to generate self-assemblies of various dimensions having aesthetic beauty and properties for possible use as functional materials are the major objectives in supramolecular chemistry/crystal engineering [1].

It is well known that the azido ligand is very useful for constructing enormous systems with abundant magnetic behaviors such as ferromagnetism, antiferromagnetism, ferrimagnetism, metamagnetism, spin-canting, spin-flop, spin glass, single-molecule magnets, and single-chain magnets [2].

The azide anion (N_3^-) plays an important role in the field of molecular magnetism as a bridging ligand because of its diverse bridging modes and its ability to effectively transmit magnetic coupling. Since copper(II) ion normally possesses four, five or six coordinate structure due to the Jahn-Teller effect, the coupling of copper complex to azide ion should enable the formation of a novel family of magnetic complexes. However, higher amounts of the coordinating ligands reduce the available coordination sites on Cu(II) for the bridging azide ligand, and thus generally azide nitrogen atoms occupy the axial positions of Cu(II) coordination sphere [3]. This weak axial coordination would weaken the magnetic coupling and frequently give rise to antiferromagnetic coupling [4]. Therefore, the change in the amount of the capping ligands should in principle change the structural pattern and even the magnetism of

Cu-azido systems [5]. The azido ligand is an efficient superexchange pathway for propagating magnetic interaction between the paramagnetic centers such as copper(II), giving dimeric, tetranuclear, cubane, 1-D, 2-D, and 3-D complexes [6]. The versatility of this ligand is due to its diverse binding modes leading to a variation in the magnetic properties that depend on its orientation with respect to the magnetic centers [7]. In general, the bridging modes observed for the azido group are end-to-end with anti-ferromagnetic interaction [8,9] and end-on with ferromagnetic interaction [10]. However, the magnetism of the latter is dependent on the M–N–M angle [11]. For copper(II) systems, ferromagnetic interaction is observed for complexes having Cu–N–Cu angles less than 108°. For angles above this value, molecules show antiferromagnetic interaction [12]. Hoffmann et al. [13] and later Ribas *et al.* [14] showed the possibility of even ferromagnetic interaction through an end-to-end azido pathway on the basis of theoretical calculations.

The azide ion in its salts is linear and symmetric, having equal N–N distances (1.167 Å). But the covalently bonded azide has unequal bond distances (in $M–N_1–N_2–N_3$, $N_1–N_2$ distance is more than $N_2–N_3$). Depending upon the coordination mode of the azide ion, IR spectra of the compounds are different [15].

The rational design and synthesis of polynuclear coordination complexes is an area of continuing interest in order to understand the structural and chemical factors that govern the exchange coupling between paramagnetic centers and to establish magnetostructural correlations in molecular systems with the aim of controlling and developing new functional molecular-based materials [16]. Although many different bridging groups and transition metal ions have been employed for the construction of such species, the Cu(II)-azide system is one of the most popular among synthetic chemists. A variety of copper-azido complexes with discrete or one-, two-, and three-dimensional polymeric structures have been reported (Fig. 3.1) depending upon the steric and electronic demands of the co-ligands.

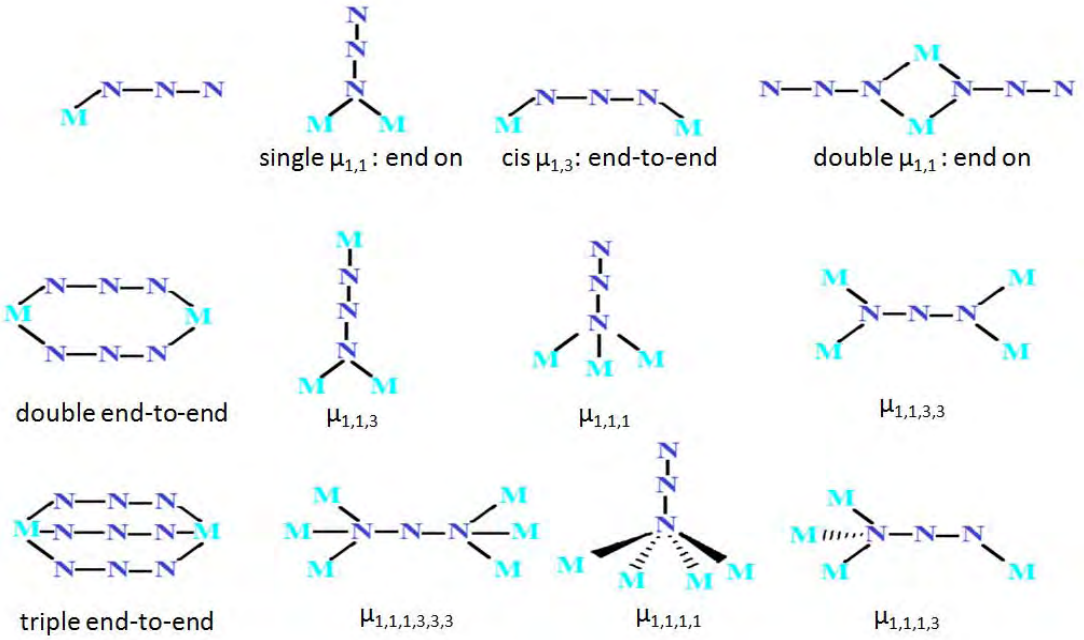

Fig. 3.1. Different binding modes of azide ion.

This diversity in the structures of the Cu(II) system is a result of its flexibility in coordination numbers (ranging from 4 to 6) and geometry [17], and taken together with its interesting magnetic properties, Cu(II) has therefore become the metal ion of choice for such studies. As a result of the extensive research of the last two decades, the superexchange mechanisms through various bridging modes of azide are now well established. For example, symmetric $\mu_{1,3}$ Cu(II) azide complexes are strongly antiferromagnetic, whereas Cu(II) complexes with double symmetric $\mu_{1,1}$-azide bridges are strongly ferromagnetic, provided that the Cu–N_{azide}–Cu angle is less than 108° [12]. Usually asymmetric $\mu_{1,3}$-azido bridges lead to weak antiferromagnetic coupling, whereas asymmetric $\mu_{1,1}$-azide bridges propagate weak to moderately strong ferro- or antiferromagnetic interactions [4]. Since other structural parameters certainly affect magnetic exchange, a number of exceptions have been reported, and it has been pointed out that other structural parameters such as Cu–N bond lengths and the $Cu(N)_3Cu$ dihedral angles [18] need also to be considered.

The magnetic study of molecular based magnetic materials has become an area of interest to physicists, material chemists and inorganic chemists. To design magnetic materials, the proper choice of bridging ligand is a major task as it

influences the magnetic strength and behavior by affecting the magnetic pathways between the paramagnetic centres, resulting in low as well as high dimensional materials. This versatile ligand has been widely used to design molecular based magnets because its diverse binding modes lead to variation in magnetic properties that depend on its orientation with respect to the magnetic centres [7]. The flexidentate azido ligand bridges metal centres in two different fashions : one is end-on ($\mu_{1,1}$) and the other is end-to-end ($\mu_{1,3}$). In the former mode the magnetism depends largely on the angle it subtends at the two metal centres. Dicopper(II) systems with smaller Cu–N–Cu bond angles (<108°) reflect a dominant ferromagnetic interaction while for larger angles (>108°) an antiferromagnetic interaction is favored [19,20]. But in the end-to-end mode, superexchange is almost always antiferromagnetic [8]. The type and the magnitude of the magnetic exchange interaction depends on the bridge identity, the metal–metal separation, the bond angles subtended to the bridging atoms, the dihedral angles between the planes containing the metal ions, the metal bridging ligand bond lengths, and the metal ion stereochemistries (Fig. 3.2).

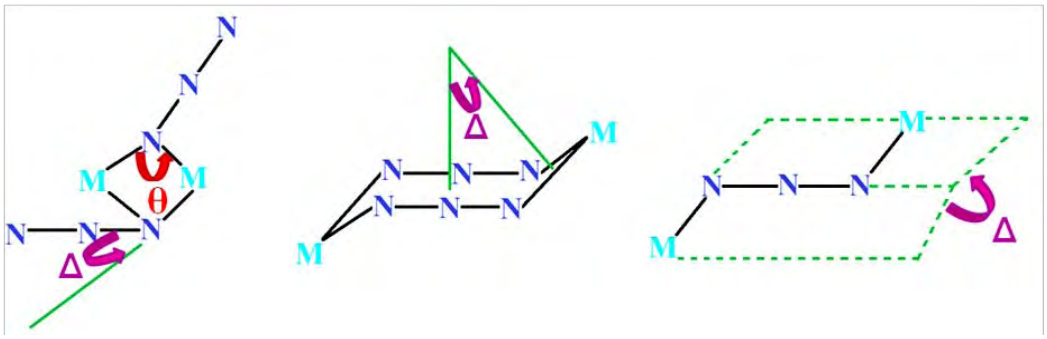

Fig. 3.2. The structural parameters for EO and EE azido bridges.

Among the transition-metal ions, Cu(II) is somewhat special in metal-azide chemistry, because more than 40% of the crystal structures containing bridging EO or EE azides involve copper [21].

During the last two decades, there has been a growing interest in the synthesis, structural characterization, and magnetic properties of polynuclear spin-coupled clusters of paramagnetic transition-metal ions exhibiting ferromagnetic and antiferromagnetic spin-exchange interactions [22]. This surge of interest in polynuclear complexes is because of their potential to provide access to new magnetic materials, which could have a possible use in quantum computing or magnetic

refrigeration [23,24,25]. Indeed, molecular-based magnetic materials have been the subject of many studies in recent years because of their physical properties in low-dimensional magnetic systems; this deals with materials such as single-molecule magnets (SMMs) [26,27]; and single-chain magnets [28,29]. Many of the molecular-based magnetic materials display long-range magnetic ordering at room temperature. Some of these materials are based on single metal centers bridged by polydentate ligands as well as doubly or triply bridging anions like N_3^-, NCS^-, CN^- etc., to form extended networks [30,31]. 1-D chain compounds with a linear or zigzag geometry are of interest in magnetochemistry and condensed matter physics due to the possibility of generating Haldane gap-type systems and single-chain magnets [32,33].

A major obstacle to a more comprehensive study of azide-based polymeric coordination complexes is the lack of rational synthetic procedures, since with the present state of knowledge it is not possible to predict which coordination mode will be adopted by azide [34,35].

The self-assembly [36] of molecular species *via* weak noncovalent interactions is one of the fundamental techniques that have been used to construct supramolecular architectures. The topology and functionality of such architectures depend on the choice of metals [37] as well as ligands [38]. Amongst various types of supramolecular architectures achieved so far, such as grid [39], helix [40], tape/ladder [41], capsule [42], cylinder [43] etc., helical architecture continues to draw attention from various research groups [44] not only due to its inherent aesthetic beauty but also due to its crucial role in biological systems of being the structural blueprint of DNA and proteins. Helical self-assembly displays a remarkable level of accuracy with inbuilt error correction mechanism due to the low energy association of noncovalent interactions in the construction of biological architectures. Induction of helicity into the system has been achieved in two ways, from inherently helical building blocks [45] and from non-helical building blocks with suitable tuning by covalent and noncovalent interactions. Following these two ways, different research groups have successfully produced single [46], double [47] and triple [48] stranded artificial materials. In the first category a type of molecules called ‘‘helicenes’’ [49] is used having inherent helical turn and several binding sites along the strand, which are forced to assemble into helical architecture with metals along the helix axis driven by

the tendency to reduce steric crowding during self-assembly. To prevent the coordination of the several binding sites to the same metal atom, a rigid spacer is generally used which assists the helication. In the other category non-helical building blocks have been selected judiciously to tune the assembly in a helical way where various non-bonded weak interactions are combined to link up the individual units. The use of complementary H-bonding in this regard is the most important and has been effectively employed for designing helices [50] but the utilization of $\pi\cdots\pi$ [51] interactions appeared in the literature. During recent years we are engaged in understanding the role of weak interactions in controlling the topology of supramolecular and coordination frameworks. In this direction our effort is to explore the design of supramolecular helical architectures using complementary H-bond donor acceptor set. The choice of linear pseudohalides is reasoned by the fact that they can act as H-bond acceptor either through S or N atoms.

3.2. Experimental

3.2.1. Synthesis of the complexes

All chemicals used for synthesis were of Analar grade. The semicarbazones and Schiff bases were formed *in situ*. **Caution:** Azide compounds are potentially explosive and should be prepared only in small quantities and handled with care.

3.2.1.1. Synthesis of $[Cu(dbsde)(N_3)]_n$ (7)

The Schiff base (Hdbsde) was prepared by heating 3,5-dibromosalicylaldehyde (0. 280 g, 1 mmol) and N,N-dimethylethylenediamine (0.088 g, 1 mmol) in methanol for 2 h. Methanolic solution of copper(II) chloride dihydrate (0.170 g, 1 mmol) and NaN_3 (0.065 g, 1 mmol) were added to the solution and refluxing was continued for another 2 h. Dark green colored crystals were isolated from the cool solution. Yield: 82%.

3.2.1.2. Synthesis of $[Cu(bsde)(N_3)]_n$ (8)

The Schiff base (Hbsde) was prepared by heating 5-bromosalicylaldehyde (0.201 g, 1 mmol) and N,N-dimethylethylenediamine (0.088 g, 1 mmol) in methanol for 2 h. Methanolic solution of copper(II) chloride dihydrate (0.170 g, 1 mmol) and

NaN_3 (0.065 g, 1 mmol) were added to the solution and refluxing was continued for another 2 h. Dark green colored crystals were isolated from the cool solution. Yield: 84%.

3.2.1.3. Synthesis of [Cu(bptsc)$\mu^2(N_3)]_2$ (9)

2-Benzoylpyridine thiosemicarbazone (Hbptsc) was prepared by refluxing a mixture of 2-benzoylpyridine (0.183 g, 1 mmol) and thiosemicarbazide (0.091 g, 1 mmol) in methanol for 2 h. Methanolic solution of copper acetate monohydrate (0.199 g, 1 mmol) and NaN_3 (0.065 g, 1 mmol) were added to the solution and refluxed continued for another 2 h. Dark green colored crystals were isolated from the cool solution. Yield: 75%.

3.2.1.4. Synthesis of [Cu(bpsc)(N_3)] (10)

2-Benzoylpyridine semicarbazone (Hbpsc) was prepared by heating 2-benzoylpyridine (0.183 g, 1 mmol) and semicarbazide hydrochloride (0.111 g, 1 mmol) in methanol for 2 h. Methanolic solution of copper(II) acetate monohydrate (0.199 g, 1 mmol) and NaN_3 (0.065 g, 1 mmol) were added to the solution and refluxing was continued for another 2 h. Dark green colored crystals were isolated from the cool solution. Yield: 53%.

3.2.2. Physical measurements

Carbon, hydrogen, nitrogen and sulfur analyses were carried out using a Vario EL III CHNS analyzer at the SAIF, Kochi, India. Infrared spectra were recorded on a JASCO FT-IR-5300 Spectrometer in the range 4000-400 cm^{-1} using KBr pellets. Electronic spectra were recorded on a Ocean Optics USB 4000 UV-Vis Fibre Optic Spectrometer in the 200-850 nm range using methanol solution. The molar conductivities of the complexes in DMF solutions (10^{-3} M) at room temperature were measured using a Systronic model 303 direct reading conductivity meter at the Department of Applied Chemistry, CUSAT, Kochi, India. Magnetic susceptibility measurements of the complexes were carried out on a Vibrating Sample Magnetometer using $Hg[Co(SCN)_4]$ as a calibrant at the SAIF, Indian Institute of Technology, Madras. The EPR spectra of the complexes in the solid state at 298 K and in DMF/DMSO at 77 K were recorded on a Varian E-112 spectrometer using

TCNE as the standard, with 100 kHz modulation frequency, 2 G modulation amplitude and 9.1 GHz microwave frequency at SAIF, IIT Bombay, India.

3.2.3. X-ray crystallography

Single crystals of compounds $[Cu(dbsde)(N_3)]_n$ (**7**), $[Cu(bsde)(N_3)]_n$ (**8**), $[Cu(bptsc)\mu^2(N_3)]_2$ (**9**) and $[Cu(bpsc)(N_3)]$ (**10**) suitable for X-ray diffraction studies were grown from their methanol solution by slow evaporation at room temperature. Single crystals were selected and mounted on a Bruker SMART APEX diffractometer, equipped with a graphite crystal, incident-beam monochromator, and a fine focus sealed tube with Mo Kα (λ = 0.71073 Å) as the X-ray source. The crystallographic data along with details of structure solution refinements are given in Table 3.1a and 3.1b. The unit cell dimensions were measured and the data collection was performed at 293(2) K. Bruker SMART software was used for data acquisition and Bruker SAINT software for data integration [52]. Absorption corrections were carried out using SADABS based on Laue symmetry using equivalent reflections [53]. The structure was solved by direct methods and refined by full-matrix least-squares calculations with the WinGX software package [54]. The molecular and crystal structures were plotted using DIAMOND version 3.2g [55]. All non-hydrogen atoms were refined anisotropically, and all H atoms on C and N were placed in calculated positions, guided by difference maps and refined isotropically, with C–H and N–H bond distances of 0.93 Å and 0.86 Å respectively. In the refinement of $[Cu(bptsc)\mu^2(N_3)]_2$ (**9**) and $[Cu(bpsc)(N_3)]$ (**10**), the hydrogen atoms of the NH_2 group were located from a difference Fourier map and restrained using DFIX and DANG instructions.

Table 3.1a. Crystallographic data and structure refinement for **7** and **8**

Parameters	$[Cu(dbsde)(N_3)]_n$ (**7**)	$[Cu(bsde)(N_3)]_n$ (**8**)
Empirical formula	$C_{11}H_{13}Br_2CuN_5O$	$C_{11}H_{14}BrCuN_5O$
Formula weight	454.62	375.72
Color	Green	Green
Temperature (T) K	296(2)	296(2)
Wavelength (Mo Kα) (Å)	0.71073	0.71073
Crystal system	Orthorhombic	Monoclinic
Space group	*Pbca*	$P2_1/n$
Cell parameters		
a	7.1185(3) Å	12.0893(9) Å
b	18.9782(11) Å	6.7671(4) Å
c	22.5112(12) Å	17.8889(10) Å
α	90°	90°
β	90°	101.866(3)°
γ	90°	90°
Volume V ($Å^3$)	3041.2(3)	1432.21(16)
Z	8	4
Calculated density (ρ)	1.986	1.742
Absorption coefficient, μ (mm^-	6.693	4.314
F(000)	1768	748
Crystal size mm^3	0.30 x 0.25 x 0.20	0.35 x 0.25 x 0.20
θ range for data collection	1.81 to 28.28°	3.23 to 27.00°
Limiting indices	-9≤h≤9,-24≤k≤24, -29≤l≤29	-11≤h≤15, -8≤k≤8, -22≤l≤17
Reflections collected	20167	10367
Unique Reflections (R_{int})	3753 [R(int) = 0.0653]	3130 [R(int) = 0.0379]
Completeness to θ	28.28 (99.4 %)	27.00 (99.8 %)
Absorption correction	Semi-empirical from equivalents	Semi-empirical from equivalents
Maximum and minimum	0.3479 and 0.2387	0.4791 and 0.3136
Refinement method	Full-matrix least-squares on F^2	Full-matrix least-squares on F^2
Data / restraints / parameters	3753 / 0 / 183	3130 / 0 / 174
Goodness-of-fit on F^2	1.174	1.027
Final R indices [I > 2σ (I)]	R_1 = 0.0676, wR_2 = 0.1352	R_1 = 0.0321, wR_2 = 0.0682
R indices (all data)	R_1 = 0.1358, wR_2 = 0.1737	R_1 = 0.0512, wR_2 = 0.0768
Largest difference peak and hole (e $Å^{-3}$)	1.247 and -0.952	0.624 and -0.658

$R_1 = \Sigma||F_o| - |F_c|| / \Sigma|F_o|$ $\quad wR_2 = [\Sigma w(F_o^2-F_c^2)^2 / \Sigma w(F_o^2)^2]^{1/2}$

Table 3.1b. Crystallographic data and structure refinement for **9** and **10**

Parameters	[Cu(bptsc)μ^2(N_3)]$_2$ (**9**)	[Cu(bpsc)(N_3)] (**10**)
Empirical formula	$C_{26}H_{22}Cu_2N_{14}S_2$	$C_{13}H_{11}CuN_7O$
Formula weight	721.78	344.83
Color	Dark green	Green
Temperature (T) K	296(2)	296(2)
Wavelength (Mo Kα) (Å)	0.71073	0.71073
Crystal system	Monoclinic	Triclinic
Space group	$P2_1/c$	$P\bar{1}$
Cell parameters		
a	11.2462(12) Å	7.6300(3) Å
b	7.2344(10) Å	8.6914(4) Å
c	18.519(2) Å	20.4022(9) Å
α	90°	96.906(2)°
β	96.653(5)°	90.001(2)°
γ	90°	90.104(2)°
Volume V (Å^3)	1496.5(3)	1343.16(10)
Z	2	4
Calculated density (ρ)	1.602	1.705
Absorption coefficient, μ (mm^{-1})	1.607	1.640
F(000)	732	700
Crystal size mm^3	0.35 × 0.30 × 0.25	0.25 x 0.25 x 0.20
θ range for data collection	3.0 to 28.3°	1.01 to 27.45°
Limiting indices	-14≤h≤15, -9≤k≤9, -24≤l≤24	-9≤h≤9, -11≤k≤11, -26≤l≤26
Reflections collected	13616	22154
Unique Reflections (R_{int})	3748 [R(int) = 0.0746]	6046 [R(int) = 0.0390]
Completeness to θ	28.40 (99.7 %)	27.45 (98.7 %)
Absorption correction	Semi-empirical from equivalents	Semi-empirical from equivalents
Maximum and minimum	0.6896 and 0.6034	0.7351 and 0.6846
Refinement method	Full-matrix least-squares on F^2	Full-matrix least-squares on F^2
Data / restraints / parameters	3748 / 0 / 199	6046 / 6 / 4136046 / 6 / 413
Goodness-of-fit on F^2	1.078	1.131
Final R indices [I > 2σ (I)]	R_1 = 0.0476, wR_2 = 0.1329	R_1 = 0.0444, wR_2 = 0.1221
R indices (all data)	R_1 = 0.0634, wR_2 = 0.1530	R_1 = 0.0628, wR_2 = 0.1327
Largest difference peak and hole (e Å^{-3})	0.580 and -0.747	0.774 and -0.565

$R_1 = \Sigma||F_o| - |F_c|| / \Sigma|F_o|$ $\quad wR_2 = [\Sigma w(F_o^2-F_c^2)^2 / \Sigma w(F_o^2)^2]^{1/2}$

3.3. Results and discussion

3.3.1. Analytical measurements

The analytical data of all the complexes are listed in Table 3.2. The CHNS obtained showed that all the complexes are analytically pure.

Table 3.2. Analytical data of Cu(II) azide complexes

Compound	Observed (Calculated)%				λ_m	μ_{eff}(B.M.)
	C	H	N	S		
[Cu(dbsde)$(N_3)]_n$ (**7**)	29.30 (29.06)	2.76 (2.88)	15.23 (15.41)	-	11	1.243
Cu(bsde)$(N_3)]_n$ (**8**)	35.10 (35.16)	3.49 (3.76)	18.91 (18.64)	-	01	1.20
[Cu(bptsc)$\mu^2(N_3)]_2$ (**9**)	43.52 (43.27)	2.85 (3.07)	27.31 (27.17)	8.74 (8.89)	04	1.3
[Cu(bpsc)$(N_3)]$ (**10**)	45.31 (45.28)	3.05 (3.22)	28.30 (28.43)	-	23	1.77

The complexes are soluble in polar solvents. The conductivity measurements were made in methanol solutions and all complexes are found to be non-electrolytes [56].

The magnetic moments of the polynuclear complexes **7**, **8** and **9** suggest considerable interaction between metal centers and the magnetic moments fall in the range 1.2-1.3 B.M. and it can be assumed to be multinuclear in nature [57]. The single end-on (EO) azido bridge in polymeric complexes **7** and **8** adopt the asymmetric basal-apical disposition and mediate relatively weak antiferromagnetic interaction based on the general magnetostructural correlation [58]. The end-on double azido-bridged copper(II) dimer **9** is weak ferromagnetic in nature [59].

But the room temperature magnetic moment of the complex of **10** formulated with one metal centre almost has the value very close to the expected spin only value of 1.73 B.M. for a d^9 copper system.

3.3.2. Crystal structure of complex [Cu(dbsde)$(N_3)]_n$ (7)

The asymmetric unit of [Cu(dbsde)$(N_3)]_n$ contains two Cu(II) ions, each one coordinated by tridentate Hdbsde ligand and linked together by an azide group. (Fig. 3.3).

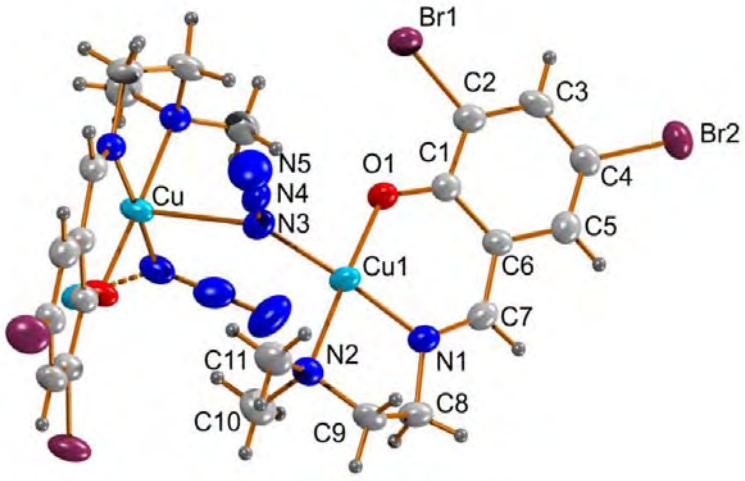

Fig. 3.3. Asymmetric unit of $[Cu(dbsde)(N_3)]_n$ (**7**) polymeric chain with atom numbering scheme.

Each azide functions as a *trans*-$\mu_{1,1}$ bridge, resulting in a one dimensional polymer. Each monomeric unit is related to its adjacent ones by a 2-fold screw axis, leading to a helical propagation along the crystallographic 'a' axis (Fig. 3.4). It is interesting to note that there are very few examples reported for helical *trans*-$\mu_{1,1}$ chains with Cu(II), whereas several $\mu_{1,3}$ -N_3 bridged helical chains have been reported [60]. The formation of helical chains in 1-D (single-stranded) coordination polymers is not unusual, with a 2_1-helix being the most common type [61].

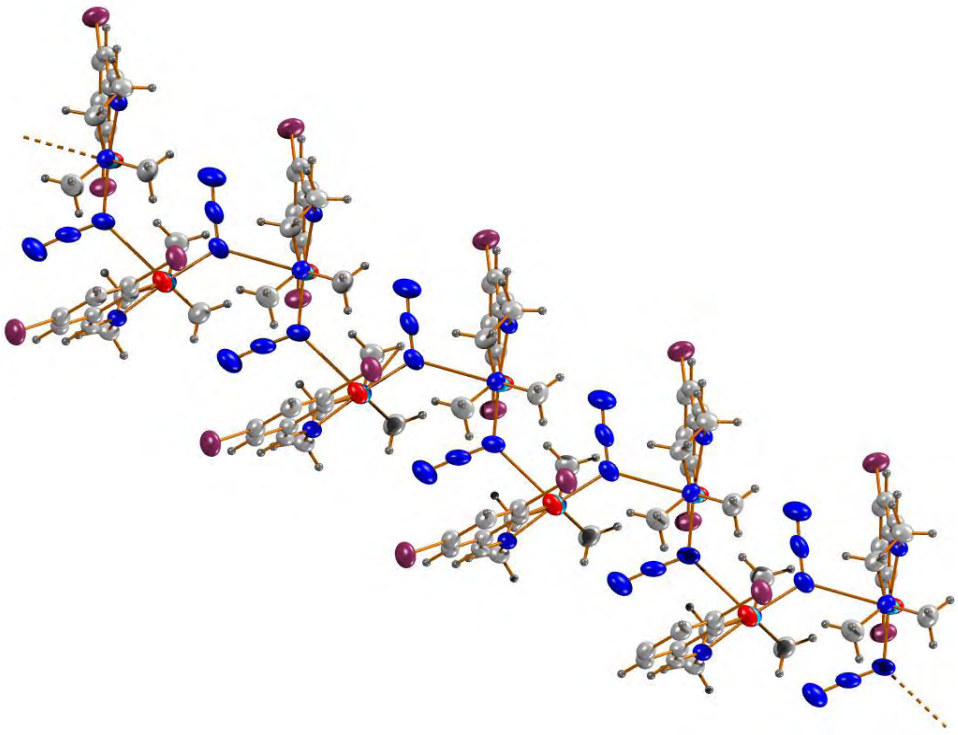

Fig. 3.4. Perspective view of helical polymeric chain of complex $[Cu(dbsde)(N_3)]_n$ (**7**) along 'a' axis.

The lattice nature is orthorhombic space group *Pbca*. The crystal structure of this compound reveals one crystallographically distinct Cu(II) center, which is pentacoordinated. The three coordination positions of the metal center are satisfied by phenoxo oxygen atom, imine nitrogen atom, and amine nitrogen atom of one deprotonated ligand. The remaining two coordination positions are satisfied by two nitrogen atoms of two end-on bridging azide ligand. The coordination geometry of the metal center is distorted square pyramidal. The basal plane is defined by two nitrogen atoms (N1 and N2) and one oxygen atom (O1) of the Schiff base ligand and one nitrogen atom (N3) of the azide ligand, while the apical position is occupied by one azide nitrogen atom. The *trans*-$\mu_{1,1}$-azide is less symmetrical that of *trans*-$\mu_{1,3}$-azides. Selected bond distances and angles are listed in the Table 3.3. Most of the angles involving central copper atoms are widely different from 90º and 180º indicating significant distortion from the square pyramidal geometry. One of the reasons for the deviation from an ideal stereochemistry is the restricted bite angle imposed by the ligands. The variation in Cu–N bond distances, Cu1–N2 (2.058(6)), Cu1–N1 (1.945(6)), and Cu1–N3 (1.990(6)) Å indicates the differences in the strength of the bonds formed by each of the coordinating N atoms.

Table 3.3. Selected bond lengths [Å] and angles [°] for $[Cu(dbsde)(N_3)]_n$ (**7**)

Bond lengths (Å)	
Cu1–N2	2.058(6)
Cu1–N1	1.945(6)
Cu1–O1	1.915(5)
Cu1–N3	1.990(6)
Br1–C1	1.893(8)
Br2–C3	1.900(8)
O1–C6	1.293(8)
Bond angles (°)	
N2–Cu1–N1	84.6(2)
N1–Cu1–O1	92.8(2)
O1–Cu1–N3	89.5(2)
N3–Cu1–N2	93.0(2)
Cu1–N3–Cu1	117.35

The intramolecular hydrogen bonding interactions (Fig. 3.5) make the molecule more rigid. A bifurcated hydrogen bonding network is established between the hydrogen atom attached at C11 carbon and the two nitrogen atoms of azide molecule (Table 3.4).

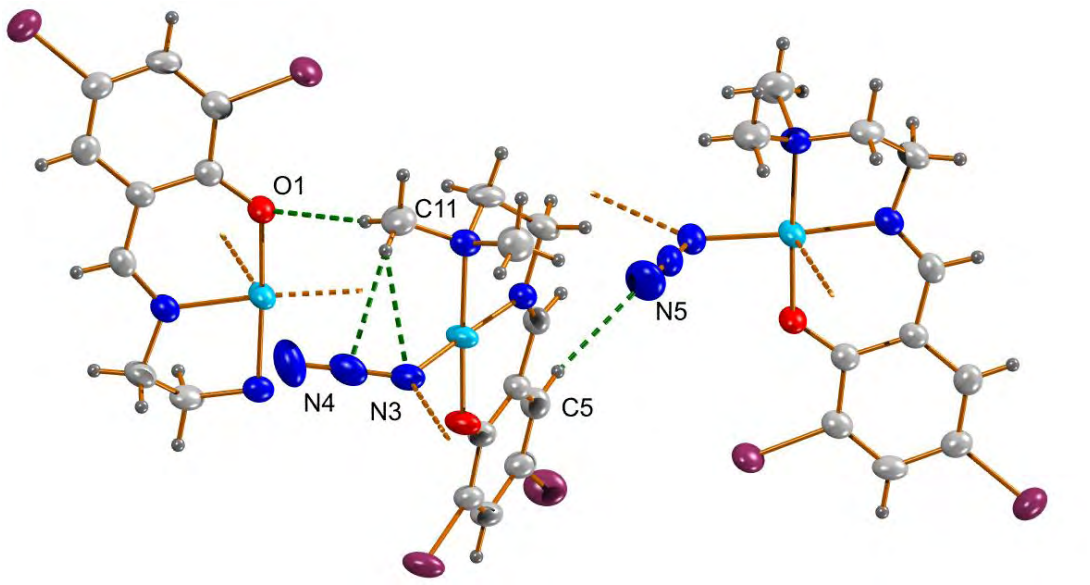

Fig. 3.5. The 1 D-polymeric chains connected with hydrogen bonds.

There are two types of C–H···π interactions (Fig. 3.6) mainly involve in the interconnection of the neighboring molecules with H···Cg distances of 3.0630 Å and 3.2369 Å (Table 3.4). There is a network of electron delocalization brought about by C–H···π interactions, which invokes a stable molecular arrangement in unit cell [62]. It is most interesting to note that complex $[Cu(dbsde)(N_3)]_n$ (**7**) is chiral. The origin of chirality and spontaneous resolution is an ill understood phenomenon to date, but recent studies [63,64] indicate that subtle interplay of weak interactions between the components, especially chiral recognition during nucleation process, may transmit the chiral information throughout the crystal and thereby spontaneous resolution may arise. It is noteworthy that no solvent molecules are present in the complexes. The solvent molecules generally fill the void space cooperatively by weak interactions within the crystalline framework.

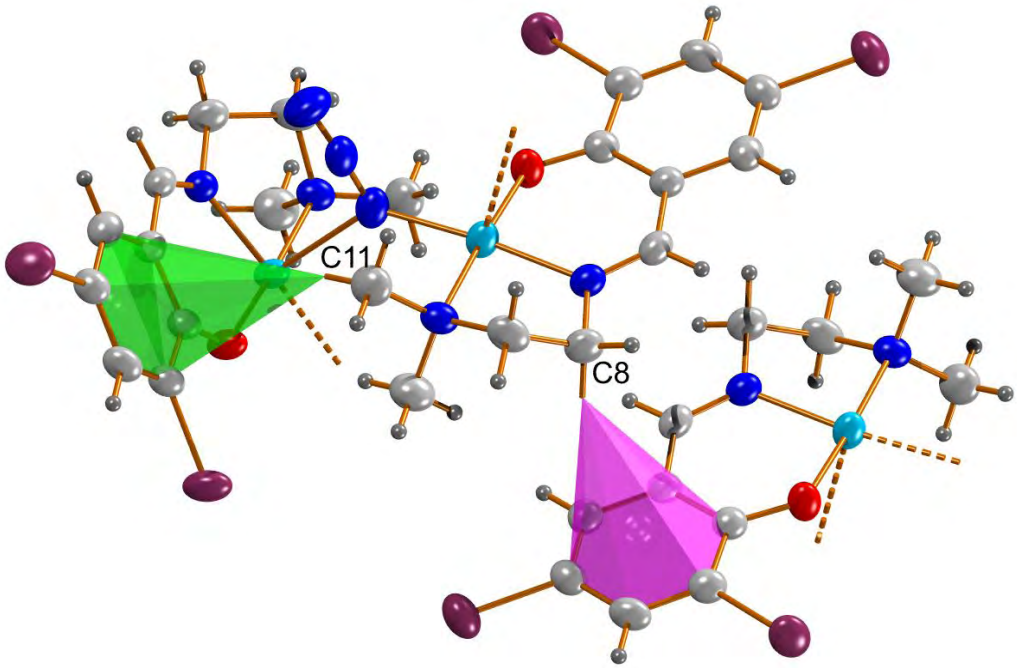

Fig. 3.6. Interconnection of the molecules *via* C–H···π interactions.

Table 3.4. Interaction parameters of the complex $[Cu(dbsde)(N_3)]_n$ (**7**)

Hydrogen bonding interactions

D–H···A	D–H (Å)	H···A (Å)	D···A (Å)	∠D–H···A (°)
C(5)–H(5)···N(5)^{a}	0.9304	2.5148	3.366(10)	152.23
C(11)–H(11A)···N(3)	0.9599	2.6229	3.089(8)	110.21
C(11)–H(11A)···N(4)	0.9599	2.5775	3.104(10)	114.73
C(11)–H(11B)···O(1)^{b}	0.9603	2.5276	3.471(9)	167.31

C–H···π interactions

X–H(I)···Cg(J)	H···Cg (Å)	X···Cg (Å)	∠X–H···Cg (°)
C(8)–H(8B)···Cg(4)^{c}	3.0630	3.975(7)	157.13
C(11)–H(11A)···Cg(4)^{d}	3.2369	4.089(8)	148.95

Equivalent position codes: a= 3/2-x,-1/2+y,z ; b= 1/2+x,1/2-y,1-z ; c= 2-x,-y,1-z ; d= 1/2+x,1/2-y,1-z ; Cg(4)= C(1), C(2), C(3), C(4), C(5), C(6) ; D, donor; A, acceptor; Cg, centroid.

The packing diagram of the coordination polymeric chain $[Cu(dbsde)(N_3)]_n$ (**7**) viewed along 'b' axis is given in the Fig. 3.7. It can be observed that the molecules are packed so that two consecutive molecules are centrosymmetrically arranged one over the other along 'a' axis (Figs. 3.8 and 3 9).

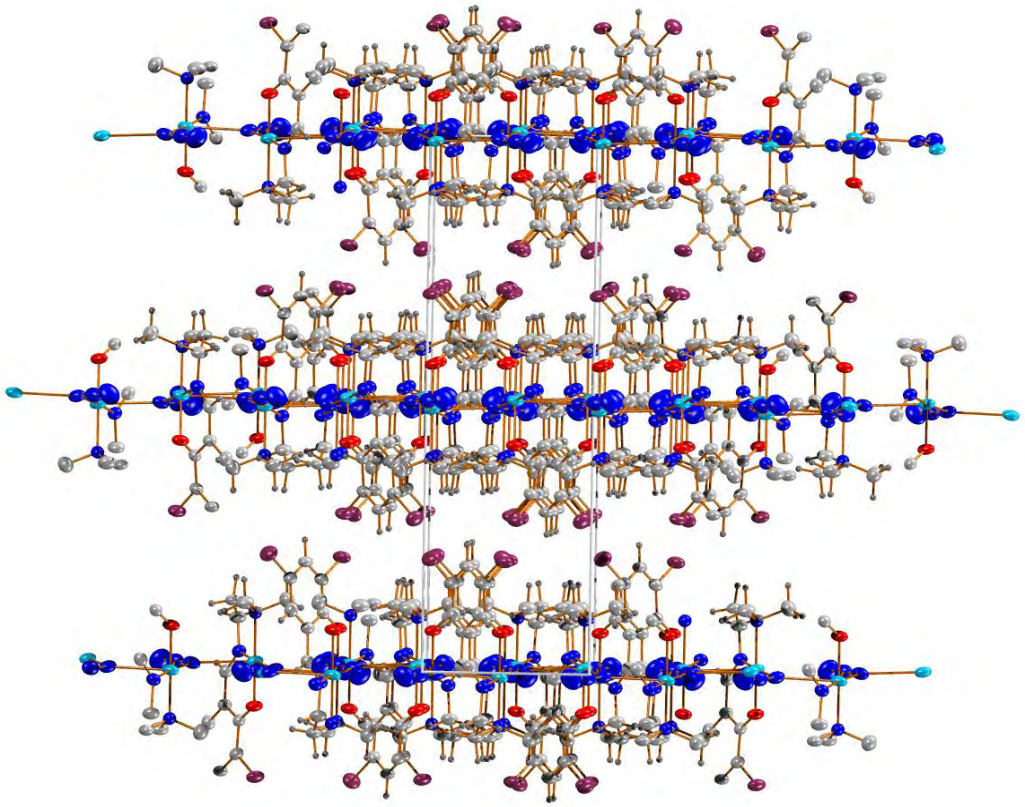

Fig. 3.7. The packing diagram of $[Cu(dbsde)(N_3)]_n$ (**7**) showing the stacking of molecules along 'b' axis.

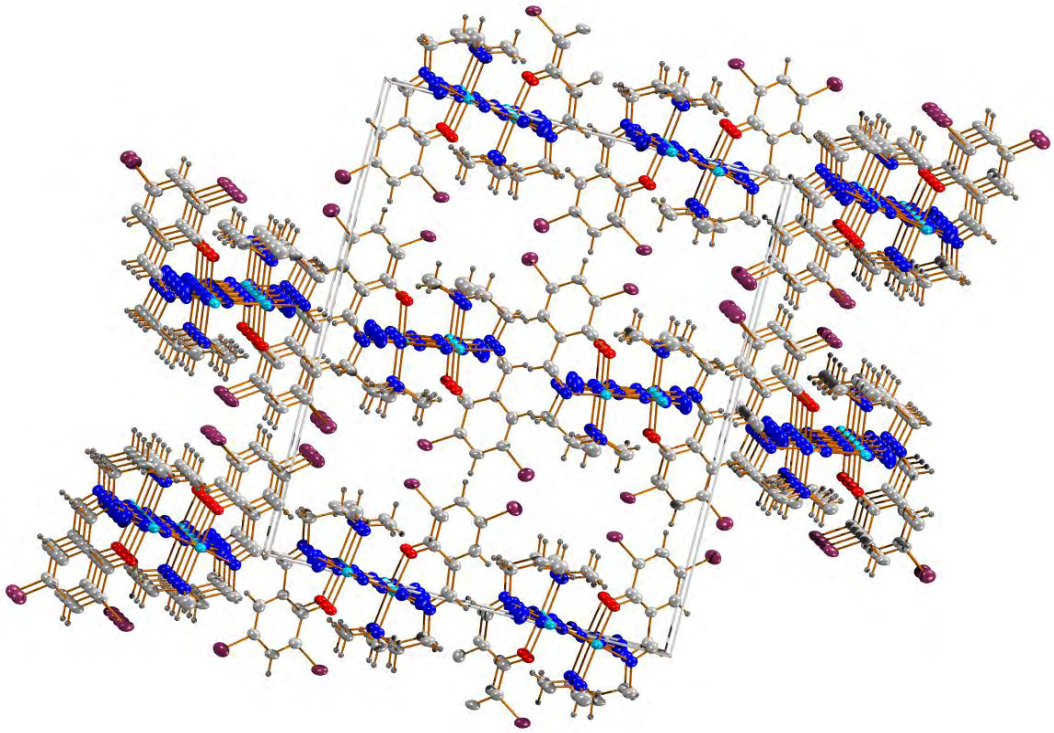

Fig. 3.8. The packing diagram of $[Cu(dbsde)(N_3)]_n$ (**7**) showing the stacking of molecules along 'a' axis.

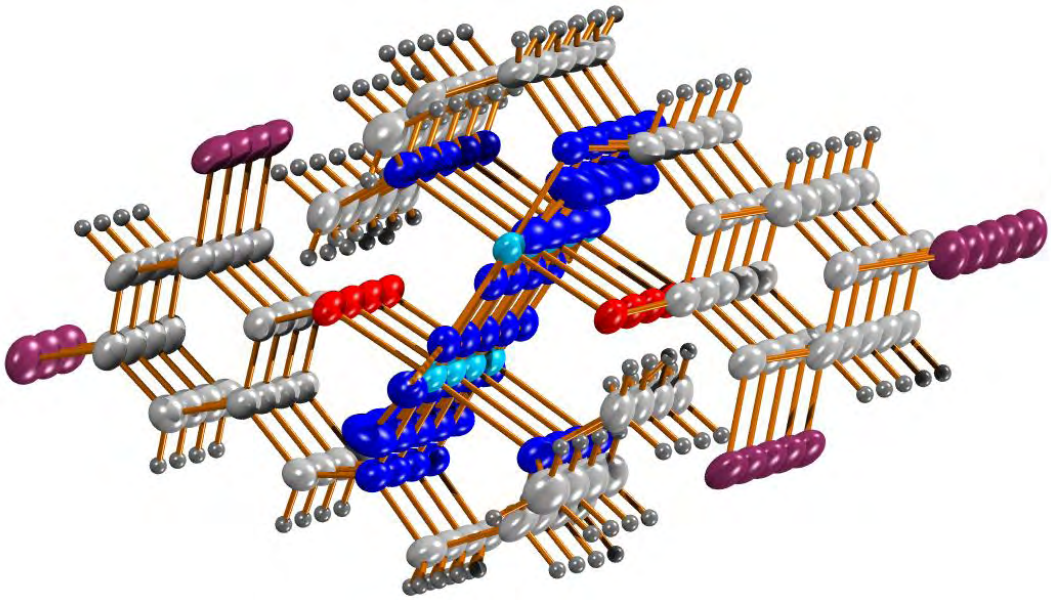

Fig. 3.9. The packing diagram of $[Cu(dbsde)(N_3)]_n$ (**7**) showing the stacking of molecules along 'a' axis.

3.3.3. Crystal structure of complex $[Cu(bsde)(N_3)]_n$ (8)

The asymmetric unit of $[Cu(bsde)(N_3)]_n$ (**8**) contains two Cu(II) ions, one tridentate Hbsde ligand and one azide group coordinated to Cu(II) (Fig. 3.10).

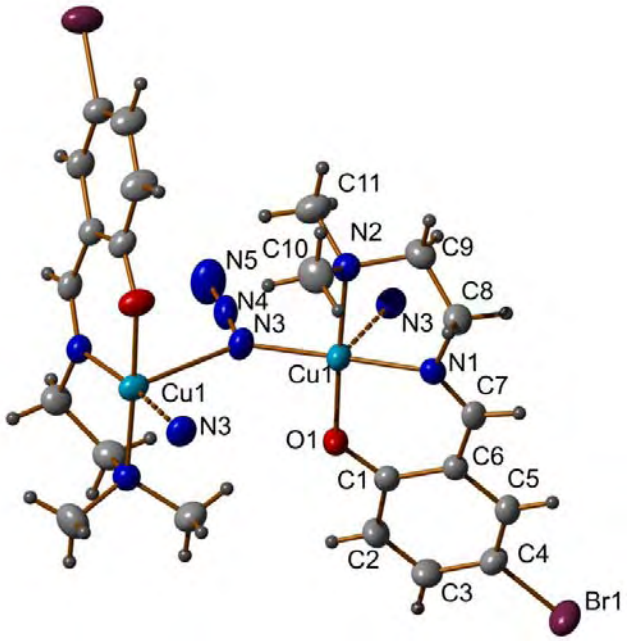

Fig. 3.10. Asymmetric unit of $[Cu(bsde)(N_3)]_n$ (**8**) polymeric chain with atom numbering scheme.

Each azide functions as a *trans*-$\mu_{1,1}$ bridge, resulting in a one dimensional polymer. Each monomeric unit is related to its adjacent ones by a 2-fold screw axis, leading to a helical propagation along the crystallographic 'b' axis (Fig. 3.11).

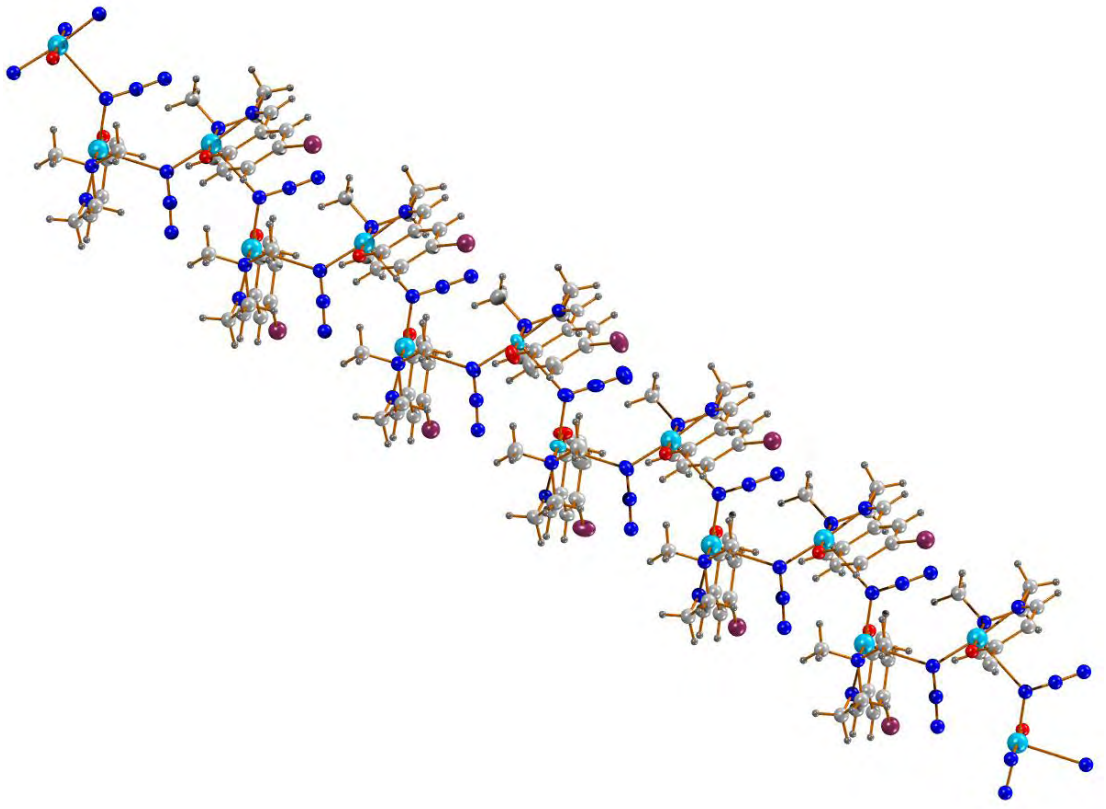

Fig. 3.11. Perspective view of helical polymeric chain of complex $[Cu(bsde)(N_3)]_n$ (**8**) along 'b ' axis.

The lattice nature is monoclinic space group $P2_1/n$. The crystal structure of this compound reveals one crystallographically distinct Cu(II) center, which is pentacoordinated. The three coordination positions of the metal center are satisfied by phenoxo oxygen atom, imine nitrogen atom, and amine nitrogen atom of one deprotonated ligand. The remaining two coordination positions are satisfied by two nitrogen atoms of two end-on bridging azide ligand. The coordination geometry of the metal center is distorted square pyramidal. The basal plane is defined by two nitrogen atoms (N1 and N2) and one oxygen atom (O1) of the Schiff base ligand and one nitrogen atom (N3) of the azide ligand, while the apical position is occupied by one azide nitrogen atom. The *trans*-$\mu_{1,1}$-azide is less symmetrical than that of *trans*-$\mu_{1,3}$-azides. Selected bond distances and angles are listed in the Table 3.5.

Table 3.5. Selected bond lengths [Å] and angles [°] for $[Cu(bsde)(N_3)]_n$ **(8)**

Bond lengths (Å)	
Cu1–N2	2.067(3)
Cu1–N1	1.953(2)
Cu1–O1	1.908(3)
Cu1–N3	1.984(3)
Bond angles (°)	
N2–Cu1–N1	84.79(11)
N1–Cu1–O1	92.63(10)
O1–Cu1–N3	89.39(12)
N3–Cu1–N2	93.10(12)
Cu1–N3–Cu1	128.85

The intramolecular hydrogen bonding interactions (Fig. 3.12) make the molecule more rigid.

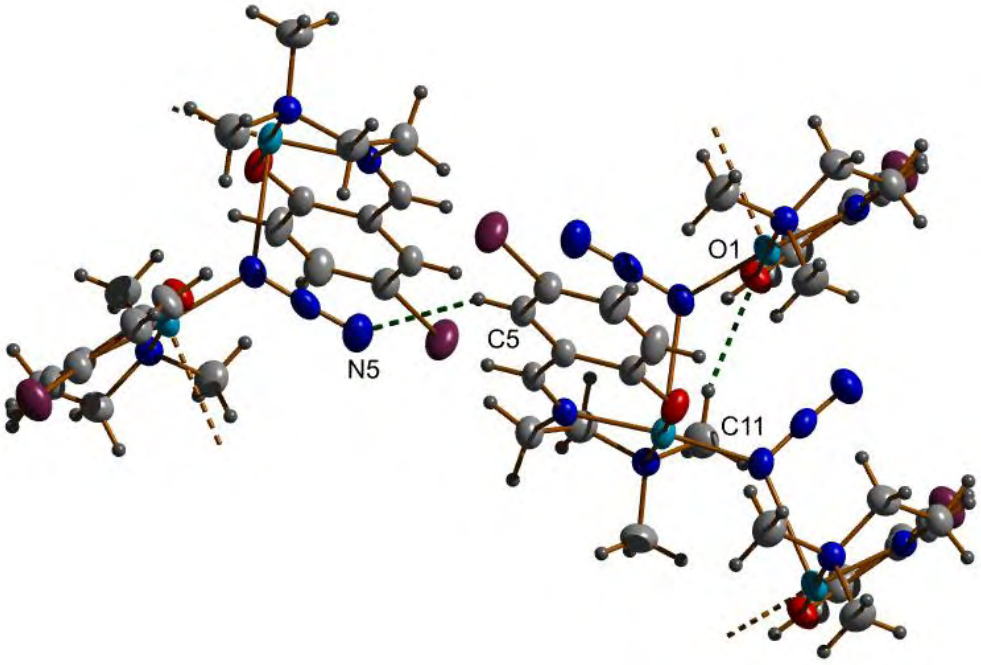

Fig. 3.12. The 1D-polymeric chains connected with hydrogen bonds.

A single type of C–H···π interaction is (Fig. 3.13) mainly involved in the interconnection of the neighboring molecules with H···Cg distances of 3.2159 Å (Table 3.6).

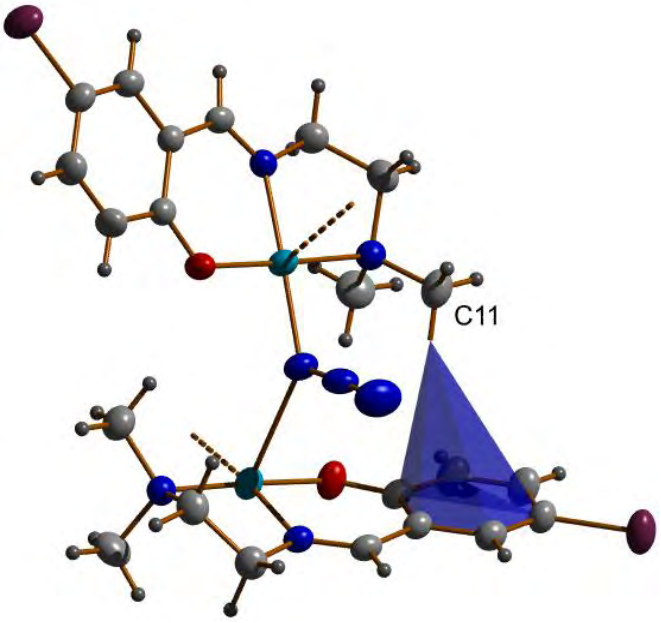

Fig. 3.13. Interconnection of the molecules via C–H···π interactions.

Table 3.6. Interaction parameters of the complex $[Cu(bsde)(N_3)]_n$ (**8**)

Hydrogen bonding interactions

D–H···A	D–H (Å)	H···A (Å)	D···A (Å)	∠D–H···A (º)
C(5)–H(5)···N(5)^a	0.9298	2.6285	3.469(4)	150.60
C(11)–H(11B)···O(1)^b	0.9594	2.3844	3.318(4)	164.11

C–H···π interactions

X–H(I)···Cg(J)	H···Cg (Å)	X···Cg (Å)	∠X–H···Cg (º)
C(11)–H(11A)···Cg(4)^c	3.2159	4.094(3)	152.93

Equivalent position codes: a= -1/2+x,1/2-y,-1/2+z ; b= 1/2-x,1/2+y,1/2-z ; c= -1/2-x,-1/2+y,1/2-z ;
Cg(3)= C(1), C(2), C(3), C(4), C(5), C(6); D, donor; A, acceptor; Cg, centroid.

The unit cell packing diagram of the coordination polymeric chain $[Cu(bsde)(N_3)]_n$ (**8**) viewed along 'a' axis is given in the Fig. 3.14. It can be observed that the molecules are packed so that two consecutive molecules are centrosymmetrically arranged one over the other along 'b' axis (Figs. 3.15 and 3.16). To design or make a chiral feature from extended helices without any chiral sources relies on the understanding of ligand effects and crystal packing, especially the latter [65].

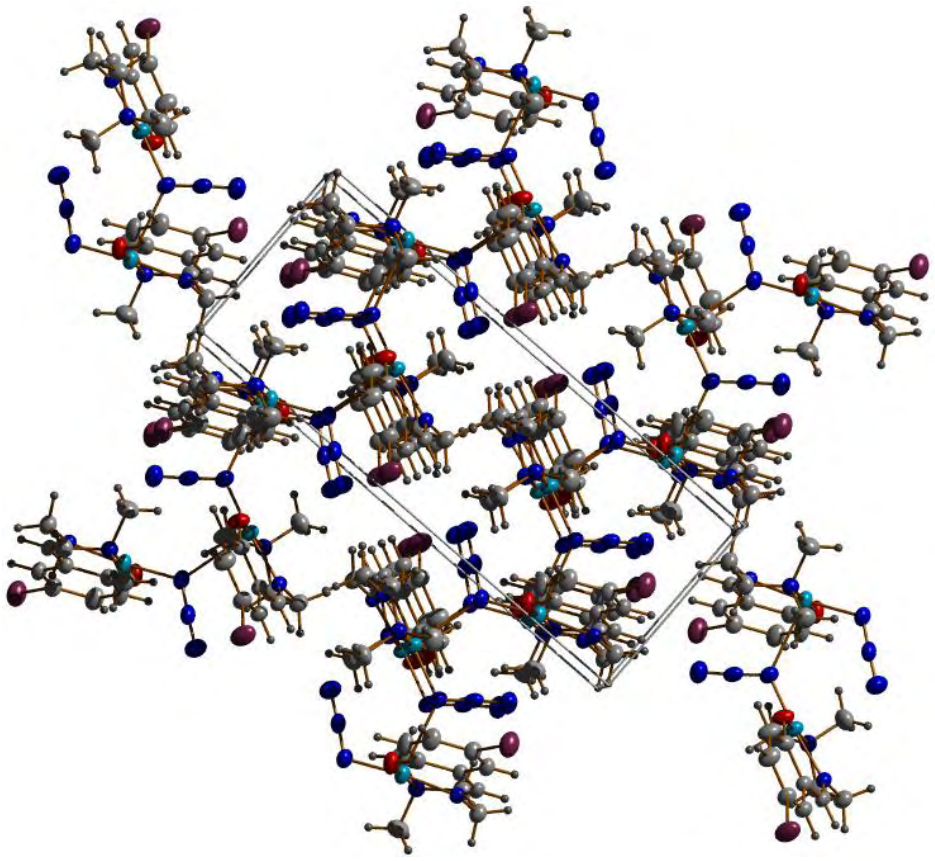

Fig. 3.14. The packing diagram of $[Cu(bsde)(N_3)]_n$ (**8**) molecules along 'a'axis.

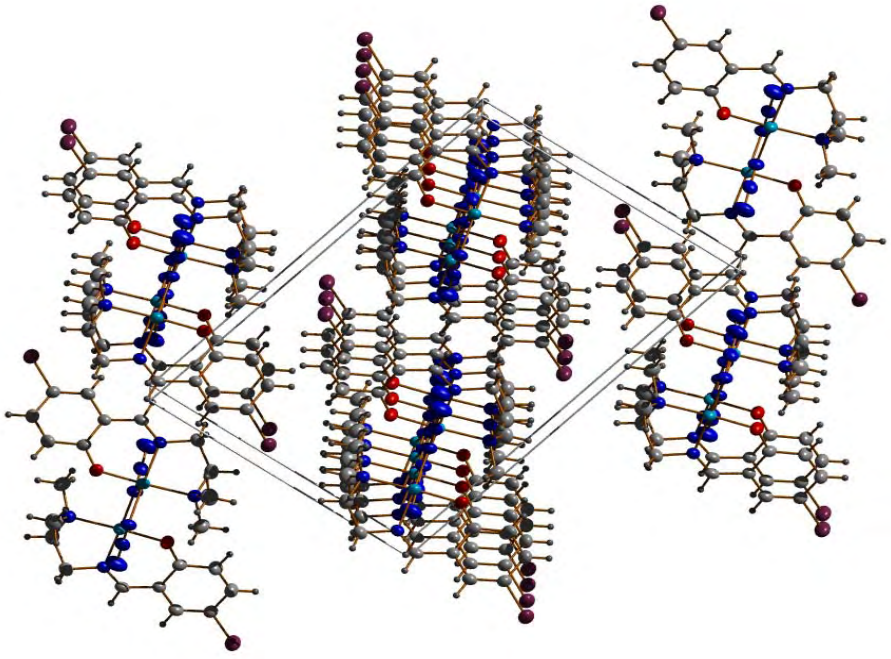

Fig. 3.15. The packing diagram of $[Cu(bsde)(N_3)]_n$ (**8**) showing the stacking of molecules along 'b' axis.

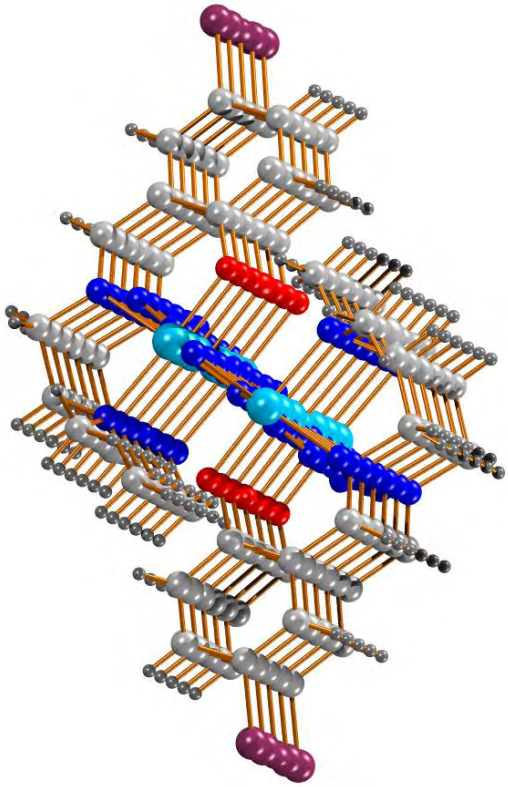

Fig. 3.16. The packing diagram of $[Cu(bsde)(N_3)]_n$ (**8**) showing the stacking of molecules along 'b' axis.

3.3.4. Crystal structure of complex $[Cu(bptsc)\mu^2(N_3)]_2$ (9)

The single crystal X-ray diffraction study of the compound $[Cu(bptsc)\mu^2(N_3)]_2$ (**9**) showed that the compound exists as an end-on azido bridged dimer. The molecular structure of the compound along with atom numbering scheme is given in Fig. 3.17.

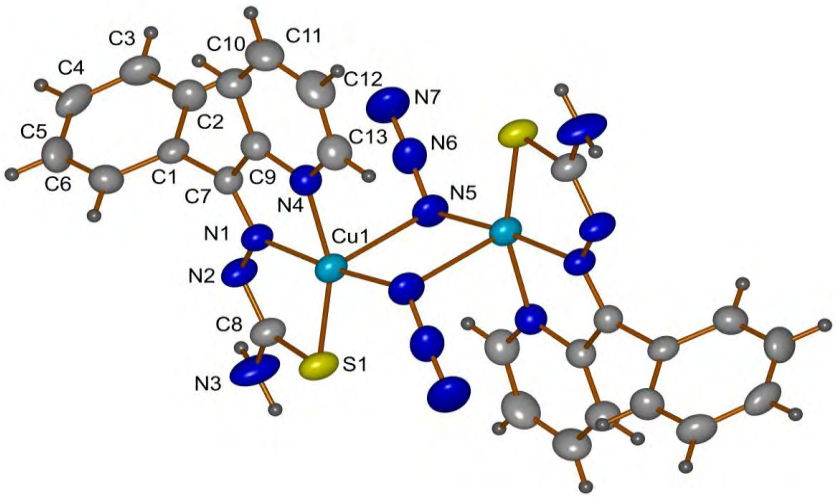

Fig. 3.17 The molecular structure of $[Cu(bptsc)\mu^2(N_3)]_2$ (**9**) along with the atom numbering scheme.

This compound crystallized in the monoclinic centrosymetric space group $P2_1/c$, with the asymmetric unit comprising one Cu(II) centre, one deprotonated thiosemocarbazone ligand and one azide N_3^- ligand. The crystal structure reveals that the compound is a centrosymmetric binuclear complex in which the Cu(II) centres are five coordinated, bonded by three NNS atoms from the deprotonated ligand and nitrogen atoms from two bridging azide anions. Each of the two azide anions bridges the Cu(II) centers in an end-on fashion and this leads to a relatively shorter Cu···Cu distance of 3.311 Å. The Cu···Cu distances within the four-member $Cu_2(N_3)_2$ ring are comparable to those found in related compounds [66]. The di-$\mu_{1,1}$-azide bridging nitrogen atoms are in a planar $Cu_2(N_3)_2$ ring around the crystallographic inversion center. The coordination polyhedron around Cu(II) may be described as an axially elongated square pyramid (for more information about the bond distances and angles see Table 3.7). The azide ion bridges in an asymmetric (basal-apical) fashion so that the Cu–N_{azide} bond lengths are significantly different, Cu1–N5 1.949 Å and Cu–N5 is 2.550 Å and the Cu1–N5–Cu bridge angle (93.82°) is considerably larger than that in related complexes reported in literature [67].

Table 3.7. Selected bond lengths [Å] and angles [°] of $[Cu(bptsc)\mu^2(N_3)]_2$ (**9**)

Bond lengths (Å)	
Cu1–N5	1.942(2)
Cu1–N1	1.9578(19)
Cu1–S1	2.2603(8)
Cu1–N4	2.022(2)
N1–N2	1.359(3)
C8–S1	1.729(3)
Bond angles (°)	
N5–Cu1–N4	94.22(9)
N1–Cu1–N4	80.26(8)
S1–Cu1–N5	101.84(7)
N1–Cu1–S1	84.08(6)

The trigonality index τ for the molecule is 0.225, which shows the coordination polyhedron around each copper atom is a distorted square pyramid. The base of each

distorted square pyramidal unit is occupied by N(1), N(4), N(5) and S(1) atoms, with the apical position occupied by the N(1A) atom of the second azido group. Each azido ligand functions as an electron donor to the coordination network through an end-on azido bridging mode. Two molecules are disposed about a center-of-inversion and the distance between the copper atom and their apical nitrogen atom of the other azide is 2.533(3) Å. In the crystal, the binuclear molecules are linked by an N–H···N hydrogen bond leading to a ribbon running along the 'a' axis (Table 3.8). These supramolecular chains close pack along the 'a' axis of the unit cell generating a considerable dense crystalline packing arrangement through hydrogen bonding (Fig. 3.18).

Table 3.8. Hydrogen bonding interactions of $[Cu(bptsc)\mu^{2}(N_3)]_2$ (**9**)

D–H···A	D–H (Å)	H···A (Å)	D···A (Å)	∠D–H···A (°)
N(3)–H(1)···N(2)^{a}	0.87(3)	2.22(3)	3.075(3)	167(3)

Equivalent position codes: a = -x,1-y,1-z.

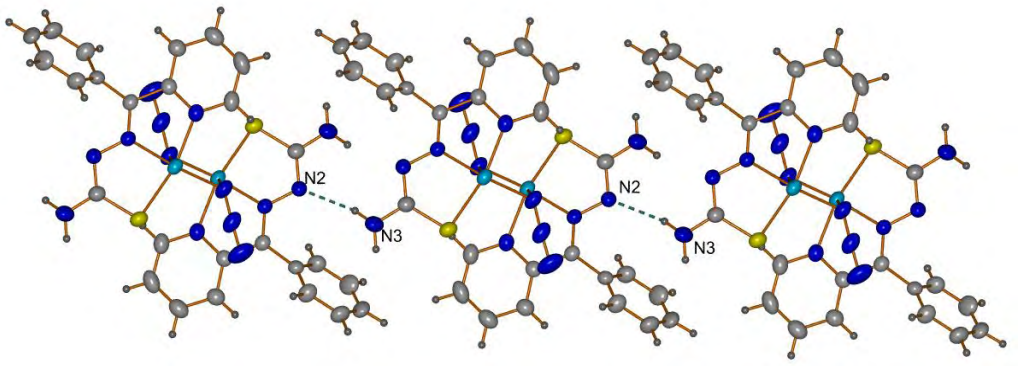

Fig. 3.18. Hydrogen bonding interactions in a ribbon maner.

The packing of the molecule in the crystal lattice is under the combined effect of hydrogen bonding, and C–H···π interactions (Table 3.9). The C–H···π interactions between the phenyl hydrogen and phenyl ring such as C(3)–H(3)···Cg(2)^{b} (b = -x,-1/2+y,1/2-z) and amino hydrogen and phenyl ring N(3)–H(2)···Cg(2)^{a} (a = -x,1-y,1-z) of the neighbouring molecules at a distances of 3.011(4) and 2.62(4) Å contribute to the stability of the unit cell packing (Fig. 3.19).

Table 3.9 C–H···π interactions of $[Cu(bptsc)\mu^{2}(N_3)]_2$ (**9**)

X–H(I)···Cg(J)	H···Cg (Å)	X···Cg (Å)	∠X–H···Cg (°)
N(3)–H(2)···Cg(2)^{a}	2.62(4)	3.168(4)	121(3)
C(3)–H(3)···Cg(2)^{b}	3.011(4)	3.704(4)	132.50

Equivalent position codes: a = -x,1-y,1-z; b = -x,-1/2+y,1/2-z; Cg (2) = C(1), C(2), C(3), C(4), C(5), C(6); D, donor; A, acceptor; Cg, centroid.

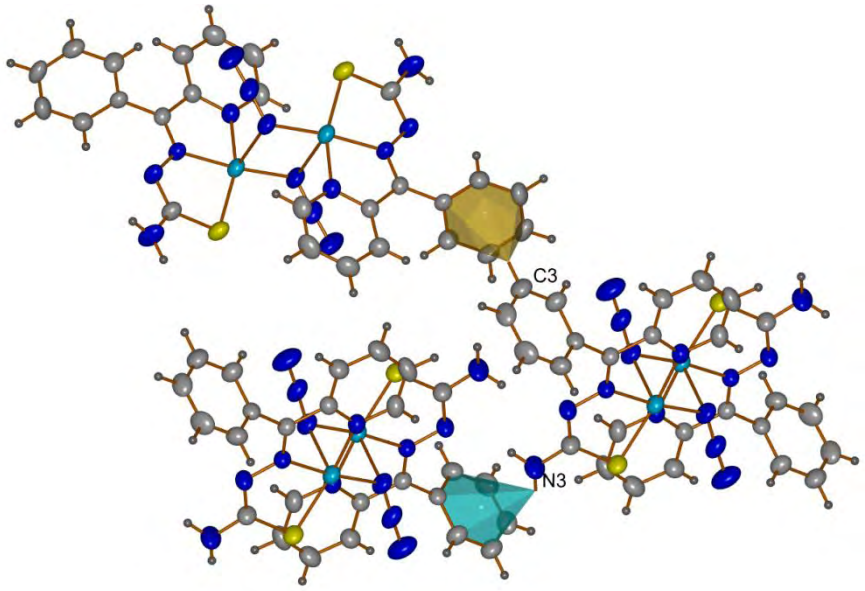

Fig. 3.19 C–H···π interactions of $[Cu(bptsc)\mu^{2}(N_3)]_2$ (**9**).

The packing diagram of the compound viewed along the 'a' and 'b' axis are shown in Figs. 3.20 and 3.21 respectively.

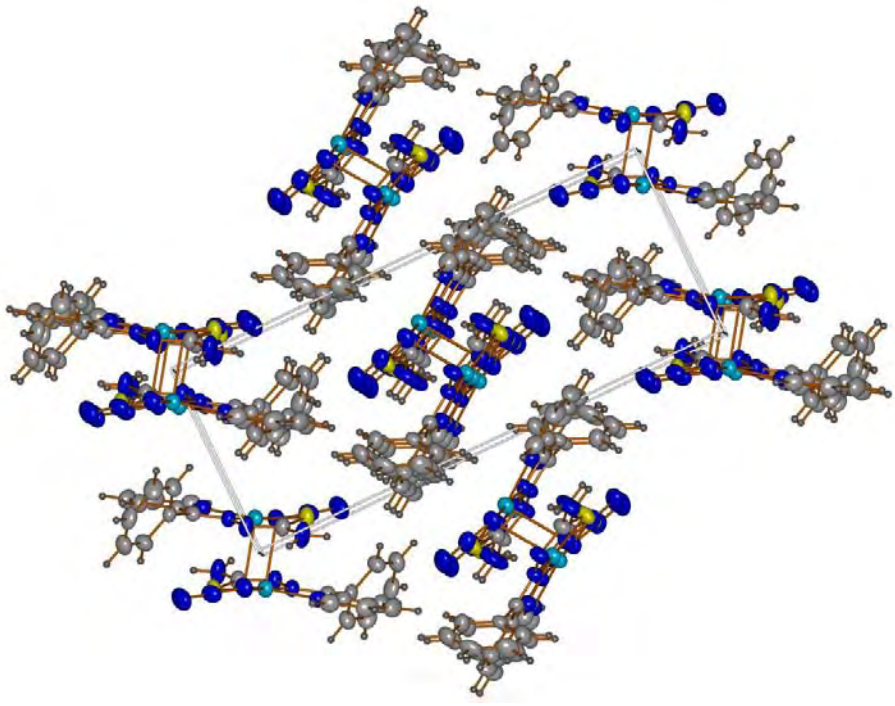

Fig. 3.20. Packing diagram of the compound viewed along the 'a' axis.

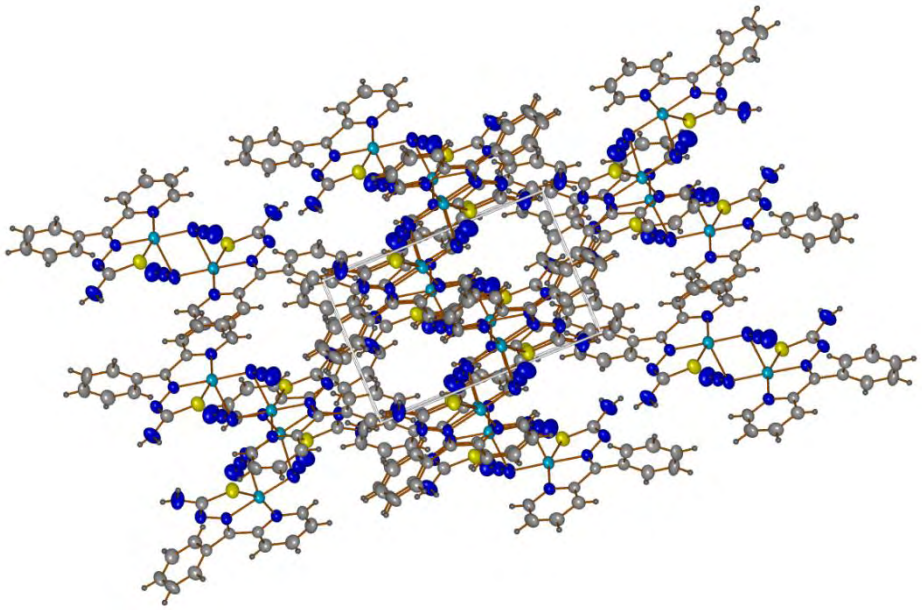

Fig. 3.21. Packing diagram of the compound viewed along the 'b' axis.

3.3.5. Crystal structure of complex [Cu(bpsc)(N_3)] (10)

The molecule crystallizes in triclinic space group $P\bar{1}$ with *E* configuration with respect to azomethine C=N double bond. Asymmetric unit contains two molecules with slightly different bond length and angles (Fig. 3.22). Metal center in the complex is four coordinate and has a distorted square planar geometry.

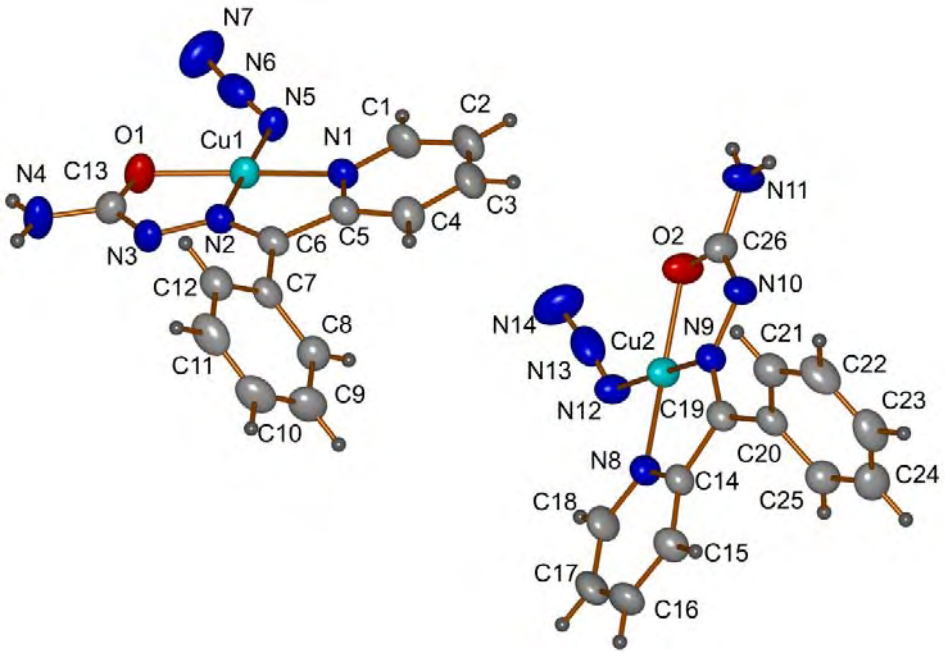

Fig. 3. 22. Asymmetric unit of compound [Cu(bpsc)(N_3)] (**10**).

The shorter Cu–$N_{azomethine}$ bond length indicates that the azomethine nitrogen coordinates more strongly than the pyridyl nitrogen [68]. The azido group has particularly a linear configuration with a N5–N6–N7 bond angle = 174.5(5) Å. The N5–N6 bond length of 1.122(5) Å is slightly larger than N6–N7 bond (1.202(6) Å). It coordinates to copper atom in a bend fashion as inferred from the Cu–N5–N6 bond angle 126.1(3)° (Table 3.10).

Table 3.10. Selected bond lengths [Å] and angles [°] for the two asymmetric units of [Cu(bpsc)(N_3)] (**10**)

Molecule 1		Molecule 2	
Bond lengths (Å)			
Cu1–O1	1.932(3)	Cu2–O2	1.931(3)
C13–O1	1.278(5)	C26–O2	1.276(5)
C13–N3	1.358(5)	C26–N10	1.359(5)
N3–N2	1.366(4)	N9–N10	1.367(4)
Cu1–N2	1.941(3)	Cu2–N9	1.942(3)
N1–Cu1	1.984(3)	N8–Cu2	1.983(3)
N5–Cu1	1.982(3)	N12–Cu2	1.980(3)
Bond angles (°)			
N5–Cu1–N1	97.29(14)	N8–Cu2–N12	97.11(14)
N5–Cu1–O1	100.94(13)	N12–Cu2–O2	101.06(13)
N2–Cu1–O1	80.60(13)	N9–Cu2–O2	80.43(13)
N2–Cu1–N1	81.01(13)	N9–Cu2–N8	81.24(13)

The packing of the molecules in the crystal lattice is reinforced by hydrogen bonding interactions (Table 3.11) and C–H···π interactions (Table 3.12). The adjacent units are interconnected through hydrogen bonding interactions (Fig. 3.23) N(4)–H(4B)···N(3)^a and N(11)–H(11B)···N(10)^b.

Table 3.11. Hydrogen bonding interactions in [Cu(bpsc)(N_3)] (**10**)

D–H···A	D–H (Å)	H···A (Å)	D···A (Å)	∠D–H···A (°)
N(4)–H(4B)···N(3)^a	0.8601	2.3052	3.150(5)	167.32
N(11)–H(11B)···N(10)^b	0.8602	2.3112	3.156(5)	167.40

Equivalent position codes: a = -x,1-y,2-z ; b= 3-x,-y,1-z.

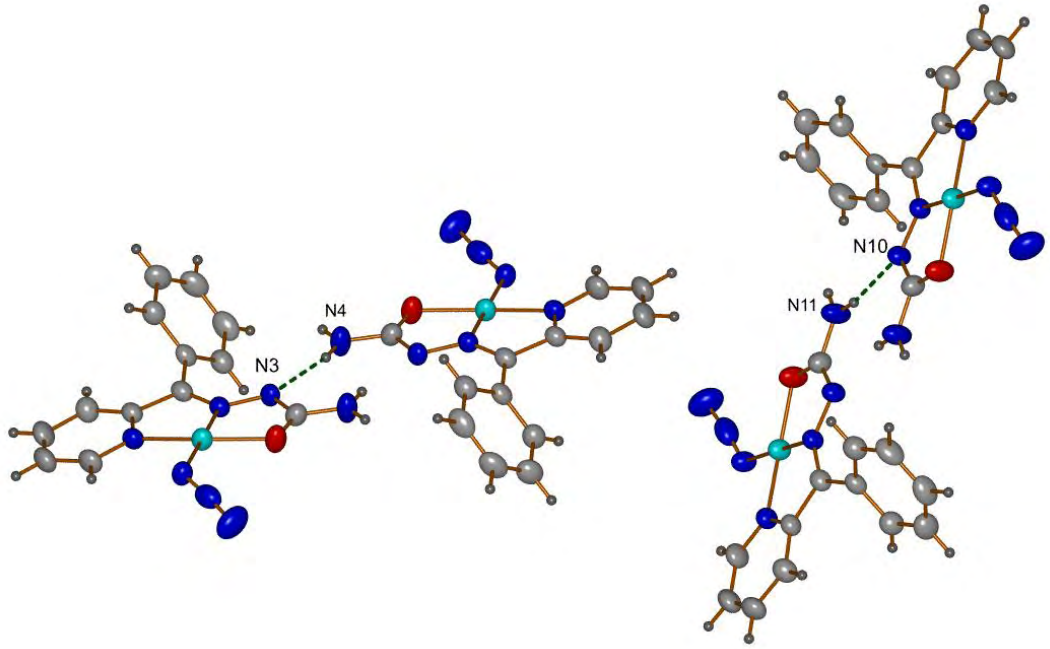

Fig. 3.23. Hydrogen bonding interactions of [Cu(bpsc)(N_3)] (**10**).

The C–H···Cg (π-ring) interactions (Fig. 3.24) involving Cg(1), Cg(2), Cg(3) and Cg(4) stabilize the packing in the unit cell.

Table 3.12. C–H···π interactions in [Cu(bpsc)(N_3)] (**10**)

X–H(I)···Cg(J)	H···Cg (Å)	X···Cg (Å)	∠X–H···Cg (°)
N(3)–H(3)···Cg(3)^{c}	3.0192	3.711(5)	132.43
C(9)–H(9)···Cg(2)^{d}	3.1205	3.898(5)	142.10
C(10)–H(10)···Cg(4)^{e}	3.0463	3.701(5)	128.77
C(16)–H(16)···Cg(4)^{f}	3.0097	3.703(5)	132.57
C(23)–H(23)···Cg(3)^{g}	3.0616	3.711(5)	128.36
C(24)–H(24)···Cg(1)^{h}	3.1301	3.907(5)	142.21

Equivalent position codes: c=1+x,y,z ; d=1-x,1-y,1-z ; e=1-x,-y,1-z ; f = -1+x,y,z ; g=2-x,-y,1-z ; h=2-x,1-y,1-z

Cg(1)= N(1), C(1), C(2), C(3), C(4), C(5) ; Cg (2) = N(8), C(14), C(15), C(16), C(17), C(18)

Cg(3)= C(7), C(8), C(9), C(10), C(11), C(12) ; Cg(4)= C(20), C(21), C(22), C(23), C(24), C(25)

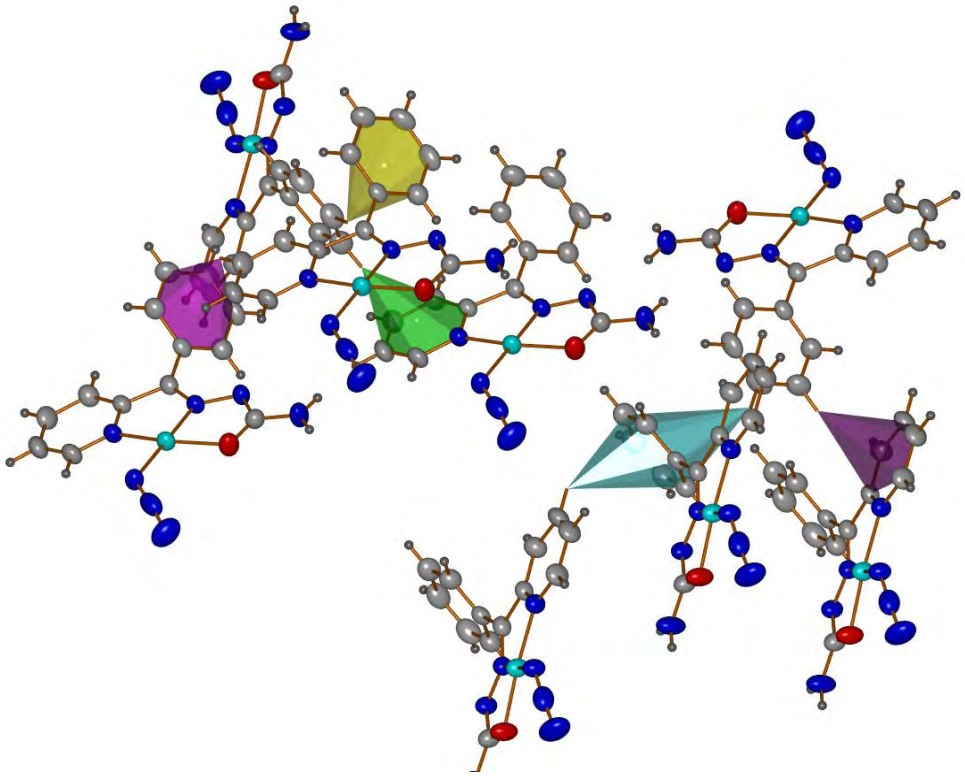

Fig. 3.24. C–H···π interactions in [Cu(bpsc)(N_3)] (**10**).

Packing diagrams of the molecule along 'a' and 'b' axes are shown in Figs. 3.25 and 3.26 respectively.

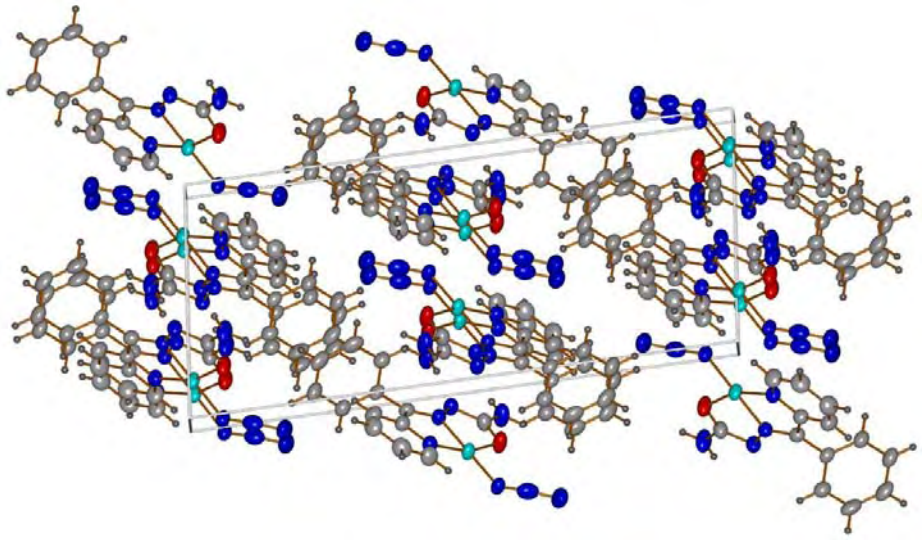

Fig. 3.25. The packing diagram of the molecule along 'a' axis.

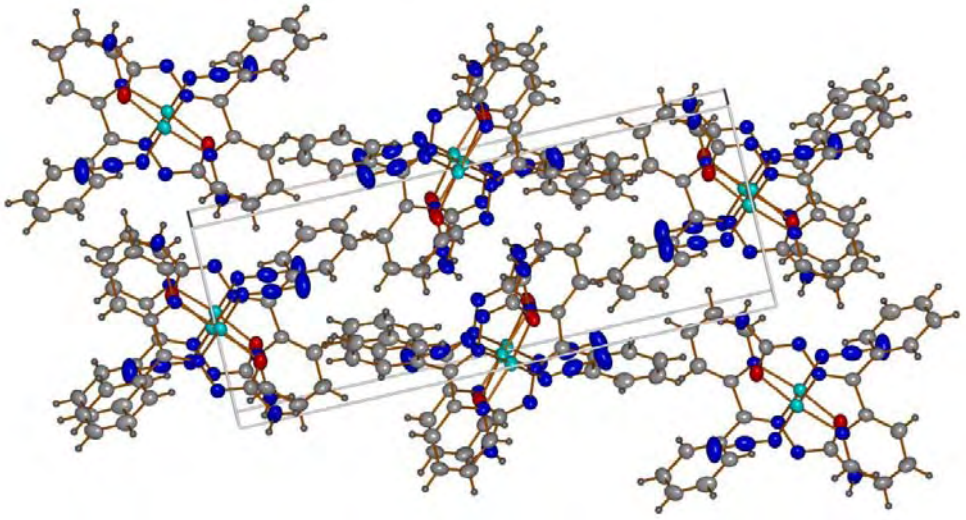

Fig. 3.26. The packing diagram of the molecule along 'b' axis.

3.3.6. Infrared spectral studies

The IR spectra of the compounds were recorded using KBr discs in range 4000-400 cm^{-1}. The characteristic IR bands of the complexes differ from their ligands and provide significant indications regarding the coordination and bonding sites. The significant IR bands with the tentative assignments of the copper(II) complexes are presented in Table 3.13.

The ν_a(NH) vibrations of the imino group is observed in the IR spectrum of ligand and this band disappears in the spectra of the complexes providing a strong evidence for the ligand coordination around copper(II) ion in the deprotonated form [69]. Coordination of azomethine nitrogen is consistent with the presence of a band at *ca*. 504-511 cm^{-1}, assignable to ν(Cu–N_{azo}) for these complexes [70,71]. The increase in ν(N–N) in the spectra of complexes in the range 1143-1154 cm^{-1} is due to enhanced double bond character through chelation, thus offsetting the loss of electron density *via* donation to the metal ion, and is supportive of azomethine coordination. Coordination of the pyridyl nitrogen causes the out of plane bending vibrational band shift from 601 cm^{-1} to higher frequencies [72].

Dinuclear azido complex [Cu(bptsc)$\mu^2(N_3)]_2$ (**9**) has a strong band at 2047 cm^{-1}, a medium band at 776 cm^{-1} and a weak band at 480 cm^{-1} corresponding to $\nu_{as}(N_3)$, $\nu_a(N_3)$ and $\delta(N_3)$ respectively [73]. The IR spectra of the complexes are shown in Figs. 3.27-3.30.

The strong ν(C=N) bands are found to be shifted to lower frequencies in the complexes indicating coordination via the azomethine nitrogen [74]. The coordination of this nitrogen is also supported by a shift in ν(N–N) to higher frequencies in the complexes. Observation of a very strong absorption band in 2000-2100 cm^{-1} is related to the coordination of azide ligand to the metal centers in these complexes [75]. This band is observed at 2046, 2046, 2047 and 2056 cm^{-1} for **7**, **8**, **9** and **10** respectively.

Table 3.13. IR spectral data of the Cu(II) azido complexes (cm^{-1})

Compounds	$\nu_a(N_3)$	$\nu_s(N_3)$	$\delta(N_3)$	ν(C=N)	ν(C=O)	ν(C=S)	ν(N–N)
$[Cu(dbsde)(N_3)]_n$ (**7**)	2046	1319	704	1634	-	-	-
$[Cu(bsde)(N_3)]_n$ (**8**)	2046	1322	704	1640	-	-	-
$[Cu(bptsc)\mu^2(N_3)]_2$ (**9**)	2047	1323	700	1596	1619	1323	1144
$[Cu(bpsc)(N_3)]$ (**10**)	2056	1320	700	1591	1624	-	1140

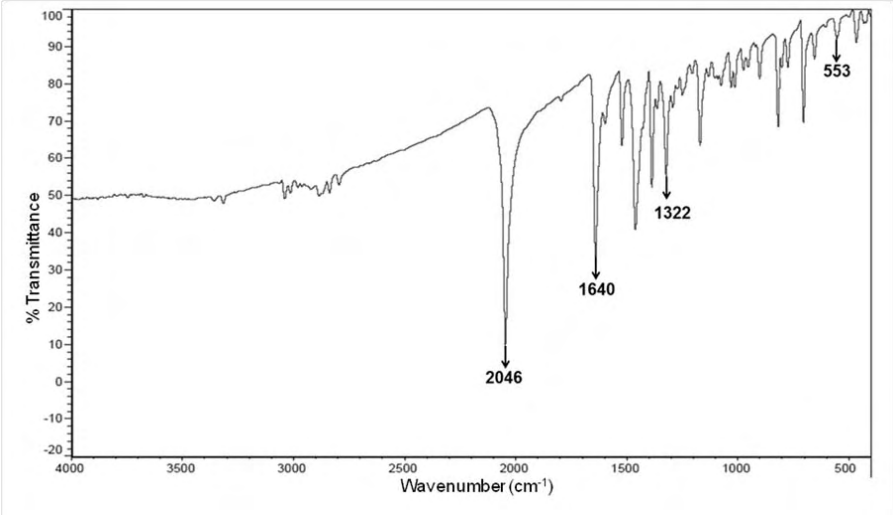

Fig. 3.27. IR spectrum of $[Cu(dbsde)(N_3)]_n$ (**7**).

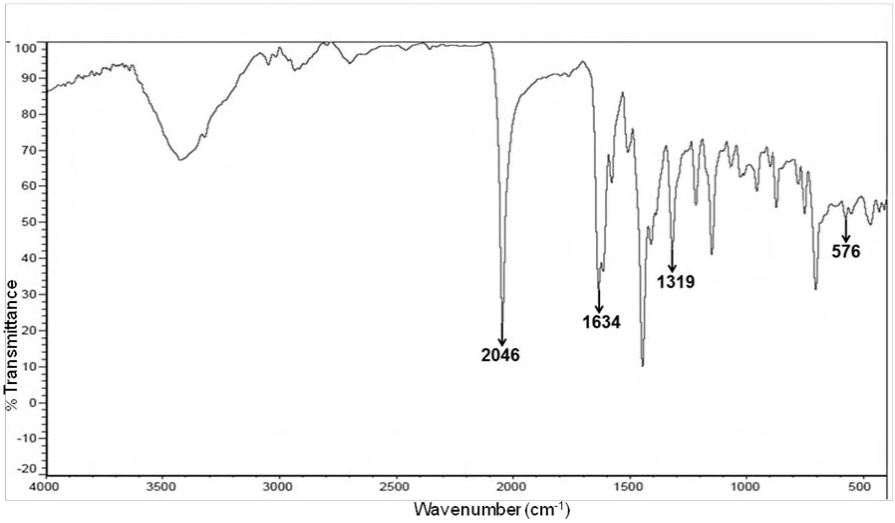

Fig. 3.28. IR spectrum of $[Cu(bsde)(N_3)]_n$ (**8**).

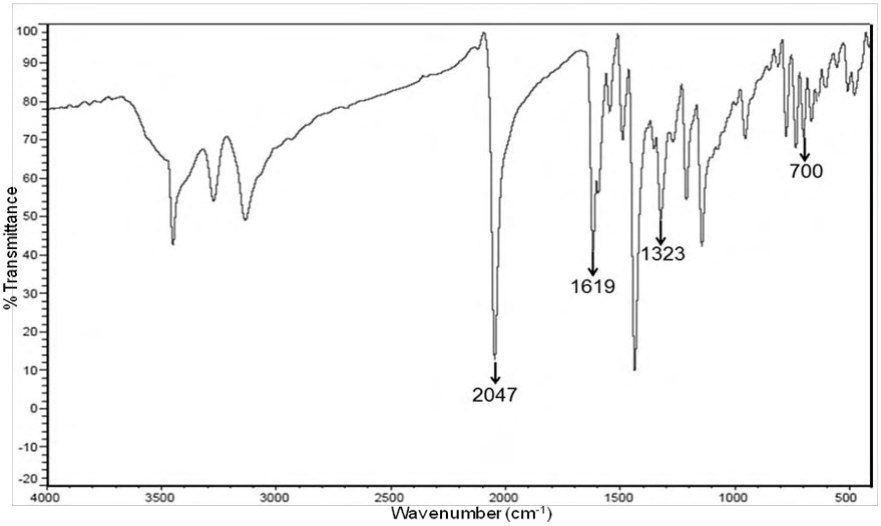

Fig. 3.29. IR spectrum of $[Cu(bptsc)\mu^2(N_3)]_2$ (**9**).

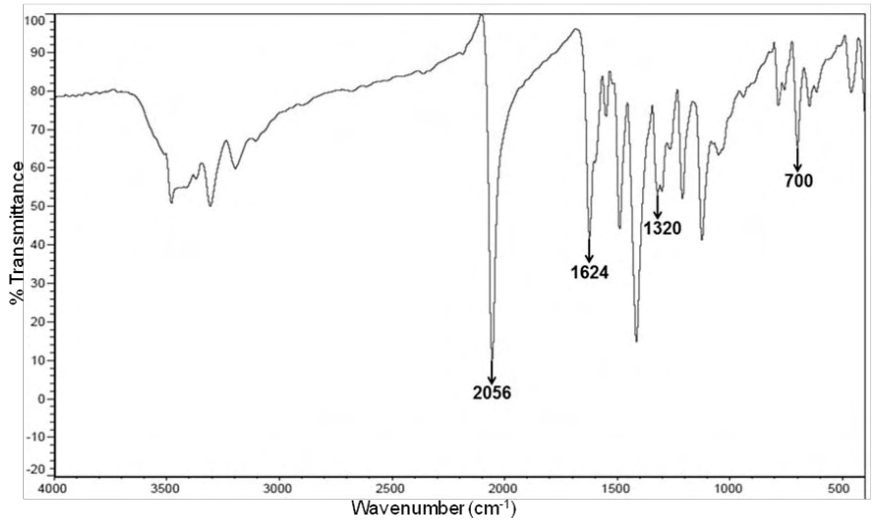

Fig. 3.30. IR spectrum of $[Cu(bpsc)(N_3)]$ (**10**).

3.3.7. Electronic spectral studies

The electronic spectral data of semicarbazones/Schiff base/thiosemicarbazone copper(II) complexes recorded in methanol solution are given in Table 3.14 and electronic spectra are shown in the Fig. 3.31-3.34. Bands in the region 28770-32200 cm^{-1} correspond to n-π* transitions of the amide function [76]. These intraligand transitions of the complexes are observed in the range 32290-28800 cm^{-1}, which undergoes shift upon complexation. This shift is may be due to the weakening of C=O bond and due to the donation of lone pair of electrons to the metal on complexation.

The high intense ligand-to-metal charge transfer (LMCT) transitions are observed at high energy region. The intensity of these transitions reflects the overlap of the ligand and metal orbitals involved in the charge transfer. In all the complexes LMCT transitions are observed in the region 22100-24050 cm^{-1} and which are assigned to O→ Cu and N→ Cu LMCT transitions. For a tetragonal field three spin allowed transitions, $^2A_{1g}\leftarrow{}^2B_{1g}$, $^2B_{2g}\leftarrow{}^2B_{1g}$ and $^2E_g\leftarrow{}^2B_{1g}$ are possible and square pyramidal complexes have the d_{yz}, $d_{xz}\leftarrow d_{x^2-y^2}$ and $d_{z^2}\leftarrow d_{x^2-y^2}$ transitions. But it is difficult to resolve them into separate bands due to the very low energy difference between these bands. All copper(II) complexes have very broad *d-d* combination bands (Fig. 3.31-3.34) in the range 14000-16000 cm^{-1} range [77,78].

Table 3.14. Electronic spectral assignments (cm^{-1}) for copper (II) azido complexes

Compounds	*d-d*	LMCT	n→π*/π→π*
$[Cu(dbsde)(N_3)]_n$ (**7**)	16200	26320	37100, 43250
$[Cu(bsde)(N_3)]_n$ (**8**)	15300	25750	36800, 43200, 47740
$[Cu(bptsc)\mu^2(N_3)]_2$ (9)	18600	24540	33740, 47610
$[Cu(bpsc)(N_3)]$ (**10**)	12860	26390	39570, 47290

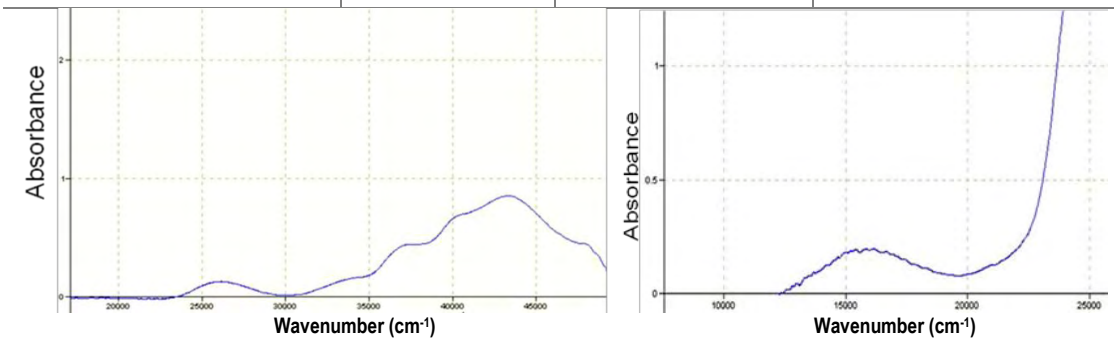

Fig. 3.31. Electronic spectra of $[Cu(dbsde)(N_3)]_n$ (**7**).

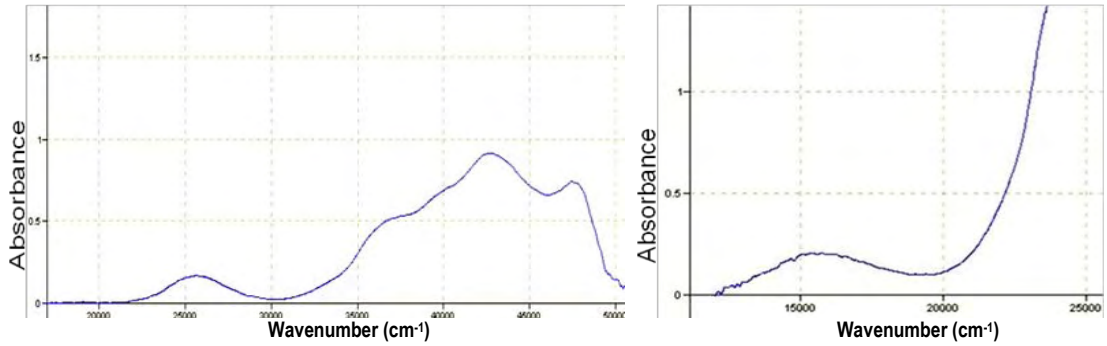

Fig. 3.32. Electronic spectra of $[Cu(bsde)(N_3)]_n$ (**8**).

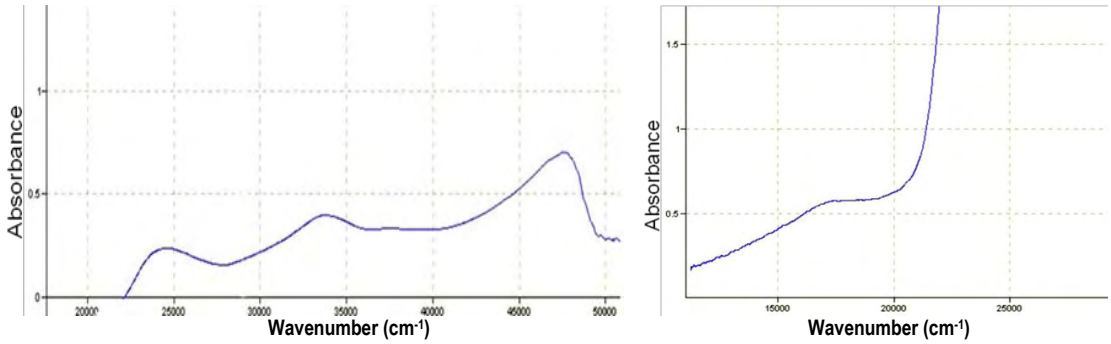

Fig. 3.33. Electronic spectra of $[Cu(bptsc)\mu^2(N_3)]_2$ (**9**).

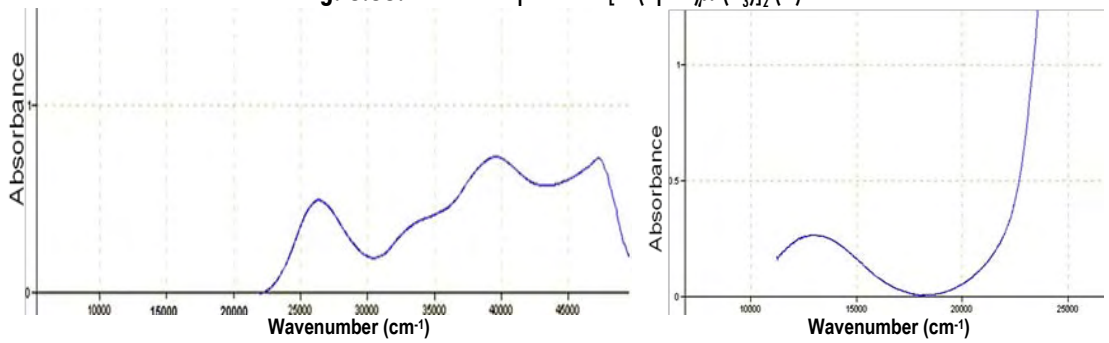

Fig. 3.34. Electronic spectra of $[Cu(bpsc)(N_3)]$ (**10**).

3.3.8. Electron paramagnetic resonance spectra

The magnetic parameters measured in EPR study are related to the structure of the paramagnetic complex, the number of ligands, nature of bonding and spatial arrangements of the ligands around the central metal ion. The copper(II) ion, with a d^9 configuration, has an effective spin of S = 1/2 and is associated with a spin angular momentum, m_s = ±1/2, leading to a doubly degenerate spin state in the absence of a magnetic field. In a magnetic field the degeneracy is lifted between these states and the energy difference between them is given by $\Delta E = h\nu = g\beta B$, where h is Planck's constant, ν is the microwave frequency for transition from m_s = +½ to m_s = -½, g is the Lande splitting factor

(equal to 2.0023 for a free electron), β is the Bohr magneton and B is the magnetic field. For the case of a $3d^9$ copper(II) ion, the appropriate spin Hamiltonian assuming a B_{1g} ground state is given by:

$$\hat{H} = \beta[g_{\|} B_a S + g_{\perp} (B_x S_x + B_y S_y)] + A_{\|} I_z S_z + A_{\perp}(I_x S_x + I_y S_y)$$

The EPR spectra of the polycrystalline samples at 298 K, DMF solution at 298 and 77 K were recorded in the X-band, using 100-kHz modulaton; *g* factors were quoted relative to the standard marker TCNE (g = 2.00277). The EPR spectra of the complexes recorded in polycrystalline state at room temperature provide information about the coordination environment around copper(II) in these complexes. The EPR spectra of the compounds **7-10** were recorded. The EPR parameters of the copper(II) complexes are presented in the Table 3.15.

Table 3.15. Spin Hamiltonian and bonding parameters of the complexes

	$[Cu(dbsde)(N_3)]_n$ (**7**)	$[Cu(bsde)(N_3)]_n$ (**8**)	$[Cu(bptsc)\mu^2(N_3)]_2$ (**9**)	$[Cu(bpsc)(N_3)]$ (**10**)
	Polycrystalline state at 298 K			
$g_{\|\|}$	2.188	2.203	$g_1 = 2.149$, $g_2 = 2.077$	2.206
$g_{\perp}$	2.069	2.069	$g_3 = 2.034$	2.061
g_{isc}/g_{rv}	2.109	2.114	2.087	2.109
G	2.784	3.013	2.864	3.495
	Solution state at 77 K			
$g_{\|\|}$	2.169	2.199	2.168	2.239
$g_{\perp}$	2.010	2.053	1.990	2.061
$A_{\|\|}$	0.0169	0.0205	19.73	18.16
α^2	0.676	0.828	0.759	0.829
β^2	0.918	0.838	0.890	0.818
γ^2	0.394	0.851	0.387	0.815
$K_{\|\|}$	0.621	0.694	0.676	0.678
$K_{\perp}$	0.267	0.704	0.294	0.675

The compounds $[Cu(dbsde)(N_3)]_n$ (**7**), $[Cu(bsde)(N_3)]_n$ (**8**), $[Cu(bptsc)\mu^2(N_3)]_2$ (**9**) and $[Cu(bpsc)(N_3)]$ (**10**) in the polycrystalline state at 298 K show axial spectra with well defined $g_{\|}$ and $g_{\perp}$ features (Figs. 3.35-3.38). The variation in the $g_{\|}$ and $g_{\perp}$ values indicate that the geometry of the compounds in the solid state is affected by the

nature of coordinating gegenions. For these complexes, the $g_{\|} > g_{\perp} > 2.0023$ and *G* values falling within the range 2.1-3.8 are consistent with a $d_{x^2-y^2}$ ground state. The geometric parameter *G* which is a measure of the exchange interaction between copper centers in the polycrystalline compound is calculated using the equation, $G = (g_{\|} - 2.0023)/ g_{\perp} - 2.0023)$. *G* values < 4.4 are consistent with a $d_{x^2-y^2}$ ground state having small exchange coupling [79]. If *G*>4, exchange interaction is negligible [80,81]. For these complexes, the $g_{\|} > g_{\perp} > 2.0023$ and *G* values falling within the range 2.1-3.8 are consistent with a $d_{x^2-y^2}$ ground state.

The spectrum of the compound $[Cu(bptsc)\mu^2(N_3)]_2$ (**9**) in the polycrystalline state at 298 K shows typical rhombic feature with three *g* values g_1, g_2 and g_3 (Fig. 3.37). without any hyperfine and superhyperfine lines.

The EPR spectra of the four coordinate copper(II) complex $[Cu(bpsc)(N_3)]$ **(10)** in DMF at 77 K (Fig. 3.38) show resolved four copper hyperfine lines. The expected superhyperfine splitting of nitrogen atoms are not observed here also. The $g_{\|} > g_{\perp}$ suggests a square planar geometry for these complexes.

The $g_{\|}$ values are nearly the same for all the complexes indicating that the bonding is dominated by the semicarbazone moiety. In all the complexes, $g_{\|} > g_{\perp} > 2.0023$. The fact that $g_{\|}$ values are less than 2.3 is an indication of significant covalent character to the M–L bond [82,83].

The EPR parameters $g_{\|}$, $g_{\perp}$, $A_{\|}$(Cu) and the energies of d-d transitions were used to evaluate the bonding parameters α^2, β^2 and γ^2 which may be regarded as measures of the covalency in the in-plane σ-bonds, in-plane π-bonds and out-of-plane π-bonds. The value of in-plane σ-bonding parameter α^2 estimated from the expression,

$$\alpha^2 = -A_{\|} / 0.036+(g_{\|} -2.0023)+ 3/7(g_{\perp} - 2.0023)+ 0.04 \text{ [84,85]}$$

The following simplified parameters were used to evaluate the bonding parameters [86],

$$K_{\|}^2 = (g_{\|} - 2.0023)\, E_{d\text{-}d} / 8\lambda_o$$

$$K_{\perp}^2 = (g_{\perp} - 2.0023)\, E_{d\text{-}d} / 2\lambda_o$$

Where $K_{\|}^2 = \alpha^2 \beta^2$ and $K_{\perp}^2 = \alpha^2 \gamma^2$, $K_{\|}$ and $K_{\perp}$ are orbital reduction factors and λo represents the one electron spin orbit coupling constant which equals -828 cm^{-1}.

Hathaway has pointed out that, for pure sigma bonding, $K_{\|} \approx K_{\perp} \approx 0.77$, and for in plane π-bonding, $K_{\|} < K_{\perp}$, while for out-of-plane π-bonding $K_{\perp} < K_{\|}$. In all complexes, it is observed that $K_{\|} < K_{\perp}$ which indicates the presence of significant in-plane π bonding. Furthermore α^2, β^2 and γ^2 have values less than 1.0, which is expected for 100% ionic character of the bonds and become smaller with increasing covalent character. Therefore, the evaluated values α^2, β^2 and γ^2 of the complexes are consistent with both strong in-plane σ- and in-plane π-bonding.

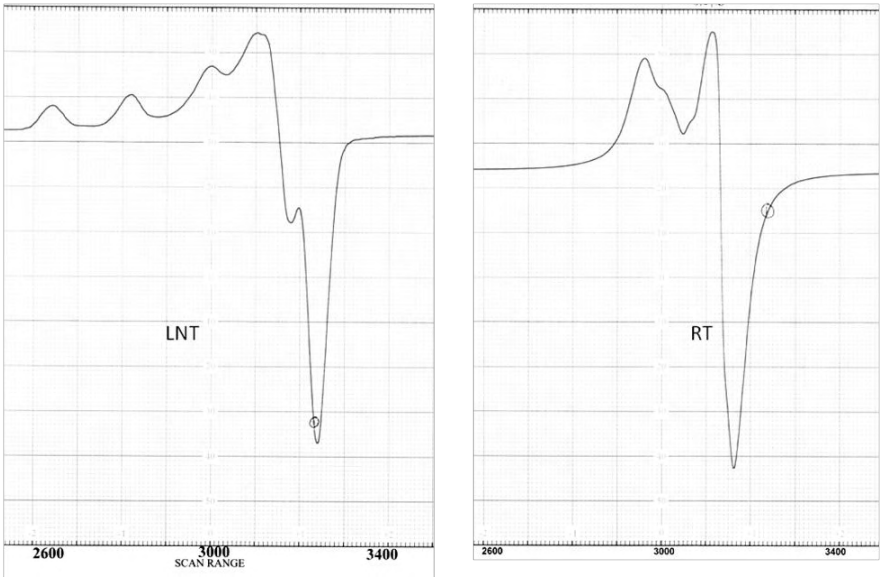

Fig. 3.35. The EPR spectra of the complex $[Cu(dbsde)(N_3)]_n$ (**7**).

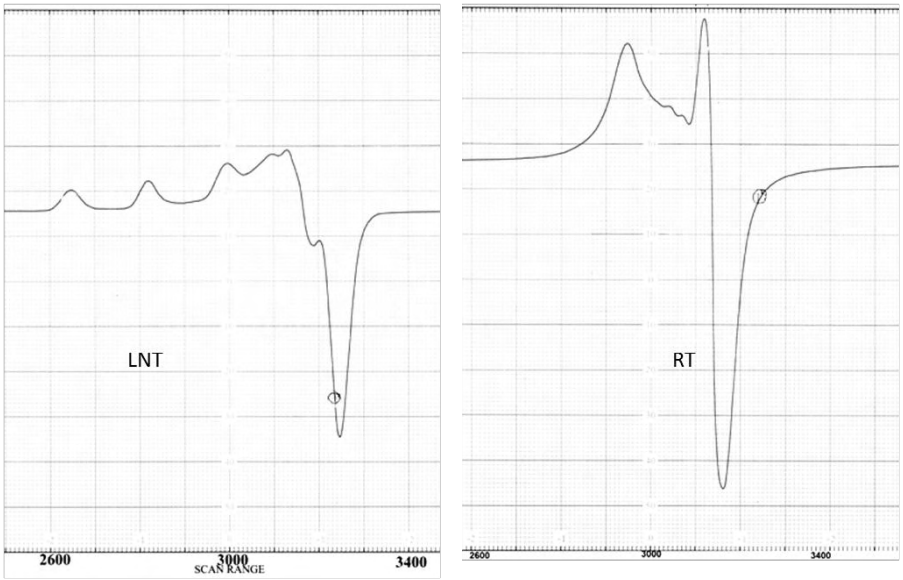

Fig. 3.36. The EPR spectra of the complex $[Cu(bsde)(N_3)]_n$ (**8**).

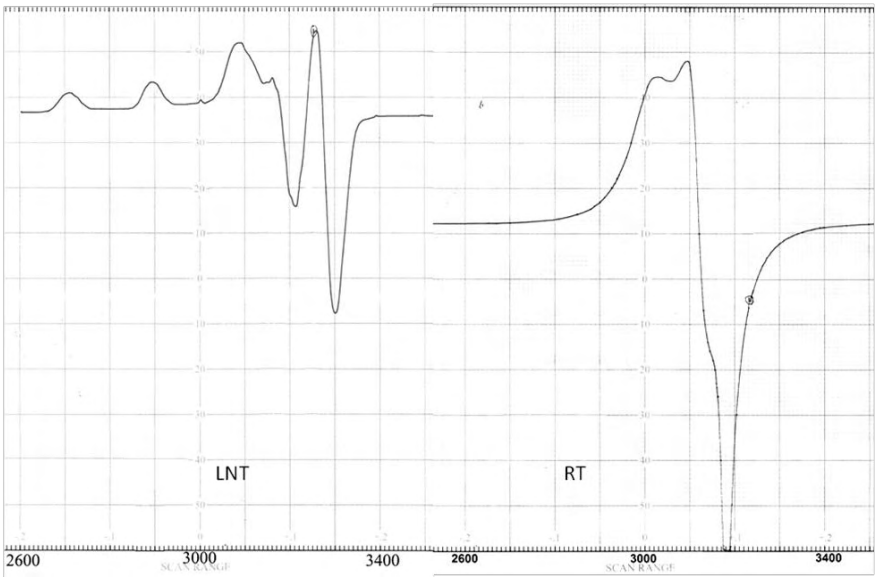

Fig. 3.37. The EPR spectra of the complex $[Cu(bptsc)\mu^2(N_3)]_2$ (**9**).

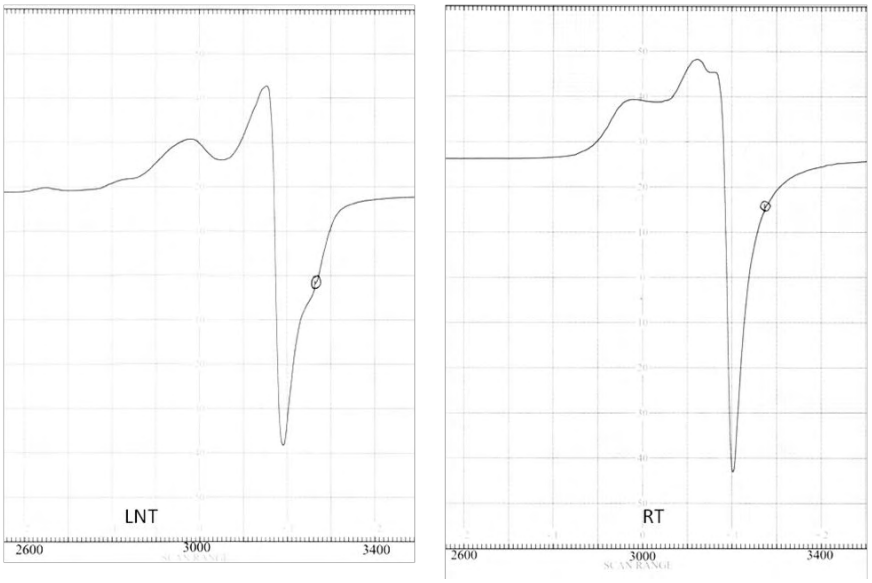

Fig. 3.38. The EPR spectra of the complex $[Cu(bpsc)(N_3)]$ (**10**).

REFERENCES

1. S. Sasmal, S. Sarkar, N.A. Alcalde, S. Mohanta. Inorg. Chem. 2011, 50, 5687.
2. Z.- G. Gu, Y.-F. Xu, X.-J. Yin, X.-H. Zhou, J.-L. Zuo, X.-Z. Youa, Dalton Trans., 2008, 5593.
3. A.M. Madalan, M. Noltemeyer, M. Neculai, H.W. Roesky, M. Schmidtmann, A. Muller, Y. Journaux, M. Andruh, Inorg. Chim. Acta, 2006, 359, 459.
4. S. Koner, S. Saha, T.Mallah, K.-I Okamoto, Inorg. Chem., 2004, 43, 840.

5. S. Mukherjee, B. Gole, R. Chakrabarty, P.S. Mukherjee, Inorg. Chem., 2009, 48, 11325.
6. P.S. Mukherjee, T.K. Maji, A Escuer, R. Vicente, J. Ribas, G. Rosair, F.A. Mautner,
N.R. Chaudhuri, Eur. J. Inorg. Chem., 2002, 943.
7. J. Ribas, M. Monfort, I. Resino, X. Solans, P. Rabu, F. Maingot, M. Drillon, Angew. Chem. Int. Ed. Engl., 1996, 35, 2671.
8. C.G. Pierpont, D.N. Hendrickson, D.M. Duggan, F. Wanger, E.K. Barefield, Inorg. Chem., 1975, 14, 604.
9. A. Escuer, R. Vicente, J. Ribas, M.S. El Fallah, X. Solans, Inorg. Chem., 1993, 32, 1033.
10. P. Chaudhuri, M. Guttmann, D. Ventur, K. Weighardt, B. Nuber, J. Weiss, J. Chem. Soc., Chem. Commun. 1985, 1618.
11. M.I. Arriortua, A.R. Cortes, L. Lezema, T. Rojo, X. Solans, Inorg. Chim. Acta, 1990, 174, 263.
12. S.S. Tandon, L.K. Thompson, M.E. Manuel, J.N. Bridson, Inorg. Chem., 1994, 33, 5555.
13. R. Hoffmann, P.J. Hay, J.C. Thibeault, J. Am. Chem. Soc., 1975, 97, 4884.
14. J. Ribas, A. Escuer, R. Vicente, M.S. El Fallah, X. Solans, M. Font-Bardia, Inorg. Chem., 1993, 32, 3727.
15. K. Nakamoto, Infrared and Raman spectra of Inorganic and Coordination compounds; 3rd Ed.; John Wiley & Sonns, Inc.: New York, 1997, 270.
16. G.E. Kostakis, A.K. Powell, Coord. Chem. Rev., 2009, 253, 2686.
17. M.A.S. Goher, F.A. Mautner, Polyhedron, 1995, 14, 1439.
18. M. Zbiri, S. Saha, C. Adhikary, S. Chaudhuri, C. Daul, S. Koner, Inorg. Chim. Acta 2006, 359, 1193.
19. O. Kahn, S. Sikorav, J. Gouteron, S. Jeannin, Y. Jeannin, Inorg. Chem., 1983, 22, 2877.
20. J. Comarmond, P. Plumere, J.M. Lehn, Y. Agnus, R. Louis, R. Weiss, O. Kahn, I. Morgesten-Badarau, J. Am. Chem. Soc., 1982, 104, 6330.

21. B. Chaitali, G.B. Michael Drew, E. Ruiz, M. Estrader, C. Diazd, A. Ghosh. Dalton Trans., 2010, 39, 7474.
22. M.M. Turnbull, T. Sugimoto, L.K. Thompson, Molecule-Based Magnetic Materials; Theory, Techniques, and Applications; American Chemical Society: Washington, DC, 1996, 644.
23. G. Christou, D. Gatteschi, D.N. Hendrickson, R. Sessoli, MRS Bull., 2000, 25, 66.
24. J.S. Miller, M. Drillon, Magnetism: Molecules to Materials; Wiley: Weinheim, Germany, 2001.
25. W. Wernsdorfer, R. Sessoli, Science, 1999, 284, 133.
26. E.K. Brechin, C. Boskovic, W. Wernsdorfer, J. Yoo, A. Yamaguchi, E.C. Sanudo, T.R. Concolino, A.L. Rheingold, H. Ishimoto, D.N. Hendrickson, G. Christou, J. Am. Chem. Soc., 2002, 124, 9710.
27. J.R. Friedman, M.P. Sarachik, J. Tejada, J. Maciejewski, R.J. Ziolo, Appl. Phys., 1996, 79, 6031.
28. A. Caneschi, D. Gatteschi, N. Lalioti, C. Sangregorio, R. Sessoli, G. Ventiru, A. Vendigni, A. Retoori, M.G. Pini, M.A. Novak, Angew. Chem., Int. Ed. 2001, 40, 1760.
29. N. Aliaga-Alcalde, R.S. Edwards, S.O. Hill, W. Wernsdorfer, K. Folting, G.J. Christou, Am. Chem. Soc., 2004, 126, 12503.
30. N.E. Chakov, W. Wernsdorfer, K.A. Abboud, G. Christou, Inorg. Chem., 2004, 43, 5919.
31. M. Ferbinteanu, H. Miyasaka, W. Wernsdorfer, K. Nakata, K. Sugiura, M. Yamashita, C. Coulon, R.J. Clerac, Am. Chem. Soc., 2005, 127, 3090.
32. J.-P. Renard, L.-P. Regnault, M. Verdaguer. Magnetism: Molecules and Materials, Wiley-VCH, Weinheim, 2001, 49.
33. A. Caneschi, D. Gatteschi, N. Lalioti, C. Sangregorio, R. Sessoli, G. Venturi, A. Vindigni, A. Rettori, M.G. Pini, M.A. Novak. Angew. Chem. Int. Ed. Engl. Engl., 2001, 40, 1760.
34. Y. Xie, Q. Liu, H. Jiang, C. Du, X. Xu, M. Yu, Y. Zhu. New J. Chem., 2002, 26, 176.

35. F. Meyer, H. Pritzkow. Inorg. Chem. Commun., 2001, 4, 305.

36. (a) J.-M. Lehn, Supramolecular Chemistry: Concepts and Perspectives, VCH, Weinheim, Germany, 1995. (b) M. Fujita, Molecular Self-Assembly Organic versus Inorganic Approaches, Structure and Bonding, Springer-Verlag, Berlin, Germany, 2000, 96. (c) G. R. Desiraju, C.V.K. Sharma, Perspectives in Supramolecular Chemistry, Wiley, Chichester, 1995.

37. (a) D. Imbert, M. Cantuel, J.-C.G. Bunzli, G. Bernardinelli, C. Piguet, J. Am. Chem. Soc., 2003, 125, 15698. (b) T. Nakano, Y. Okamoto, Chem. Rev., 2001, 101, 4013.

38. (a) R.-G. Xiong, J.-L. Zuo, X.-Z. You, F. B. Abrahams, Z.-P. Bai, C.-M. Che, H.-K. Fun, Chem. Commun., 2000, 2061. (b) S. Zang, Y. Su, Y. Li, Z. Ni, Q. Meng, Inorg. Chem., 2006, 45, 174. (c) Y.-Z. Tang, X.-F. Huang, Y.-M. Song, P. W. H. Chan and R.-G. Xiong, Inorg. Chem., 2006, 45, 4868.

39. (a) Y. Gong, W. Tang, W. Hou, Z. Zha, C. Hu, Inorg. Chem., 2006, 45, 4987. (c) D. Ghoshal, T. K. Maji, T. Mallah, T.-H. Lu, G. Mostafa, N. Ray Chaudhuri, Inorg. Chim. Acta, 2005, 358, 1027.

40. (a) D.M. Bassani, J.-M. Lehn, G. Baum, D. Fenske, Angew. Chem., Int. Ed. Engl., 1997, 36, 1845. (b) P.N.W. Baxter, H. Sleiman, J.-M. Lehn, K. Rissanen, Angew. Chem. Int. Ed. Engl., 1997, 36, 1297.

41. (a) D. Ghoshal, A.D. Jana, T.K. Maji, G. Mostafa, Inorg. Chim. Acta, 2006, 359, 690. (b) M.-S. Wang, G.-C. Guo, M.-L. Fu, L. Xu, L.-Z. Cai, J.-S. Huang, Dalton Trans., 2005, 2899.

42. (a) Y.-S. Yoo, J.-H. Choi, J.-H. Song, N.-K. Oh, W.C. Zin, S. Park, T. Chang, M. Lee, J. Am. Chem. Soc., 2004, 126, 6294. (b) S.A. Dalrymple, M. Parvez, G.K.H. Shimizu, Inorg. Chem., 2002, 41, 6987.

43. A. Christensen, C. Mayer, F. Jensen, A.D. Bond, C.J. McKenzie, Dalton Trans., 2006, 108.

44. (a) C. Goze, J.-C. Chambron, V. Heitz, D. Pomeranc, X.J. Salom- Roig, J.-P. Sauvage, A.F. Morales, F. Barigelletti, Eur. J. Inorg. Chem., 2003, 3752. (b) H.-T. Zhang, Y.-Z. Li, H.-Q. Wang, E.N. Nfor, X.-Z. You, Cryst. Eng. Comm., 2005, 7, 578.

45. M. Albrecht, Chem. Rev., 2001, 101, 3457.

46. S.R. Halper, S.M. Cohen, Angew. Chem., Int. Ed., 2004, 43, 2385.

47. (a) D.A. Beauchamp, S.J. Loeb, Chem. Commun., 2002, 2484. (b) A. Jouaiti, M.W. Hosseini, N. Kyritsakas, Chem. Commun., 2003, 472. (c) P. Grosshans, A. Jouaiti, V. Bulach, J.-M. Planeix, M.W. Hosseini, J.-F. Nicoud, Chem. Commun., 2003, 1336.

48. (a) H. Imai, K. Inoue, K. Kikuchi, Y. Yoshida, M. Ito, T. Sunahara, S. Onaka, Angew. Chem., Int. Ed., 2004, 43, 5618. (b) N. Giuseppone, J.-L. Schmitt, J.-M. Lehn, Angew. Chem., Int. Ed., 2004, 43, 4902. (c) L. Han, M. Hong, R. Wang, J. Luo, Z. Lin, D. Yuan, Chem. Commun., 2003, 2580. (d) M. Cantuel, G. Bernardinelli, G. Muller, J.P. Riehl, C. Piguet, Inorg. Chem., 2004, 43, 1840. (e) C.-D. Wu, C.-Z. Lu, S.-F. Lu, H.-H. Zhuang, J.-S. Huang, Dalton Trans., 2003, 3192.

49. (a) L.J. Childs, N.W. Alcock, M.J. Hannon, Angew. Chem., Int. Ed., 2001, 40, 1079. (b) J.-M. Lehn, A. Marquis-Rigault, Angew. Chem., Int. Ed. Engl., 1988, 27, 1095. (c) D.M. Bassani, J.-M. Lehn, G. Baum, D. Fenske, Angew. Chem., Int. Ed., 1997, 36, 1845. (d) C. Piguet, G. Bernardinelli, G. Hopfgartner, Chem. Rev., 1997, 2005.

50. (a) V. Balamurugan, R. Mukherjee, Cryst. Eng. Comm., 2005, 7, 337. (b) S. Khatua, H. Stoeckli-Evans, T. Harada, R. Kuroda, M. Bhattacharjee, Inorg. Chem., 2006, 45, 9619. (c) V. Berl, I. Huc, R. G. Khoury, J.-M. Lehn, Chem. Eur. J., 2001, 7, 2810. (d) C.C.A. Fraser, D.J. Eisler, M.C. Jennings, R.J. Puddephatt, Chem. Commun., 2002, 1224. (e) I. Odriozola, N. Kyristsakas, J.-M. Lehn, Chem. Commun., 2004, 62.

51. (a) X.-M. Chen, G.-F. Liu, Chem. Eur. J., 2002, 8, 4811; (b) T.B. Norsten, R. McDonald, N.R. Brand, Chem. Commun., 1999, 719.

52. SMART and SAINT, Area Detector Software Package and SAX Area Detector Integration Program, Bruker Analytical X-ray; Madison, WI, USA, 1997.

53. SADABS, Area Detector Absorption Correction Program; Bruker Analytical X-ray; Madison, WI, 1997.

54. L.J. Farrugia, J. Appl. Cryst., 2012, 45, 849.

55. K. Brandenburg, Diamond Version 3.2g, Crystal Impact GbR, Bonn, Germany, 2010.

56. W.J. Geary, Coord. Chem. Rev., 1971, 7, 81.

57. D.X. West, J.K. Swearingen, Transition Met. Chem., 2001, 26, 260.

58. (a) E.-Q. Gao, S.-Q. Bai, C.-F. Wang, Y.-F. Yue, C.-H. Yan, Inorg. Chem., 2003, 42, 8456. (b) E.-Q. Gao, Y.-F. Yue, S.-Q. Bai, Z. He, C.-H. Yan, Cryst. Growth Des., 2005, 5, 1119. (c) H.-R. Wen, J.-L. Zuo, W. Liu, Y. Song, X.-Z. You, Inorg. Chim. Acta, 2005, 358, 2565. (d) C.-Y. Wang, J. Coord. Chem., 2009,62, 2860. (e) J. Carranza, J. Sletten, F. Lloret, M. Julve, J. Mol. Struct., 2008, 890, 31.

59. (a) M.S. Ray, A. Ghosh, R. Bhattacharya, G. Mukhopadhyay, M.G.B. Drew, J. Ribas, Dalton Trans., 2004, 252. (b) S.-Q. Bai, E.-Q. Gao, Z. He, C.-J. Fang, C.-H. Yan, New J. Chem., 2005, 29, 935. (c) K. Matsumoto, S. Ooi, K. Nakatsura, W. Mori, S. Suzuki, A. Nakahara, Y. Nakao, J. Chem. Soc. Dalton Trans., 1985, 2095.(d) J.P. Costés, F. Dahan, J. Ruiz, J.P. Laurent, Inorg. Chim. Acta, 1995, 239, 53. (e) X.-Z. Li, L.-N. Zhu, C.-Q. Li, D.-Z. Liao, Inorg. Chem. Commun., 2006, 9, 1297. (f) J. Lin, Z. Shen, Y. Song, H.-J. Xu, Y.-Z. Li, X.-Z. You, Inorg. Chim. Acta, 2005, 358, 1963. (g) S. Sen, S. Mitra, D.L. Hughes, G. Rosair, C. Desplanches, Polyhedron, 2007, 26, 1740.

60. (a) C. Biswas, M.G.B. Drew, E. Ruiz, M. Estrader, C. Diaz, A. Ghosh, Dalton Trans., 2010, 39, 7474. (b) S. Naiya, C. Biswas, M.G.B. Drew, C.J.G. Garcia, J.M.C. Juan, A. Ghosh, Inorg. Chem., 2010, 49, 6616. (c) S. Sasmal, S. Sarkar, N.A. Alcalde, S. Mohanta, Inorg. Chem., 2011, 50, 5687.

61. L. Han, M. Hong, Inorg. Chem. Commun., 2005, 8, 406.

62. H. Masui, Coord. Chem. Rev. 2001, 957, 219.

63. B.-H. Ye, B. -B Ding, Y.-Q. Weng, X.-M. Chen, Cryst. Growth Des., 2005, 5, 801.

64. (a) S. Decurtins, H.W. Schmalle, P. Schneuwly, J. Ensling, P. Gutlich, J. Am. Chem. Soc., 1994, 116, 9251. (b) E. Coronado, J.R. Galan-Mascaros, C.J. Gomez-Garcia, J.M. Martinez- Agudo, Inorg. Chem., 2001, 40, 1331. (c) C.Y. Su, B.S. Kang, Q.C. Yang, T.C.W. Mak, J. Chem. Soc., Dalton Trans., 2000,

1857. (d) R. Custelcean, M. E. Ward, Cryst. Growth Des. 2005, 5, 2277. (e) B. Kesanli, W. Lin, Coord. Chem. Rev., 2003, 246, 305. (f) I. Katsuki, Y. Motoda, Y. Sunatsuki, N. Mastumoto, M. Kojima, J. Am. Chem. Soc., 2002, 124, 629.

65. L. Han, M. Hong, Inorg. Chem. Commun., 2005, 8, 406.
66. (a) A. Ray, S. Banerjee, R.J. Butcher, C. Desplanches, S. Mitra, Polyhedron, 2008, 27, 2409. (b) Y.F. Wu, D.R. Zhu, Y. Song, K. Shen, Z. Shen, X. Shen, Y. Xu, Chem. Commun., 2009, 12, 959.(c) C. Adhikary, D. Mal, R. Sen, B.B. Ashis, P. Gutlich, S. Chaudhuri, S. Koner, Polyhedron, 2007, 26, 1658.
67. V.A. Sawant, B.A. Yamgar, S.K. Sawant, S.S. Chavan, Spectrochim. Acta, Part A, 2009, 74, 1100.
68. D.X. West, J.K. Swearingen, J. Vades-Martinez, S. Hernandez-Ortega, A.K. El-Sawaf, F.V. Meurs, A. Castineiras, I. Garcia, E. Bermejo, Polyhedron, 1999, 18, 2919.
69. J. Jezierska, B. Jezowska-Trzebiatowska, G. Petrova, Inorg. Chim. Acta, 1981, 50, 153.
70. B.S. Garg, M.R.P. Kurup, S.K. Jain, Y.K. Bhoon, Transition Met. Chem., 1988, 13, 247.
71. P.B. Sreeja, M.R.P. Kurup, Spectrochim. Acta, Part A, 2005, 61, 331.
72. V. Philip, V. Suni, M.R.P. Kurup, Polyhedron, 2006, 25, 1931.
73. A.B.P. Lever, E. Mantovani, B.S. Ramaswami, Can. J. Chem., 1971, 49, 1957.
74. (a) T.A. Reena, E.B. Seena, M.R. Kurup, Polyhedron, 2008, 27, 1825. (b) S. Basak, S. Sen, C. Marrschner, J. Baumgartner, S.R. Batten, D.R. Turner, S. Mitra, Polyhedron, 2008, 27, 1193.
75. (a) W.-W. Sun, X.-B. Qian, C.-Y. Tian, E.-Q. Gao, Inorg. Chem. Acta, 2009, 362, 2744.
76. C.R.K. Rao, P.S. Zacharias, Polyhedron, 1997, 16, 1201.
77. R.P. John, A. Sreekanth, V. Rajakannan, T.A. Ajith, M.R.P. Kurup, Polyhedron, 2004, 23, 2549.
78. M. Joseph, M. Kuriakose, M.R.P. Kurup, E. Suresh, A. Kishore, G. Bhat, Polyhedron, 2006, 25, 61.
79. J.R. Wasson, C. Trapp, J. Phys. Chem., 1969, 73, 3763.

80. J.A. De Bolfo, T.D. Smith, J.F. Boas, J.R. Pilbrow, J. Chem. Soc., Faraday II, 1976, 72, 481.

81. M.J. Bew, B.J. Hathaway, R.J. Faraday, J. Chem. Soc. Dalton Trans., 1972, 1229.

82. A.H. Maki, B.R. McGarvey, J. Chem. Phys., 1958, 29, 35.

83. D. Kivelson, R. Neiman, J. Chem. Soc, Dalton Trans., 1961, 49.

84. B.N. Figgis, Introduction to ligand Fields, Interscience, New York, 1996, 295.

85. B.J. Hathaway, G. Wilkinson, R.D. Gillard, J.A. McCleverty (Ed), In Comprehensive Coordination Chemistry, Permagon: Oxford, 1987, 5, 533.

86. A.W. Addison, T.N. Rao, J. Reedijk, J. van Rijn and G.C. Vershoor, J. Chem. Soc., Dalton Trans., 1984, 1349.

Chapter 4

Copper(II) complexes containing cyanate as coligand

Contents

4.1. Introduction

Bi- and poly-nuclear copper cyanate systems are of considerable interest due to the broad range of their structural and magnetic properties. They act as synthetic models for the natural copper proteins and their derivatives. The end-on coordination mode is usually found in cyanato bridged polynuclear copper(II) compounds [1]. In contrast to azide, another pseudo-halide, cyanate, appears to be less versatile; so far only two common bridging modes, $\mu_{1,1}$ [2,3,4] and $\mu_{1,3}$ [5,6] and two rarely bridging modes, $\mu_{1,1,3}$ [7] and $\mu_{1,1,1,1}$ [8] have been observed for the cyanate anion. Although much less in comparison to the azide systems, a number of cyanate-bridged dinuclear, oligonuclear cluster, and 1-D metal complexes have been reported, and their structure-dependent magnetic properties have been investigated. In spite of extensive research previously carried out, it is difficult to judge the nature of a metallopseudo-halide product to be obtained from a reaction mixture. For a particular pseudohalide, the composition, topology, and nuclearity of the product depend on the metal ion and its simple salt, organic ligand, solvent, stoichiometric ratio of the reactants, etc., and therefore, new topologies may be attained by modifying these parameters.

The ability of the cyanate to facilitate magnetic exchange has only been scarcely studied. The cyanate anion, like the most widely studied azide, can act as a bridging ligand between metal atoms. It shows preference for the end-on (EO) bridging mode through the nitrogen atom. In this kind of bridging, the cyanato ligand has been shown to be able to mediate ferromagnetic interactions.

The linear cyanato ligand may coordinate to the metal centre through the nitrogen (M–NCO) or the oxygen (M–OCN) or both nitrogen and oxygen (M–NCO–

M) (Fig. 4.1). The N–C and C–O bond distances of the cyanato ion are 1.17 Å and 1.23 Å respectively. Majority of the reported complexes are N-bonded. The observed range for asymmetric stretching, symmetric stretching and bending vibrations of the cyanate are 2050-2250, 1200-1400 and 420-480 cm^{-1} respectively. It shows preference for the end-on (EO) bridging mode through the nitrogen atom. In this kind of bridging, the cyanato ligand has been shown to be able to mediate ferromagnetic interactions. The design and synthesis of novel coordination architectures controlled by varying the reaction conditions (including temperature [9], metal/ligand ratio [10], pH values [11], solvents [12], and counter anions [13]) are of great interest in coordination chemistry. Appropriate control of the reaction conditions make it possible to construct new materials with useful properties.

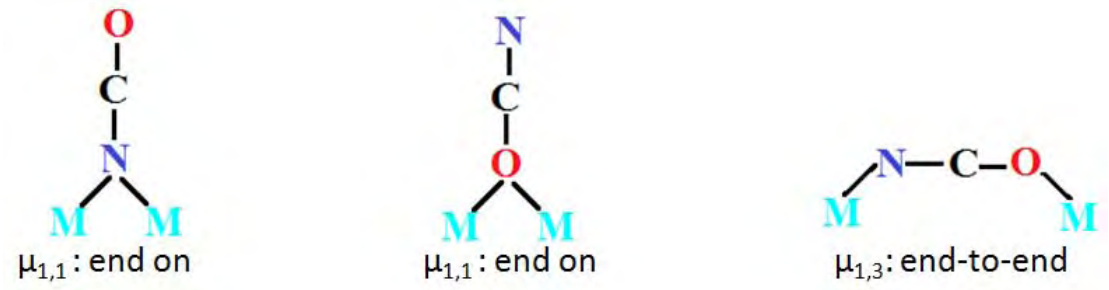

Fig. 4.1. Different binding modes of cyanate ion.

Polymorphism is defined as the ability of a substance to exist in two or more crystalline phases that have different arrangements or conformations of the molecules in the crystal lattice. It essentially means that in different polymorphs, the same molecule exists in different ways [14]. In general, polymorphs are classified into three major categories based on the geometry of molecular assembly in the crystal lattice. Of these, conformational polymorphism, which involves changes at the molecular level, occurs predominantly in flexible molecules. In the case of rigid molecules, the differences occur mainly in the packing motifs directed by the intermolecular interactions, which results in packing polymorphism. The third category is a consequence of the presence of solvent molecules in the crystal lattice, referred to as pseudo or solvato-morphism, which involves large changes in crystal density and packing. In the recent literature, several careful studies have been made to evaluate the role of the solvent in the formation of polymorphism. These highlight the importance of the kinetics in solution rather than the formation of molecular

assemblies [15]. Inorganic materials and discrete coordination complexes also show different packing polymorphism [16].

Dinuclear distorted square pyramidal structures of Cu(II) can show magnetic interactions whereas the perfect square pyramids are not reported to show any such interactions. This is due to the fact that in the latter geometry the magnetically active [$d_{x^2-y^2}$ orbital in case of Cu(II)] orbitals on each monomeric unit are orthogonal to each other and there is no suitable orbital on the ligand, which participates in the bridging, through which magnetic interaction can take place. As a consequence greater distortion from the perfect square pyramidal geometry will give rise to greater magnetic interaction between the paramagnetic metal centers. Due to lack of magnetic data, no definite conclusion could be drawn about the magnetostructural correlation in pentacoordinated cyanato bridged Cu(II) dinuclear structures. We take the θ/R ratio [where θ is the Cu–N–Cu bridge angle and R is the longer Cu–N separation in the axial bond length in Cu and bridging NCO^-] as an authentic parameter for magnetostructural correlation as done by Marsh *et.al.* [17]. It could be stated that with increase in θ/R ratio the interaction changes from ferromagnetic to antiferromagnetic gradually.

4.2. Experimental

4.2.1. Synthesis of the complexes

All chemicals used for synthesis were of Analar grade. The proligands were formed *in situ*.

4.2.1.1. Synthesis of [Cu(bpsc)μ^2(NCO)]$_2$ (11)

Methanolic solutions (20 mL) of 2-benzoylpyridine semicarbazone (Hbpsc) (0.240 g, 1 mmol), copper acetate monohydrate (0.199 g, 1 mmol) and sodium cyanate (0.075 g, 1 mmol) were mixed and the resulting mixture was refluxed for 5 h. The dark green solid was collected and recrystallized from methanol. Yield: 15%.

4.2.1.2. Synthesis of [Cu(bpsc)μ^2(NCO)]$_2$ (12)

Methanolic solutions (20 mL) of 2-benzoylpyridine semicarbazone (0.240 g, 1 mmol) copper sulfate pentahydrate (0.250 g, 1 mmol) and sodium cyanate (0.075 g, 2 mmol) were mixed and the resulting mixture was refluxed for 5 h. The dark green solid was collected and recrystallized from methanol. Yield: 68%.

4.2.2. Physical measurements

Carbon, hydrogen and nitrogen analyses were carried out using a Vario EL III CHNS analyzer at the SAIF, Kochi, India. Infrared spectra were recorded on a JASCO FT-IR-5300 Spectrometer in the range 4000-400 cm^{-1} using KBr pellets. Electronic spectra were recorded on Ocean Optics USB 4000 UV-Vis Fiber Optic Spectrometer in the 200-850 nm range using solutions in methanol. Magnetic susceptibility measurements of the complexes were carried out on a Vibrating Sample Magnetometer using $Hg[Co(SCN)_4]$ as a calibrant at the SAIF, Indian Institute of Technology, Madras.

4.2.3. X-ray crystallography

Single crystals of polymorphs of the compound $[Cu(bpsc)\mu^2(NCO)]_2$ suitable for X-ray diffraction studies were grown from their methanolic solution by slow evaporation at room temperature. Single crystals were selected and mounted on a Bruker SMART APEX diffractometer, equipped with a graphite crystal, incident-beam monochromator, and a fine focus sealed tube with Mo Kα (λ = 0.71073 Å) as the X-ray source. The crystallographic data along with details of structure solution refinements are given in Table 4.1. The unit cell dimensions were measured and the data collection was performed at 293(2) K. Bruker SMART software was used for data acquisition and Bruker SAINT software for data integration [18]. Absorption corrections were carried out using SADABS based on Laue symmetry using equivalent reflections [19]. The structure was solved by direct methods and refined by full-matrix least-squares calculations with WinGX software package [20]. The molecular and crystal structures were plotted using DIAMOND version 3.2g [21]. All non-hydrogen atoms were refined anisotropically, and all H atoms on C and N were placed in calculated positions, guided by difference maps and refined isotropically, with C–H and N–H bond distances of 0.93 Å and 0.86 Å respectively.

In the refinement of both polymorphs of $[Cu(bpsc)\mu^2(NCO)]_2$, carbon-bound H-atoms were placed in calculated positions (C–H = 0.93 Å) and were included in the refinement in the riding model approximation, with *U*iso(H) set to 1.2 *U*eq(C). The amino H-atoms were located from difference Fourier map, and were refined with a distance restraint of N–H = 0.88±0.01 Å and their displacement parameters refined. Only one H-atom is involved in the formation of a hydrogen bond.

Table 4.1. Crystallographic data and structure refinement for **11** and **12**

Parameters	[Cu(bpsc)μ^2(NCO)]$_2$ (**11**) Polymorph **A**	[Cu(bpsc)μ^2(NCO)]$_2$ (**12**) Polymorph **B**
Empirical formula	$C_{28}H_{22}Cu_2N_{10}O_4$	$C_{28}H_{22}Cu_2N_{10}O_4$
Formula weight	689.66	689.66
Color	Dark Green	Dark Green
Temperature (T) K	296(2)	296(2)
Wavelength (Mo Kα) (Å)	0.71073	0.71073
Crystal system	Triclinic	Monoclinic
Space group	$P\bar{1}$	$P2_1/n$
Cell parameters		
a	7.401(5) Å	8.7601(1) Å
b	9.992(5) Å	7.6732(1) Å
c	10.979(5) Å	20.0819(3) Å
α	104.590(5)°	90°
β	99.225(5)°	96.7467(7)°
γ	109.260(5)°	90°
Volume V (Å^3)	714.9(7)	1340.52(3)
Z	1	4
Calculated density (ρ) (Mg m^{-3})	1.602	1.709
Absorption coefficient, μ (mm^{-1})	1.542	1.644
F(000)	350	700
Crystal size mm^3	0.3 x 0.25 x 0.2	0.30 × 0.25 × 0.20
θ range for data collection	2.28 to 24.99°	2.4 to 28.3°
Limiting indices	-8≤h≤8, -11≤k≤11, -10≤l≤10	-10≤h≤10, -8≤k≤9, -23≤l≤23
Reflections collected	9943	9798
Unique Reflections (R_{int})	2517 [R(int) = 0.0618]	2355 [R(int) = 0.0303]
Completeness to θ	24.99 (99.4%)	25.00 (99.8%)
Absorption correction	Semi-empirical from equivalents	Semi-empirical from equivalents
Maximum and minimum transmission	0.735 and 0.636	0.7345 and 0.6383
Refinement method	Full-matrix least-squares on F^2	Full-matrix least-squares on F^2
Data / restraints / parameters	2505 / 3 / 208	2351 / 3 / 208
Goodness-of-fit on F^2	1.113	1.061
Final R indices [I > 2σ (I)]	R_1 = 0.0450, wR_2 = 0.1266	R_1 = 0.0262, wR_2 = 0.0741
R indices (all data)	R_1 = 0.0480, wR_2 = 0.1291	R_1 = 0.0289, wR_2 = 0.0770
Largest difference peak and hole (e Å^{-3})	0.459 and -0.511	0.309 and -0.362

$R_1 = \Sigma||F_o| - |F_c|| / \Sigma|F_o|$ $\quad$ $wR_2 = [\Sigma w(F_o^2-F_c^2)^2 / \Sigma w(F_o^2)^2]^{1/2}$

4.3. Results and discussion

4.3.1. Analytical measurements

The analytical data of all the complexes are listed in Table 4.2. The CHN obtained showed that all the complexes are analytically pure.

Table 4.2. Preliminary analytical data of Cu(II) cyanato complexes.

Compounds	Observed (Calculated)%			λ_m	μ_{eff}(B.M.)
	C	H	N		
$[Cu(bpsc)(NCO)]_2$ Polymorph **A**	48.32 (48.77)	3.41 (3.22)	19.96 (20.31)	13	1.335
$[Cu(bpsc)(NCO)]_2$ Polymorph **B**	48.38 (48.77)	3.33 (3.22)	20.10 (20.31)	29	1.343

From the crystal data and magnetic susceptibility, we confirm that polymorphs **A** and B shows ferromagnetic interactions due to the end-on (EO) bridging mode of cyanato ligand [22]. The complexes are soluble in polar solvents. The conductivity measurements were made in DMF solutions and all complexes are found to be non-electrolytes [23].

4.3.2. Crystal structure of polymorphs of $[Cu(bpsc)\mu^2(NCO)]_2$

The molecular structure obtained in the polymorphs **A** and **B** differ only very marginally in the geometrical parameters. Therefore, the two structures are described together. The single crystal X-ray diffraction study of the polymorphs $[Cu(bpsc)\mu^2(NCO)]_2$ revealed that these compounds are cyanato bridged Cu(II) dimer. The molecular structures of the polymorphs with the atom numbering scheme are shown in Fig. 4.2. The structures of polymorphs **A** and **B** consists of the dinuclear $[Cu_2(bpsc)_2(\mu_{1,1}\text{-NCO})]$ species. Two copper(II) atoms [Cu(1) and Cu(1A)] are bridged by cyanate ion in an end-on fashion, giving the dinuclear structures with semicarbazone as the ligand attached to each copper centers. The coordination polyhedron around the Cu(1) is best described as an elongated (4+1) square pyramid. Two nitrogen atoms, N(1) and N(2), and one oxygen atom, O(1), from the deprotonated semicarbazone ligand, (bpsc) and one nitrogen atom N(5) from a terminal OCN ligand define the equatorial plane, having bond lengths from the Cu(I) atom at 2.007(3), 1.942(3), 1.976(2) and 1.971(3) Å, in polymorph **A** and 1.934(16), 1.940(16), 1.980(17) and 1.960(18) in polymorph **B** respectively. Cu(II) ion has a

distorted square pyramidal geometry with a CuN_4O chromophore and τ value of 0.258 and 0.295 in polymorph **A** and **B** respectively (τ = 0 for a square pyramidal geometry, and τ = 1 for a trigonal bipyramidal geometry) [24]. From the crystallographic literature, it is seen that Cu(II) dinuclear $\mu_{1,1}$-NCO bridged compounds have a Cu–N_{NCO}–Cu angle in the narrow range 92.3-96.3 [25]. However in polymorph **A** and **B**, these angles are at 90.07° and 92.98° respectively. The Cu(1) and Cu(1A) separation in polymorph **A** and **B** are 3.171 and 3.355 Å respectively. In polymorph **B**, the metal center shows square-planar coordination that is distorted towards square-pyramidal coordination owing to an intermolecular Cu···$N_{cyanate}$ interaction [2.623(2) Å], which generates a centrosymmetric dimer. The geometry is better interpreted as square planar as the Cu···$N_{cyanate}$···Cu angle is too acute [92.98°].

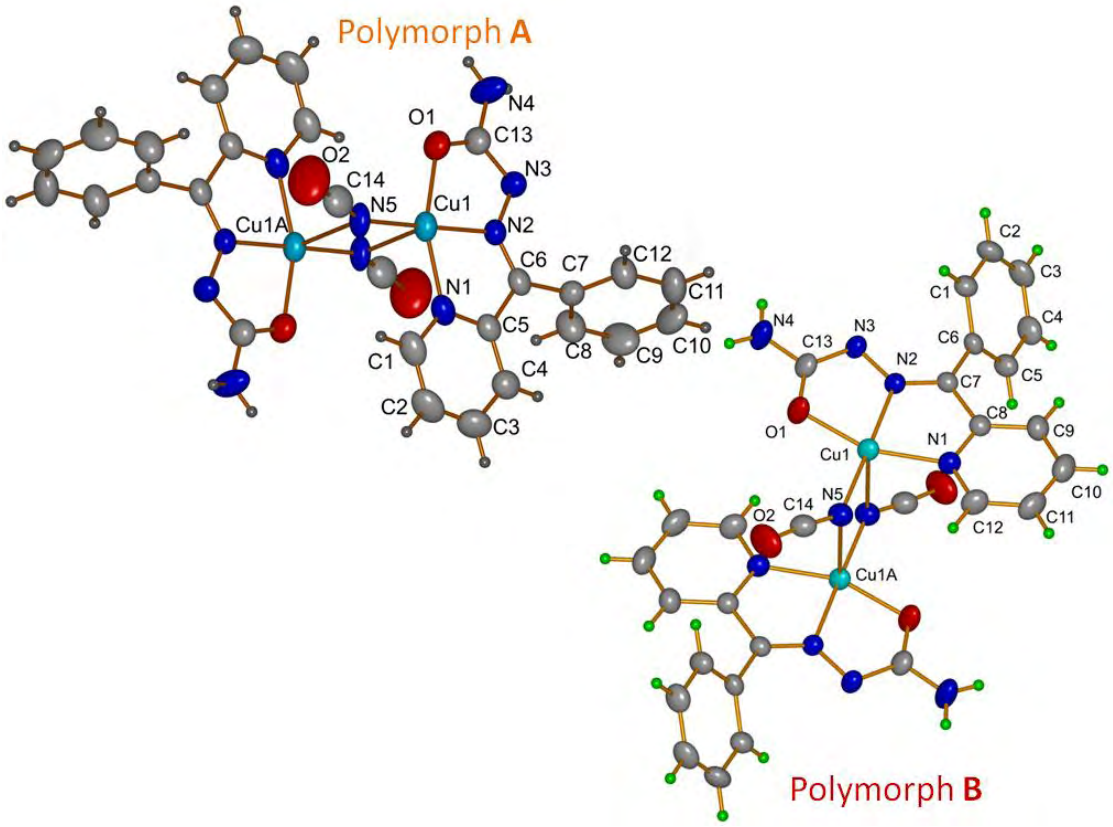

Fig. 4.2. The molecular structures of the polymorphs $[Cu(bpsc)\mu_{1,1}\text{-}(NCO)]_2$ with the atom numbering scheme.

Selected bond lengths and bond angles are given in Table 4.3.

Table 4.3. Selected bond lengths [Å] and angles [°] for the two polymorphs of $[Cu(bpsc)\mu^2(NCO)]_2$

	Polymorph **A**	Polymorph **B**
Bond lengths (Å)		
C13–O1	1.252(4)	1.273(3)
C13–N3	1.367(4)	1.352(3)
N3–N2	1.355(3)	1.356(2)
Cu1–N1	2.007(3)	1.934(16)
Cu1–N2	1.942(3)	1.940(16)
Cu1–O1	1.976(2)	1.980(17)
Cu1–N5	1.971(3)	1.960(18)
Bond angles (°)		
N2–Cu1–O1	79.16(10)	80.00(6)
N2–Cu1–N1	80.38(10)	81.20(7)

The difference in the intermolecular interactions present in complexes enabled a variation in the packing motifs, thus resulting in packing polymorphism; Polymorph A and B (Fig. 4.3a and 4.3b). Formation of the centrosymmetric molecular dimers *via* C–H···π interactions and hydrogen bonding is the major structural feature that stabilizes the molecular packing.

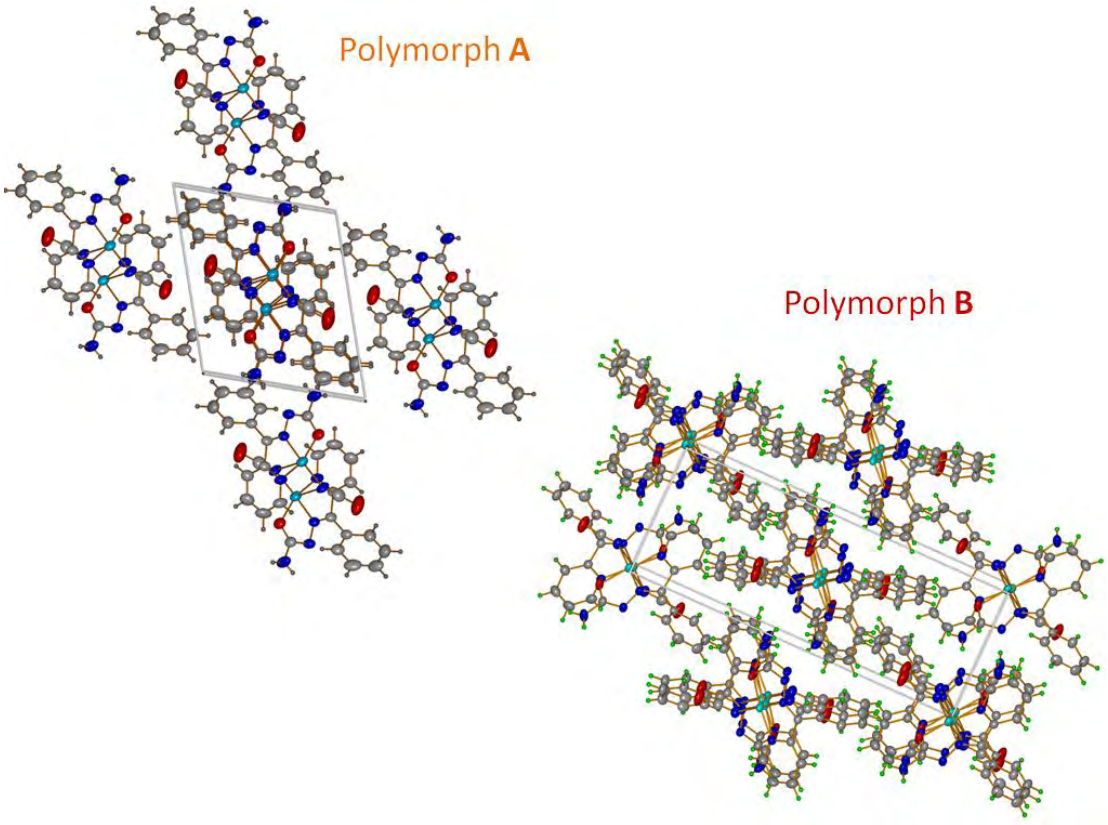

Fig. 4.3a. Packing polymorphism exhibited by $[Cu(bpsc)\mu^2(NCO)]_2$ along 'a' axis.

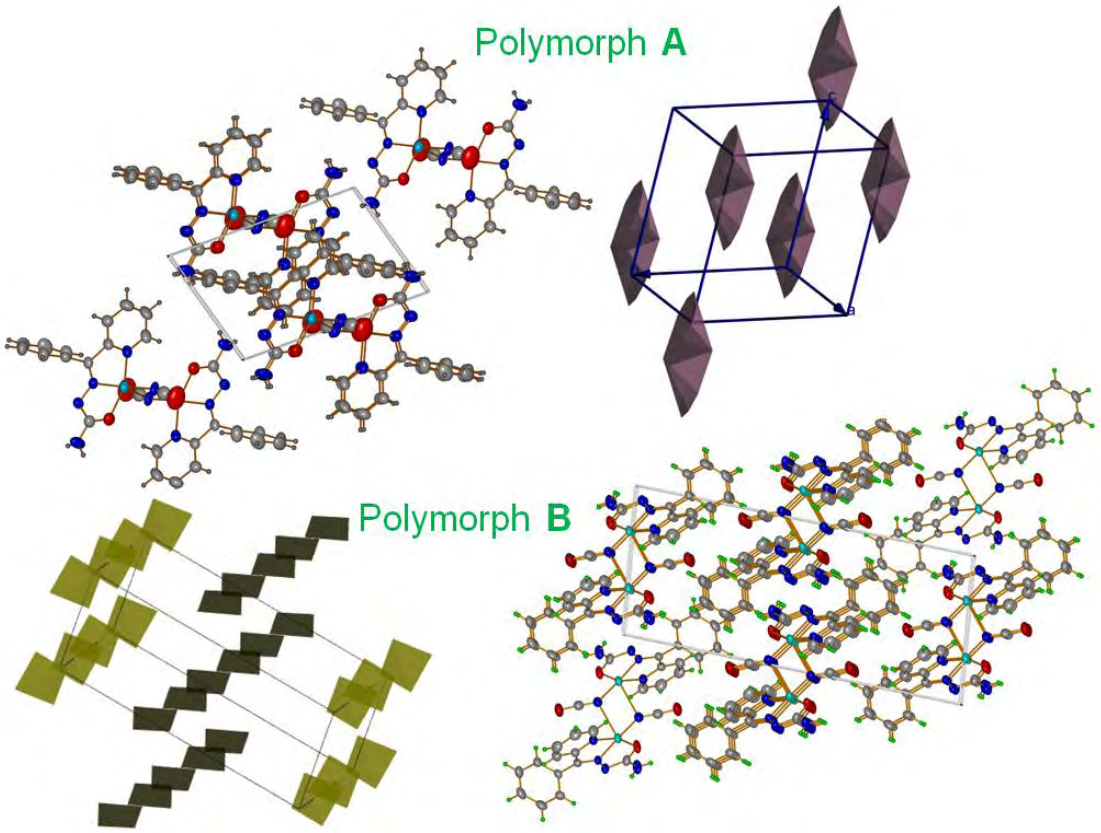

Fig. 4.3b. Packing polymorphism exhibited by $[Cu(bpsc)\mu^{2}(NCO)]_2$ along 'b' axis.

In the crystal, adjacent complex dimers are linked by an amine N–H···N hydrogen-bond pair (Fig. 4.4 and Table 4.4), also giving a centrosymmetric cyclic association [graph set $R_2^2(8)$], generating a linear chain parallel to [110].

Table 4.4. Hydrogen bonding interactions in the polymorphs of $[Cu(bpsc)\mu^{2}(NCO)]_2$

D–H···A	D–H (Å)	H–A (Å)	D–A (Å)	∠D–H···A (°)
N(4)–H(4B)···N(3)^{a}	0.80(3)	2.24(3)	3.039(5)	177(2)
C(4)–H(4)···O(2)^{b}	0.9294	2.4124	3.035(6)	124.33
C(9)–H(9)···O(1)^{b}	0.9300	2.5933	3.391(6)	144.17

Equivalent position codes: a = -x,1-y,-z ; b = 1+x,1+y,z.

D–H···A	D–H (Å)	H···A (Å)	D···A (Å)	∠D–H···A (°)
N(4)–H(1N4)···N(3)^{a}	0.85(3)	2.29(2)	3.139(3)	174(3)

Equivalent position codes: a= 1-x,-y,1-z.

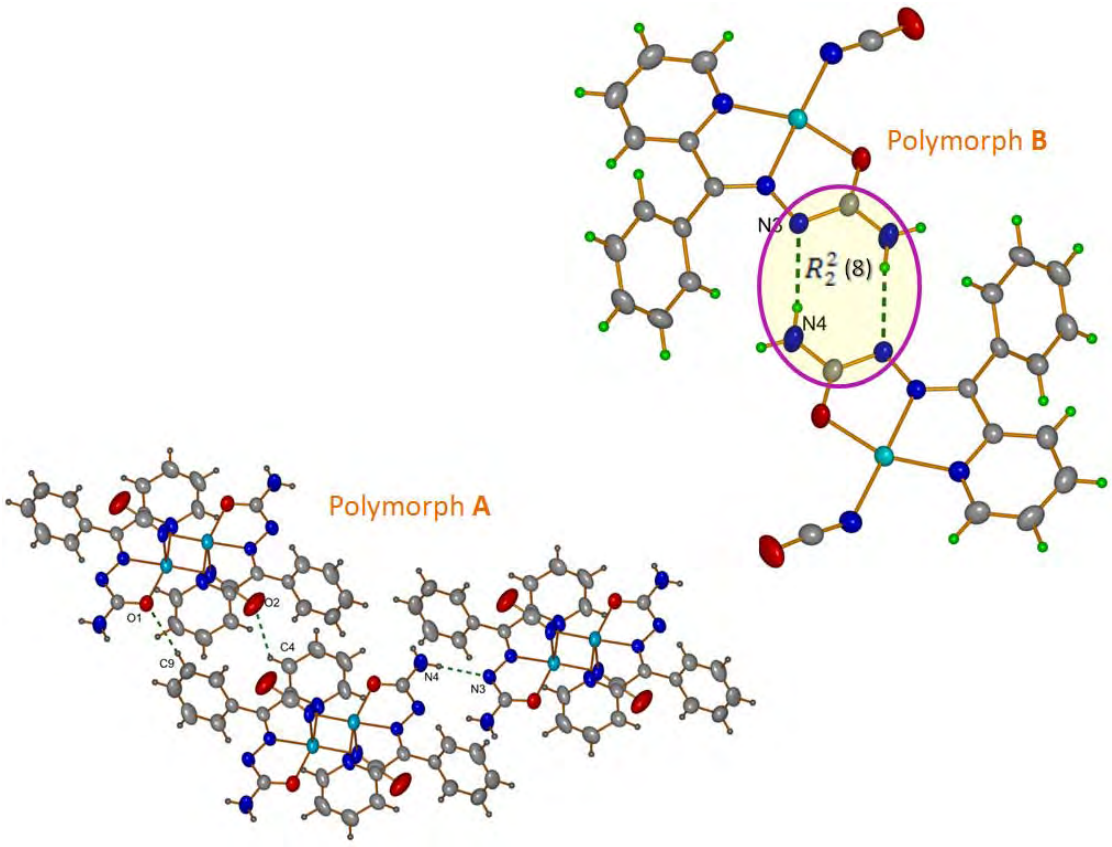

Fig. 4.4. Hydrogen bonding interactions in the polymorphs of $[Cu(bpsc)\mu^2(NCO)]_2$.

For the polymorphic compound **A**, π···π interaction is perceived at 3.645(3) Å for Cg(5)···Cg(7)^c [Cg(5) = Cu(1), N(1), C(5), C(6), N(2); Cg(7) = N(1), C(1), C(2), C(3), C(4), C(5); c = 1-x,1-y,1-z.]. The Cg···Cg stacking interactions between rings with Cg···Cg distances of 3.9094(10) and 3.9237(9) Å can support the packing stability in polymorph **B** (Table 4.5 and Fig. 4.5).

Table 4.5. π···π interactions in polymorphs of $[Cu(bpsc)\mu^2(NCO)]_2$

Polymorph **A**

Cg(I)···Cg(J)	Cg···Cg (Å)	α (°)	β (°)	γ (°)
Cg(5)···Cg(7)^c	3.645(3)	2.69	23.23	25.36

Equivalent position codes: c = 1-x,1-y,1-z.

Polymorph **B**

Cg(I)···Cg(J)	Cg···Cg (Å)	α (°)	β (°)	γ (°)
Cg(3)···Cg(7)^b	3.9094(10)	88.98	33.54	69.98
Cg(4)···Cg(5)^c	3.9237(9)	4.59	19.70	17.11

Equivalent position codes: b=x,y,z; c=1-x,1-y,1-z.

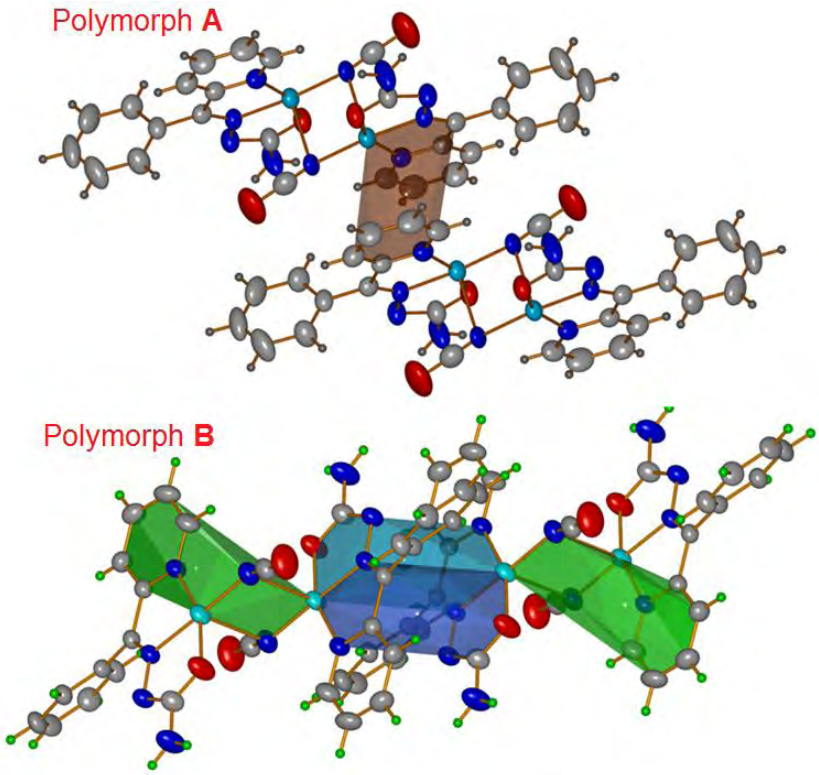

Fig. 4.5. $\pi\cdots\pi$ interactions in polymorphs of $[Cu(bpsc)\mu^2(NCO)]_2$.

The complexes show significant C–H$\cdots\pi$ interactions (Fig. 4.6 and Table. 4.6).

Table 4.6. C–H$\cdots\pi$ interactions of the polymorphs of $[Cu(bpsc)\mu^2(NCO)]_2$

Polymorph **A**

X–H(I)···Cg(J)	H···Cg (Å)	X···Cg (Å)	∠X–H···Cg (°)
C(1)–H(1)···Cg(5)^c	3.3781	3.304(5)	77.47
N(4)–H(4A)···Cg(8)^a	2.85(4)	3.407(5)	126(3)
C(2)–H(2)···Cg(4)^c	3.3516	3.466(5)	89.21
C(8)–H(8)···Cg(7)^d	3.3279	4.047(5)	135.70

Equivalent position codes:c = 1-x,1-y,1-z; d = 1-x,2-y,1-z. Cg (4) = Cu(1), O(1), C(13), N(3), N(2);
Cg (5) = Cu(1), N(1), C(5), C(6), N(2); Cg (7) = N(1), C(1), C(2), C(3), C(4), C(5); Cg (8)= C(7), C(8), C(9), C(10), C(11), C(12).

Polymorph **B**

X–H(I)···Cg(J)	H···Cg (Å)	X···Cg (Å)	∠X–H···Cg (°)
C(3)–H(3)···Cg(8)^d	3.1131	3.741(2)	126.40
C(4)–H(4)···Cg(7)^e	3.0848	3.851(2)	140.80
C(10)–H(10)···Cg(8)^f	3.0335	3.729(3)	132.90
C(11)–H(11)···Cg(4)^f	3.3549	3.820(3)	113.34
C(12)–H(12)···Cg(3)^g	3.0703	3.250(2)	92.72

Equivalent position codes: d=3/2-x,-1/2+y,3/2-z ; e=1/2-x,-1/2+y,3/2-z; f=x,1+y,z ; g=-x,1-y,1-z
Cg(3) = Cu1, N5, Cu1A, N5A; Cg (4) = Cu1, O1, C13, N3, N2; Cg (7) = N1, C8, C9, C10, C11, C12; Cg (8) = C1, C2, C3, C4, C5, C6.

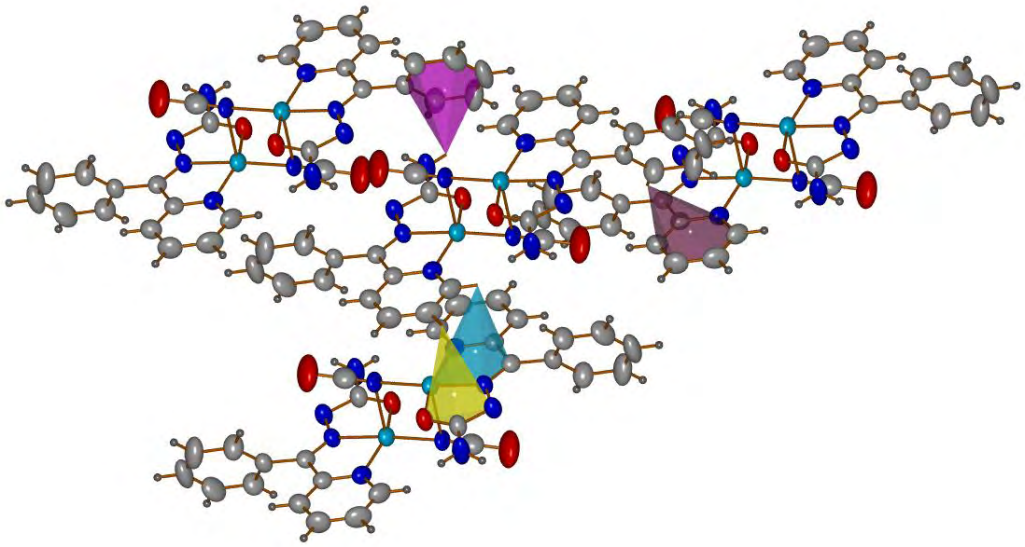

Polymorph **A**

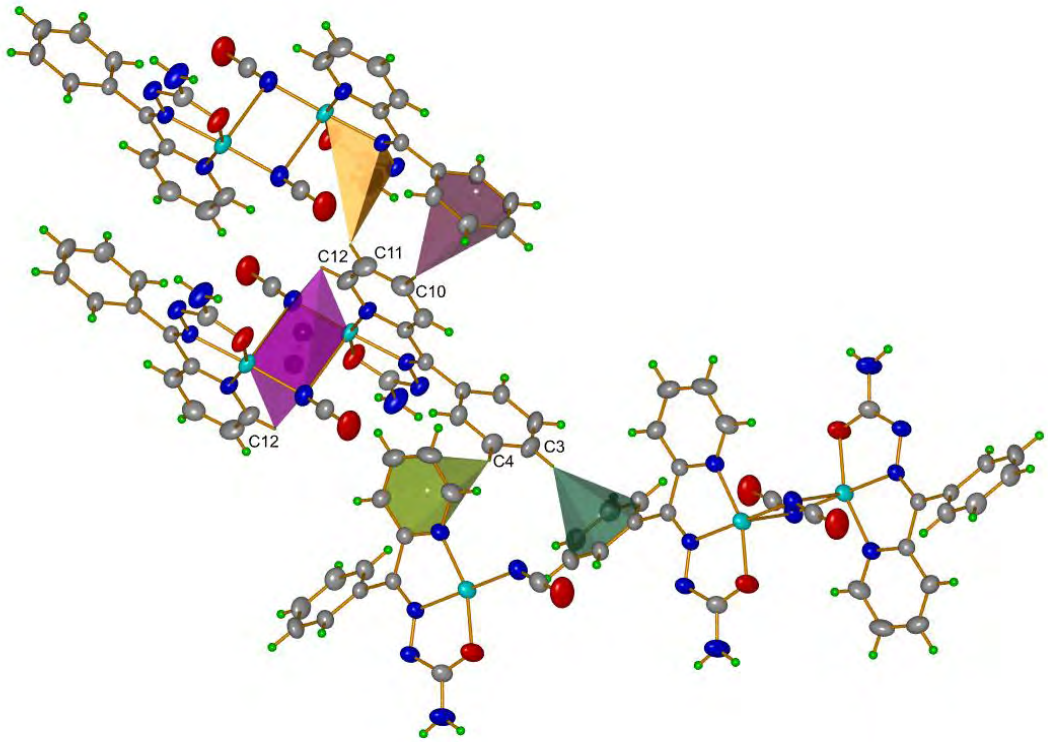

Polymorph **B**

Fig. 4.6. C–H ··π interactions in polymorphs of $[Cu(bpsc)\mu^2(NCO)]_2$.

There are two distinct types of π···π interactions present in polymorph **B**, between the rings Cg(4)···Cg(5)^c and Cg(3)···Cg(7)^b (b = x,y,z) with Cg···Cg distances of 3.9237(9) and 3.9094(10) respectively, whereas in polymorph **A**, only one type of π···π interaction between rings Cg(5)···Cg(7)^c (c = 1-x,1-y,1-z) with

Cg···Cg distance of 3.645(3). Interestingly, in polymorph **A** the supramolecular assembly is also supported by Cu···π interactions with distance of 3.447 Å (Fig. 4.7 and Table 4.7). The molecular conformation is found to be significantly deviating from planarity in order to accommodate various modes of intermolecular interactions.

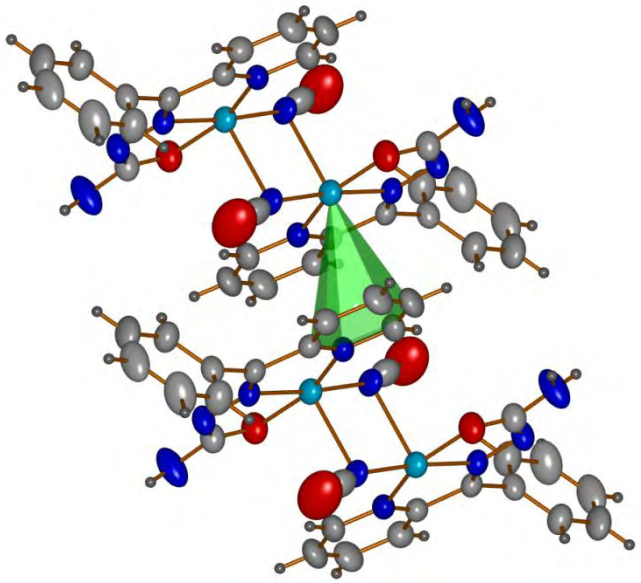

Fig. 4.7. Ring-metal interactions in polymorph A.

Table 4.7. Ring-metal interactions in polymorph **A**

Cg(I)···M(J)	Cg(I)-M(J) (Å)	β (°)
Cg(7)···Cu(1)^{c}	3.447	10.80

Equivalent position codes: c = 1-x,1-y,1-z.

4.3.3. Infrared spectral studies

IR spectroscopy is a useful tool to confirm the coordination of various atoms and groups to the metal atom. However, it cannot be used alone to determine the stereochemistry and has to be coupled with other spectral techniques like EPR, electronic spectroscopy etc. The significant bands observed in the spectra of cyanato complexes with the tentative assignments are presented in Table 4.8.

Table 4.8. IR spectral data of the Cu(II) cyanato complexes (cm^{-1})

Compound $[Cu(bpsc)\mu^{2}(NCO)]_2$	ν_a(NCO)	ν_s(NCO)	δ(NCO)	ν(C=N)	ν(C=O)	ν(N–N)
Polymorph **A**	2183	1302	618	1551	1624	1124
Polymorph **B**	2184	1305	620	1552	1625	1125

In the IR spectrum of polymorph **A** (Fig. 4.8), the medium sharp peak 1551 cm^{-1} is assigned as the ν(C=N) stretching mode of the azomethine function of the semicarbazone, the position of which is in agreement with the previous reports and is thus indicative of the coordination of azomethine nitrogen [26,27]. The most relevant and the interesting bands in the IR spectra are those associated with the cyanato group. In IR spectra, characteristic asymmetric and symmetric cyanato stretching vibration at ~ 2180 and ~ 1300 cm^{-1} respectively are observed in all complexes. The IR spectrum of polymorph **B** is shown in Fig 4.9.

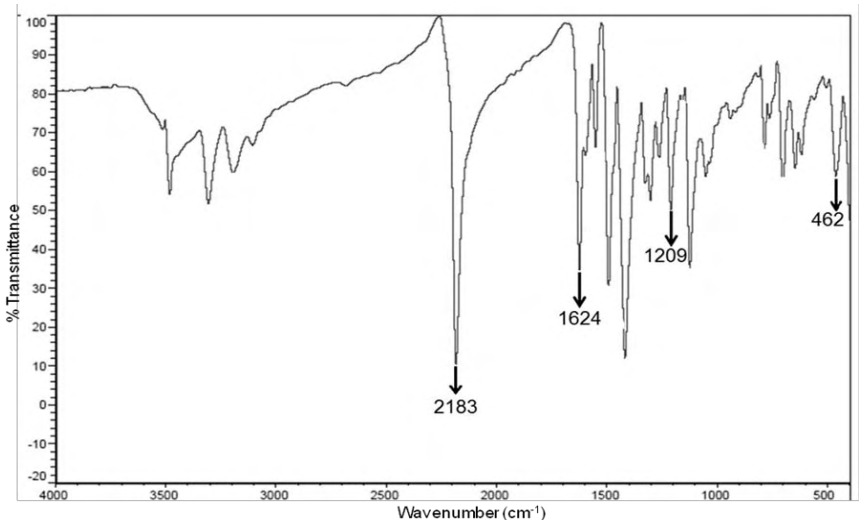

Fig. 4.8. IR spectrum of polymorph **A**.

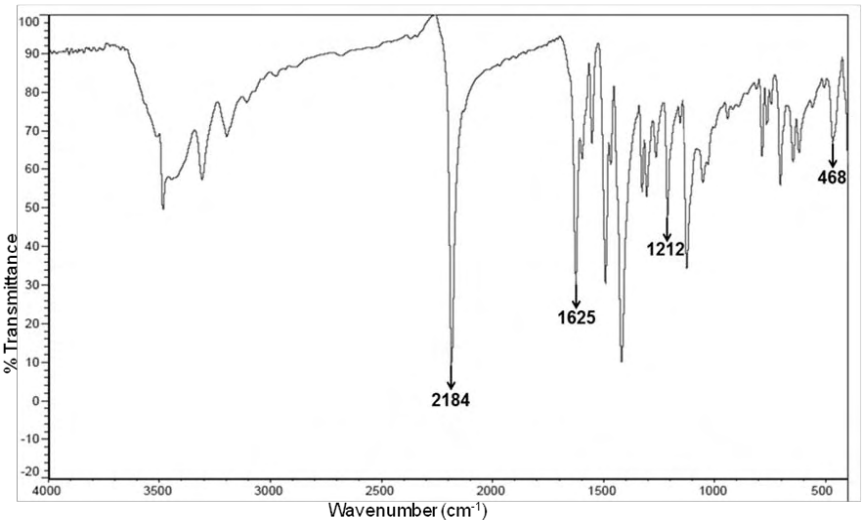

Fig. 4.9. IR spectrum of polymorph **B**.

4.3.4. Electronic spectral studies

The electronic spectral data of polymorphs are given in Table 4.8.

Table 4.8. Electronic spectral assignments (cm^{-1}) for cyanato complexes

$[Cu(bpsc)\mu^2(NCO)]_2$	*d-d*	LMCT	n→π*/π→π*
Polymorph **A** (11)	14500	26020	33750, 39530, 46965
Polymorph **B** (12)	13520	26250	33750, 39500, 47180

The semicarbazone and copper(II) polymorphs have two bands; one centered in the 37295-45360 cm^{-1} region and the other in the 30150-33170 cm^{-1} region. These bands are due to π→π* and n→π* transitions (Fig. 4.10-4.11) of phenyl rings and semicarbazide moiety [28]. The charge transfer bands were observed in the 24660-26150 cm^{-1} region and its broadness can be explained as due to the combination of O→Cu and N→Cu LMCT transitions [29]. It is rather difficult to interpret electronic spectra of Cu(II) complexes as they possess flexible stereochemistry. The outer electronic configuration for copper(II) ion is $3d^9$ with ^2D as ground state term which will be split by an octahedral field in to two levels $^2T_{2g}$ and ^2E_g. So the expected excitation in an octahedral d^9 system is from ^2E_g to $^2T_{2g}$ results in a single absorption band. However the geometry around copper(II) ion lacks cubic symmetry and the tetragonal distortion yields other distorted forms of basic stereochemistries. Jahn-Teller distortions cause further splitting of the $^2T_{2g}$ and ^2E_g. So the possible spin allowed excitations *viz.* $^2A_{1g} \leftarrow {}^2B_{1g}$, $^2B_{2g} \leftarrow {}^2B_{1g}$ and $^2E_g \leftarrow {}^2B_{1g}$ which occur in the region 11760-18180, 15500-18010 and 17240-20000 cm^{-1} respectively. But the energy difference between these levels is too small to resolve them into separate bands. The ligand field at the metal center affects the splitting of *d*-orbitals and so the associated *d-d* transitions are sensitive probes of the ligand geometry. The *d-d* absorption maxima range from 16394-11560 cm^{-1} and tend to be indicative of tetragonal geometries [30].

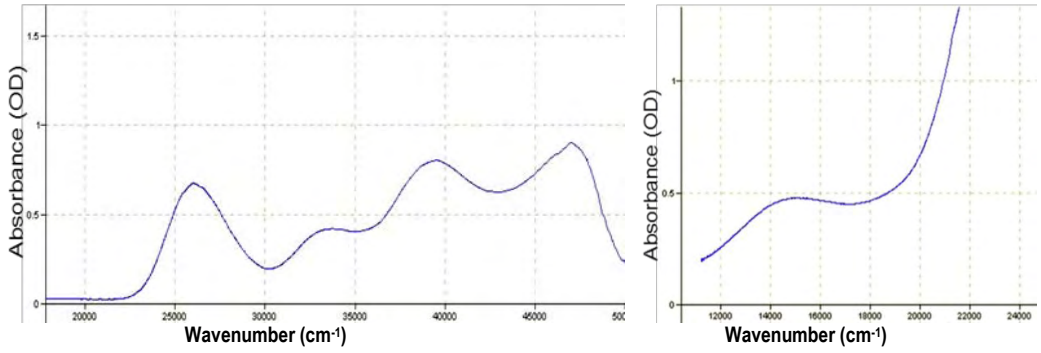

Fig. 4.10. Electronic spectra of polymorph A.

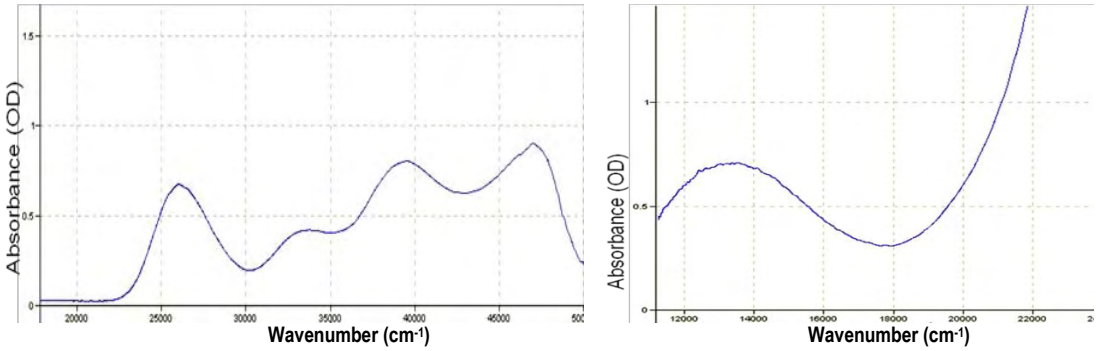

Fig. 4.11.. Electronic spectra of polymorph B.

4.3.5. EPR spectral studies

The EPR spectra of the polymorphs **A** and **B** were recorded in the X-band frequency. The various magnetic interaction parameters are summarized in Table 4.9.

Table 4.9. Spin Hamiltonian and bonding parameters of the complexes

Polycrystalline state at 298 K					Solution state at 77 K							
Compounds	$g_{\|\|}$	$g_{\perp}$	g_{rv}	G	$g_{\|\|}$	$g_{\perp}$	$A_{\|\|}$	α^2	β^2	γ^2	$K_{\|\|}$	$K_{\perp}$
Polymorph **A**	2.135	2.056	2.082	4.128	2.216	2.056	20	0.851	0.804	0.806	0.684	0.686
Polymorph **B**	2.228	2.056	2.113	4.203	2.211	2.056	20	0.845	0.773	0.784	0.653	0.662

The EPR spectra of polymorphs in the polycrystalline state at 298 K show axial spectra with well defined $g_{||}$ and $g_{\perp}$ features. Hyperfine lines are not well resolved.

The EPR spectrum of polymorph **A** in solution at 77 K (Fig. 4.12) is a typical axial spectrum with $g_{||}$= 2.135 and $g_{\perp}$ = 2.056. The g_{av} values calculated as $g_{av} = 1/3(g_{||}+2g_{\perp})$ has the value 2.082. The parallel region of the spectrum is well resolved and consists of a set of four hyperfine lines due to the interaction of the electron with the Cu(II) nucleus (No: of hyperfine lines = $2nI+1$ and for ^{63}Cu, I=3/2). The perpendicular region of the spectrum is devoid of hyperfine splitting. The $g_{||}$ values provide information regarding the nature of metal-ligand bond [31]. The $g_{||}$ value is normally 2.3 or larger for ionic and less than 2.3 for covalent metal-ligand bonds. The $g_{||}$ values obtained indicate a significant degree of covalency in the metal-ligand bonds.

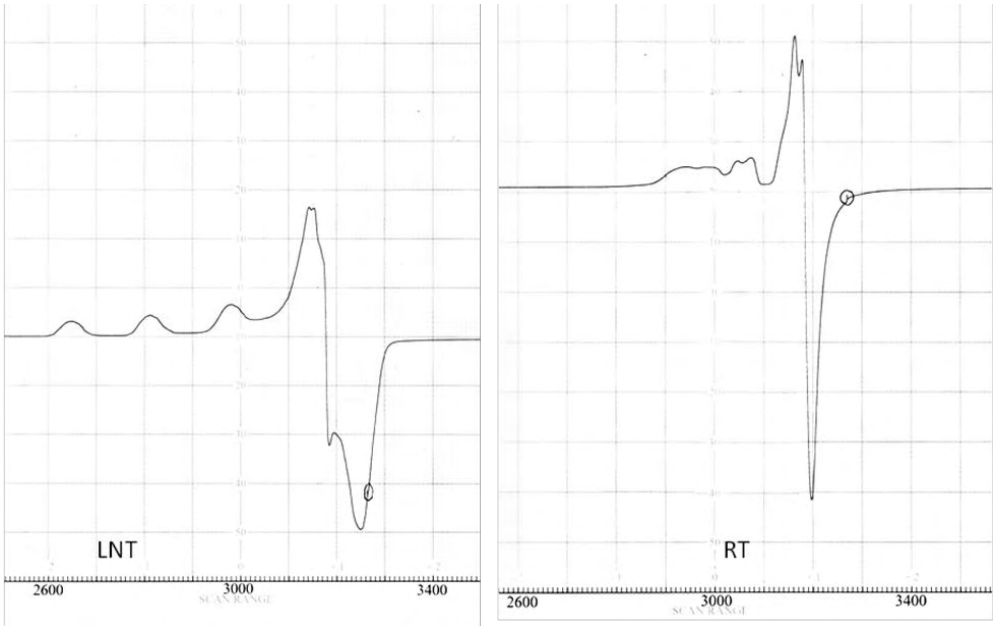

Fig. 4.12. EPR spectra of Polymorph A (**11**).

The spectrum of polymorph **B** in DMF at 77 K (Fig. 4.13) is axial in character, $g_{||}$ = 2.228, $g_{\perp}$ = 2.056 and g_{av} = 2.113. The parallel region is well resolved into a set of four hyperfine lines as a result of the interaction of the electron spin with the spin of the nuclei of ^{63}Cu.

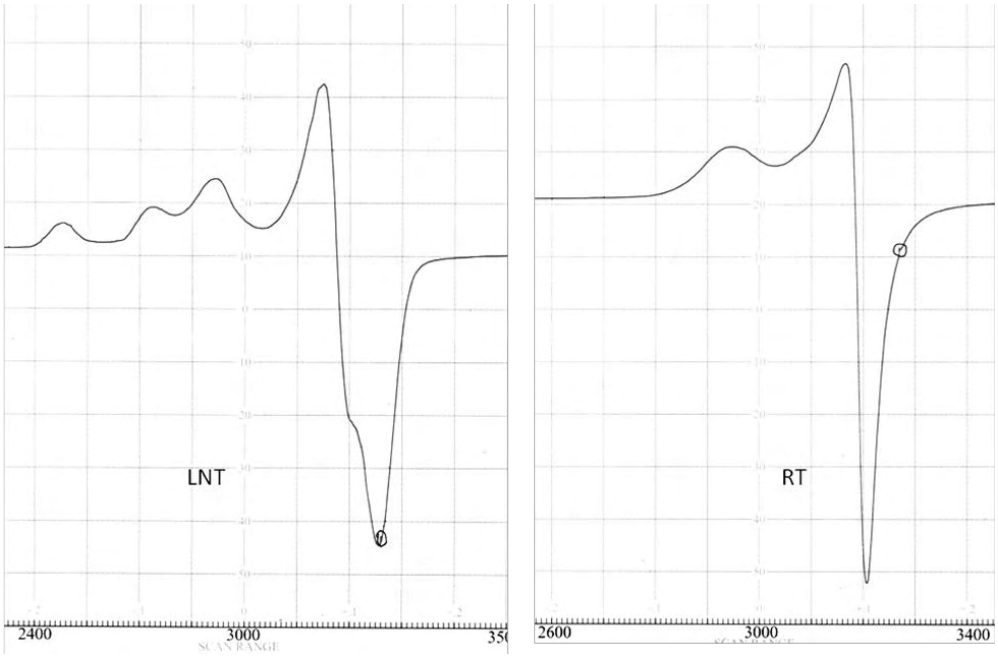

Fig. 4.13. EPR spectra of polymorph B (**12**).

REFERENCES

1. O.J. Parker, M.P. Wolther, G.L. Breneman, Acta Cryst., 1996, C52, 1089.
2. M.I. Arriortua, R. Cortes, J.L. Mesa, L. Lezama, T. Rojo, G. Villeneuve, Transit. Met. Chem., 1988, 13, 371.
3. S. Hazra, R. Koner, P. Lemoine, E.C. Sanudo, S. Mohanta, Eur. J. Inorg. Chem., 2009, 3458.
4. (a) M. Habib, T.K. Karmakar, G. Aromi, J. Ribas-Arino, H.-K. Fun, S. Chantrapromma, S.K. Chandra, Inorg. Chem., 2008, 47, 4109. (b) C.D. Nicola, Effendy, F. Fazaroh, C. Pettinari, B.W. Skelton, N. Somers, A.H. White, Inorg. Chim. Acta, 2005, 358, 720. (c) J.M. Clemente-Juan, C. Mackiewicz, M. Verelst, F. Dahan, A. Bousseksou, Y. Sanakis, J.-P. Tuchagues, Inorg. Chem., 2002, 41, 1478. (d) M.A.S. Goher, F.A.J. Mautner, Chem. Soc., Dalton Trans., 1999, 1923.
5. (a) P. Talukder, A. Datta, S. Mitra, G. Rosair, M.S.E. Fallah, J. Ribas, Dalton Trans., 2004, 4161. (b) R. Vicente, A. Escuer, E. Penalba, X. Solans, M.J. Font-Bardía, Chem. Soc., Dalton Trans., 1994, 3005.
6. A. Escuer, M. Font-Bardía, E. Penalba, X. Solans, R. Vicente, Inorg. Chim. Acta, 1999, 286, 189.
7. (a) J. Luo, X.-G. Zhou, L.-H. Weng, X.-F. Hou, Acta Cryst., 2003, C59, m519.
8. A.K. Boudalis, Y. Sanakis, J.M. Clemente-Juan, B. Donnadieu, V. Nastopoulos, A. Mari, Y. Coppel, J.-P. Tuchagues, S.P. Perlepes, Chem. Eur. J., 2008, 14, 2514.
9. (a) P.M. Forster, A.R. Burbank, C. Livage, G. Freyb, A.K. Cheetham, J. Chem. Soc., Chem. Commun., 2004, 4, 368. (b) S.-M. Chen, C.-Z. Lu, Q.-Z. Zhang, J.-H. Liu, X.-Y. Wu, Eur. J. Inorg. Chem., 2005, 2, 423.
10. A.J. Blake, N.R. Brooks, N.R. Champness, P.A. Cooke, A.M. Deveson, D. Fenske, P. Hubberstey, W.-S. Li, M. Schröder, J. Chem. Soc., Dalton Trans., 1999, 2103.
11. X.-X. Hu, J.-Q. Xu, P. Cheng, X.-Y. Chen, X.-B. Cui, J.-F. Song, G.-D. Yang, T.-G. Wang, Inorg. Chem., 2004, 43, 2261.

12. M.A. Withersby, A.J. Blake, N.R. Champness, P.A. Cooke, P. Hubberstey, W.-S. Li, M. Schröder, Inorg. Chem., 1999, 38, 2259.

13. (a) J.R. Black, N.R. Champness, W. Levason, G. Reid. J. Chem. Soc., Chem. Commun., 1995, 12, 1277. (b) J.R. Black, N.R. Champness, W. Levason, G. Reid, J. Chem. Soc., Dalton Trans., 1995, 3439.

14 B. Moulton, M.J. Zaworotko, Chem. Rev., 2001, 101, 1629.

15. (a) R.M. Vrcelj, G.H. Gallagher, J.N. Sherwood, J. Am. Chem. Soc., 2001, 123, 2291. (b) R.J. Davey, N. Blagden, S. Righini, H. Alison, M.J. Quayle, S. Fuller, Cryst. Growth Des., 2001, 1, 59.

16. X.M. Zhang, M.L. Tong, M.L. Gong, H.K. Lee, L. Luo, K.F. Li, Y.X. Tong, X.M. Chen, Chem. Eur. J., 2002, 8, 3187.

17. W.E. Marsh, W.E. Hatfield, D.J. Hodgson, Inorg. Chem., 1982, 21, 2679.

18. SMART and SAINT, Area Detector Software Package and SAX Area Detector Integration Program, Bruker Analytical X-ray; Madison, WI, USA, 1997.

19. SADABS, Area Detector Absorption Correction Program; Bruker Analytical X-ray; Madison, WI, 1997.

20. L. J. Farrugia, J. Appl. Cryst., 2012, 45, 849.

21. K. Brandenburg, Diamond Version 3.2g, Crystal Impact GbR, Bonn, Germany, 2010.

22. (a) S. Youngme, J. Phatchimkun, U. Suksangpanya, C. Pakawatchai, G.A. van Albada, J. Reedijk, Inorg. Chem.Commun., 2005, 8, 882. (b) C. Diaz, J. Ribas, M.S. El Fallah, X. Solans, M. Font-Bardìa, Inorg. Chim. Acta, 2001, 312, 1.

23. W.J. Geary, Coord. Chem. Rev. 1971, 7, 81.

24. A.W. Addison, J. Reedijk, J. van Rijn, G.C. Verschoor, J. Chem. Soc., Dalton Trans., 1984, 1349.

25. (a) A.E. Mauro, S.I. Klein, J.S. Saldan, C.A.D. Simone, J. Zukerman-Schpector, E.E. Castellano, Polyhedron, 1990, 9, 2937. (b) J. Zukerman-Schpector, E.E. Castellano, C.A.D. Simone, G. Oliva, A.E. Mauro, Acta Cryst., 1991, C47, 957. (c) C. Diaz, J. Ribas, M.S. El Fallah, X. Solans, M. Font-Bardia, Inorg. Chim. Acta, 2001, 1, 312. (d) H. Grove, M. Julve, F. Lloret, P.E. Kruger, K.W. Törnroos, J. Sletten, Inorg. Chim. Acta, 2001, 325, 115.

26. E.-Q, Gao, S.-Q. Bai, Y.-F. Yue, Z.-M. Wang, C.-H. Yan, Inorg. Chem., 2003, 39, 3642.

27. E.-Q, Gao, Y.-F. Yue, S.-Q. Bai, Z. He, C.-H. Yan, Cryst. Growth. Des., 2005, 5, 1119.

28. M.R.P Kurup, B. Varghese M. Sithambaresan, S. Krishnan, S.R. Sheeja, E. Suresh, Polyhedron, 2010, 30, 70.

29. R.P. John, A. Sreekanth, V. Rajakannan, T.A. Ajith, M.R.P. Kurup, Polyhedron, 2004, 23, 2549.

30. P.B. Sreeja, M.R.P. Kurup, A. Kishore, C. Jasmin, Polyhedron, 2004, 23, 575.

31. T. D. Smith, J. Pilbrow, Coord. Chem. Rev., 1974, 13, 173.

Chapter 5

Copper(II) complex containing dicyanamide as coligand

Contents

5.1. Introduction

The dicyanamide ion, $N(CN)_2^-$ (dca) has the ability to form a wide variety of transition metal compounds of different architectures and topologies. The π-electrons of the nitrile groups interact with the π-system of the central nitrogen, allowing electron delocalization which in principle should facilitate the transmission of electrons between the metal centers across the bridging dca ligand and should lead to long range magnetic interaction between the metallic centers. Dicyanamide is a popular bridging ligand, which has already been used extensively for the synthesis of homo-polymetallic complexes with interesting supramolecular architectures [1]. A large variety of topologies and magnetic properties are observed in dicyanamide based complexes due to their different bridging modes [2]. Coordination polymers based on the dicyanamide ($[NCNCN]^-$) ligand have also attracted much attention because they can facilitate the syntheses of metal-organic frameworks containing channels and cavities with various sizes and shapes [3]. In contrast to what we expected, the dca anion is not planar as a result of the dihedral angle (30°-37°) between the two nitrile fragments of $N(CN)_2$ [4]. The geometrical nature of dca precludes the possibility of formation of chelated coordination compounds but instead it enforces the anion to act as a terminal or a bridging ligand through the nitrile groups. In polynuclear complexes bridged by dca ligand, the anion displays a wide range of bonding modes either through its terminal nitrile nitrogen group(s) or the central amide nitrogen or by both.

Among the several coordination modes of dca, the $\mu_{1,5}$ bridging mode is by far the most usual one (68%) and 32% contain a terminal dca ligand coordinated through one of the nitrile groups [5,6].

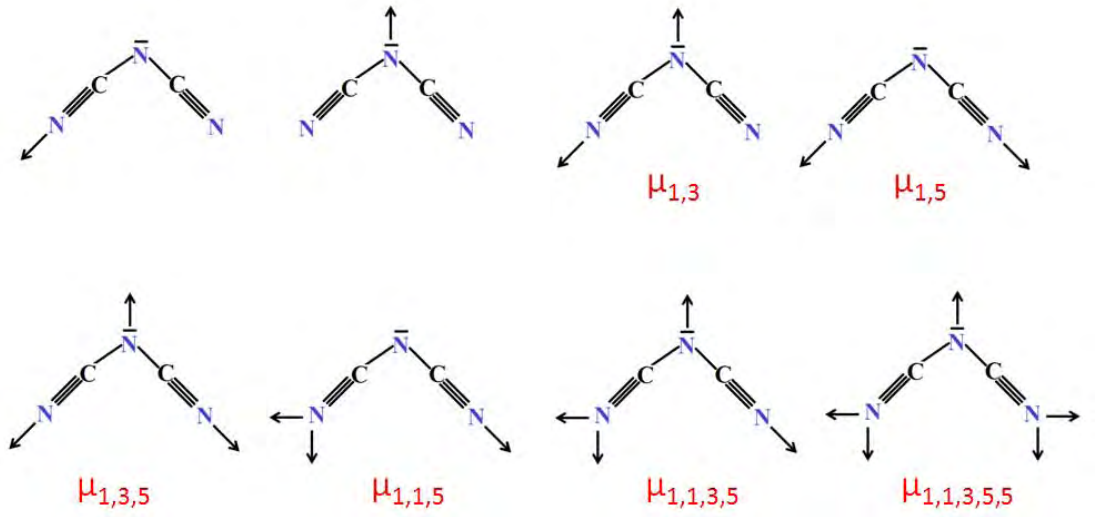

Fig. 5.1. Bridging modes of dicyanamide.

The end-to-end $\mu_{1,5}$ bridging mode of dca (Fig. 5.1) with metal ions give rise to a weak antiferromagnetic coupling. The $\mu_{1,5}$ -dicyanamide bridging generally show weak coupling inside the chain which is due to longer distance between the Cu(II) ions. The weak interaction can also be explained by the fact that one end of the dca bridge is in the apical position of the square pyramidal copper. The magnetic orbital ($d_{x^2-y^2}$) being perpendicular to that direction, no overlap between magnetic orbitals is expected. The $\mu_{1,3,5}$ -bridging mode is able to produce weak or strong ferromagnetic interactions between the metal centres.

Self-assembly processes that lead to helical structures are common throughout biology and chemistry [7,8]. Protein α-helices and the DNA double helix are well known biological examples which have inspired the work of synthetic chemists aiming to create chemical analogs of these complex structures [9]. However, there is a little known about *meso*-helical self-assembling systems within this very active field of helical structure research in supramolecular chemistry [10].

5.2. Experimental

5.2.1. Synthesis of the complex

All chemicals used for synthesis were of Analar grade. The semicarbazone was formed *in situ*.

5.2.1.1. Synthesis of $[Cu(bpsc)N(CN)_2]_n.nH_2O$ (13)

2-Benzoylpyridine semicarbazone (Hbpsc) was synthesized *in situ* by heating a mixture of 2-benzoylpyridine (0.183 g, 1 mmol) and semicarbazide hydrochloride (0.112 g, 1 mmol) in methanol for 2 h. A methanolic solution of copper acetate monohydrate (0.199 g, 1 mmol) and sodium dicyanamide (0.09 g, 1 mmol) was added to it and the mixture was heated for 3 h. The dark green solid was collected and recrystallized from methanol. Yield: 74%.

5.2.2. Physical measurements

Carbon, hydrogen and nitrogen analyses were carried out using a Vario EL III CHNS analyzer at the SAIF, Kochi, India. Infrared spectra were recorded on a JASCO FT-IR-5300 Spectrometer in the range 4000-400 cm^{-1} using KBr pellets. Electronic spectra were recorded on Ocean Optics USB 4000 UV-Vis Fiber Optic Spectrometer in the 200-850 nm range using solutions in methanol. Magnetic susceptibility measurements of the complexes were carried out on a Vibrating Sample Magnetometer using $Hg[Co(SCN)_4]$ as a calibrant at the SAIF, Indian Institute of Technology, Madras. The EPR spectra of the complexes in the solid state at 298 K and in DMF/DMSO at 77 K were recorded on a Varian E-112 spectrometer using TCNE as the standard, with 100 kHz modulation frequency, 2 G modulation amplitude and 9.1 GHz microwave frequency at SAIF, IIT Bombay, India.

5.2.3. X-ray crystallography

Single crystals of compound $[Cu(bpsc)N(CN)_2]_n \cdot nH_2O$ (**13**) suitable for X-ray diffraction studies were grown from their methanolic solution by slow evaporation at room temperature. Single crystals were selected and mounted on a Bruker SMART

APEX diffractometer, equipped with a graphite crystal, incident-beam monochromator, and a fine focus sealed tube with Mo Kα (λ = 0.71073 Å) as the X-ray source. The crystallographic data along with details of structure solution refinements are given in Table 5.1. The unit cell dimensions were measured and the data collection was performed at 293(2) K. Bruker SMART software was used for data acquisition and Bruker SAINT software for data integration [11]. Absorption corrections were carried out using SADABS based on Laue symmetry using equivalent reflections [12]. The structure was solved by direct methods and refined by full-matrix least-squares calculations with the WinGX software package [13]. The molecular and crystal structures were plotted using DIAMOND version 3.2g [14].

In the refinement of $[Cu(bpsc)N(CN)_2]_n \cdot nH_2O$ (**13**) carbon-bound H-atoms were placed in calculated positions (C–H=0.93 Å) and were included in the refinement in the riding model approximation, with U(H) set to 1.2U(C). The amino H-atoms were similarly treated (N–H=0.88 Å) and their temperature factors tied by a factor of 1.2 times. Omitted owing interference from the beam stop were (2 1 0), (0 0 2), (1 1 2), (1 1 4) and (1 2 1). The presence of water was indicated by an infrared spectral measurement. The two independent water molecules are both disordered over two positions; the occupancy could not be refined, and was assumed as a 1:1 type of disorder. For one molecule, the disorder is such that two components are separated by about 2 Å, so that one hydrogen atom should be midway between two oxygen atoms. For the other, the two are separated by about 1 Å, so that one hydrogen atom should be occupying the site of the other oxygen atom. For both, hydrogen atoms were positioned on only one component oxygen atom so that each water molecule forms only one hydrogen bond. Furthermore, the hydrogen atoms were given full occupancy, i.e., hydrogen atoms were not placed on those atoms that do not engage in hydrogen bonding.

Table 5.1. Crystallographic data and structure refinement for **13**

Parameters	$[Cu(bpsc)N(CN)_2]_n \cdot nH_2O$
Empirical formula	$C_{15}H_{13}CuN_7O_2$
Formula weight	386.86
Color	Green
Temperature (T) K	296(2)
Wavelength (Mo Kα) (Å)	0.71073
Crystal system	Orthorhombic
Space group	*Pbca*
Cell parameters	
a	12.3996(2) Å
b	21.0115(4) Å
c	26.7059(5) Å
α	90°
β	90°
γ	90°
Volume V ($Å^3$)	6957.8(2)
Z	16
Calculated density (ρ) ($Mg\ m^{-3}$)	1.477
Absorption coefficient, μ (mm^{-1})	1.28
F(000)	3152
Crystal size mm^3	0.40 x 0.30 x 0.20
θ range for data collection	2.7 to 26.5°
Limiting indices	$-14 \le h \le 14$, $-24 \le k \le 24$, $-31 \le l \le 31$
Reflections collected	97863
Unique Reflections (R_{int})	6113 [R(int) = 0.0526]
Completeness to θ	25.00 (99.9 %)
Absorption correction	Semi-empirical from equivalents
Maximum and minimum transmission	0.7845 and 0.6294
Refinement method	Full-matrix least-squares on F^2
Data / restraints / parameters	6113 / 6 / 481
Goodness-of-fit on F^2	1.168
Final R indices [$I > 2\sigma(I)$]	$R_1 = 0.0442$, $wR_2 = 0.1117$
R indices (all data)	$R_1 = 0.0742$, $wR_2 = 0.1435$
Largest difference peak and hole (e $Å^{-3}$)	0.611 and -0.381

$R_1 = \Sigma||F_o| - |F_c|| / \Sigma|F_o|$ $\quad$ $wR_2 = [\Sigma w(F_o^2-F_c^2)^2 / \Sigma w(F_o^2)^2]^{1/2}$

5.3. Results and discussion

5.3.1. Analytical measurements

The analytical data of the complex is listed in Table 5.2. The CHN obtained showed that the complex is analytically pure.

Table 5.2. Preliminary analytical data of $[Cu(bpsc)N(CN)_2]_n \cdot nH_2O$

Compound	Observed (Calculated)%			λ_m	μ_{eff}(B.M.)
	C	H	N		
$[Cu(bpsc)N(CN)_2]_n \cdot nH_2O$ (**13**)	48.62 (48.85)	3.07 (3.01)	26.30 (26.58)	16	1.71

5.3.2. Crystal structure of complex $[Cu(bpsc)N(CN)_2]_n \cdot nH_2O$ (13)

The structure determination reveals that the complex **13** consists of chains in which two neighboring [Cu(bpsc)] units are linked by a bridging $\mu_{1,5}$-NCNCN ligand. Adjacent metal atoms are bridged by the dicyanamide ion to generate a chain that propagates along the 'b' axis of the orthorhombic unit cell (Fig. 5.2).

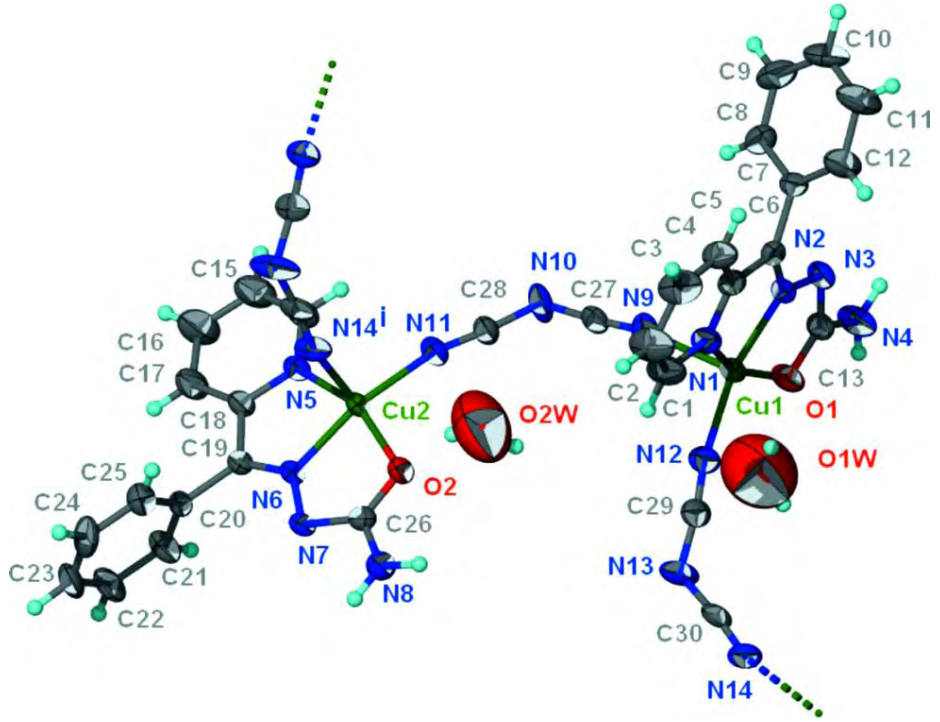

Fig. 5.2. Thermal ellipsoid plot of a portion of the chain structure of $[Cu(bpsc)N(CN)_2]_n \cdot nH_2O$ (**13**) at the 50% probability level; hydrogen atoms are drawn as spheres of arbitrary radius. The disorder in the water molecules is not shown.

Table 5.3. Selected bond lengths [Å] and angles [°] for $[Cu(bpsc)N(CN)_2]_n \cdot nH_2O$ (**13**)

Bond lengths (Å)			
Cu1–O1	1.966(3)	Cu2–O2	1.977(3)
Cu1–N2	1.946(3)	Cu2–N6	1.940(3)
Cu1–N1	2.004(4)	Cu2–N5	2.016(3)
Cu1–N12	1.955(3)	Cu2–N14^{i}	2.228(4)
Cu1–N9	2.205(4)	Cu2–N11	1.941(3)
N2–N3	1.358(4)	N6–N7	1.358(4)
C13–N3	1.349(5)	C26–N7	1.353(5)
O1–C13	1.278(4)	O2–C26	1.281(4)
Bond angles (°)			
O1–Cu1–N12	97.91(14)	O2–Cu2–N11	96.58(13)
O1–Cu1–N2	79.14(12)	O2–Cu2–N6	79.29(12)
N2–Cu1–N1	80.51(13)	N6–Cu2–N5	80.58(12)
N1–Cu1–N9	94.37(16)	N14^{i}–Cu2–N5	94.34(14)
N1–Cu1–N12	97.91(15)	N14^{i}–Cu1–N11	98.04(14)

Selected bond lengths and angles are summarized in Table 5.3. In the chain of complex, each copper atom has a distorted square pyramidal environment [with trigonality index, τ (Addison parameter) = 0.101 (for Cu1) and 0.120 (for Cu2)], in which two nitrogen atoms, N(1) and N(2), and the iminolate oxygen atom, O(1), of the tridentate semicarbazone ligand and the nitrile nitrogen atom, N(12), of the dicyanamide anion coordinate to define an equatorial plane around the copper atom. The apical fifth coordination site of the square pyramid is occupied by the nitrogen atom N(9) of the dicyanamide group. All the equatorial bond lengths are shorter than the apical Cu–N bond distances for both complexes and are in good agreement with those previously reported in the literature [15].

The Cu(II) atoms are linked by $N(CN)_2^-$ anions leading to infinite *meso* helical chains along 'b' axis. Similar to helix, several 1D *meso*-helix coordination polymers have been characterized [16]. As shown in Fig. 5.3, a *meso*-helix is a 3D presentation of a lemniscate.

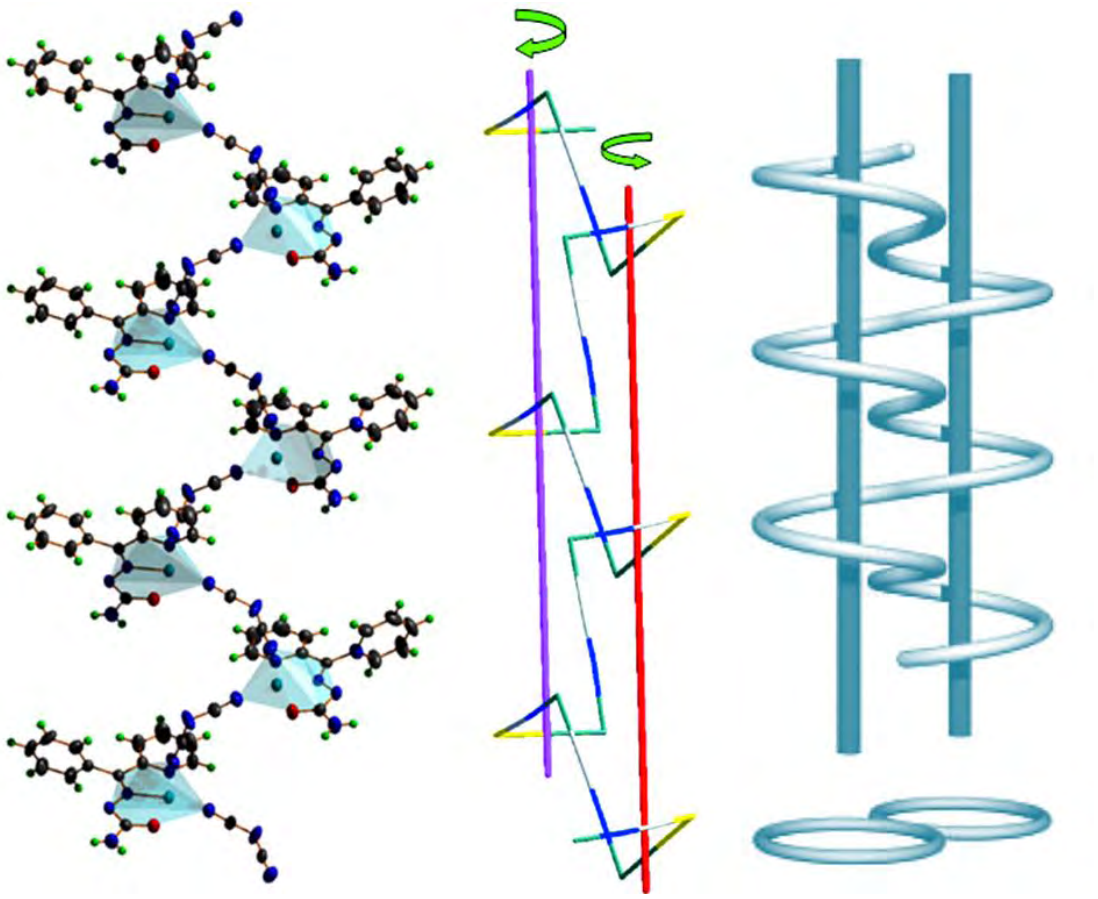

Fig. 5.3. Generation of *meso*-helix from a lemniscate in $[Cu(bpsc)N(CN)_2]_n \cdot nH_2O$ (**13**).

The details of the H-bonding distances are given in Table 5.4. The two independent water molecules are disordered over two positions; each water molecule is a hydrogen-bond donor to a carbonyl O atom. Each water molecule is a hydrogen-bond donor to a carbonyl O atom. Weak N–H···N hydrogen bonding is also observed (Fig. 5.4).

Table 5.4. Hydrogen bonding interactions of the complex $[Cu(bpsc)N(CN)_2]_n \cdot nH_2O$ (**13**)

D–H···A	D–H (Å)	H···A (Å)	D···A (Å)	∠D–H···A (°)
O(1W)–H(1W1)···O(1)	0.8409	2.0503	2.88(2)	168.91
O(2W)–H(2W1)···O(2)	1.3077	2.3462	2.95(2)	104.29
N(4)–H(42)···N(7)[a]	0.8787	2.1294	3.006(5)	175.64
N(8)–H(482)···N(3)[b]	0.8804	2.1446	3.025(5)	178.88

Equivalent position codes: a= x,1/2-y,1/2+z; b= x,1/2-y,-1/2+z.

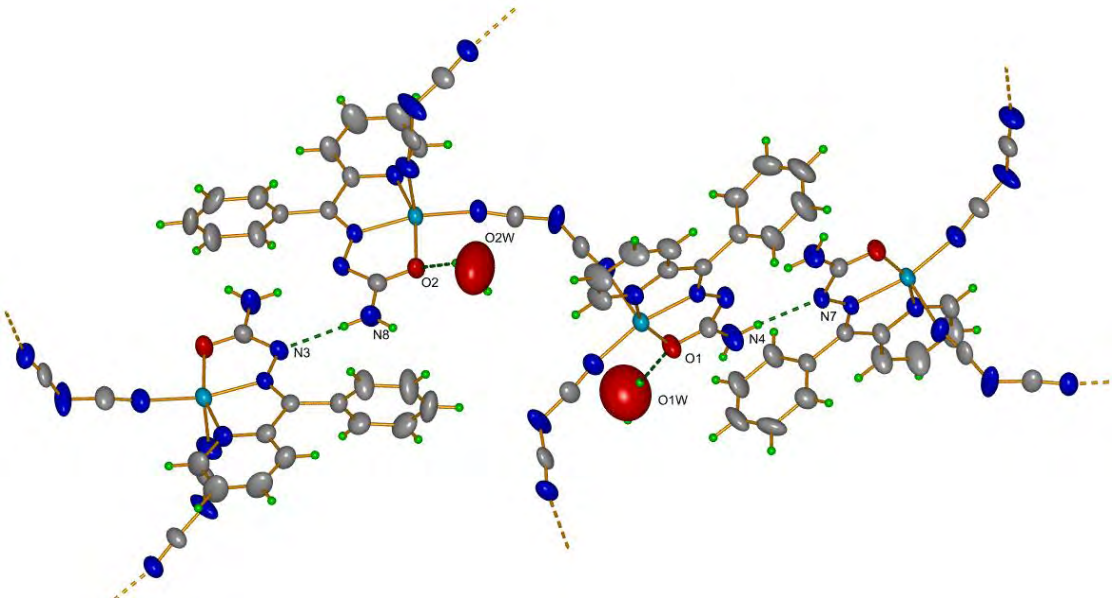

Fig. 5.4. Hydrogen bonding interactions in $[Cu(bpsc)N(CN)_2]_n \cdot nH_2O$ (**13**).

Geometric features of the π···π stacking interactions are given in Table 5.5. In complex **13** mononuclear unit of two adjacent 1D polymeric chains shows π···π interactions with each other, Cg(5)···Cg(8)^c and Cg(6)···Cg(7)^c (c=1/2+x,1/2-y,1-z) (centroid-centroid separation: 3.8487(19) and 3.7429(19) Å, as shown in Fig. 5.5).

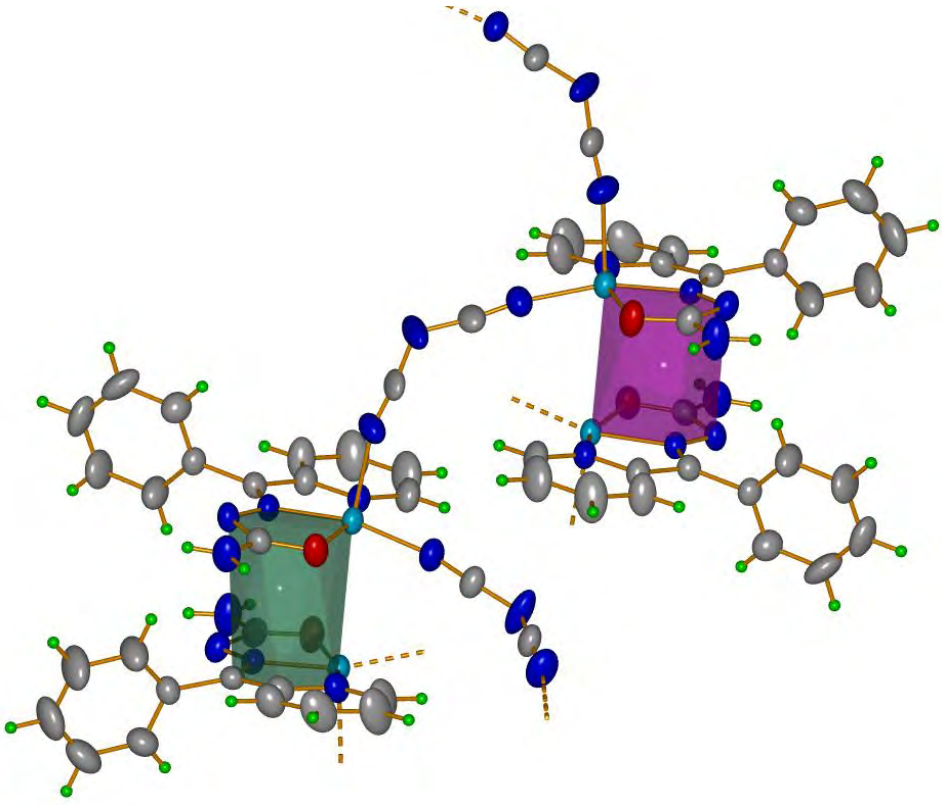

Fig. 5.5. π···π interactions in $[Cu(bpsc)N(CN)_2]_n \cdot nH_2O$ (**13**).

Table 5.5. π···π interactions of $[Cu(bpsc)N(CN)_2]_n \cdot nH_2O$ (**13**)

Cg(I)···Cg(J)	Cg···Cg (Å)	α (°)	β (°)	γ (°)
Cg(5)···Cg(8)[c]	3.8487(19)	4.54	10.10	9.95
Cg(6)···Cg(7)[c]	3.7429(19)	8.69	13.86	8.71

Equivalent position codes: c=1/2+x,1/2-y,1-z; Cg(5) = Cu1, O1, C13, N3, N2; Cg(6) = Cu1, N1, C5, C6, N2; Cg(7) = Cu2, O2, C26, N7, N6; Cg(8) = Cu2, N5, C18, C19, N6

The complex shows significant C–H···π interactions. Geometric features of the C–H···π interactions (Fig. 5.6) are given in Table 5.6.

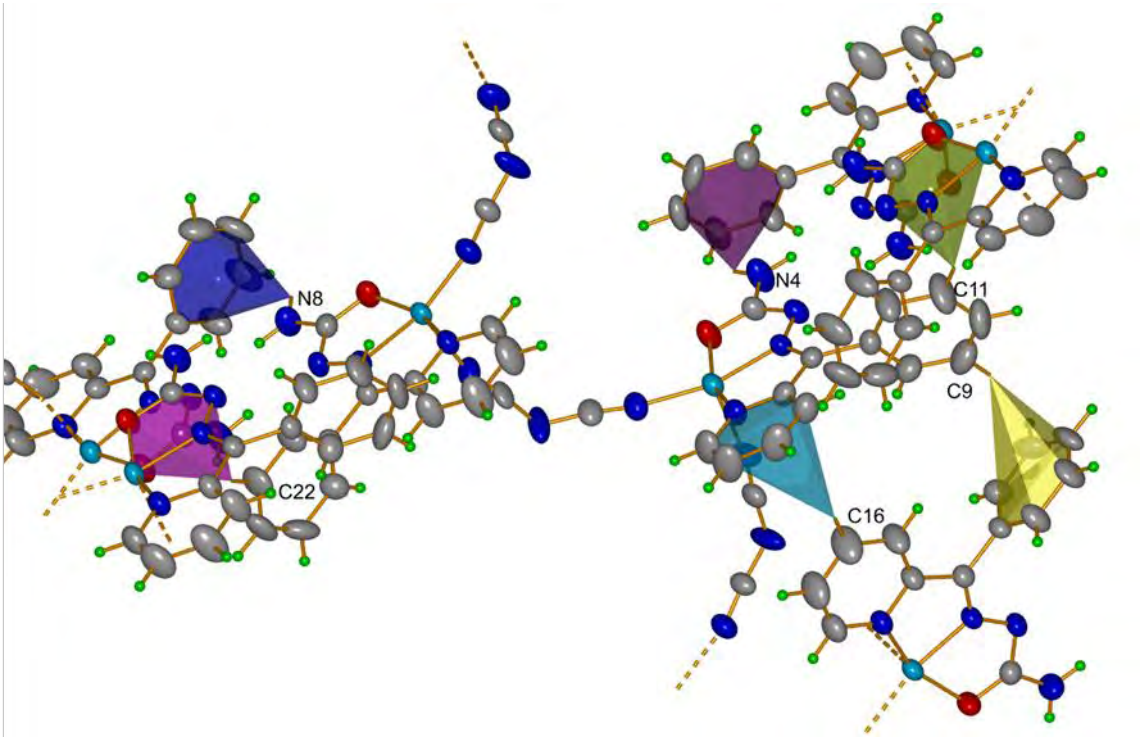

Fig. 5.6. C–H···π and N–H ···π interactions of $[Cu(bpsc)N(CN)_2]_n \cdot nH_2O$ (**13**).

Table 5.6. C–H···π and N–H···π interactions of $[Cu(bpsc)N(CN)_2]_n \cdot nH_2O$ (**13**)

X–H(I)···Cg(J)	H···Cg (Å)	X···Cg (Å)	∠X–H···Cg (°)
C(9)–H(9)···Cg(14)[d]	3.2318	4.068(5)	150.77
C(11)–H.(11)···Cg(5)[e]	3.1600	3.994(6)	149.96
C(16)–H(16)···Cg(11)[d]	3.2349	4.115(7)	158.56
C(22)–H(22)···Cg(7)[f]	3.0624	3.914(5)	153.06
N(4)–H(41)···Cg(14)[a]	2.6117	3.182(4)	122.30
N(8)–H(81)···Cg(13)[b]	2.8401	3.392(4)	122.30

Equivalent position codes: d=1-x,-y,1-z; e=-1/2+x,y,3/2-z; f=-1/2+x,y,1/2-z

Cg(11)= N1, C1, C2, C3, C4, C5; Cg(13)= C7, C8, C9, C10, C11, C12; Cg(14)= C20, C21, C22, C23, C24, C25

Unit cell packing diagram of the molecule is given in Fig. 5.7.

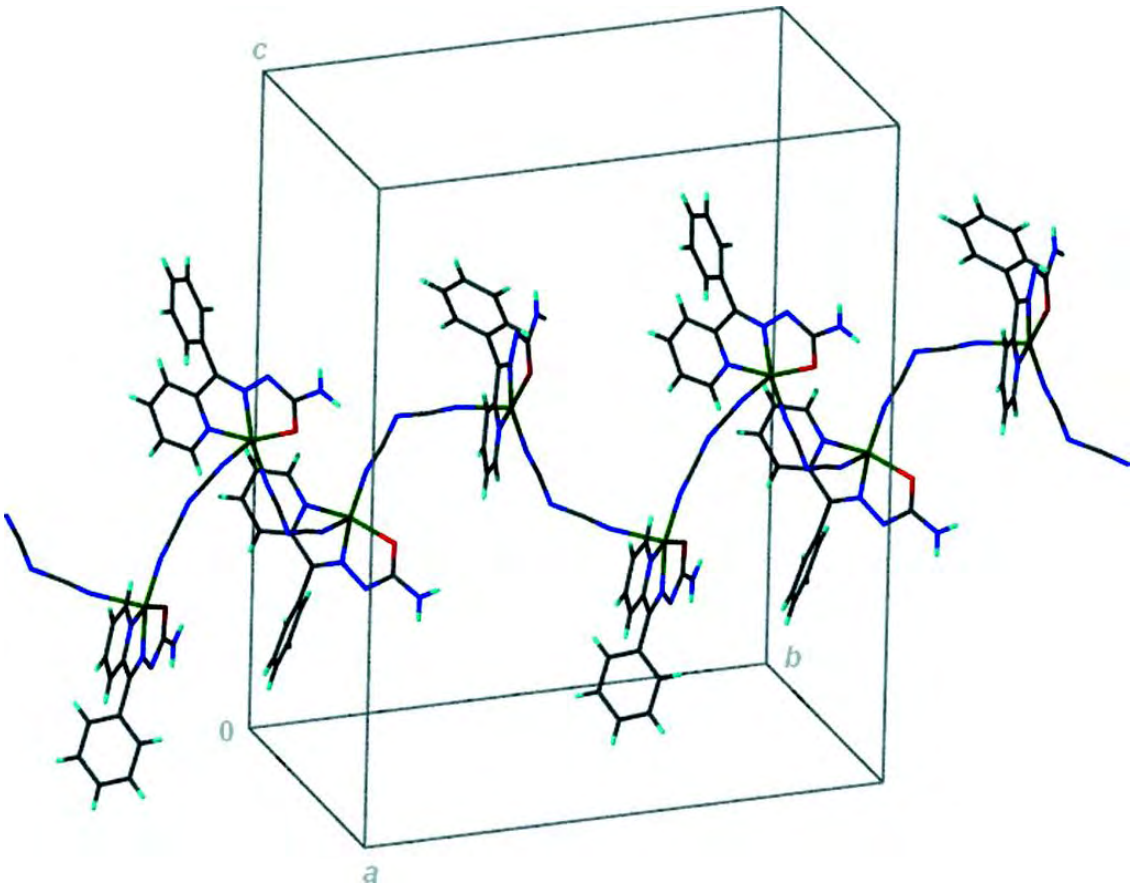

Fig. 5.7. Unit cell packing diagram of $[Cu(bpsc)N(CN)_2]_n \cdot nH_2O$ (**13**).

5.3.3. Infrared spectral studies of $[Cu(bpsc)N(CN)_2]_n \cdot nH_2O$ (13)

The distinct band due to the azomethine group at 1634 cm^{-1} is noticed in the IR spectrum of this complex [17]. In the IR spectrum of the dicyanamido complex, three peaks of very strong to medium intensities are observed in the 2155-2283 cm^{-1} region, attributed to the asymmetric stretching of the C≡N bond. The splitting of the CN band most probably results from the presence of the coordinated dicyanamide $[NCNCN]^-$ ion in two different environments and from the unequal C≡N bond lengths [18].

The dicyanamide anion in $NaN(CN)_2$ shows three sharp and strong characteristic bands in the frequency region 2290-2170 cm^{-1} attributed to ν_s(C≡N) combination modes (2286 cm^{-1}), ν_s(C≡N) (2232 cm^{-1}) and ν_s(C=N) (2179 cm^{-1}), respectively [19]. The shift towards higher frequencies of these peaks in **13** as compared to the free dca anion is due to the bridging coordination modes of dca in the complex (Fig. 5.8).

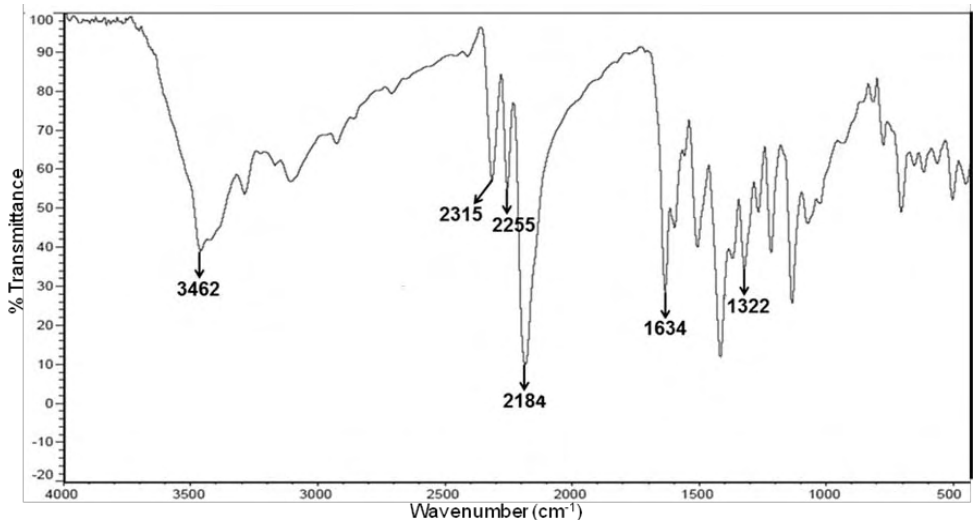

Fig. 5.8. IR spectrum of $[Cu(bpsc)N(CN)_2]_n \cdot nH_2O$ (**13**)

5.3.4. Electronic spectral studies of $[Cu(bpsc)N(CN)_2]_n \cdot nH_2O$ (13)

The semicarbazone and its copper(II) complex have two bands; one centered in the 37295-45360 cm^{-1} region and the other in the 30150-33170 cm^{-1} region (Fig. 5.9 and Table 5.7). These bands are due to $\pi \rightarrow \pi^*$ and $n \rightarrow \pi^*$ transitions of phenyl rings and semicarbazide moiety [20]. The charge transfer bands were observed at 26460 cm^{-1} region and its broadness can be explained as due to the combination of O→Cu and N→Cu LMCT transitions [21]. It is rather difficult to interpret electronic spectra of Cu(II) complexes as they possess flexible stereochemistry. The outer electronic configuration for copper(II) ion is $3d^9$ with ^2D as ground state term which will be split by an octahedral field in to two levels $^2T_{2g}$ and ^2E_g. So the expected excitation in an octahedral d^9 system is from ^2E_g to $^2T_{2g}$ results in a single absorption band. However the geometry around copper(II) ion lacks cubic symmetry and the tetragonal distortion yields other distorted forms of basic stereochemistries. Jahn-Teller distortions cause further splitting of the $^2T_{2g}$ and ^2E_g. So the possible spin allowed excitations *viz.* $^2A_{1g} \leftarrow {}^2B_{1g}$, $^2B_{2g} \leftarrow {}^2B_{1g}$ and $^2E_g \leftarrow {}^2B_{1g}$ which occur in the region 11760-18180, 15500-18010 and 17240-20000 cm^{-1} respectively. But the energy difference between these levels is too small to resolve them into separate bands. The ligand field at the metal center affects the splitting of *d*-orbitals and so the associated *d-d* transitions are sensitive probes of the ligand geometry. The *d-d* absorption maxima range from 16394-11560 cm^{-1} and tend to be indicative of tetragonal geometries [22].

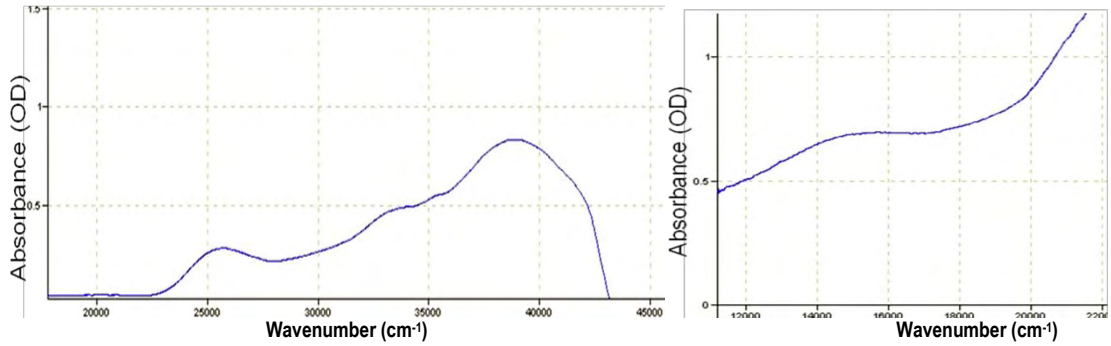

Fig. 5.9. Electronic spectra of $[Cu(bpsc)N(CN)_2]_n \cdot nH_2O$ (**13**).

Table 5.7. Electronic spectral assignments (cm^{-1}) for copper(II) dicyanamido complex

Compound	*d-d*	LMCT	$n \rightarrow \pi^*/\pi \rightarrow \pi^*$
$[Cu(bpsc)N(CN)_2]_n \cdot nH_2O$ (**13**)	15100	26460	34190, 39200

5.3.5. EPR spectral studies of $[Cu(bpsc)N(CN)_2]_n \cdot nH_2O$ (13)

The complex **13** in polycrystalline state at 298 K (Fig. 5.10) gave a typical axial spectrum with $g_{||}$= 2.164 and $g_{\perp}$= 2.064. The g_{av} values calculated as g_{av} =1/3($g_{||}$ +2$g_{\perp}$) has the value 2.097. Hyperfine splitting is not well resolved. The EPR spectrum of **13** at 77 K (Fig. 5.10) also exhibits well defined axial spectrum with $g_{||}$= 2.245 and $g_{\perp}$= 2.054. The parallel region of the spectrum is well resolved and consists of a set of four hyperfine lines due to the interaction of the electron with the Cu(II) nucleus (number of hyperfine lines = 2n*I*+1 and for ^{63}Cu, *I*=3/2). The perpendicular region of the spectrum is devoid of hyperfine splitting. The $g_{||}$ values provide information regarding the nature of metal-ligand bond [23]. The $g_{||}$ value is normally 2.3 or larger for ionic and less than 2.3 for covalent metal-ligand bonds. The $g_{||}$ values obtained indicate a significant degree of covalency in the metal-ligand bonds.

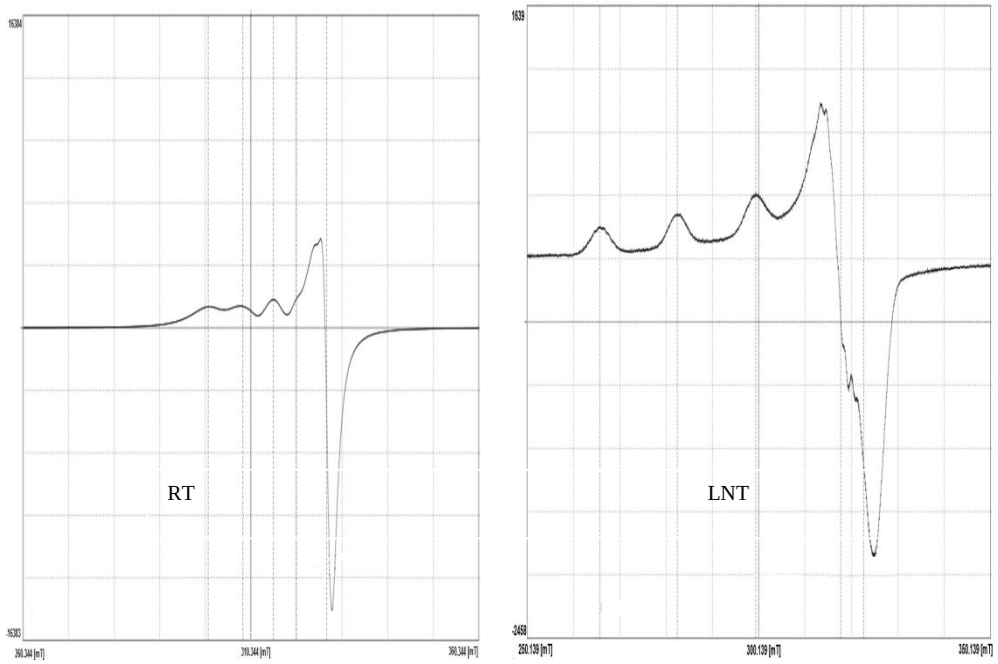

Fig. 5.10. EPR spectra of complex $[Cu(bpsc)N(CN)_2]_n \cdot nH_2O$ (**13**).

Spin Hamiltonian and bonding parameters of the complex is shown in Table 5.8.

Table 5.8. Spin Hamiltonian and bonding parameters of the complex $[Cu(bpsc)N(CN)_2]_n \cdot nH_2O$ (**13**)

Polycrystalline state at 298 K				**Solution state at 77 K**							
$g_{\|\|}$	$g_{\perp}$	g_{rv}	G	$g_{\|\|}$	$g_{\perp}$	$A_{\|\|}$	α^2	β^2	γ^2	$K_{\|\|}$	$K_{\perp}$
2.164	2.064	2.097	2.621	2.245	2.054	18.968	0.857	0.868	0.801	0.744	0.687

REFERENCES

1. J.-Y. Xu, C.-Z. Xie, F. Xue, L.-F. Hao, Z.-Y. Ma, D.-Z. Liaob, S.-P. Yan, Dalton Trans., 2010, 39, 7159. (b) M. Maiti, D. Sadhukhan, S. Thakurta, S. Roy, G. Pilet, R.J. Butcher, A. Nonat, L.J. Charbonnière, S. Mitra, Inorg. Chem., 2012, 51, 12176. (c) A. Majumder, G. Pilet, M.T.G. Rodriguez, S. Mitra, Polyhedron, 2006, 25, 2550. (d) K. Ma, Q. Shi, M. Hu, X. Cai, S. Huang, Inorg. Chim. Acta, 2009, 362, 4926.
2. E. Colacio, I.B. Maimoun, F. Lloret, J. Suárez-Varela, Inorg. Chem., 2005, 44, 3771. (b) M. Kurmoo, C.J. Kepert, New J. Chem., 1998, 1515. (c) D. Ghoshal, H. Bialas, A. Escuer, T.K. Maji, J. Ribas, X. Solans, R. Vicente, E. Zangrando, N.R. Chaudhuri, Eur. J. Inorg. Chem., 2003, 3929.
3. Z.-G. Gu, X.-H. Zhou, Y.-B. Jin, R.-G. Xiong, J.-L. Zuo, X.-Z. You, Inorg. Chem., 2007, 46, 5462. (b) X.-J. Zhao, Q. Wang, M. Du, Inorg. Chim. Acta, 2007, 360, 1970. (c) D. Mal, R. Sen, E. Rentschler, K.-I. Okamoto, Y. Miyashita, S. Koner, Inorg. Chim. Acta, 2012, 385, 27. (d) J. Luo, M. Hong, J. Weng, Y. Zhao, R. Cao, Inorg. Chim. Acta, 2002, 329, 59.
4. S. Benmansour, F. Setifi, S. Triki, J.-Y. Salaün, F. Vandervelde, J. Sala-Pala, C.J. Gómez-García, T. Roinset, Eur. J. Inorg. Chem., 2007, 186.
5. D. Sadhukhan, A. Ray, R.J. Butcher, C.J. Gómez Garclá, B. Dede, S. Mitra, Inorg. Chim. Acta, 2011, 376, 245.
6. D.R. Turner, A.S.R. Chesman, K.S. Murray, G.B. Deacon, S.R. Batten, Chem. Commun., 2011, 47, 10189.
7. X.-J. Luan, X.-H. Cai, Y.-Y. Wang, D.-S. Li, C.-J. Wang, P. Liu, H.-M. Hu, Q.-Z. Shi, S.-M. Peng, Chem. Eur. J., 2006, 12, 6281.
8. C. Piguet, G. Bermardinelli, G. Hopfgartner, Chem. Rev., 1997, 97, 2005.
9. L.M. Greig, D. Philp, Chem. Soc. Rev., 2001, 30, 287.
10. L. Cheng, J.-B. Lin, J.-Z. Gong, A.-P. Sun, B.-H. Ye, X.-M. Chen, Cryst. Growth Des., 2006, 6, 2739.
11. SMART and SAINT, Area Detector Software Package and SAX Area Detector Integration Program, Bruker Analytical X-ray; Madison, WI, USA, 1997.

12. SADABS, Area Detector Absorption Correction Program; Bruker Analytical X-ray; Madison, WI, 1997.
13. L.J. Farrugia, J. Appl. Cryst., 2012, 45, 849.
14. K. Brandenburg, Diamond Version 3.2g, Crystal Impact GbR, Bonn, Germany, 2010.
15. M. Fondo, A.M. Garcia-Deibe, N. Ocampo, R. Vicente, J. Sanmartin, C. Sanudo, Inorg. Chim. Acta, 2011, 373, 73.
16. (a) L. Plasseraud, H. Maid, F. Hample, R.W. Saalfrank, Chem. Eur. J., 2001, 7, 4007. (b) G. Becker, B. Eschbach, O. Mundt, N. Seidler, Z. Anorg, Allg. Chem., 1994, 620, 1381. (c) R.A. Bartlett, M.M. Olmstead, P.P. Power, Inorg. Chem., 1986, 25, 1243.
17. D. Maity, S. Chattopadhyay, A. Ghosh, M.G.B. Drew, G. Mukhopadhyay, Polyhedron, 2009, 28, 812.
18. F.A. Mautner, C.N. Landry, A.A. Gallo, S.S. Massoud, J. Mol. Struct., 2007, 837, 72.
19. H. Köhler, A. Kolbe, G. Lux, Z. Anorg. Allg. Chem., 1977, 428, 103.
20. M.R.P Kurup, B. Varghese M. Sithambaresan, S. Krishnan, S.R. Sheeja, E. Suresh, Polyhedron, 2010, 30, 70.
21. R.P. John, A. Sreekanth, V. Rajakannan, T.A. Ajith, M.R.P. Kurup, Polyhedron, 2004, 23, 2549.
22. P.B. Sreeja, M.R.P. Kurup, A. Kishore, C. Jasmin, Polyhedron, 2004, 23, 575.
23. T.D. Smith, J. Pilbrow, Coord. Chem. Rev., 1974, 13, 173.

Chapter 6

Copper(II) complexes containing chloride as coligand

Contents

6.1. Introduction

The design of high or low nuclearity transition metal clusters with novel magnetic properties is a major goal of current research. Copper(II) clusters are of present interest in bioinorganic chemistry, multi-electron transfer, catalysis, and magnetostructural correlations. In fact, 1-D magnetic materials are becoming a very fruitful area of investigation owing to their potential to afford a large variety of interesting structural types with unusual magnetic properties, such as spin-ladder and spin frustrated systems, single chain magnets etc [1,2]. This has led to an increasing interest in the study of magnetic properties of 1-D copper(II) systems. Studies in this area have been further fuelled by a prediction that spin-ladders with mobile charge carriers could become superconducting [3]. The prediction has been confirmed in several copper oxide spin-ladders in recent studies [4,5]. Towards this end, quite a few halide bridged copper(II) complexes with spin-ladder type structure have been studied [6,7].

During the past decade, particular interest has been directed towards the investigation of copper(II) complexes with halogen bridging ligands as well as pseudohalogens, due to their correlative structures and ability to transmit magnetic interactions. The chloride anion has the capability of acting as either a bridging or a terminal ligand, occupying either axial or equatorial coordination positions [8]. As a result, mono- or polynuclear complexes as well as 1-D chain-like compounds have been obtained. However, up to now, most researchers focus on dimeric Cu(II) complexes. The investigations on the structure and magnetic properties of chloro-bridged Cu(II) chain complexes are rarely reported [9,10].

Schiff bases play a very important role as chelating ligands in main group metal and transition metal coordination chemistry, due to their ease of synthesis, stability under a variety of oxidative and reductive conditions, and their structural versatility, which is associated with their various applications [11,12]. Schiff bases are frequently used in designing molecular ferromagnets, biological modeling applications, catalysis and in preparing liquid crystals [13]. Definitely the salen type ligands, prepared from the condenzation of a diamine with salicylaldehyde or its derivative, are receiving the most attention among all the Schiff bases, because of the ability of the phenoxo oxygen atoms to form μ^2-bridges, thus affording high nuclearity complexes [14] which could act as promising candidates to offer valuable insight into various natural electron-transfer events [15]. N_2O donor tridentate Schiff bases can also be easily prepared by refluxing an N-substituted diamine with salicylaldehyde or 2-hydroxy-1-naphthaldehyde [16,17]. The ligands can then be used to form complexes with several transition metals [18]. Supra-molecular interactions like H bonding, $\pi\cdots\pi$ and C–H$\cdots\pi$ interactions are responsible for the variations in the molecular as well as crystalline architectures of the complexes. Herein, we report the synthesis, structural features, spectroscopic characterization and X-ray crystal structures of six new complexes of copper(II).

6.2. Experimental

6.2.1. Synthesis of the complexes

All chemicals used for synthesis were of Analar grade. The semicarbazones and Schiff bases were formed *in situ*.

6.2.1.1. Synthesis of [Cu(Hmssc)Cl] (14)

A mixture of 2-Hydroxy-4-methoxybenzaldehyde (0.152 g, 1 mmol) and semicarbazide hydrochloride (0.111 g, 1 mmol) in methanol was refluxed for 3 h. Copper(II) chloride dihydrate (0.170 g, 1 mmol) dissolved in methanol was added to this solution and refluxed for another 2 h. Dark green colored crystals were isolated from the cool solution. Yield: 12%.

6.2.1.2. Synthesis of $[Cu(bpap)Cl_2]\cdot H_2O$ (15)

1-[(*E*)-[Phenyl(pyridin-2-yl)methylidene]amino]pyrrolidin-2-one was synthesized *in situ* by heating 2-benzoylpyridine (0.183 g, 1 mmol) and 1-aminopyrrolidin-2-one (0.100 g, 1 mmol) in methanol for 2 h. Copper(II) chloride

dihydrate (0. 170 g, 1 mmol) dissolved in methanol was added to it, and the mixture was heated for 3 h. The resulting pale green solid was collected and recrystallized from methanol. Yield: 82%.

6.2.1.3. Synthesis of $[Cu(bsde)Cl]_n$ (16)

The Schiff base was prepared by heating a mixture of 5-bromosalicylaldehyde (0.201 g, 1 mmol) and N,N-dimethylethylenediamine (0.088 g, 1 mmol) in methanol for 2 h. Copper(II) chloride dihydrate (0.170 g, 1 mmol) dissolved in methanol was added to the solution and refluxed for another 2 h. Dark green colored crystals were isolated from the cool solution. Yield: 78%.

6.2.1.4. Synthesis of $[Cu(csde)Cl]_n$ (17)

The Schiff base was prepared by heating a mixture of 5-chlorosalicylaldehyde (0.157 g, 1 mmol) and N,N-dimethylethylenediamine (0.088 g, 1 mmol) in methanol for 2 h. Copper(II) chloride dihydrate (0.170 g, 1 mmol) dissolved in methanol was added to the solution and refluxed for another 2 h. Dark green colored crystals were isolated from the cool solution. Yield: 80%.

6.2.1.5. Synthesis of [Cu(dbsap)Cl] (18)

(1-{(E)-[3,5-dibromo-2-oxidobenzylidene]pyrrolidin-2-one was synthesized *in situ* by heating a mixture of 3,5-dibromosalicylaldehyde (0.280 g, 1 mmol) and 1-aminopyrrolidin-2-one (0.100 g, 1 mmol) in methanol for 2 h. Copper(II) chloride dihydrate (0.170 g, 1 mmol) dissolved in methanol was added to it, and the mixture was heated for 5 h. The resulting pale green solid was collected and recrystallized from methanol. Yield: 77%.

6.2.1.6. Synthesis of $[Cu(Hdbssc)Cl]\cdot H_2O$ (19)

The 3,5-dibromosalicylaldehyde semicarbazone was prepared by heating a mixture of 3,5-dibromosalicylaldehyde (0.280g, 1mmol) and semicarbazide hydro-chloride (0.111 g,1 mmol) in methanol for 3 h. Copper(II) chloride dihydrate (0.170 g, 1 mmol) dissolved in methanol was added to the solution and refluxed for another 2 h. Dark green colored crystals were isolated from the cool solution. Yield: 12%.

6.2.2. Physical measurements

Carbon, hydrogen and nitrogen analyses were carried out using a Vario EL III CHNS analyzer at the SAIF, Kochi, India. Infrared spectra were recorded on a

JASCO FT-IR-5300 Spectrometer in the range 4000-400 cm^{-1} using KBr pellets. Electronic spectra were recorded on Ocean Optics USB 4000 UV-Vis Fiber Optic Spectrometer in the 200-850 nm range using solutions in methanol.

6.2.3. X-ray crystallography

Crystallographic data and structure refinement for all the complexes were shown in Tables 6.1a, 6.1b and 6.1c. Single crystals of [Cu(Hmssc)Cl] (**14**), $[Cu(bpap)Cl_2]\cdot H_2O$ (**15**), $[Cu(bsde)Cl]_n$ (**16**), $[Cu(csde)Cl]_n$ (**17**), [Cu(dbsap)Cl] (**18**) and $[Cu(Hdbssc)Cl]\cdot H_2O$ (**19**) suitable for X-ray diffraction studies were obtained from their methanolic solutions by slow evaporation at room temperature. Crystal with appropriate sizes were mounted on a Bruker SMART APEX diffractometer, equipped with a graphite crystal, incident-beam monochromator, and a fine focus sealed tube with Mo Kα (λ = 0.71073 Å) as the X-ray source. The unit cell dimensions were measured and the data collections were performed at 296(2) K. Bruker SMART software was used for data acquisition and Bruker SAINT software for data integration [19]. Absorption corrections were carried out using SADABS based on Laue symmetry using equivalent reflections [20]. The structure was solved by direct methods and refined by full-matrix least-squares calculations with the WinGX software package [21]. The graphics tool used was DIAMOND version 3.2g [22]. All non-hydrogen atoms were refined anisotropically. All the H atoms on C of [Cu(Hmssc)Cl] (**14**) were placed in calculated positions, guided by difference maps and refined isotropically. Carbon-bound H-atoms were placed in calculated positions (C–H = 0.93 Å) and were included in the refinement in the bridging model approximation, with *U*(H) set to 1.2*U*(C). The amino H-atoms were located from fourier maps restrained to (N–H = 0.88 ± 0.01 Å). The water H-atoms were located in a difference Fourier map, and were refined with a distance restraint of O–H = 0.84±0.01 Å, with their displacement parameters refined. The (0 1 0) reflection was omitted owing to interference from the beam stop.

In all the other complexes, the carbon bound hydrogen atoms were placed in calculated positions, guided by difference Fourier map and refined isotropically using riding model approximation. In $[Cu(Hdbssc)Cl]\cdot H_2O$ (**19**), hydrogen atoms on N2, N3, and O1W were located from difference Fourier maps and restrained using DFIX and DANG instructions.

Table 6.1a. Crystallographic data and structure refinement for **14** and **15**

Parameters	[Cu(Hmssc)Cl] (**14**)	$[Cu(bpap)Cl_2]\cdot H_2O$ (**15**)
Empirical formula	$C_9H_{10}ClCuN_3O_3$	$C_{16}H_{17}Cl_2CuN_3O_2$
Formula weight	307.20	417.77
Color	Dark green	Green
Temperature (T) K	296(2)	296(2)
Wavelength (Mo Kα) (Å)	0.71073	0.71073
Crystal system	monoclinic	triclinic
Space group	$P2_1/n$	$P\bar{1}$
Cell parameters		
a	11.8413(6) Å	9.1289(4) Å
b	14.2791(7) Å	9.4017(4) Å
c	13.5751(6) Å	10.6798(4) Å
α	90°	90.4350(10)°
β	102.501(2)°	99.163(2)°
γ	90°	105.491(2)°
Volume V ($Å^3$)	2240.90(19)	870.84(6)
Z	8	2
Calculated density (ρ) ($Mg\ m^{-3}$)	1.821	1.593
Absorption coefficient, μ (mm^{-1})	2.186	1.574
F(000)	1240	426
Crystal size (mm^3)	0.30 x 0.25 x 0.20	0.30 x 0.30 x 0.30
θ range for data collection	2.10 to 25.00°	2.25 to 28.22°
Limiting indices	$-13\le h\le 14$, $-16\le k\le 16$, $-11\le l\le 16$	$-12\le h\le 12$, $-12\le k\le 12$, $-14\le l\le 14$
Reflections collected	16965	15376
Unique Reflections (R_{int})	3942 [R(int) = 0.0441]	4252 [R(int) = 0.0326]
Completeness to θ	25.00 (99.8%)	28.22 (99.2%)
Absorption correction	Semi-empirical from equivalents	Semi-empirical from equivalents
Maximum and minimum transmission	0.646 and 0.524	0.6495 and 0.6495
Refinement method	Full-matrix least-squares on F^2	Full-matrix least-squares on F^2
Data / restraints / parameters	3935 / 8 / 333	4252 / 3 / 225
Goodness-of-fit on F^2	1.087	1.089
Final R indices [$I > 2\sigma(I)$]	$R_1 = 0.0346$, $wR_2 = 0.0823$	$R_1 = 0.0272$, $wR_2 = 0.0809$
R indices (all data)	$R_1 = 0.0532$, $wR_2 = 0.0938$	$R_1 = 0.0297$, $wR_2 = 0.0839$
Largest difference peak and hole ($e\ Å^{-3}$)	0.524 and -0.299	0.438 and -0.445

$R_1 = \Sigma||F_o| - |F_c|| / \Sigma|F_o|$ $\qquad$ $wR_2 = [\Sigma w(F_o^2-F_c^2)^2 / \Sigma w(F_o^2)^2]^{1/2}$

Table 6.1b. Crystallographic data and structure refinement for **16** and **17**

Parameters	$[Cu(bsde)Cl]_n$ (**16**)	$[Cu(csde)Cl]_n$ (**17**)
Empirical formula	$C_{11}H_{14}BrClCuN_2O$	$C_{11}H_{14}Cl_2CuN_2O$
Formula weight	369.14	324.68
Color	Green	Green
Temperature (T) K	296(2)	296(2)
Wavelength (Mo Kα) (Å)	0.71073	0.71073
Crystal system	orthorhombic	orthorhombic
Space group	*Pbca*	*Pbca*
Cell parameters		
a	8.5735(8) Å	8.575(2) Å
b	14.4041(8) Å	14.448(5) Å
c	20.7243(17) Å	20.468(6) Å
α	90°	90°
β	90°	90°
γ	90°	90°
Volume V ($Å^3$)	2559.3(3)	2536.0(13)
Z	8	8
Calculated density (ρ) (Mg m^{-3})	1.916	1.701
Absorption coefficient, μ (mm^{-1})	5.022	2.127
F(000)	1464	1320
Crystal size (mm^3)	0.40 x 0.30 x 0.20	0.40 x 0.35 x 0.30
θ range for data collection	2.83 to 26.79°	2.94 to 27.99
Limiting indices	$-10\leq h\leq 10$, $-17\leq k\leq 18$, $-20\leq l\leq 26$	$-11\leq h\leq 7$, $-19\leq k\leq 16$, $-22\leq l\leq 27$
Reflections collected	19157	10966
Unique Reflections (R_{int})	2732 [R(int) = 0.0374]	3052 [R(int) = 0.0458]
Completeness to θ	26.79 (100.0%)	27.99 (99.9%)
Absorption correction	Semi-empirical from equivalents	Semi-empirical from equivalents
Maximum and minimum transmission	0.4333 and 0.2386	0.5678 and 0.4833
Refinement method	Full-matrix least-squares on F^2	Full-matrix least-squares on F^2
Data / restraints / parameters	2732 / 0 / 156	3052 / 0 / 156
Goodness-of-fit on F^2	1.094	1.065
Final R indices [$I > 2\sigma(I)$]	$R_1 = 0.0373$, $wR_2 = 0.0805$	$R_1 = 0.0450$, $wR_2 = 0.1161$
R indices (all data)	$R_1 = 0.0550$, $wR_2 = 0.0891$	$R_1 = 0.0758$, $wR_2 = 0.1388$
Largest difference peak and hole (e $Å^{-3}$)	0.587 and -0.602	0.640 and -0.570

$R_1 = \Sigma||F_o| - |F_c|| / \Sigma|F_o|$ $\qquad$ $wR_2 = [\Sigma w(F_o^2-F_c^2)^2 / \Sigma w(F_o^2)^2]^{1/2}$

Table 6.1c. Crystallographic data and structure refinement for **18**, and **19**

Parameters	[Cu(dbsap)Cl] (**18**)	[Cu(Hdbssc)Cl]·H_2O (**19**)
Empirical formula	$C_{11}H_9Br_2C_{l1}CuN_2O_2$	$C_8H_8Br_2ClCuN_3O_3$
Formula weight	477.50	452.98
Color	Dark green	Green
Temperature (T) K	296(2)	296(2)
Wavelength (Mo Kα) (Å)	0.71073	0.71073
Crystal system	triclinic	monoclinic
Space group	$P\bar{1}$	$P2_1/n$
Cell parameters		
a	7.8288(11) Å	7.3794(10) Å
b	12.1863(12) Å	13.5324(15) Å
c	13.8014(17) Å	12.9543(13) Å
α	90.051(7)°	90°
β	90.066(7)°	97.536(6)°
γ	96.588(8)0°	90°
Volume V ($Å^3$)	1308.0(3)	1282.5(3)
Z	4	4
Calculated density (ρ) (Mg m^{-3})	2.425	2.346
Absorption coefficient, μ (mm^{-1})	7.807	8.144
F(000)	904	868
Crystal size (mm^3)	0.40 x 0.30 x 0.20	0.35 x 0.25 x 0.20
θ range for data collection	1.48 to 28.40	2.19 to 26.00
Limiting indices	-10≤h≤9, -14≤k≤16, -17≤l≤18	-6≤h≤9, -16≤k≤16, -15≤l≤14
Reflections collected	10529	7434
Unique Reflections (R_{int})	6106 [R(int) = 0.0876]	2492 [R(int) = 0.1150]
Completeness to θ	28.40 (92.7%)	26.00 (99.3%)
Absorption correction	Semi-empirical from equivalents	Semi-empirical from equivalents
Maximum and minimum	0.3043 and 0.1463	0.2927 and 0.1628
Refinement method	Full-matrix least-squares on F^2	Full-matrix least-squares on F^2
Data / restraints / parameters	6106 / 0 / 343	2492 / 6 / 179
Goodness-of-fit on F^2	1.033	1.272
Final R indices [I > 2σ (I)]	R_1 = 0.1073, wR_2 = 0.2737	R_1 = 0.1128, wR_2 = 0.3221
R indices (all data)	R_1 = 0.1963, wR_2 = 0.3350	R_1 = 0.1415, wR_2 = 0.3514
Largest difference peak and hole (e $Å^{-3}$)	2.303 and -2.328	2.253 and -2.147

$R_1 = \Sigma||F_o| - |F_c|| / \Sigma|F_o|$ $\quad wR_2 = [\Sigma w(F_o^2-F_c^2)^2 / \Sigma w(F_o^2)^2]^{1/2}$

6.3. Results and discussion

6.3.1. Analytical measurements

The analytical data of all the complexes are listed in Table 6.2. The CHN data obtained showed that all the complexes are analytically pure. The conductivity measurements were made in DMF solutions and all complexes are found to be non-electrolytes. Room temperature magnetic moments of these complexes show that all the copper(II) complexes have μ_{eff} values in the range 1.60-1.72 B. M., corresponding to the presence of one unpaired electron. These results suggest that no copper-copper interactions at room temperature are present in the complexes.

Table 6.2. Analytical data of Cu(II) chloride complexes

Compounds	Observed (Calculated)%			λ_m	μ_{eff}(B.M.)
	C	H	N		
[Cu(Hmssc)Cl] (**14**)	35.11 (35.19)	3.32 (3.28)	13.47 (13.68)	12	1.726
[Cu(bpap)Cl_2]·H_2O (**15**)	45.87 (46.00)	4.31 (4.10)	10.12 (10.06)	09	1.713
[Cu(Hbsde)Cl]$_n$ (**16**)	35.62 (35.79)	3.73 (3.82)	7.78 (7.59)	04	1.722
[Cu(Hcsde)Cl]$_n$ (**17**)	40.88 (40.69)	4.12 (4.35)	8.92 (8.63)	16	1.719
[Cu(Hdbsap)Cl] (**18**)	28.85 (28.72)	1.64 (1.97)	6.21 (6.09)	23	1.682
[Cu(Hdbssc)Cl]·H_2O (**19**)	21.42 (21.21)	1.52 (1.78)	9.34 (9.28)	19	1.698

6.3.2. Crystal structure of complex [Cu(Hmssc)Cl] (14)

The compound [Cu(Hmssc)Cl] (**14**) crystallizes in monoclinic space group $P2_1/n$. Fig. 6.1 shows the asymmetric unit consisting of two molecule of this complex with atom numbering scheme. The Cu(II) cation is *N,O,O'*-chelated by the deprotonated semicarbazone ligand and is further coordinated by a Cl^- anion in a distorted ClNOO square-planar geometry. The two copper atom in these molecules are coordinated by azomethine nitrogens (N1 and N4), phenolate oxygens (O2 and O5) and amido oxygens (O3 and O6). The coordination of the semicarbazone to the Cu atom through amido oxygen is confirmed by the bond lengths C9–O3 [1.257(4)] and C18–O6 [1.250(4)] Å which are very close to the reported values of complexes of semicarbazone [23]. Selected bond lengths (Å) and bond angles (°) of [Cu(Hmssc)Cl] (**14**) are shown in Table 6.3.

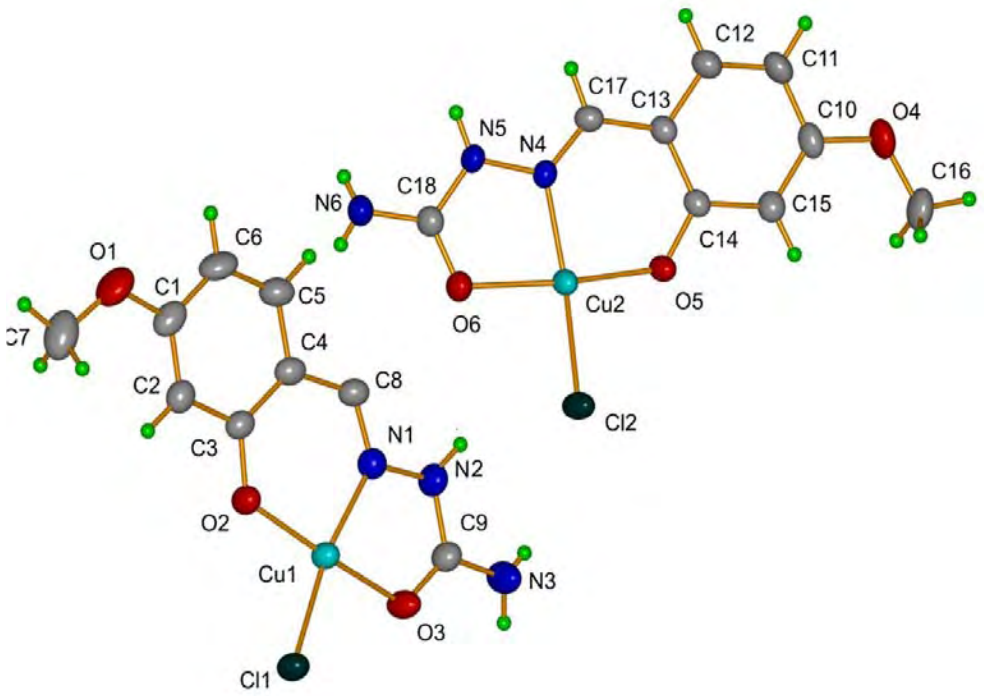

Fig. 6.1. Asymmetric unit of compound [Cu(Hmssc)Cl] (**14**).

Table 6.3. Selected bond lengths [Å] and angles [°] for the two molecules of [Cu(Hmssc)Cl] (**14**)

Molecule 1		Molecule 2	
Bond lengths (Å)			
Cu1–O2	1.880(2)	Cu2–O5	1.897(2)
Cu1–N1	1.920(3)	Cu2–N4	1.918(2)
Cu1–O3	1.963(2)	Cu2–O6	1.976(2)
Cu1–Cl1	2.2225(9)	Cu2–Cl2	2.2179(9)
N1–N2	1.376(4)	N4–N5	1.377(3)
N2–C9	1.353(4)	N5–C18	1.355(4)
O3–C9	1.257(4)	O6–C18	1.250(4)
Bond angles (°)			
O2–Cu1–N1	92.42(10)	O5–Cu2–N4	2.63(10)
O2–Cu1–O3	169.71(10)	O5–Cu2–O6	169.86(10)
N1–Cu1–O3	81.91(10)	N4–Cu2–O6	81.48(10)
O2–Cu1–Cl1	95.08(7)	O5–Cu2–Cl2	94.59(7)
N1–Cu1–Cl1	168.53(8)	N4–Cu2–Cl2	169.05(8)
O3–Cu1–Cl1	91.89(7)	O6–Cu2–Cl2	92.49(7)

Two independent but very identical [Cu(Hmssc)Cl] molecules are bridged by intermolecular hydrogen bonds. In the crystal, adjacent molecules are linked by N–H

···O and N–H···Cl hydrogen bonds, forming a two-dimensional network parallel to [100]. A supramolecular hydrogen bonding network is established between the molecules as shown in the Fig. 6.2. The intermolecular hydrogen bonding interactions are shown in Table 6.4.

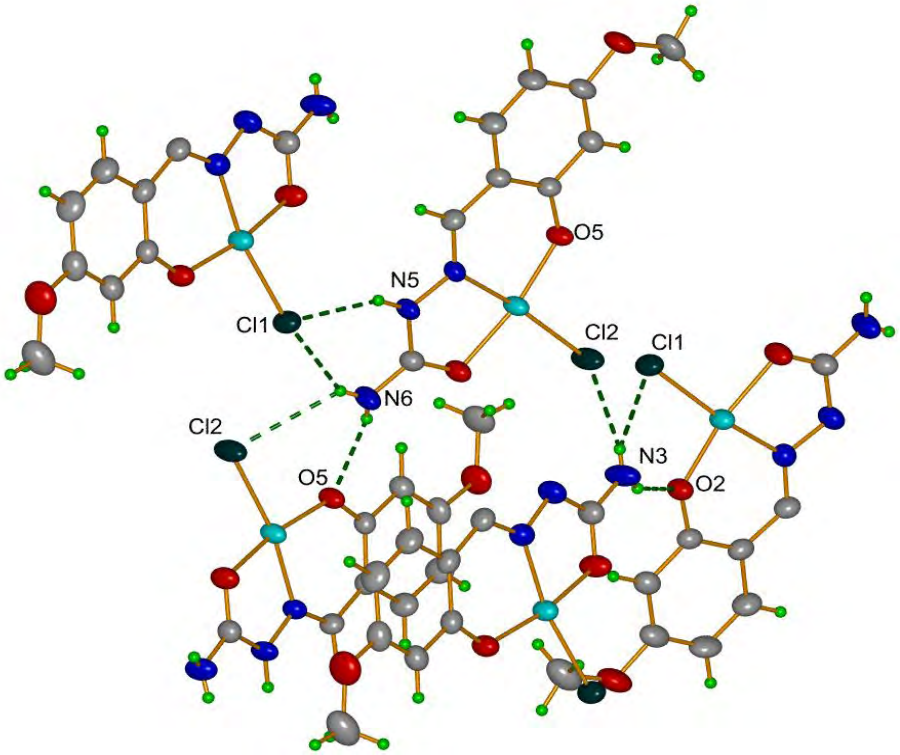

Fig. 6.2. Intermoleccular hydrogen bonding network of the compound [Cu(Hmssc)Cl] (**14**).

Table 6.4. Hydrogen bonding interactions of [Cu(Hmssc)Cl] (**14**)

D–H···A	D–H (Å)	H···A (Å)	D···A (Å)	∠D–H···A(°)
N(6)–H(1A)···O(5)^{a}	0.72(4)	2.24(4)	2.904(4)	154(4)
N(6)–H(1B)···Cl(1)^{b}	0.68(5)	2.79(5)	3.346(4)	142(5)
N(6)–H(1B)···Cl(2)^{a}	0.68(5)	2.77(5)	3.243(3)	129(5)
N(3)–H(1C)···O(2)^{c}	0.83(5)	2.03(4)	2.825(5)	160(4)
N(3)–H(1D)···Cl(2)	0.62(5)	2.74(5)	3.301(5)	150(5)
N(3)–H(1D)···Cl(1)^{c}	0.62(5)	2.83(5)	3.210(4)	123(5)
N(5)–H(8)···Cl(1)^{b}	0.8594	2.4215	3.214(3)	153.69

Equivalent position codes: a= 1/2-x,1/2+y,1/2-z; b=1+x,y,z; c=-1/2-x,-1/2+y,1/2-z. D, donor; A, acceptor.

The diverse π···π stacking is present in the molecular arrangement (Fig. 6.3) with Cg···Cg distances shown in Table 6.5. Four significant π···π interactions are also giving strength to the molecular system by the interaction between the rings of two

adjacent molecules with the distances of 3.6728(19), 3.5913(19), 3.7150(15) and 3.878(2) Å between the centroids of the corresponding interacting rings.

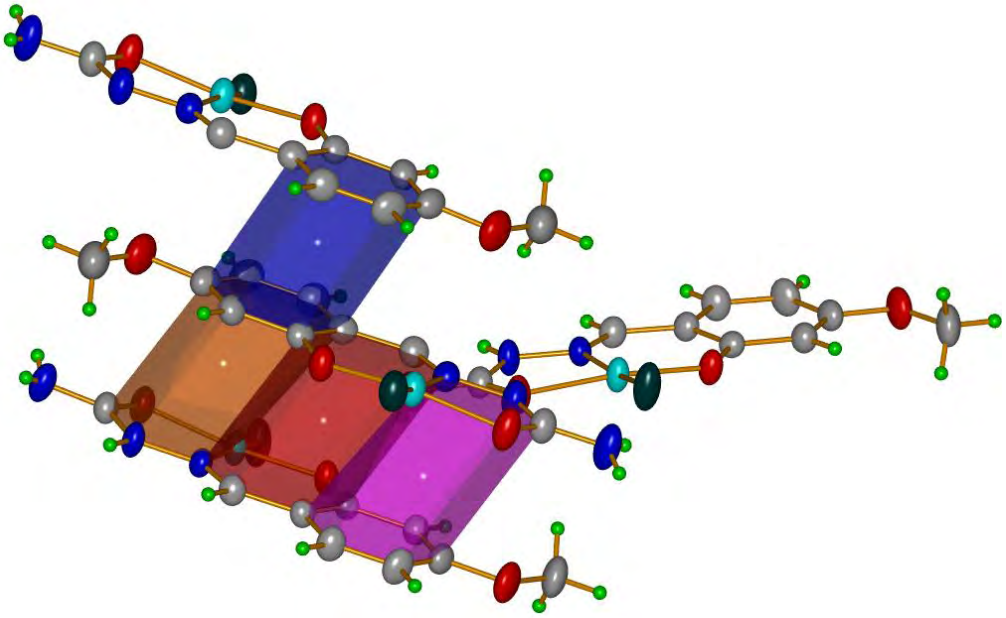

Fig. 6.3. π···π interactions between the molecules of the [Cu(Hmssc)Cl] (**14**).

Table 6.5. π···π interactions of the [Cu(Hmssc)Cl] (**14**)

Cg(I)···Cg(J)	Cg···Cg (Å)	α (°)	β (°)	γ(°)
Cg(5)···Cg(10)[a]	3.6728(19)	4.55	22.26	22.88
Cg(6)···Cg(9)[d]	3.5913(19)	3.26	20.33	23.09
Cg(7)···Cg(8)[a]	3.7150(15)	1.68	28.64	26.99
Cg(9)···Cg(9)[e]	3.878(2)	0.02	28.06	28.06

Equivalent position codes: a= 1/2-x,1/2+y,1/2-z; d=1/2-x,-1/2+y,1/2-z; e=-x,2-y,1-z. Cg(5) = Cu(1), O(3), C(9), N(2), N(1); Cg (6) = Cu(2), O(6), C(18), N(5), N(4); Cg (7) = Cu(1), O(2), C(3), C(4), C(8), N(1); Cg (8) = Cu(2), O(5), C(14), C(13), C(17), N(4); Cg (9) = C(1), C(2), C(3), C(4), C(5), C(6); Cg (10)= C(10), C(11), C(12), C(13), C(14), C(15)

In addition to this, ring metal interactions exist (Fig. 6.4) and the ring-metal distance required for such interactions are given in Table 6.6. The packing of this molecule involves a hydrogen bonding network supported by π···π and metal-π interactions throughout the entire lattice.

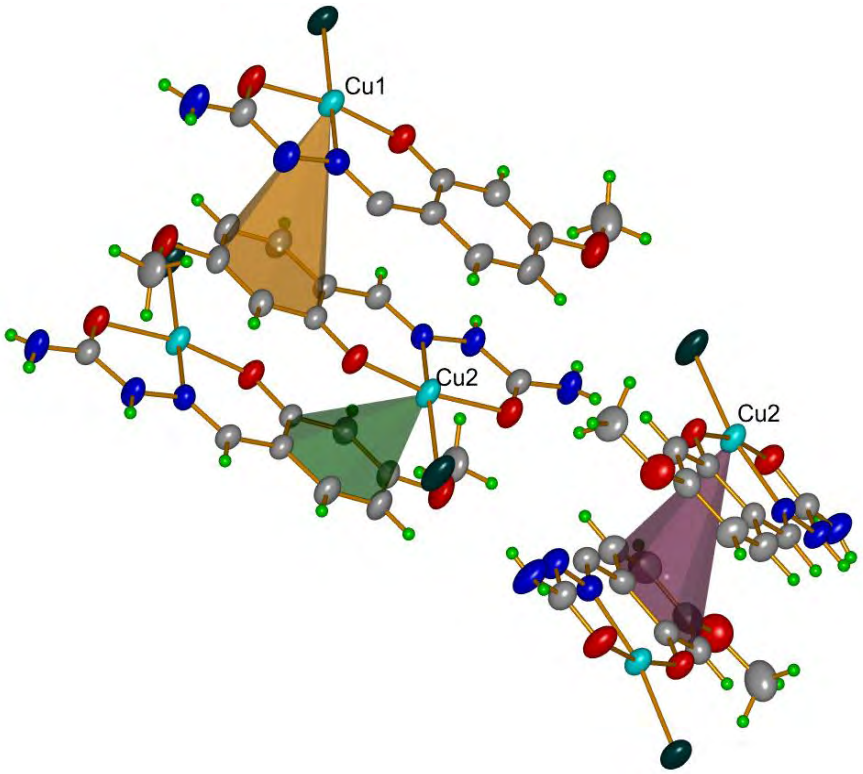

Fig. 6.4. Ring metal interactions of the [Cu(Hmssc)Cl] (**14**).

Table 6.6. Ring metal interactions of the [Cu(Hmssc)Cl] (**14**)

Cg(I)···Metal(J)	Cg(I)-Metal(J) (Å)	β(°)
Cg(9)···Cu(2)[a]	3.747	25.04
Cg(10)···Cu(1)[d]	3.804	22.33
Cg(10)···Cu(2)[f]	3.559	26.03

Equivalent position codes: a= 1/2-x,1/2+y,1/2-z; d=1/2-x,-1/2+y,1/2-z; f=1-x,1-y,1-z

Cg, centroid; α, dihedral angles between planes I and J; β, angle between Cg-Cg and Cg(J)_perp; γ, angle between Cg-Cg and Cg(I)_perp.

The arrangements of the molecules along 'a' and 'c' axes are shown in Figs. 6.5. and 6.6.

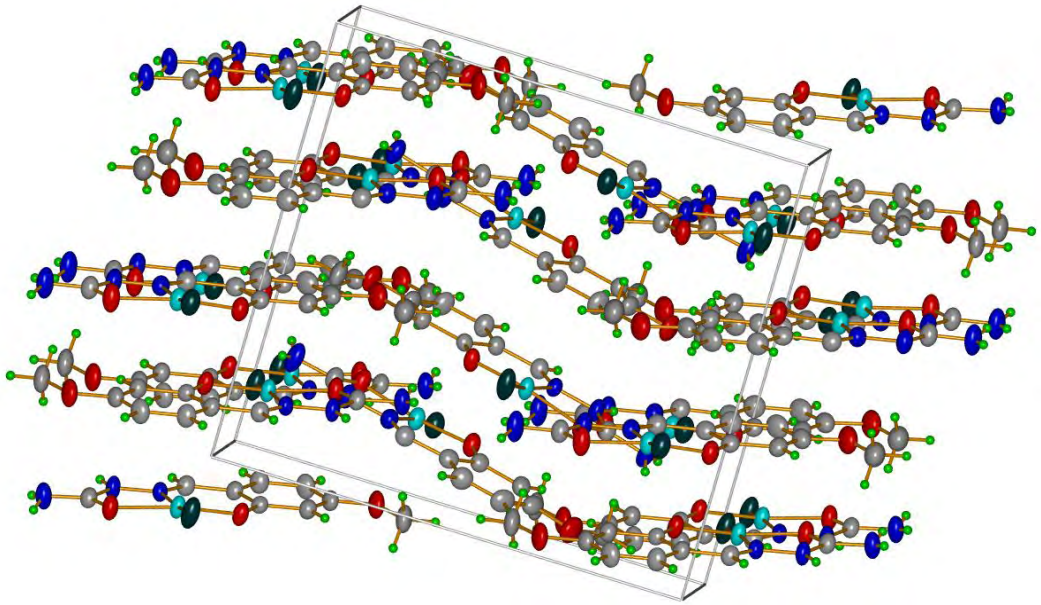

Fig. 6.5. The packing diagram of the molecule along 'a' axis.

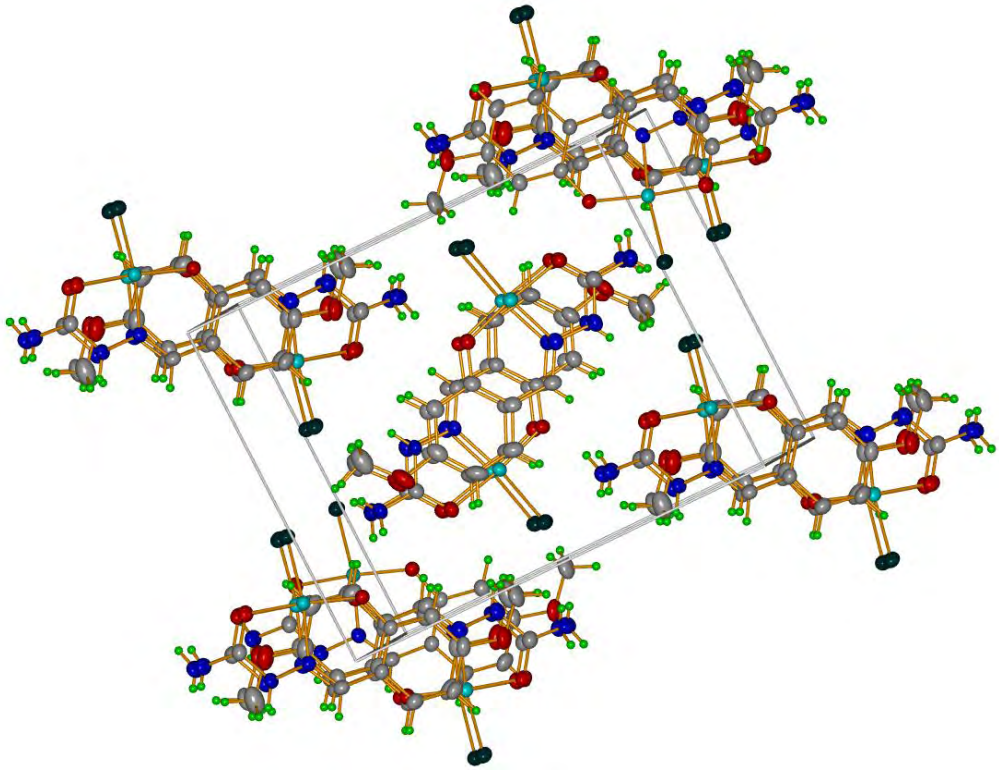

Fig. 6.6. The packing diagram of the molecule along 'c' axis.

6.3.3. Crystal structure of complex $[Cu(bpap)Cl_2]\cdot H_2O$ (15)

The complex crystallizes in triclinic space group, $P\bar{1}$. The molecular structure of $[Cu(bpap)Cl_2]$ along with the atom numbering is given in Fig. 6.7. Selected bond lengths and angles are given in Table 6.7.

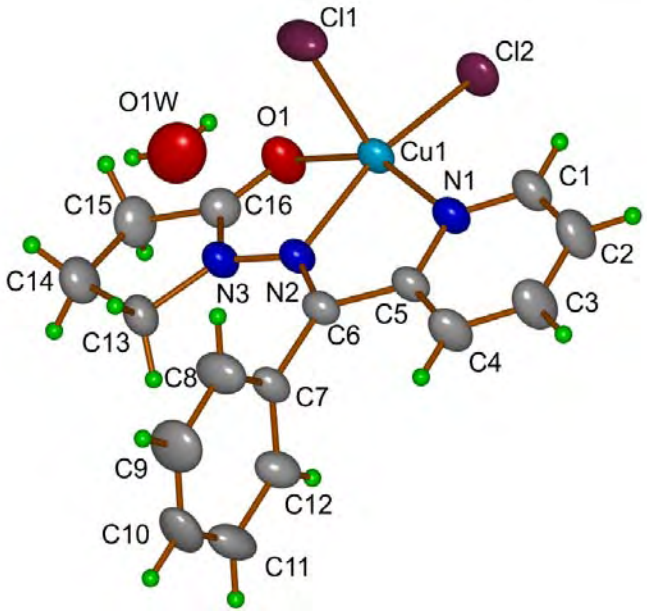

Fig. 6.7. Molecular structure of $[Cu(bpap)Cl_2]\cdot H_2O$ (**15**).

Table 6.7 Selected bond lengths [Å] and angles [°] for $[Cu(bpap)Cl_2]\cdot H_2O$ (**15**)

Bond lengths (Å)	
Cu1–N2	1.9888(13)
Cu1–N1	2.0213(14)
Cu1–O1	2.0878(13)
Cu1–Cl2	2.2125(4)
Cu1–Cl1	2.4240(5)
O1–C16	1.231(2)
N2–N3	1.3518(19)
Bond angles (°)	
N2–Cu1–N1	78.77(5)
N2–Cu1–O1	78.29(5)
N1–Cu1–O1	152.34(6)
N1–Cu1–Cl2	100.41(4)
N2–Cu1–Cl2	163.34(4)
O1–Cu1–Cl2	97.17(4)
N2–Cu1–Cl1	95.08(4)
N1–Cu1–Cl1	100.24(4)
O1–Cu1–Cl1	96.99(5)
Cl2–Cu1–Cl1	101.40(2)

The Cu(II) atom in this complex is *N*,*N*′,*O*-chelated by the neutral Schiff ligand and has a square-pyramidal geometry, with the atom displaced out of the square plane

in the direction of the apical Cl atom by 0.316(1) Å. The apical Cl atoms of adjacent complex units are hydrogen-bond acceptors to two water molecules, the interaction generating a centrosymmetric dimer (Fig. 6.8) through a cyclic $R_4^2(8)$ association (Fig. 6.9) [24].

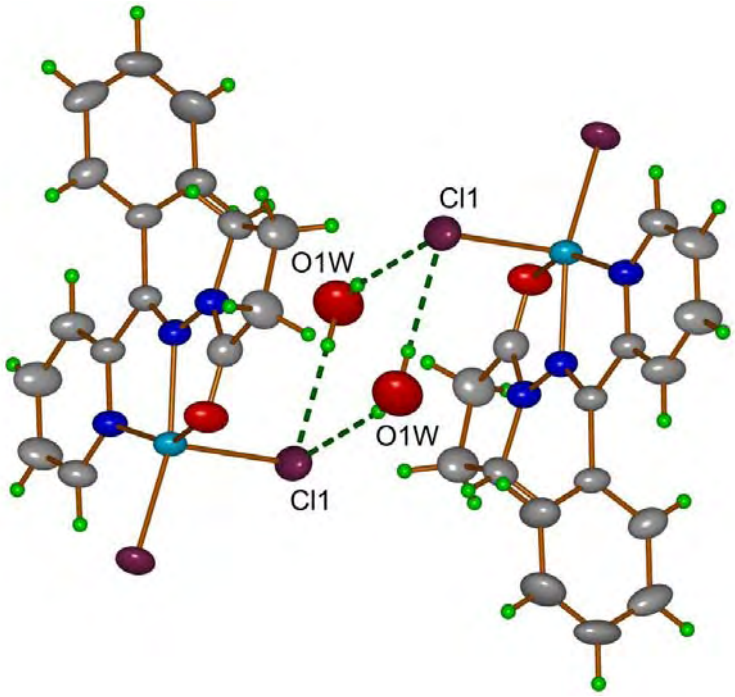

Fig. 6.8. Intermolecular hydrogen bonding of $[Cu(bpap)Cl_2]\cdot H_2O$ (**15**).

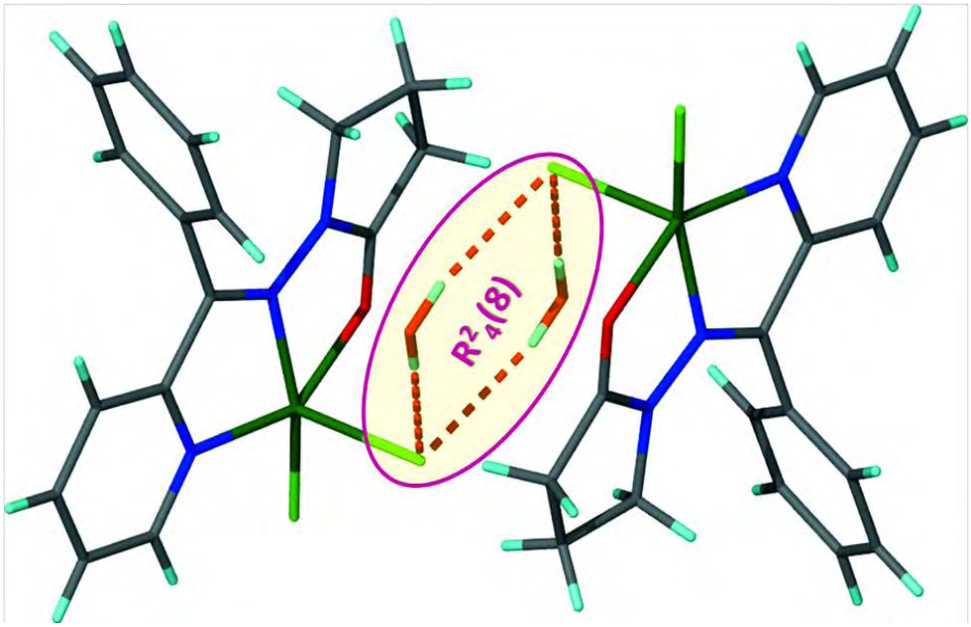

Fig. 6.9. View of the hydrogen bonded motif $R_4^2(8)$.

The hydrogen bonding interactions are shown in Table 6.8. The intermolecular hydrogen bonding interactions (Fig. 6.10) make the molecule more rigid.

Table 6.8. Hydrogen bonding interactions of $[Cu(bpap)Cl_2]\cdot H_2O$ (**15**)

D–H···A	D–H (Å)	H···A (Å)	D···A (Å)	∠D–H···A (°)
O(1W)–H(1)···Cl(1)	0.83(3)	2.34(3)	3.175(2)	178(2)
O(1W)–H(2)···Cl(1)[a]	0.83(3)	2.41(3)	3.220(2)	165(4)
C(4)–H(4)···O(1W)[b]	0.9304	2.5164	3.225(3)	133.18
N(8)–H(8)···O1(W)	0.9295	2.5280	3.319(3)	143.15
N(10)–H(10)···Cl(1)[c]	0.9298	2.7970	3.585(2)	143.25

Equivalent position codes: a= 1-x,2-y,-z; b= -1+x,y,z; c= -1+x,-1+y,z

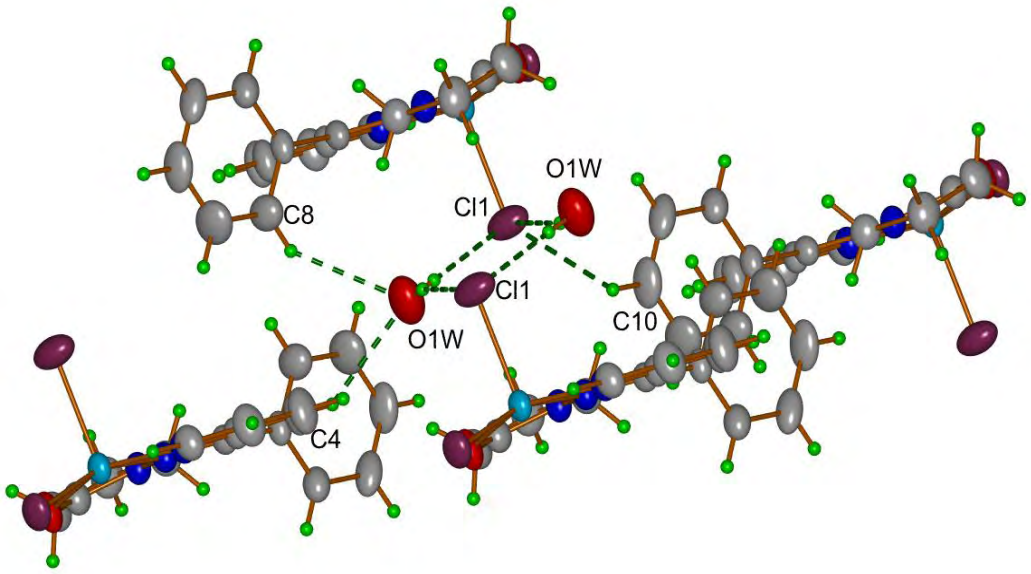

Fig. 6.10. Hydrogen bonding interactions of $[Cu(bpap)Cl_2]\cdot H_2O$ (**15**).

C–H···π interactions of the complex $[Cu(bpap)Cl_2]\cdot H_2O$ (**15**) are given in the Table 6.9. There are three types of C–H···π interactions (Figs. 6.11a and 6.11b) mainly involve in the inter connection of the neighbouring molecules with H···Cg distances of 3.32(3), 3.2125 and 2.8119 Å.

Table 6.9. C–H···π interactions of $[Cu(bpap)Cl_2]\cdot H_2O$ (**15**)

X-H(I)···Cg(J)	H···Cg (Å)	X···Cg (Å)	∠X-H···Cg (°)
O(1W)–H(1)···Cg(5)[a]	3.32(3)	3.439(2)	91(2)
C(9)–H(9)···Cg(7)[b]	3.2125	4.022(2)	146.72
C(15)–H(15B)···Cg(8)[d]	2.8119	3.629(2)	142.43

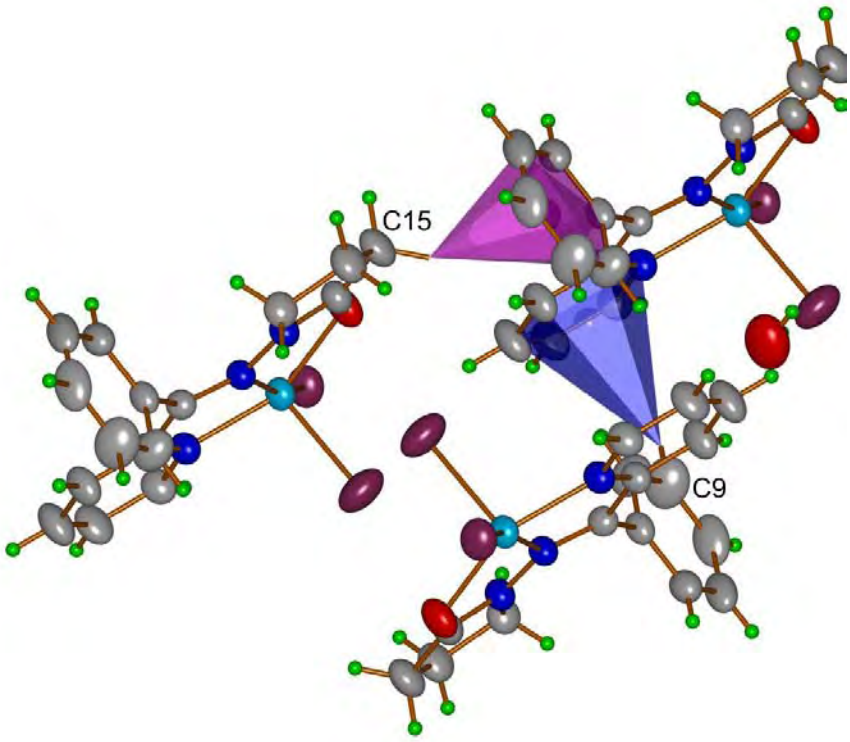

Fig. 6.11a. C–H···π interactions of $[Cu(bpap)Cl_2]\cdot H_2O$ (**15**).

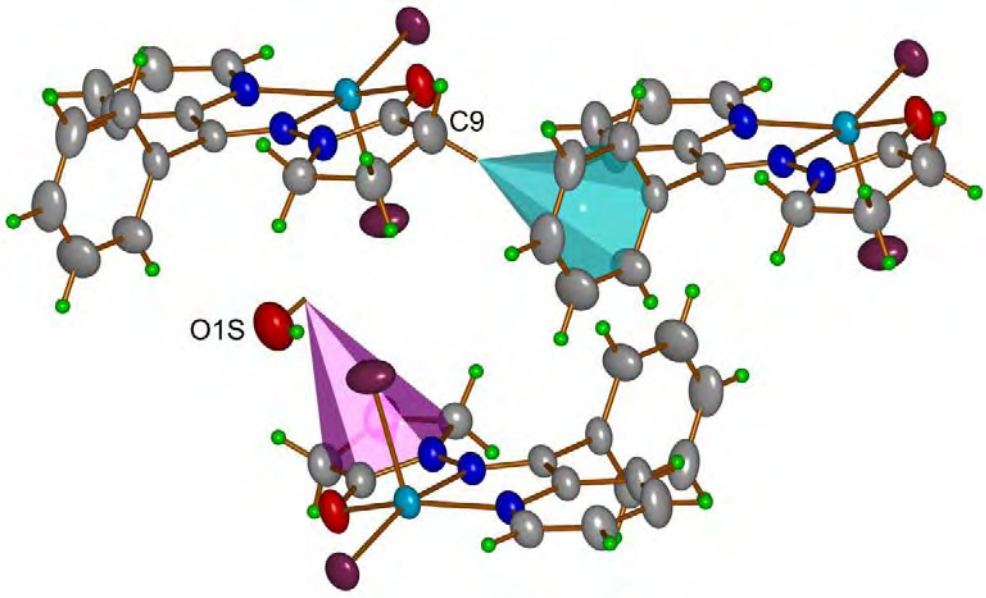

Fig. 6.11b. C–H···π interactions of $[Cu(bpap)Cl_2]\cdot H_2O$ (**15**).

The arrangement of the molecules in the unit cell along 'c' axis is shown in Fig. 6.12.

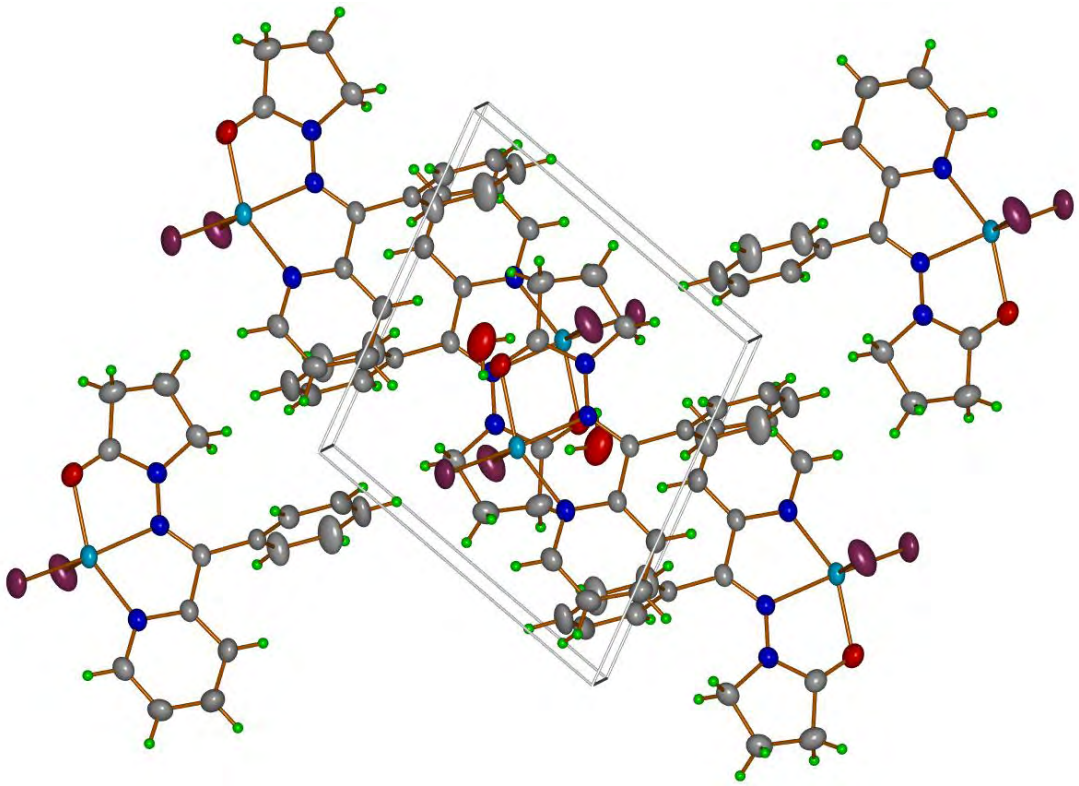

Fig. 6.12. The packing diagram of $[Cu(bpap)Cl_2]\cdot H_2O$ (**15**) along 'c' axis.

6.3.4. Crystal structures of complexes $[Cu(bsde)Cl]_n$ (16) and $[Cu(csde)Cl]_n$ (17)

The use of tridentate Schiff-base ligands with Cu(II) and potentitally bridging ligand as chloride anions has afforded 1-D polymeric chains. These complexes confirm the ability of tridentate Schiff base ligands to chelate and bridge Cu(II) ions while leaving some coordination positions vacant that can be easily occupied by diverse bridging or terminal ligands. The use of chloride anions has led to the formation of novel chloro-bridged 1-D chains.

The complexes crystallize in centrosymmetric orthorombic space group *Pbca* of which makes the molecule, a mesomer. The bridging chloride ion occupies the apical site and bridges adjacent Cu(II) ions to form the uniform chain. The Cu···Cu distance in the chains are 4.367 and 4.372 Å in complexes **16** and **17** respectively, which is longer than the similar compounds with single chlorido bridging. Weak antiferromagnetic coupling is very common in single chlorido bridged Cu(II) complexes [25].

Crystals of $[Cu(bsde)Cl]_n$ **(16)** and $[Cu(bsde)Cl]_n$ (**17**) suitable for X-ray diffraction studies were grown by slow evaporation of their methanolic solutions. Molecular structure of the compounds together with the atom labeling scheme is shown in Fig. 6.13. A summary of the key crystallographic information is given in Table 6.1b. The coordination environment around the copper atom is distorted square pyramidal in these complexes. The asymmetric unit consists of a copper(II) centre, one deprotonated Schiff base ligand and a chloride ion (Fig. 6.13).

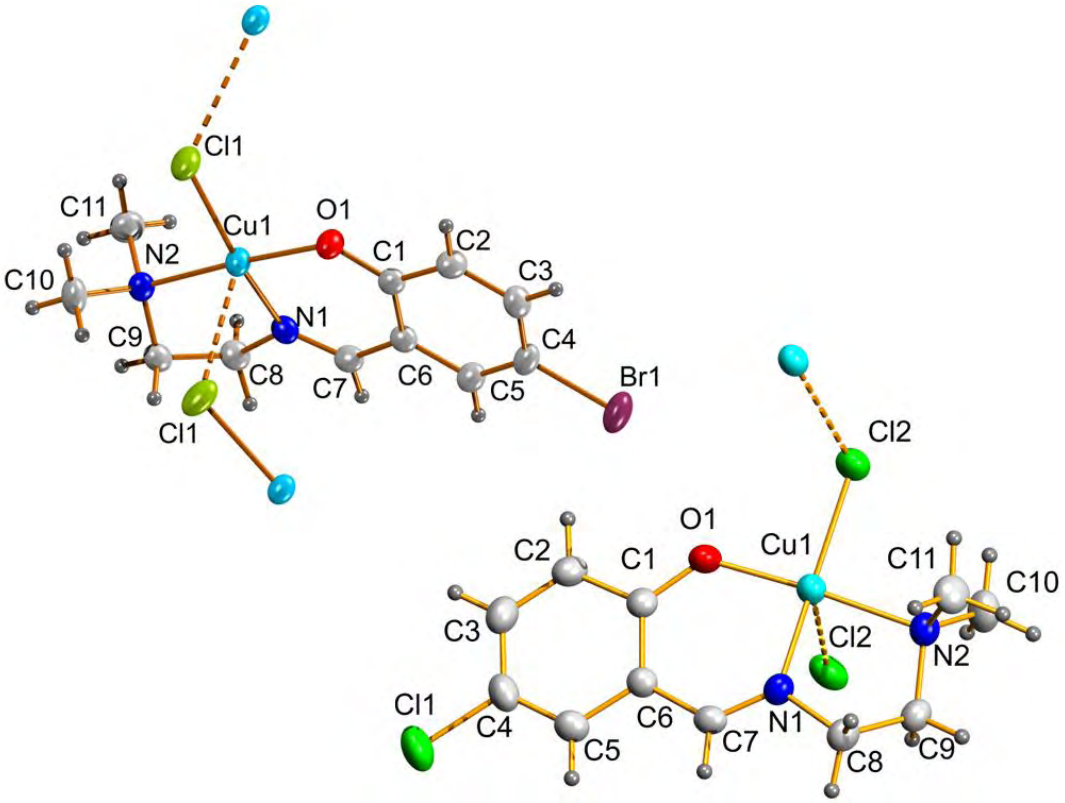

Fig. 6.13. Asymmetric unit of $[Cu(bsde)Cl]_n$ (**16**) and $[Cu(csde)Cl]_n$ (**17**).

The geometry of the pentacoordinated metal center can be determined by the Addison parameter (τ), which is 0.183 and 0.195 in **16** and **17** respectively. The copper(II) centre is coordinated by two nitrogen atoms, N(1) and N(2), and one oxygen atom, O(1), of the tridentate deprotonated Schiff base and one Cl atom in the equatorial plane. Another Cl atom from a symmetry related molecule coordinates the metal in its apical position to form a chloro-bridged 1-D chain, with alternating short and long Cu–Cl distances of 2.248 and 3.064 Å in **16** and 2.261 and 3.047 Å in **17** (Figs. 6.14 and 6.15).

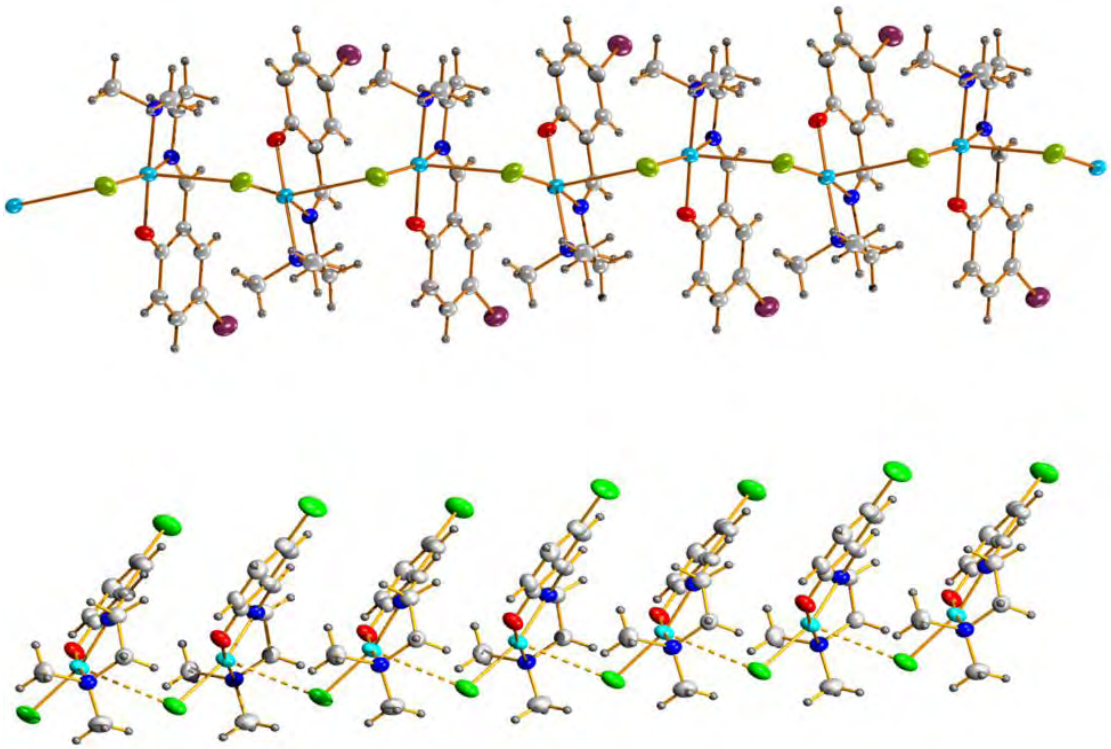

Fig. 6.14. 1D chain of Cu(II) complexes with single-μ-chloride bridging.

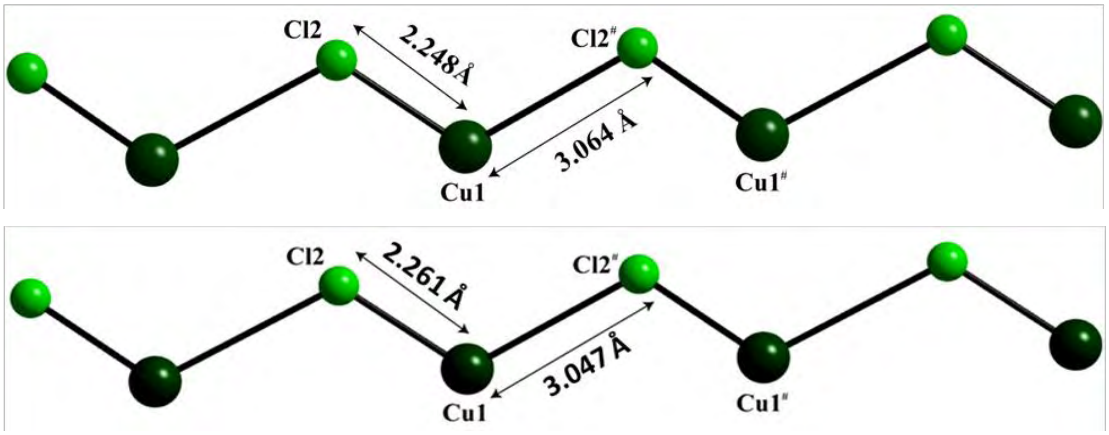

Fig. 6.15. Chloride bridged polynuclear chain with alternating short and long Cu–Cl bonds.

This is comparable with the Cu–Cl bond lengths found for several Cu(ligand)Cl (here ligand corresponds to a tridentate Schiff base) cores in different complexes [26]. As is usual for a square pyramidal structure, the copper atom is slightly pulled out of the mean squares plane towards the apical donor atom Cl. The Cu(II)···Cu(II) distance in the complex **16** is 4.367 Å and the Cu(1)–Cl(2)–Cu(1) angle is 106.60°, whereas in **17** it is 4.372 Å and 110.05° respectively, which falls in the normal range [27]. Selected bond lengths and angles are listed in Table 6.10.

Table 6.10. Selected bond lengths [Å] and angles [°] for $[Cu(bsde)Cl]_n$ (**16**) and $[Cu(csde)Cl]_n$ (**17**)

$[Cu(bsde)Cl]_n$ (**16**)		$[Cu(csde)Cl]_n$ (**17**)	
Bond lengths (Å)			
Cu1–N2	2.075(5)	Cu1–N2	2.082(3)
Cu1–N1	1.947(5)	Cu1–N1	1.954(3)
Cu1–O1	1.905(5)	Cu1–O1	1.910(3)
Cu1–Cl1	2.248(18)	Cu1–Cl2	2.260(11)
C4–Br1	1.895(4)	C4–Cl1	1.752(4)
Bond angles (°)			
N2–Cu1–N1	84.2(2)	N2–Cu1–N1	84.29(12)
N1–Cu1–O1	92.1(2)	N1–Cu1–O1	92.14(11)
O1–Cu1–Cl1	91.10(13)	O1–Cu1–Cl2	91.04(8)
Cl1–Cu1–N2	92.63(14)	Cl2–Cu1–N2	92.62(9)
O1–Cu1–N2	176.26(18)	O1–Cu1–N2	176.33(11)
Cl1–Cu1–N1	165.31(16)	Cl2–Cu1–N1	164.59(9)

The molecular structure highlighting the hydrogen bonding in compounds **16** and **17** are shown in Fig. 6.16. The relevant H–bonding interactions of the compounds are given in Tables 6.11a and 6.11b.

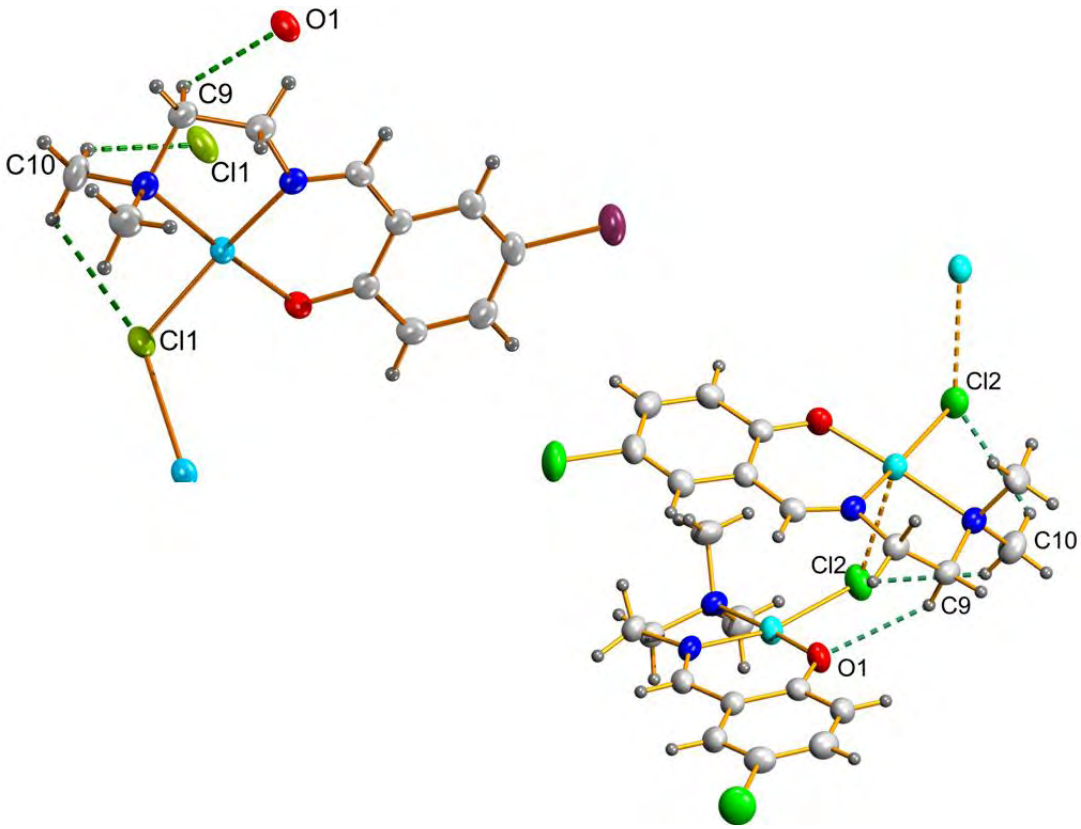

Fig. 6.16. Hydrogen bonding interactions.

Table 6.11a. Hydrogen bonding interactions of $[Cu(bsde)Cl]_n$ (**16**)

D–H···A	D–H (Å)	H···A (Å)	D···A (Å)	∠D–H···A (°)
C(9)–H(9B)···O(1)^a	0.9704	2.5400	3.282(4)	133.22
C(10)–H(10B)···Cl(1)	0.9606	2.7873	3.346(4)	117.90
C(10)–H(10B)···Cl(1)^a	0.9592	2.7246	3.489(4)	137.11

Equivalent position codes: a= 1/2+x,y,3/2-z

Table 6.11b. Hydrogen bonding interactions of $[Cu(csde)Cl]_n$ (**17**)

D–H···A	D–H (Å)	H···A (Å)	D···A (Å)	∠D–H···A (°)
C(9)–H(9B)···O(1)^a	0.97	2.56	3.300(4)	133
C(10)–H(10B)···Cl(2)	0.96	2.82	3.364(4)	117
C(15)–H(15)···Cl(1)^a	0.96	2.73	3.501(4)	137

Equivalent position codes: a= 1/2+x,y,1/2-z.

The complex shows significant C–H···π interactions. In **16** two of the methyl groups, C(10) and C(11) of the Schiff base are involved in two C–H···π interactions with two phenyl groups present in Schiff base of adjacent moieties, whereas in **17** only one methyl group C(11) of the Schiff base are involved in C–H···π interaction with phenyl group present in a Schiff base of an adjacent moiety (Fig. 6.17).

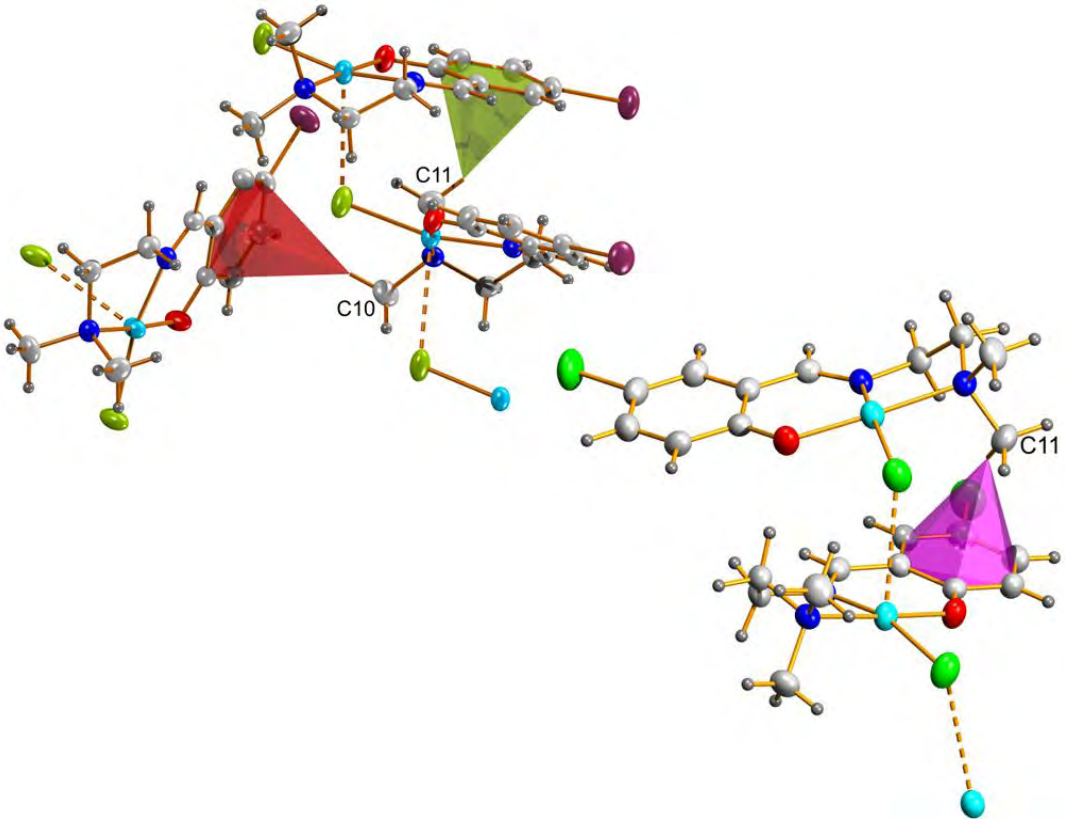

Fig. 6.17. C–H···π interactions of $[Cu(bsde)Cl]_n$ (**16**) and $[Cu(csde)Cl]_n$ (**17**).

In complex **16** the C(10)–H(10B)···Cg(3)^{b} and C(11)–H(11A)···Cg(3) (symmetry codes: b=-x,-1/2+y,3/2-z ;c=-1/2+x,y,3/2-z) distances are 3.0622 and 2.5838 Å, respectively, and the C(10)–H(10B)···Cg(3)^{b} and C(11)–H(11A)···Cg(3)^{c} angles are 150.27 and 145.64° respectively. In complex **17** the C(11)–H(11A)···Cg(3)^{b} (b= -1/2+x,y,1/2-z) distance is 2.57 Å and the angle is 146°. So each mononuclear unit of the polymeric complexes **16** and **17** have C–H···π interactions, forming a 1-D array along the polymerization axis. The C–H···π ring interactions of the compounds are given in Tables 6.12a and 6.12b contribute to the stability of the unit cell packing (Figs. 6.18- 6.21).

Table 6.12a. C–H···π interactions of [Cu(bsde)Cl]$_n$ (**16**)

X–H(I)···Cg(J)	H···Cg (Å)	X···Cg (Å)	∠X–H···Cg (°)
C(10)–H(10B)···Cg(3)^{b}	3.0622	3.925(4)	150.27
C(11)–H(11A)···Cg(3)^{c}	2.5838	3.419(4)	145.64

Equivalent position codes: b=-x,-1/2+y,3/2-z ; c=-1/2+x,y,3/2-z ; Cg(3)= C(1), C(2), C(3), C(4), C(5), C(6)

Table 6.12b. C–H···π interactions of [Cu(csde)Cl]$_n$ (**17**)

X–H(I)···Cg(J)	H···Cg (Å)	X···Cg (Å)	∠X–H···Cg (°)
C(11)–H(11A)···Cg(3)^{b}	2.57	3.421(5)	146

Equivalent position codes: b= -1/2+x,y,1/2-z; Cg (3) = C(1), C(2), C(3), C(4), C(5), C(6).

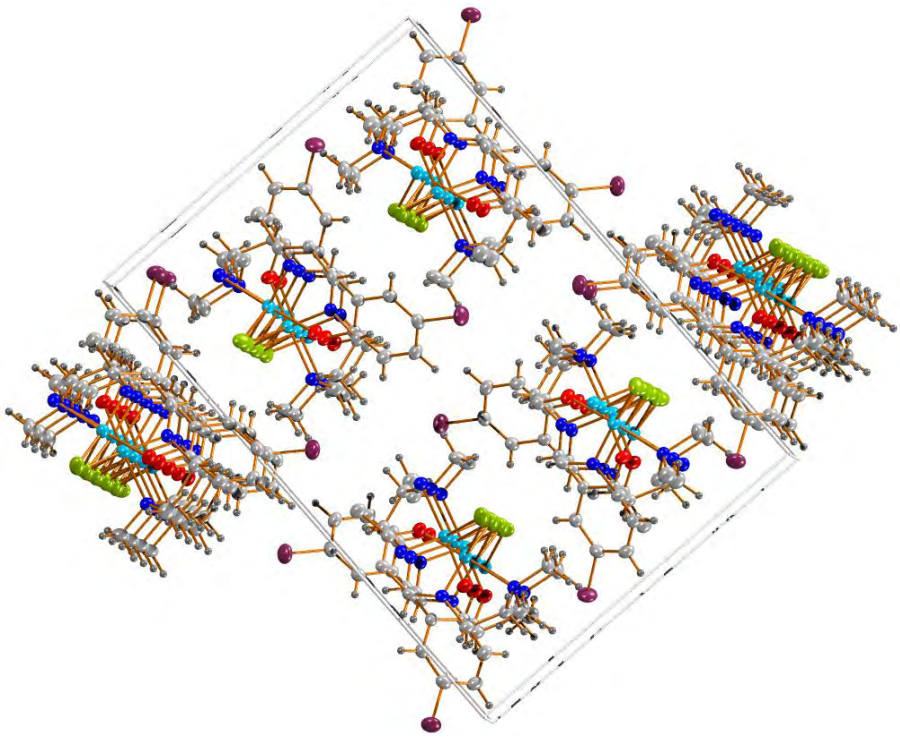

Fig. 6.18. The packing diagram of the [Cu(bsde)Cl]$_n$ (**16**) molecule along 'a' axis.

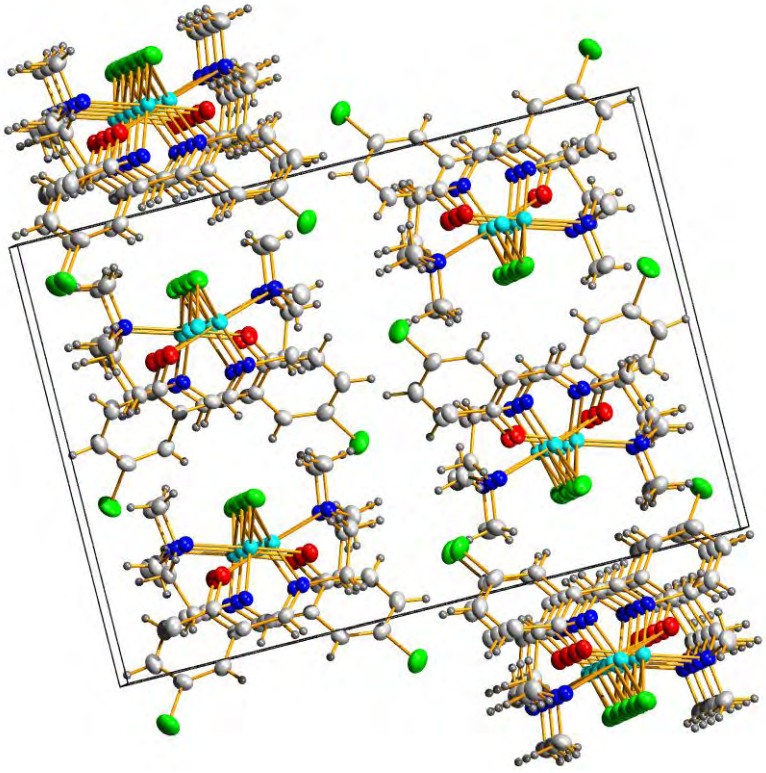

Fig. 6.19. The packing diagram of the $[Cu(csde)Cl]_n$ (**17**) along 'a' axis.

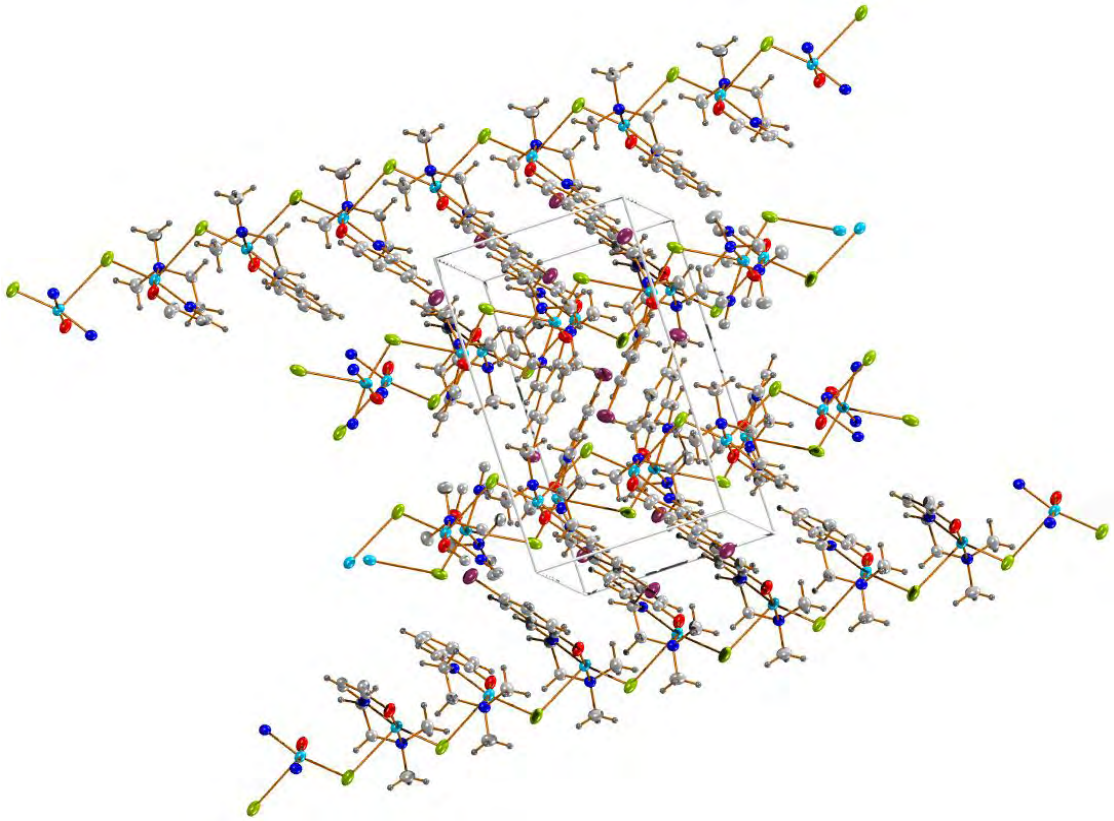

Fig. 6.20. The packing diagram of the $[Cu(bsde)Cl]_n$ (**16**) molecule along 'c' axis.

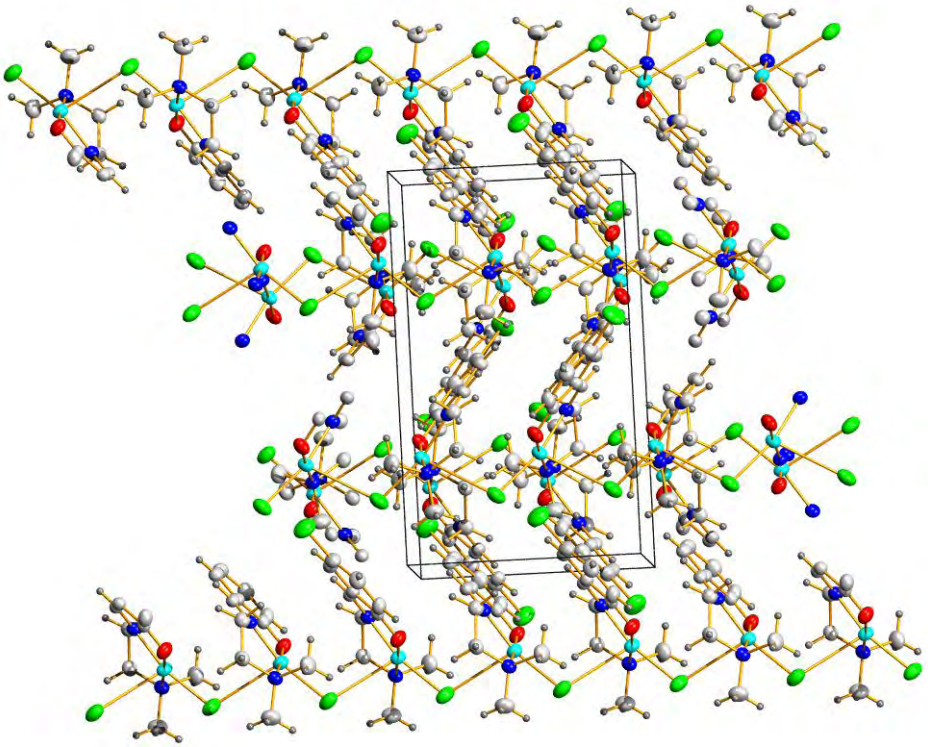

Fig. 6.21. The packing diagram of the $[Cu(csde)Cl]_n$ (**17**) molecule along 'c' axis.

6.3.5. Crystal structure of complex [Cu(dbsap)Cl] (18)

The asymmetric unit of the mononuclear Cu(II) complex with the atom numbering scheme is shown in the Fig. 6.22. The Cu(II) cation is *N,O,O'*-chelated by the deprotonated Schiff base ligand and is further coordinated by a Cl^- anion in a distorted ClNOO square-planar geometry. Copper atoms in these compounds are coordinated by azomethine nitrogens (N1 and N3), phenolate oxygens (O1 and O3) and amido oxygens (O2 and O4). Selected bond lengths and angles are given in Table 6.13.

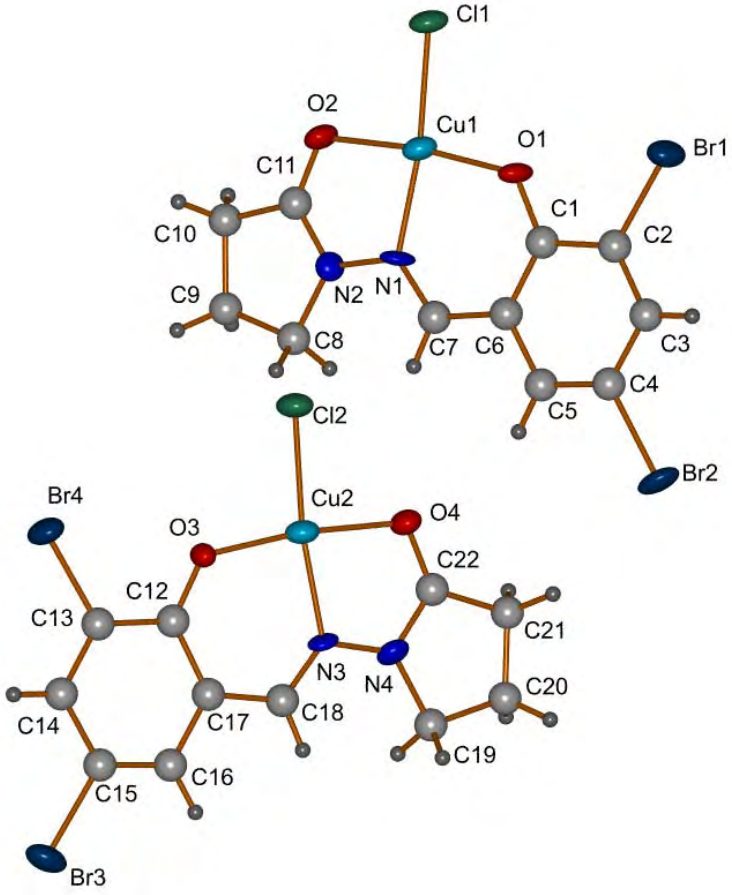

Fig. 6.22. Asymmetric unit of the structure of [Cu(dbsap)Cl] (**18**).

Table 6.13. Selected bond lengths [Å] and angles [°] for the two asymmetric units of [Cu(dbsap)Cl] (**18**)

Molecule 1		Molecule 2	
Bond lengths (Å)			
Cu1–O1	1.914(11)	Cu2–O3	1.904(10)
Cu1–N1	1.936(11)	Cu2–N3	1.936(11)
Cu1–O2	2.002(12)	Cu2–O4	2.013(11)
Cu1–Cl1	2.199(4)	Cu2–Cl2	2.194(4)
O2–C11	1.257(18)	O4–C22	1.27(2)
Bond angles (°)			
N1–Cu1–O2	81.9(5)	N3–Cu2–O4	82.0(5)
O1–Cu1–Cl1	95.3(3)	O3–Cu2–Cl2	95.7(3)
N1–Cu1–Cl1	172.7(4)	N3–Cu2–Cl2	172.7(4)
O2–Cu1–Cl1	92.1(3)	O4–Cu2–Cl2	92.0(3)
O1–Cu1–O2	172.1(4)	O3–Cu2–O4	171.7(4)
O1–Cu1–N1	91.0(5)	O3–Cu2–N3	90.5(5)

The intermolecular hydrogen bonding interaction exists between adjacent molecules giving a beautiful hydrogen bonding network in zig zag manner in the

lattice as shown in the Fig. 6.23 and 6.24. Hydrogen bonding interactions of [Cu(dbsap)Cl] (**18**) are given in Table 6.14.

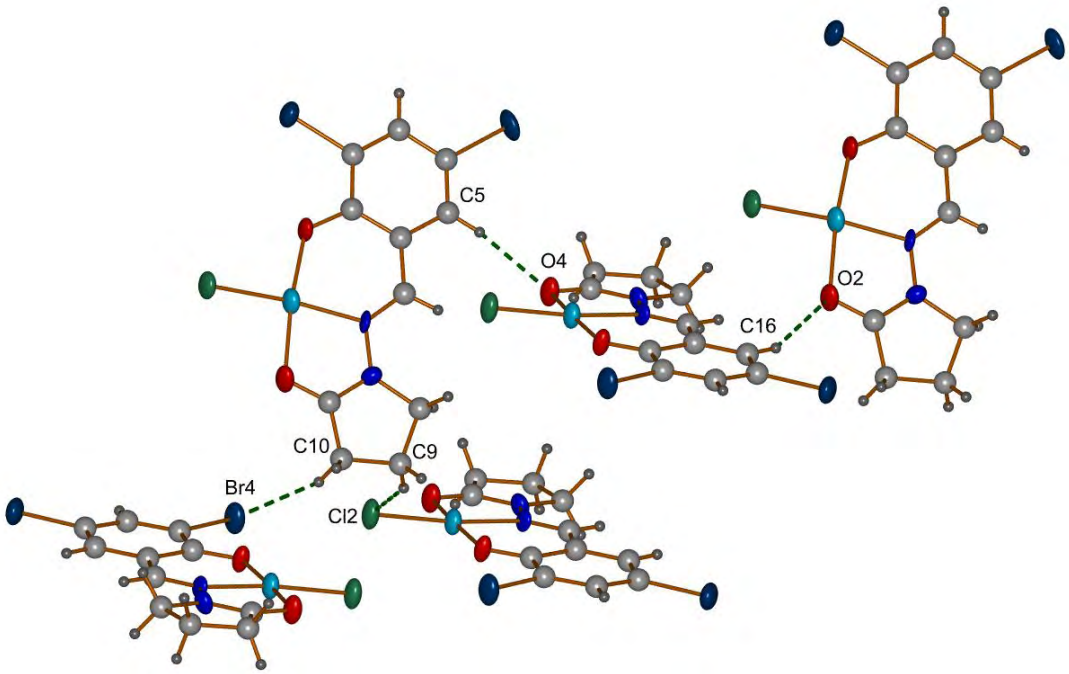

Fig. 6.23. Hydrogen bonding interactions of [Cu(dbsap)Cl] (**18**).

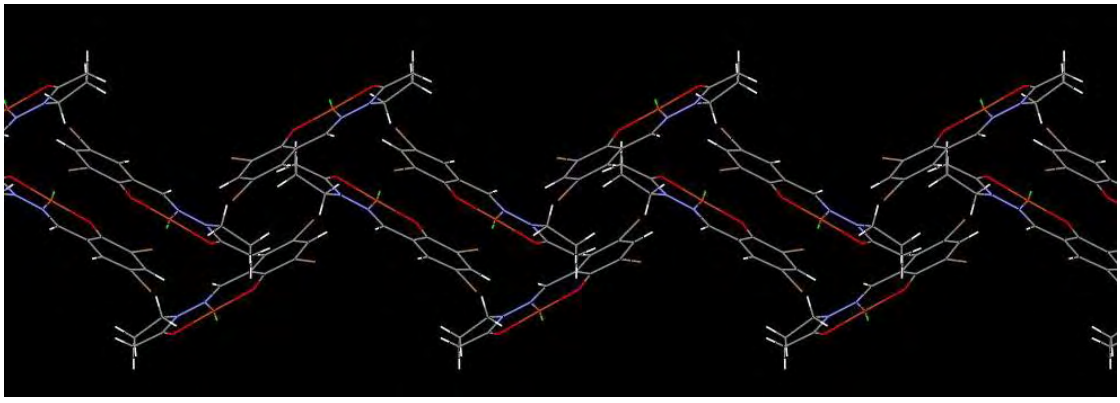

Fig. 6.24. Arrangement of the molecules along 'b' direction.

Table 6.14. Hydrogen bonding interactions of [Cu(dbsap)Cl] (**18**)

D–H···A	D–H (Å)	H···A (Å)	D···A (Å)	∠D–H···A (°)
C(5)–H(5)···O(4)	0.9295	2.4786	3.322(19)	151.03
C(9)–H(9B)···Cl(2)^{a}	0.9706	2.7382	3.594(17)	147.37
C(10)–H(10A)···Br(4)^{b}	0.9734	2.9186	3.85(2)	161.49
C(16)–H(16)···O(2)^{c}	0.9304	2.4629	3.337(18)	156.49

Equivalent position codes: a = 1+x,y,z; b = 2-x,1-y,1-z; c = -1+x,-1+y,z

The significant π···π interactions (Fig. 6.25) are also giving strength to the molecular system by the interaction between the rings of two adjacent molecules with the distances of 3.633(8) and 3.640(8) Å between the centroids of the corresponding interacting rings (Table 6.15).

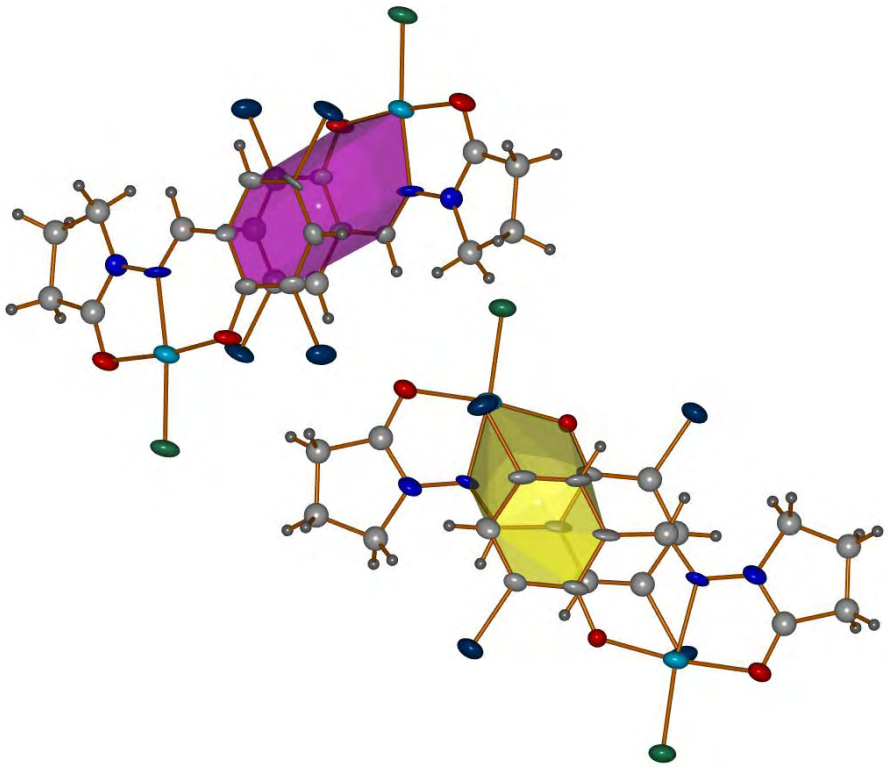

Fig. 6.25. Molecular structure showing π···π interactions of [Cu(dbsap)Cl] (**18**).

Table 6.15. π···π interactions of [Cu(dbsap)Cl] (**18**)

Cg(I)···Cg(J)	Cg···Cg (Å)	α (°)	β (°)	γ (°)
Cg(9)···Cg(11) [d]	3.633(8)	0.49	23.45	22.98
Cg(10)···Cg(12) [e]	3.640(8)	0.21	23.22	23.13

Equivalent position codes: d = 1-x,1-y,2-z ; e= .1-x,-y,1-z ; f= 1-x,-y,2-z. ; Cg (9) = Cu(1, O(1), C(1), C(6), C(7), N(1); Cg (10) = Cu(2, O(3), C(12, C(17, C(18, N(3); Cg (11) = C(1), C(2), C(3), C(4), C(5), C(6); Cg (12)= C(12, C(13, C(14, C(15, C(16, C(17). D, donor; A, acceptor; Cg, centroid; α, dihedral angles between planes I and J; β, angle between Cg-Cg and Cg(J)_perp; γ, angle between Cg-Cg and Cg(I)_perp.

There are two types of C–H···π interactions (Fig. 6.26) with H···Cg distances of 3.0572 and 2.9866 Å (Table 6.16).

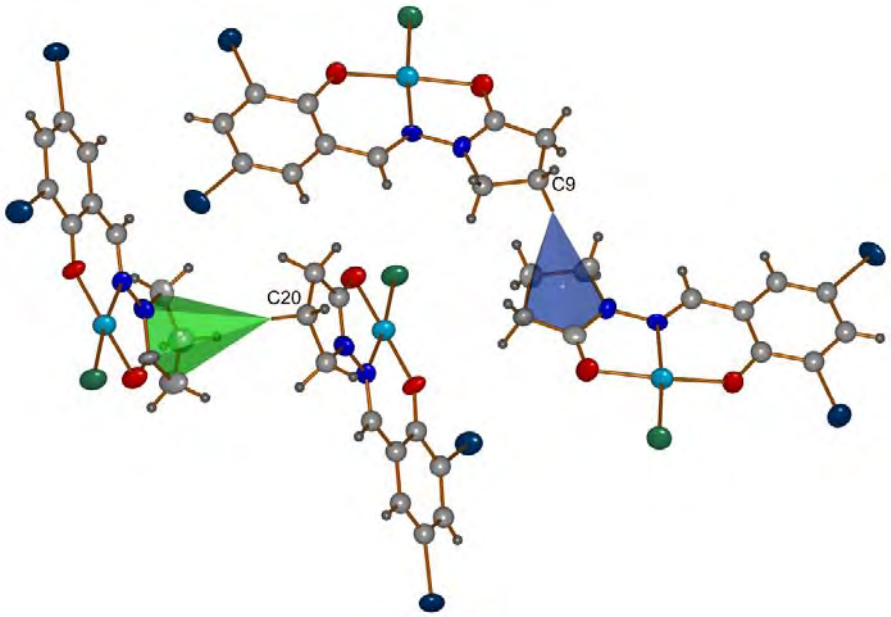

Fig. 6.26. Interconnection of the molecules *via* C–H···π interactions of [Cu(dbsap)Cl] (**18**).

Table 6.16. C–H···π interactions of [Cu(dbsap)Cl] (**18**)

X–H(I)···Cg(J)	H···Cg (Å)	X···Cg (Å)	∠X–H···Cg (°)
C(9)–H(9A)···Cg(7)^{b}	3.0572	3.96(2)	155.69
C(20)–H(20A)···Cg(8)^{f}	2.9866	3.91(2)	159.82

The arrangements of the molecules along 'a' and 'b' axes are shown in Fig. 6.27 and 6.28.

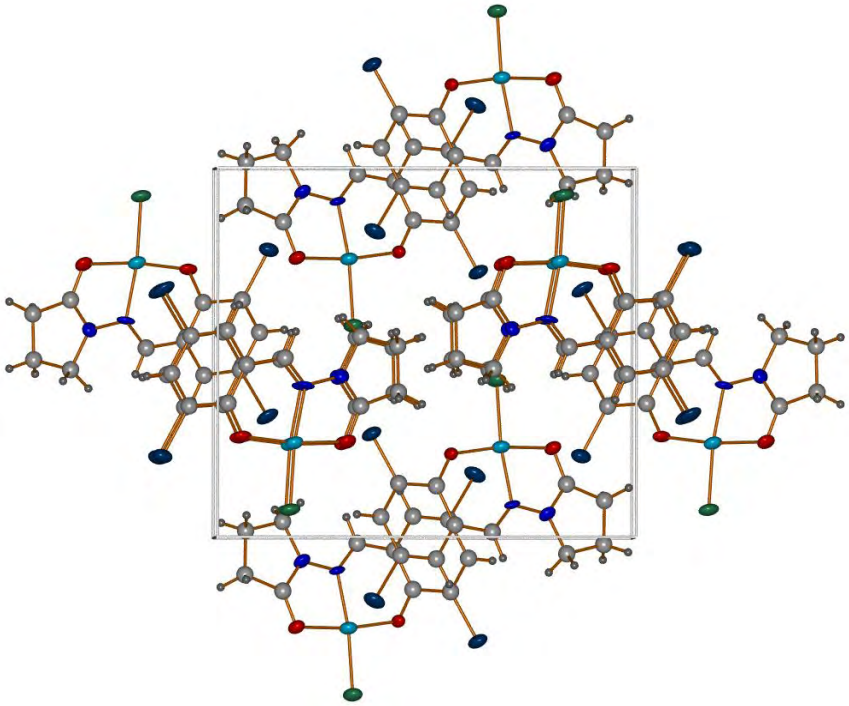

Fig. 6.27. Packing diagram of the [Cu(dbsap)Cl] (**18**) along 'a' axis.

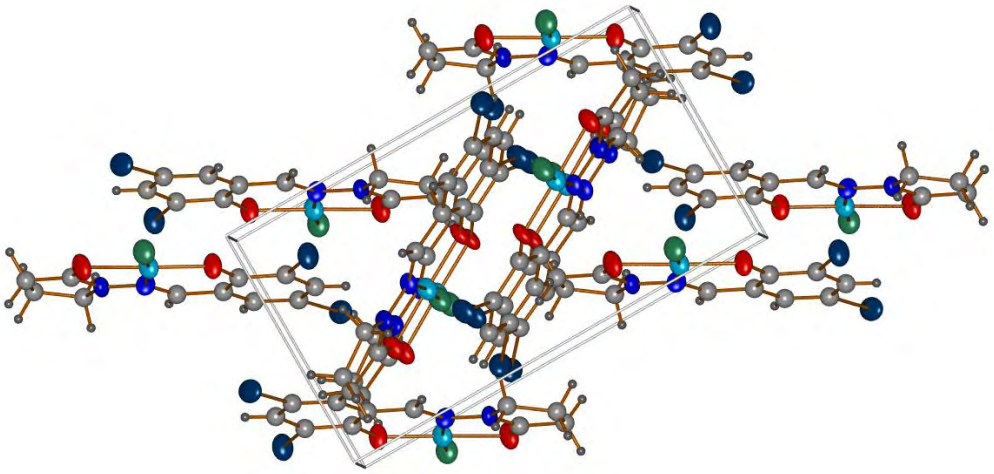

Fig. 6.28. Packing diagram of the [Cu(dbsap)Cl] (**18**) along 'b' axis.

6.3.6. Crystal structure of complex [Cu(Hdbssc)Cl]·H_2O (19)

This compound crystallizes in the monoclinic space group $P2_1/n$. Fig. 6.29 shows the molecular structure of this complex with atom numbering scheme. The Cu(II) cation is *N,O,O'*-chelated by the deprotonated semicarbazone and is further coordinated by a Br^- anion in a distorted BrNOO square-planar geometry. Copper atom are coordinated by azomethine nitrogen (N1), phenolate oxygen (O1) and amido oxygen (O2). Selected bond lengths and angles are given in Table 6.17. The coordination of the semicarbazone to the Cu atom through amido oxygen is confirmed by the bond length C8–O2 [1.197(16)] Å which is very close to the reported values of semicarbazone complexes.

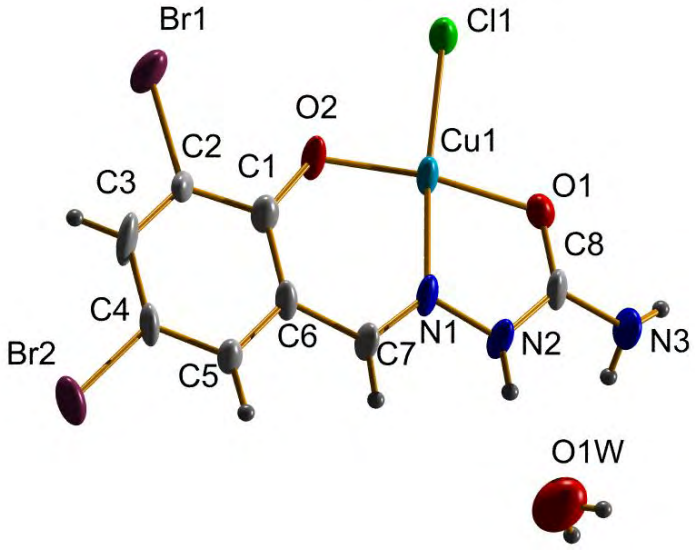

Fig. 6.29. Molecular structure of [Cu(Hdbssc)Cl]·H_2O (**19**) along with atom numbering scheme.

Table 6.17 Selected bond lengths [Å] and angles [°] for [Cu(Hdbssc)Cl]·H_2O (**19**)

Bond lengths (Å)	
Cu1–O2	1.900(9)
Cu1–N1	1.937(11)
Cu1–O1	1.986(9)
Cu1–Cl1	2.226(4)
C8–O1	1.262(17)
O2–C1	1.325(15)
N2–N1	1.375(14)
Bond angles (°)	
N1–Cu1–O1	81.2(4)
N1–Cu1–Cl1	172.8(3)
O1–Cu1–O2	171.4(5)
O1–Cu1–Cl1	95.1(3)
N1–Cu1–O2	92.2(4)

A supramolecular hydrogen bonding network is established between the molecules as shown in the Fig. 6.30. The intermolecular hydrogen bonding interactions are shown in Table 6.18.

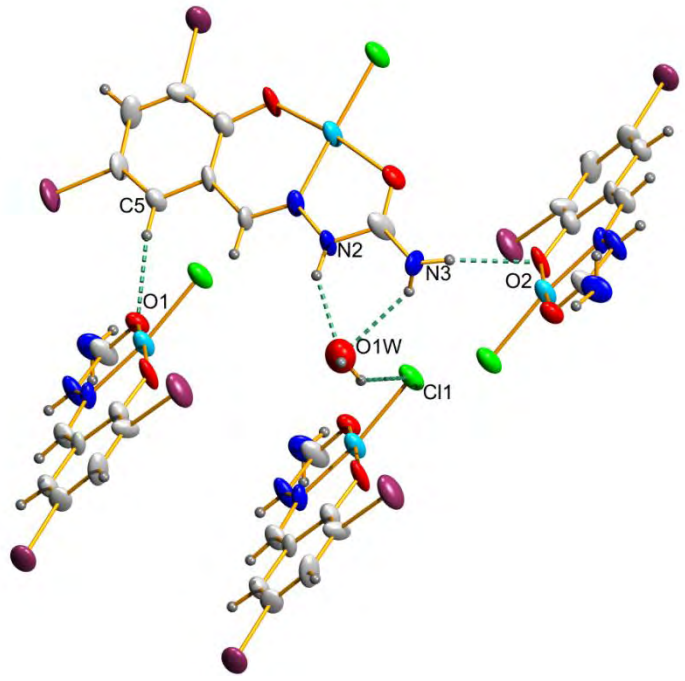

Fig. 6.30. Hydrogen bonding interactions of [Cu(Hdbssc)Cl]·H_2O (**19**).

Table 6.18. Hydrogen bonding interactions of [Cu(Hdbssc)Cl]·H_2O (**19**)

D–H···A	D–H (Å)	H···A (Å)	D···A (Å)	∠D–H···A (°)
O(1W)–H(1A)···Cl(1)[a]	0.86(8)	2.75(7)	3.34(2)	128(8)
N(2)–H(2)···O(1W)	0.86	2.06	2.79(2)	141
N(3)–H(3A)···O(1W)	0.86(11)	2.31(9)	2.98(2)	134(11)
N(3)–H(31B)···O(2)[b]	0.86(9)	2.24(11)	3.091(18)	173(11)
C(5)–H(5)···O(1)[c]	0.93	2.39	3.306(16)	167

Equivalent position codes: a= -1/2+x,1/2-y,1/2+z; b=1/2-x,-1/2+y,1/2-z; c=1/2+x,1/2-y,1/2+z.

The intermolecular hydrogen bonding interactions (Fig. 6.30) make the molecule more rigid and the two types of C–H···π interactions (Fig. 6.31), mainly involve in the interconnection of the neighbouring molecules with H···Cg distances of 3.380(6) and 3.273(6) Å (Table 6.19).

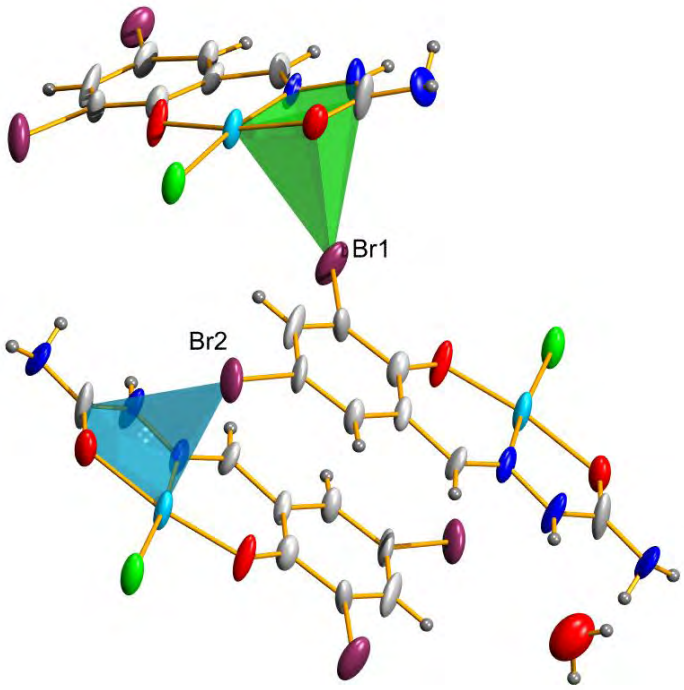

Fig. 6.31. C–H···π interactions of [Cu(Hdbssc)Cl]·H_2O (**19**).

Table 6.19. C–H···π interactions of [Cu(Hdbssc)Cl]·H_2O (**19**)

Y–X(I)···Cg(J)	X···Cg (Å)	Y···Cg (Å)	∠Y–X···Cg (°)
C(2)–Br(1)···Cg(1)[d]	3.380(6)	4.479(15)	113.2(5)
C(4)–Br(2) ···Cg(1)[e]	3.273(6)	3.796(15)	90.5(5)

Equivalent position codes: d=3/2-x,1/2+y,1/2-z ; e= 1-x,1-y,1-z ; Cg(1) = Cu(1), O(1), C(8), N(2), N(1).

The π···π interactions present in the complex are given in Table 6.20.

Table 6.20. $\pi\cdots\pi$ interactions of $[Cu(Hdbssc)Cl]\cdot H_2O$ (**19**)

Cg(I)···Cg(J)	Cg···Cg (Å)	α (°)	β (°)	γ (°)
Cg(2)···Cg(3)^e	3.621(8)	0.8(6)	26.5	26.2

Cg (2) = Cu(1), O(2), C(1), C(6), C(7), N(1); Cg (3) = C(1), C(2), C(3), C(4), C(5), C(6); Cg, centroid; α, dihedral angles between planes I and J; β, angle between Cg-Cg and Cg(J)_perp; γ, angle between Cg-Cg and Cg(I)_perp.

The arrangement of the molecules in the unit cell along 'a', 'b' and 'c' axes are shown in Figs. 6.32, 6.33 and 6.34 respectively.

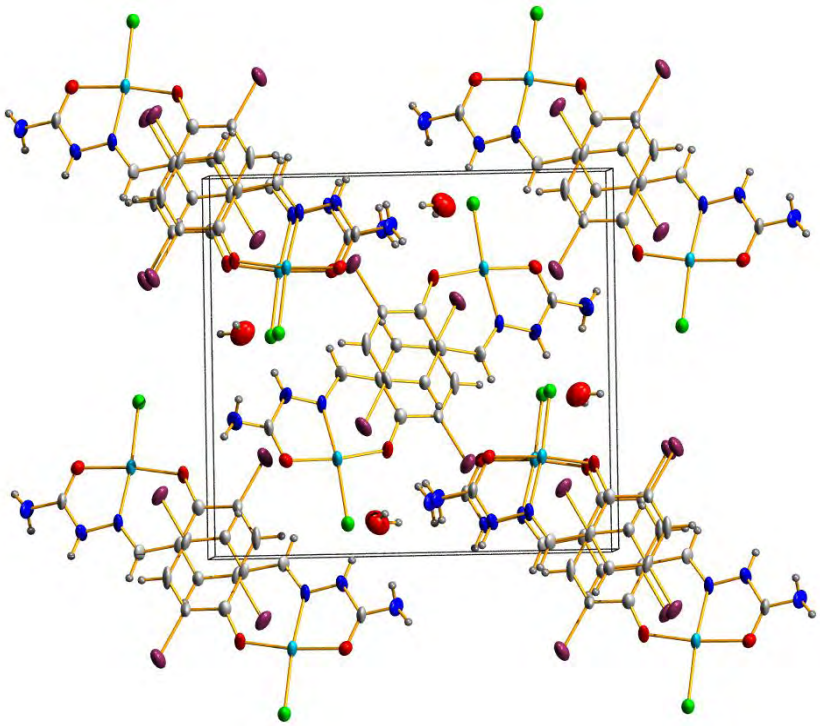

Fig. 6.32. Packing diagram along 'a' axis.

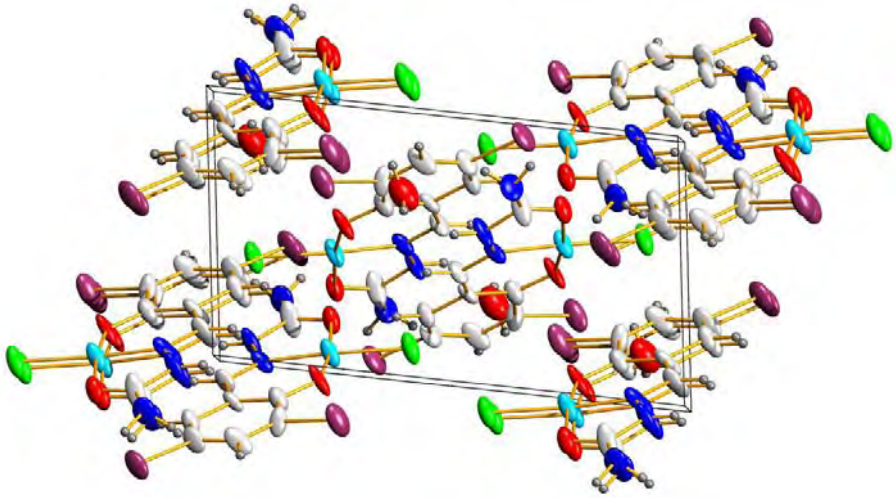

Fig. 6.33. Packing diagram along 'b' axis.

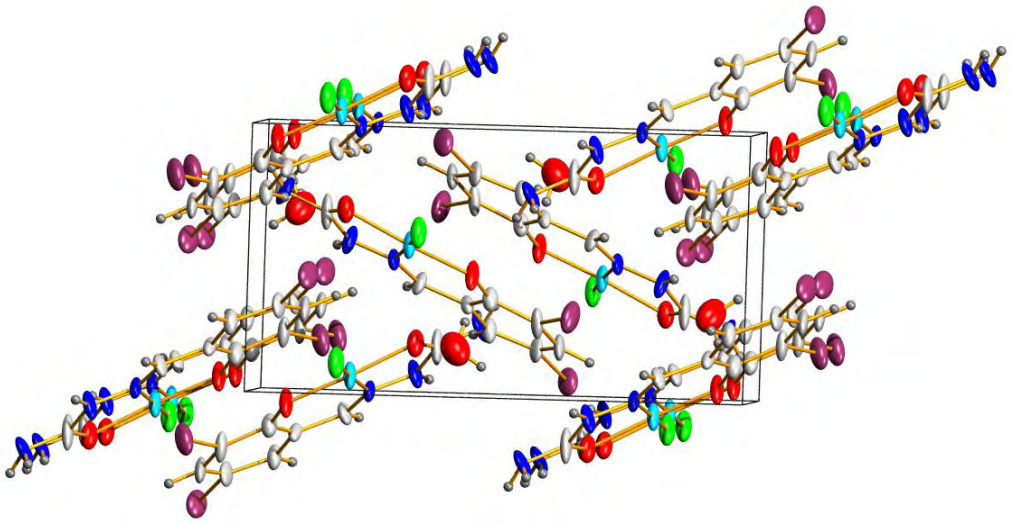

Fig. 6.34. Packing diagram along 'c' axis.

6.3.7. Infrared spectral studies

The tentative assignments of the significant IR spectral bands of copper(II) chloride complexes are useful for determining the ligand's mode of coordination (Table 6.21). The infrared spectra of all the complexes are very similar to each other. The distinct bands due to the azomethine (C=N) group within the range 1619-1625 cm^{-1} are noticed in the IR spectra of all the complexes [28].

The increase in ν(N–N) value in the spectra of complexes is due to the increase in double bond character, off-setting the loss of electron density *via* donation to the metal and is a confirmation of the coordination of the ligand through the azomethine nitrogen. The IR spectra of complexes are presented in Figs. 6.35-6.40. The strong phenolic ν(C–O) band observed at 1225 cm^{-1} confirms the deprotonation and coordination of the phenolate oxygen atom to the Cu atom in **16** and **17**. Bands in the region 3530-3540 cm^{-1} in the complex **19** can be assigned to ν(OH) from water.

Table 6.21. IR spectral data of the Cu(II) chlorido complexes (cm^{-1})

Compound	ν(C=N)	ν(C=N)	ν(N–N)	ν(C–O)	ν(C=O)
[Cu(Hmssc)Cl] (**14**)	1607	1525	1025	1222	1648
$[Cu(bpap)Cl_2]\cdot H_2O$ (**15**)	1593	1456	1023	-	1633
$[Cu(Hbsde)Cl]_n$ (**16**)	1647	1540	1160	1225	-
$[Cu(Hcsde)Cl]_n$ (**17**)	1650	1544	1162	1228	-
[Cu(Hdbsap)Cl] (**18**)	1531	1498	1109	1230	1611
$[Cu(Hdbssc)Cl]\cdot H_2O$ (**19**)	1653	1542	1164	1225	1580

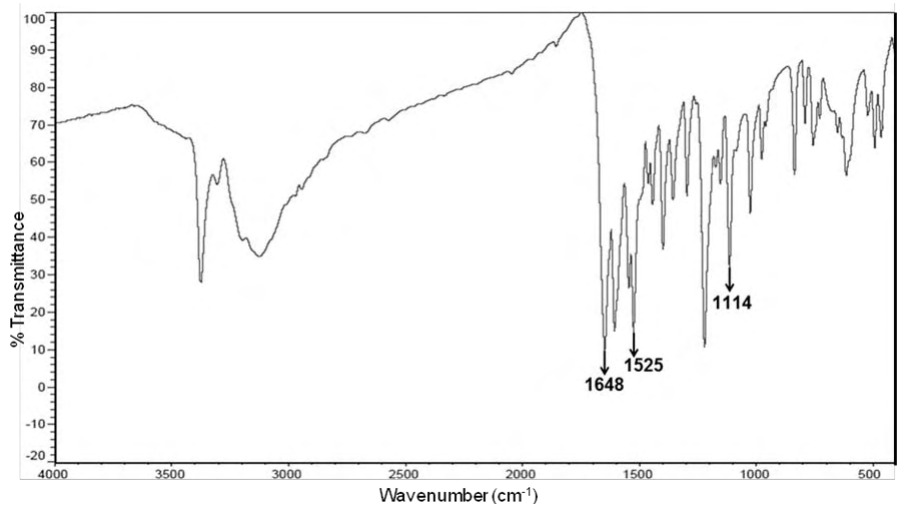

Fig. 6.35. IR spectrum of [Cu(Hmssc)Cl] (**14**).

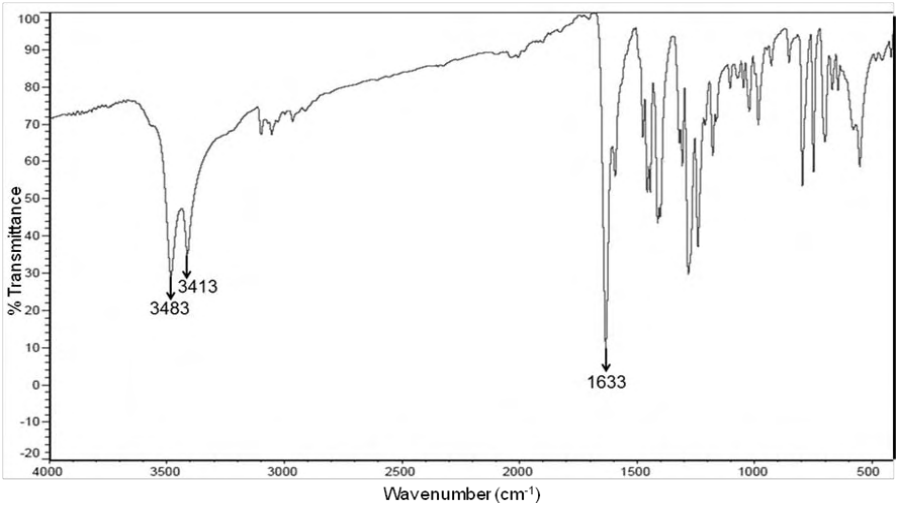

Fig. 6.36. IR spectrum of $[Cu(bpap)Cl_2]\cdot H_2O$ (**15**).

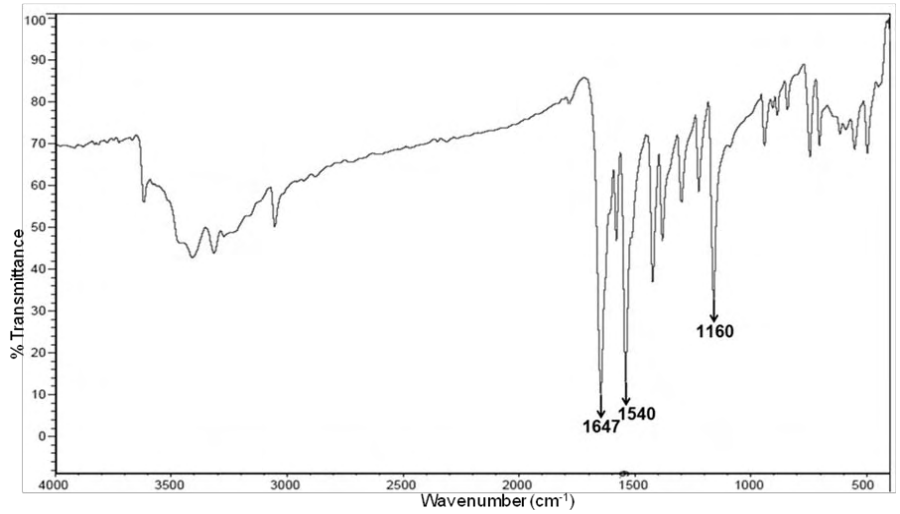

Fig. 6.37. IR spectrum of $[Cu(bsde)Cl]_n$ (**16**)

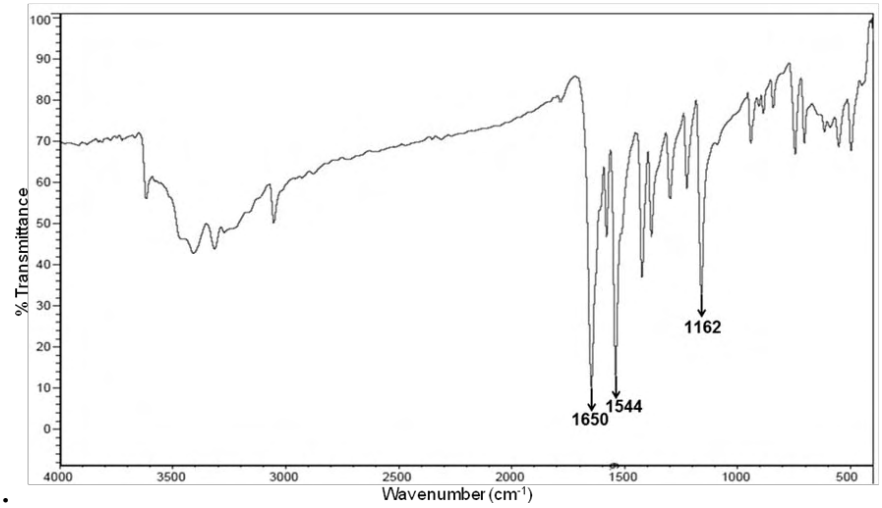

Fig. 6.38. IR spectrum of $[Cu(csde)Cl]_n$ (**17**).

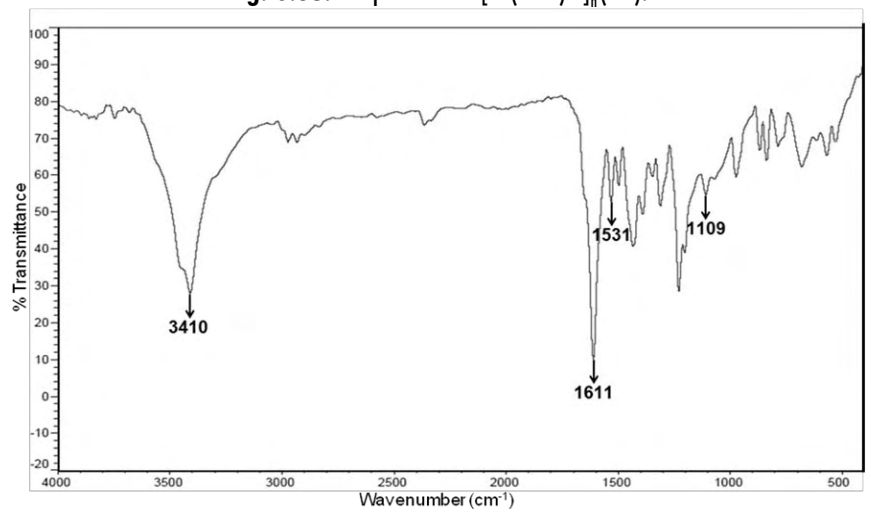

Fig. 6.39. IR spectrum of [Cu(dbsap)Cl] (**18**).

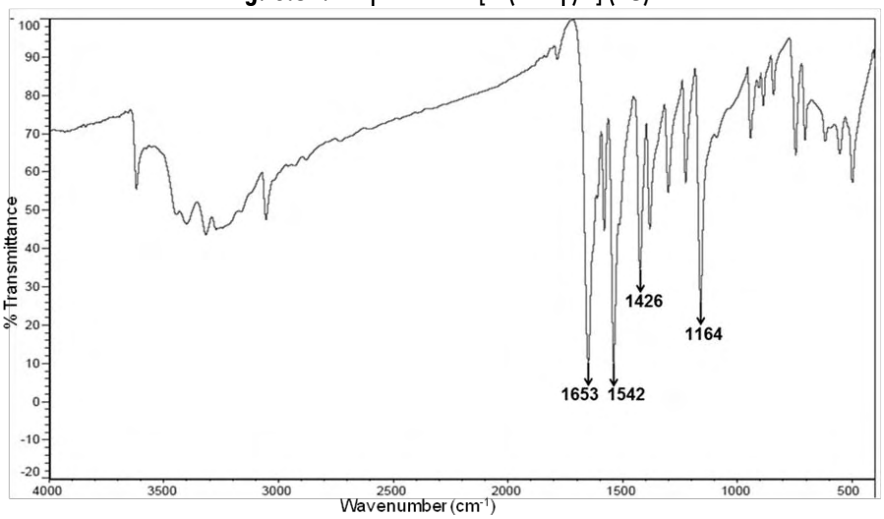

Fig.6.40. IR spectrum of $[Cu(Hdbssc)Cl]\cdot H_2O$ (**19**).

6.3.8. Electronic spectral studies

The electronic spectra of Cu(II) complexes consist of bands in the region 31000-38000 cm^{-1}. These broad bands can be regarded as a combination of n→π* transitions and π→π* of aromatic rings and semicarbazide/Schiff base moiety respectively [29]. The broad charge transfer bands were observed between 24000 and 27500 cm^{-1}, and their broadness can be explained as due to the combination of O→Cu and N→Cu LMCT transitions [30].

For copper(II) complexes, there are three spin allowed transitions, A_{1g}←B_{1g}, B_{2g} ←B_{1g} and E_g←B_{1g}. But it is very difficult to resolve the three spin allowed transitions into separate bands due to the very low energy difference between these bands. All the complexes gave *d-d* bands in the 12000-17000 cm^{-1} range [31].

The n→π* band which is found at 33900 cm^{-1} in the spectrum of uncomplexed semicarbazone was slightly shifted on complexation. This is an indication of the enolization followed by the deprotonation of the ligand during complexation. The significant electronic absorption bands in all the complexes recorded in methanol solution are presented in Table 6.22. Electronic spectra of the complexes are shown in Figs 6.41- 6.46.

Table 6.22. Electronic spectral assignments (cm^{-1}) for copper (II) chlorido complexes

Compounds	*d-d*	LMCT	n→π*/π→π*
[Cu(Hmssc)Cl] (**14**)	12130	27450	36010 , 38160 , 43530
$[Cu(bpap)Cl_2]\cdot H_2O$ (**15**)	12440	27450	36020, 38150, 43500, 47410
$[Cu(Hbsde)Cl]_n$ (**16**)	16100	26050	37500, 40180, 44020, 47900
$[Cu(Hbsde)Cl]_n$ (**17**)	16050	26000	37750, 40100, 43500,48200
[Cu(Hdbsap)Cl] (**18**)	14190	24290	32150, 40250, 47280
$[Cu(Hdbssc)Cl]\cdot H_2O$ (**19**)	14200	25600	33800, 38900, 42250, 47500

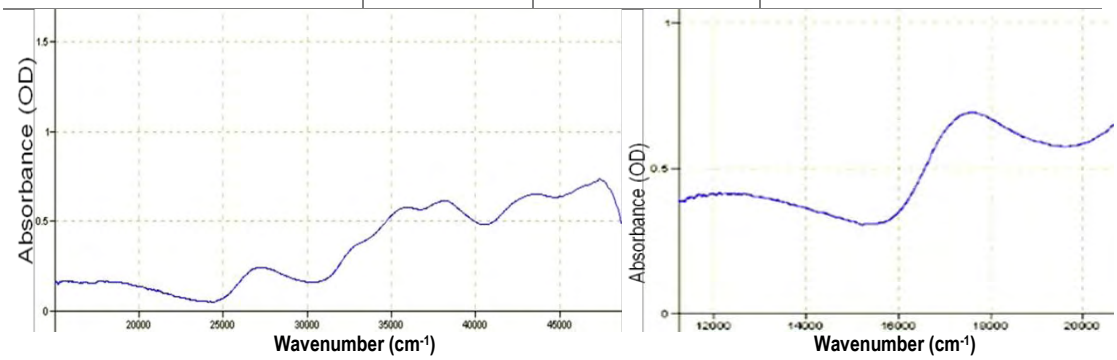

Fig. 6.41. Electronic spectra of complex [Cu(Hmssc)Cl] (**14**).

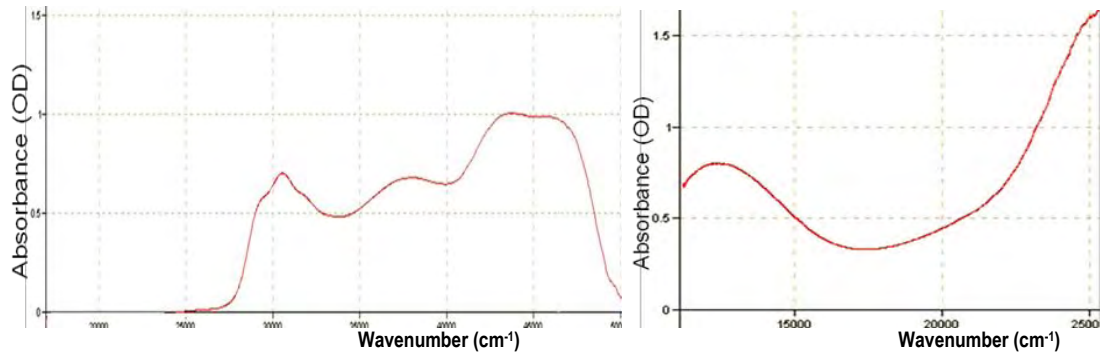

Fig. 6.42. Electronic spectra of complex $[Cu(bpap)Cl_2]\cdot H_2O$ (**15**).

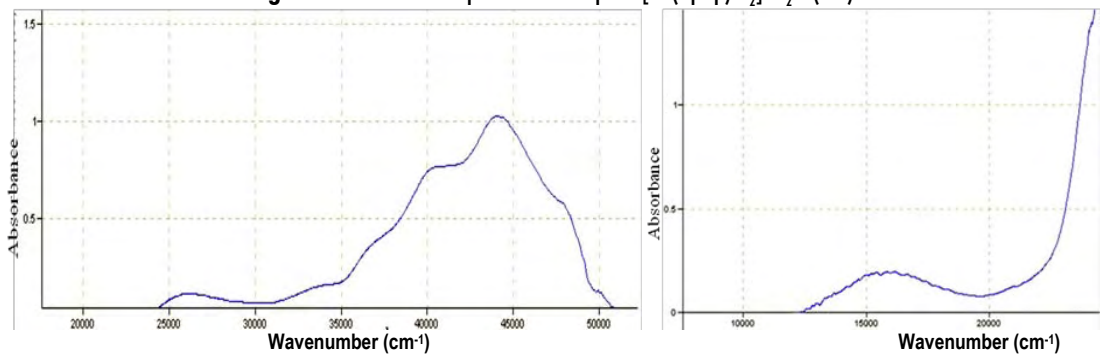

Fig. 6.43. Electronic spectra of complex $[Cu(bsde)Cl]_n$ (**16**).

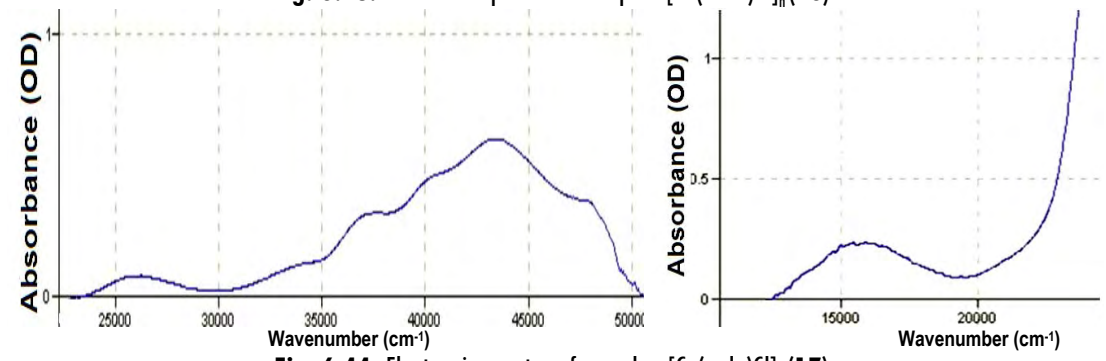

Fig. 6.44. Electronic spectra of complex $[Cu(csde)Cl]_n$ (**17**).

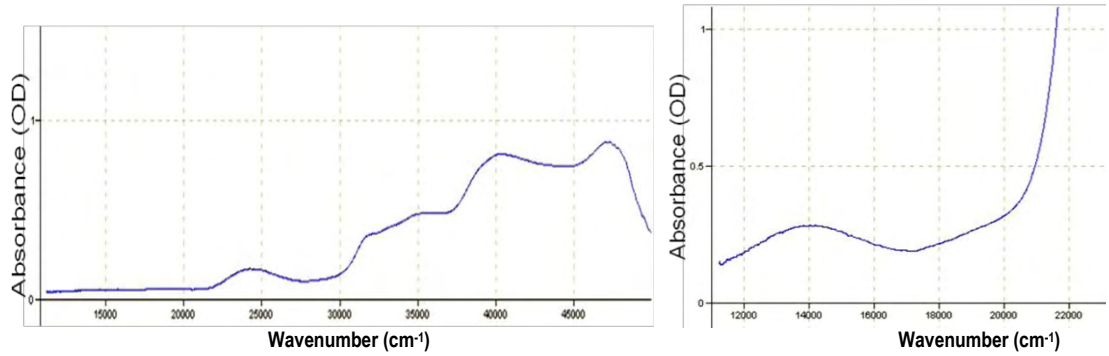

Fig. 6.45. Electronic spectra of complex [Cu(dbsap)Cl] (**18**).

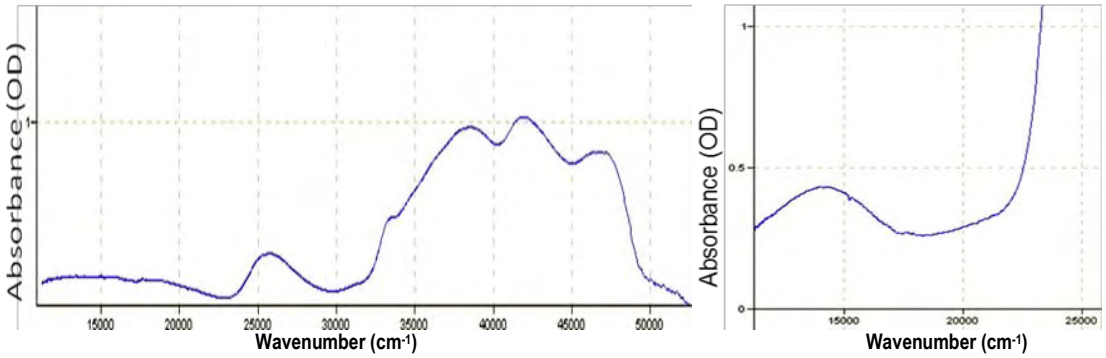

Fig. 6.46. Electronic spectra of [Cu(Hdbssc)Cl]·H_2O (**19**).

6.3.9. EPR spectral studies

The geometric parameter *G*, which is a measure of exchange interaction between the copper centers in the polycrystalline compound, is calculated and the value of *G* is found to be in the range 2.4-3.8. It is perceived that, if *G*>4, the exchange interaction is negligible and vice versa in the complexes. The *G* values indicate that the exchange interactions are strong in all these complexes. In all the complexes, **14**, **15**, **16** and **18;** $g_{\|} > g_{\perp} > 2.0023$ is consistent with a $d_{x^2-y^2}$ ground state in a square planar or square pyramidal geometry [36].

Spin Hamiltonian and bonding parameters of the complexes are given in Table 6.23. The EPR spectra of **14, 15, 16** and **17** in DMF solution at 77 K are axial in nature with four well resolved hyperfine splitting lines in the region (Figs. 6.47-6.50). The spectrum shows four hyperfine splitting lines both in the parallel region and no superhyperfine splitting is observed. In the epr spectrum of copper (II) complexes **14**, **16** and **18** in frozen DMF, the four fairly resolved hyperfine lines [^{63,65}Cu, I = 3/2]corresponding to -3/2, -1/2, +1/2 and +3/2 transitions. As $g_{\|} > g_{\perp}$ a square pyramidal geometry can be assigned and rules out the possibility of a triagonal bipyramidal structure which would be expected to have $g_{\perp} > g_{\|}$. The accuracy of epr spectral data is proved by single crystal XRD results. The α^2, β^2, γ^2 values of the complex **16** are less than one which indicates that the complex have stong in-plane π bonding. The orbital reduction factor $K_{\|} < K_{\perp}$ also support that the complex involved in in-plane π bonding.

Table 6.23. Spin Hamiltonian and bonding parameters of the complexes

	[Cu(Hmssc)Cl] (**14**)	$[Cu(bpap)Cl_2]\cdot H_2O$ (**15**)	$[Cu(bsde)Cl]_n$ (**16**)	[Cu(dbsap)Cl] (**18**)
	Polycrystalline state at 298 K			
$g_{\|\|}$	2.086	2.219	-	2.178
$g_{\perp}$	2.043	2.128	-	2.075
g_{isc}/g_{rv}	2.0573	2.1583	2.149	2.1093
G	2.0565	1.7239	-	2.4168
	Solution state at 77 K			
$g_{\|\|}$	-	-	2.202	2.324
$g_{\perp}$	-	-	2.044	2.078
$A_{\|\|}$	-	-	20.16	10.028
α^2	-	-	0.833	0.696
β^2	-	-	0.837	1.192
γ^2	-	-	0.765	1.157
$K_{\|\|}$	-	-	0.697	0.8301
$K_{\perp}$	-	-	0.637	0.8054

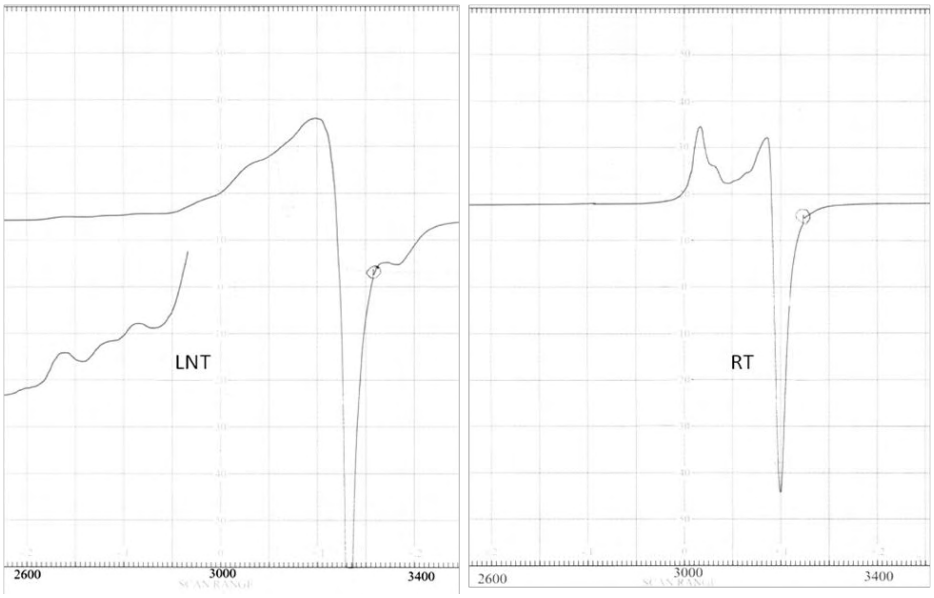

Fig. 6.47. EPR spectra of complex [Cu(Hmssc)Cl] (**14**).

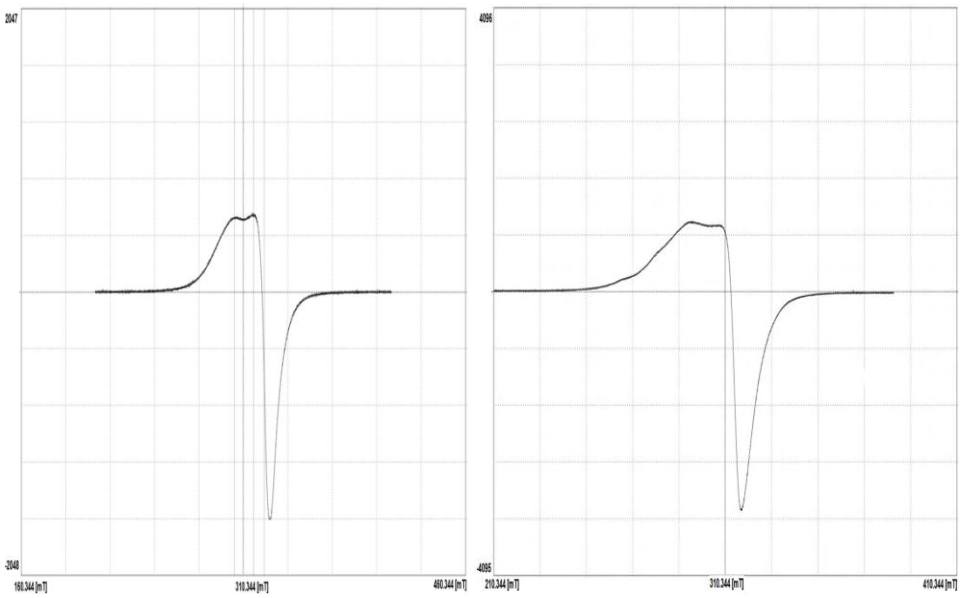

Fig. 6.48. EPR spectra of complex $[Cu(bpap)Cl_2]\cdot H_2O$ (**15**).

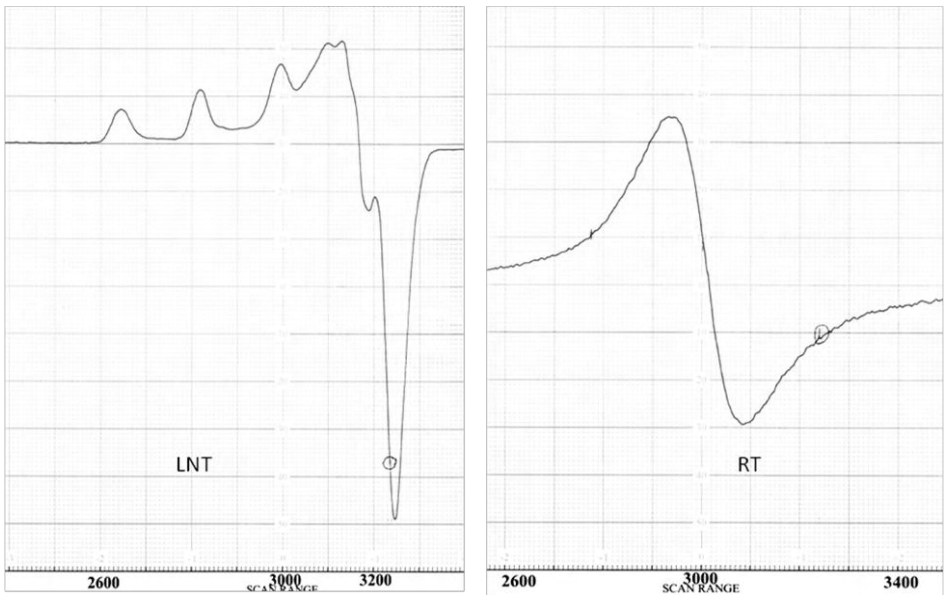

Fig. 6.49. EPR spectra of complex $[Cu(bsde)Cl]_n$ (**16**).

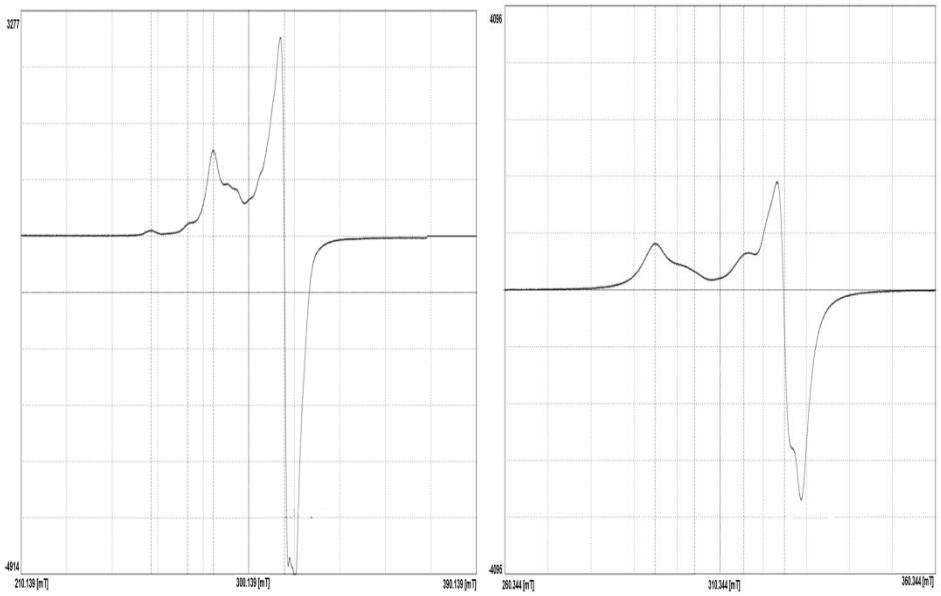

Fig. 6.50. EPR spectra of complex [Cu(dbsap)Cl] (**18**).

REFERENCES

1. A. Dhalenne, R. Revcolevschi, Science, 1998, 279, 345.
2. E. Dagotto, T.M. Rice, Science, 1996, 271, 618.
3. T. Barnes, E. Dagotto, J. Riera, E.S. Swanson, Phys. Rev. B, 1993, 47, 3196.
4. E. Dagotto, J. Riera, D.J. Scalapino, Phys. Rev. B, 1992, 45, 5744.
5. T. Nagato, M. Uehara, J. Goto, J. Akimitsu, N. Motoyama, H. Eisaki, S. Uchida, H. Takahashi, T. Nakanishi, N. Mori, Phys. Rev. Lett., 1998, 81, 90.
6. B.C. Watson, V.N. Kotov, M.W. Meisel, D.W. Hall, G.E. Granoth, W.T. Montfrooij, S.E. Nagnler, D.A. Jensen, R. Backov, M.A. Petruska, G.E. Fanucci, D.R. Talham, Phys. Rev. Lett., 2001, 86, 5168.
7. A. Luque, J. Sertucha, L. Lezama, T. Rojo, P. Roman, J. Chem. Soc., Dalton Trans., 1997, 847.
8. Y. B. Jiang, H. Z. Kou, R. J. Wang, A. L. Cui. Eur. J. Inorg. Chem., 2004, 4608.
9. G.H.-Molina, J.G.-Platas, C.R.-Pérez, F. Lloret, M. Julve, Inorg. Chim. Acta, 1999, 284, 258.
10. M.T. Garland, D. Grandjean, E. Spodin, A.M. Atria, J. Manzur, Acta Cryst., 1988, C44, 1209.
11. M. Orio, O. Jarjayes, H. Kanso, C. Philouze, F. Neese, F. Thomas, Angew. Chem. Int. Ed., 2010, 49, 4989.

12. R. Ziessel, Coord. Chem. Rev., 2001, 216, 195.
13. (a) S. Sasmal, S. Sarkar, N.A. Alcalde, S. Mohanta, Inorg. Chem., 2011, 50, 5687. (b) M. Shaker, S. Adama, A.D. Mohamad, P.G. Jones, M.K. Kindermann, J. W. Heinicke, Polyhedron, 2013, 50, 101. (c) E.S. Aazam, M.M. Ghoneim, M.A.E. Attar, J. Coord. Chem., 2011, 64, 2506. (d) K. Pal, U.N. Maiti, T.P. Majumder, S.C. Debnath, N. Bennis, J.M. Oton, J. Mol. Struct., 2013, 1035, 76.
14. (a) P. Bhowmik, H.P. Nayek, M. Corbella, N.A. Alcalde, S. Chattopadhyay, Dalton Trans., 2011, 40, 7916. (b) S. Jana, S. Chatterjee, S. Chattopadhyay, Polyhedron, 2012, 48, 189. (c) P. Bhowmik, K. Harms, S. Chattopadhyay, Polyhedron, 2013, 49, 113.
15. L. Canali, D.C. Sherrington, Chem. Soc. Rev., 1999, 28, 85.
16. M. Das, S. Chattopadhyay, Transit. Met. Chem., 2013, 38, 191.
17. P. Bhowmik, S. Chattopadhyay, A. Ghosh, Inorg. Chim. Acta, 2013, 396, 66.
18. (a) S. Biswas, A. Ghosh, J. Mol. Struct., 2012, 1019, 32. (b) C.R. Bhattacharjee, P. Goswami, P. Mondal, Inorg. Chim. Acta, 2012, 387, 86. (c) P. Kar, A. Ghosh, Inorg. Chim. Acta, 2013, 395, 67.
19. SMART and SAINT, Area Detector Software Package and SAX Area Detector Integration Program, Bruker Analytical X-ray; Madison, WI, USA, 1997.
20. SADABS, Area Detector Absorption Correction Program; Bruker Analytical X-ray; Madison, WI, 1997.
21. L.J. Farrugia, J. Appl. Cryst., 2012, 45, 849.
22. K. Brandenburg, Diamond Version 3.2g, Crystal Impact GbR, Bonn, Germany, 2010.
23. J,-L. Wang, B. Liu, B.-S. Yang, S.-P. Huang, J. Struc. Chem. 2008, 49,570.
24. M. C.Etter, J.C. MacDonald, J. Bernstein, Acta Cryst., 1990, B46, 256.
25. X.-L. Li, B.-L. Liu, Y. Song, Inorg. Chem. Commun., 2008, 11, 1100.
26. M.K. Paira, T.K. Mondal, E. López-Torres, J. Ribas, C. Sinha, Polyhedron, 2010, 29, 3147.
27. W.A. Alves, I.O. Matos, P.M. Takahashi, E.L. Bastos, H. Martinho, J.G. Ferreira, C.C. Silva, R.H.A. Santos, A. Paduan-Filho, A.M.D.C. Ferreira, Eur. J. Inorg. Chem., 2009, 2219.

28. D. Maity, S. Chattopadhyay, A. Ghosh, M.G.B. Drew, G. Mukhopadhyay, Polyhedron, 2009, 28, 812.

29. C.R.K. Rao, P.S. Zacharias, Polyhedron, 1997, 16, 1201.

30. H. Sacconi, G.Speroni, J. Am. Chem. Soc., 1965, 87, 3102.

31. (a) R.P. John, A. Sreekanth, V. Rajakannan, T.A. Ajith, M.R.P. Kurup, Polyhedron, 2004, 23, 2549. (b) M. Joseph, M. Kuriakose, M.R.P. Kurup, E. Suresh, A. Kishore, G. Bhat, Polyhedron, 2006, 25, 61. (c) B.N. Bessy Raj, M.R.P. Kurup, E. Suresh, Spectrochim. Acta, Part A, 2008, 71, 1253.

Chapter 7

Copper(II) complexes containing bromide as coligand

Contents

7.1. Introduction

The potential role played by copper ions, present in the active sites of many metalloproteins [1,2] has stimulated the design of new N_2O donor ligand frames and their copper complexes as models for providing a better understanding of biological systems [3,4,5]. The syntheses and characterization of di- or poly-nuclear copper complexes are of immense interest for understanding the structural and chemical factors that govern the exchange coupling between paramagnetic centers and magnetostructural correlations in molecular systems, and for developing new functional molecular-based materials [6]. Schiff base ligands are ubiquitous in coordination chemistry being used in the synthesis of a large variety of transition metal complexes, which remains an important area of research due to their simple synthesis, good yield, high purity and wide range of applications [7]. Semicarbazone based ligands are versatile molecules and can coordinate to metal either in neutral or anionic form [8]. This family of molecules has been demonstrating high potential in numerous applications such as anticancer, antibacterial, antifungal and antivirus agents [9]. Usually their metal complexes revealed enhanced antimicrobial activities than the metal free ligands [10].

7.2. Experimental

7.2.1. Synthesis of complexes

All chemicals used for synthesis were of Analar grade. The semicarbazones and Schiff bases were formed in solution and complexes are isolated on reaction with copper(II) dibromide.

7.2.1.1. Synthesis of $[Cu(dpktsc)Br]_2 \cdot CH_3OH$ (20)

The di-2-pyridylketone thiosemicarbazone was prepared by heating a mixture of di-2-pyridylketone (0.185 g, 1 mmol) and thiosemicarbazide (0.091 g, 1 mmol) in methanol for 3 h. Copper(II) bromide (0.223 g, 1 mmol) was added to this solution and continued to reflux for another 2 h. Dark green colored crystals separated on cooling and were isolated from the solution. Yield: 64%.

7.2.1.2. Synthesis of $[Cu(Hbpsc)Br_2] \cdot H_2O$ (21)

2-Benzoylpyridine semicarbazone was prepared by heating a mixture of 2-benzoylpyridine (0.183 g, 1 mmol) and semicarbazide hydrochloride (0.111 g, 1 mmol) in methanol for 3 h. Copper(II) bromide (0.223 g, 1 mmol) was added to this solution and reflux was continued for another 2 h. Dark green colored crystals separated on cooling and were isolated from the solution. Yield: 82%.

7.2.1.3. Synthesis of [Cu(bptsc)Br] (22)

2-Benzoylpyridine thiosemicarbazone was prepared by heating a mixture of 2-benzoylpyridine (0.183 g, 1 mmol) and thiosemicarbazide (0.091 g, 1 mmol) in methanol for 3 h. Copper(II) bromide (0.223 g, 1 mmol) was added to this solution and reflux was continued for another 2 h. Dark green colored crystals separated on cooling and were isolated from the solution. Yield: 76%.

7.2.1.4. Synthesis of $[Cu(bpap)Br_2] \cdot H_2O$ (23)

1-[(*E*)-[Phenyl(pyridin-2-yl)methylidene]amino]pyrrolidin-2-one was synthesized *in situ* by heating a mixture of 2-benzoylpyridine (0.183 g, 1 mmol) and 1-aminopyrrolidin-2-one (0.100 g, 1 mmol) in methanol for 2 h. Copper(II) bromide (0.223 g, 1 mmol) was added, and the mixture heated for 5 h. The resulting pale green solid was collected and recrystallized from methanol. Yield: 78%.

7.2.1.5. Synthesis of $[Cu(Hdbssc)Br] \cdot H_2O$ (24)

3,5-Dibromosalicylaldehyde semicarbazone was prepared by heating a mixture of 3,5-dibromosalicylaldehyde (0.280 g, 1 mmol) and semicarbazide hydrochloride (0.111 g, 1 mmol) in methanol for 3 h. Copper(II) bromide (0.223 g, 1 mmol) was added to this solution and reflux was continued for another 2 h. Dark green colored crystals separated on cooling and were isolated from the solution. Yield: 55%.

7.2.2. Physical measurements

Carbon, hydrogen and nitrogen analyses were carried out using a Vario EL III CHNS analyzer at the SAIF, Kochi, India. Infrared spectra were recorded on a JASCO FT-IR-5300 Spectrometer in the range 4000-400 cm^{-1} using KBr pellets. Electronic spectra were recorded on Ocean Optics USB 4000 UV-Vis Fiber Optic Spectrometer in the 200-850 nm range using solutions in methanol.

7.2.3. X-ray crystallography

Single crystals of **20-24** suitable for X-ray diffraction studies were obtained from their methanol solution by slow evaporation at room temperature. Crystals with appropriate dimensions were mounted on a Bruker SMART APEX diffractometer, equipped with a graphite crystal, incident-beam monochromator, and a fine focus sealed tube with Mo Kα (λ = 0.71073 Å) as the X-ray source. The unit cell dimensions were measured and the data collections were performed at 296(2) K. Bruker SMART software was used for data acquisition and Bruker SAINT software for data integration [11]. Absorption corrections were carried out using SADABS based on Laue symmetry using equivalent reflections [12]. The structure was solved by direct methods and refined by full-matrix least-squares calculations with the WinGX software package [13]. The graphics tool used was DIAMOND version 3.2g [14]. In $[Cu(dpktsc)Br]_2 \cdot CH_3OH$ (**20**), $[Cu(Hbpsc)Br_2] \cdot H_2O$ (**21**), [Cu(bptsc)Br] (**22**) and $[Cu(Hdbssc)Br] \cdot H_2O$ (**24**), the hydrogen atoms of the NH_2 group were located from a difference Fourier map and restrained using DFIX and DANG instructions. In all complexes, hydrogen atoms bound to carbon atoms were placed in geometrically idealized positions and constrained to ride on their parent atoms, with C–H distances of 0.93 Å, and with isotropic displacement parameters 1.2 times that of the parent carbon atoms. In $[Cu(Hbpsc)Br_2] \cdot H_2O$ (**21**) and $[Cu(Hdbssc)Br] \cdot H_2O$ (**24**), N–H hydrogen atoms were located from Fourier maps and restrained to a distance of 0.88±0.01. In $[Cu(Hbpsc)Br_2] \cdot H_2O$ (**21**), the lattice water was disordered over two sites A and B with occupancies of 65% and 35% respectively. In [Cu(bptsc)Br] (**22**), the (0 2 0) and (-1,1,1) reflections were omitted owing to interference from the beam stop. In $[Cu(bpap)Br_2] \cdot H_2O$ (**23**), the hydrogen atoms on the solvent molecule were unable to locate from the difference maps. The key crystallographic information of the isolated single crystals of the complexes is tabulated (Tables 7.1a and 7.1b).

Table 7.1a. Crystallographic data and structure refinement for **20, 21** and **22**

Parameters	$[Cu(dpktsc)Br]_2 \cdot CH_3OH$ (**20**)	$[Cu(Hbpsc)Br_2] \cdot H_2O$ (**21**)	[Cu(bptsc)Br] (**22**)
Empirical formula	$C_{26}H_{28}Br_2Cu_2N_{10}O_2S_2$	$C_{26}H_{24}Br_4Cu_2N_8O_3$	$C_{13}H_{11}BrCuN_4S$
Formula weight	863.62	943.23	398.78
Color	Dark Green	Green	Dark Green
Temperature (T) K	296(2)	296(2)	296(2)
Wavelength (Mo Kα) (Å)	0.71073	0.71073	0.71073
Crystal system	Triclinic	Triclinic	Monoclinic
Space group	$P\bar{1}$	$P\bar{1}$	*C*2/c
Cell parameters			
a	8.3052(7) Å	9.3587(5) Å	11.0424(7) Å
b	9.2120(7) Å	13.0232(5) Å	22.2919(16) Å
c	11.0500(9) Å	14.2224(9) Å	12.1004(7) Å
α	68.341(2)°	83.853(2)°	90°
β	79.127(3)°	71.523(2)°	105.043(2)°
γ	84.913(2)°	84.5670(10)°	90°
Volume V ($Å^3$)	771.45(11)	1631.23(15)	2876.5(3)
Z	1	2	8
Calculated density (ρ) ($Mg\ m^{-3}$)	1.859	1.920	1.842
Absorption coefficient, μ (mm^{-1})	4.148	6.244	4.435
F(000)	430	916	1576
Crystal size mm^3	0.30 x 0.25 x 0.25	0.35 x 0.20 x 0.20	0.35 x 0.30 x 0.25
θ range for data collection	2.38 to 25.00°	1.51 to 27.00 °	2.53 to 25.00°
Limiting indices	-9≤h≤9, -9≤k≤10, -13≤l≤13	-11≤h≤11,-16≤k≤16, -18≤l≤18	-13≤h≤13, -26≤k≤26, -14≤l≤14
Reflections collected	11266	27391	19205
Unique Reflections (R_{int})	2708 [R(int) = 0.0650]	7117 [R(int) = 0.0451]	2546 [R(int) = 0.0952]
Completeness to θ	25.00 (99.3%)	27.00 (99.9%)	25.00 (99.9%)
Absorption correction	Semi-empirical from equivalents	Semi-empirical from equivalents	Semi-empirical from equivalents
Maximum and minimum transmission	0.349 and 0.298	0.3682 and 0.2185	0.4035 and 0.3059
Refinement method	Full-matrix least-squares on F^2	Full-matrix least-squares on F^2	Full-matrix least-squares on F^2
Data / restraints / parameters	2688 / 3 / 209	7113 / 1 / 398	2543 / 3 / 189
Goodness-of-fit on F^2	1.052	1.059	1.052
Final R indices [$I > 2\sigma(I)$]	$R_1 = 0.0398$, $wR_2 = 0.1063$	$R_1 = 0.0871$, $wR_2 = 0.2720$	$R_1 = 0.0293$, $wR_2 = 0.0831$
R indices (all data)	$R_1 = 0.0460$, $wR_2 = 0.1125$	$R_1 = 0.1140$, $wR_2 = 0.3053$	$R_1 = 0.0333$, $wR_2 = 0.0865$
Largest difference peak and hole (e $Å^{-3}$)	0.741 and -0.610	3.103 and -3.689	0.526 and -0.500

$R_1 = \Sigma||F_o| - |F_c|| / \Sigma|F_o|$ $\qquad$ $wR_2 = [\Sigma w(F_o^2-F_c^2)^2 / \Sigma w(F_o^2)^2]^{1/2}$

Table 7.1b. Crystallographic data and structure refinement for **23** and **24**

Parameters	$[Cu(bpap)Br_2]\cdot H_2O$ (**23**)	$[Cu(Hdbssc)Br]\cdot H_2O$ (**24**)
Empirical formula	$C_{16}H_{15}Br_2CuN_3O_2$	$C_8H_8Br_3CuN_3O_3$
Formula weight	504.66	497.44
Color	Green	Dark green
Temperature (T) K	296(2)	296(2)
Wavelength (Mo Kα) (Å)	0.71073	0.71073
Crystal system	Triclinic	Monoclinic
Space group	$P\bar{1}$	$P2_1/n$
Cell parameters		
a	9.1838(8) Å	7.3969(6) Å
b	9.3704(9) Å	13.5754(12) Å
c	10.9403(11) Å	12.7995(13) Å
α	88.959(4)°	90°
β	79.518(3)°	96.569(5)°
γ	75.217(3)°	90°
Volume V ($Å^3$)	894.73(15)	1276.8(2)
Z	2	4
Calculated density (ρ) ($Mg\ m^{-3}$)	1.814	2.588
Absorption coefficient, μ(mm^{-1})	5.692	11.100
F(000)	494	940
Crystal size mm^3	0.40 x 0.30 x 0.20	0.35 x 0.30 x 0.25
θ range for data collection	1.89 to 28.16°	3.00 to 26.99°
Limiting indices	$-12\le h\le 10$, $-12\le k\le 12$, $-14\le l\le 14$	$-6\le h\le 9$, $-17\le k\le 17$, $-16\le l\le 16$
Reflections collected	13632	8976
Unique Reflections (R_{int})	4264 [R(int) = 0.0384]	2779 [R(int) = 0.0984]
Completeness to θ	28.16 (96.9%)	26.99 (99.7%)
Absorption correction	Semi-empirical from equivalents	Semi-empirical from equivalents
Maximum and minimum transmission	0.3956 and 0.2092	0.1679 and 0.1123
Refinement method	Full-matrix least-squares on F^2	Full-matrix least-squares on F^2
Data / restraints / parameters	4264 / 0 / 217	2779 / 6 / 179
Goodness-of-fit on F^2	1.597	1.049
Final R indices [$I > 2\sigma(I)$]	$R_1 = 0.1087$, $wR_2 = 0.3510$	$R_1 = 0.0898$, $wR_2 = 0.2394$
R indices (all data)	$R_1 = 0.1324$, $wR_2 = 0.3811$	$R_1 = 0.1196$, $wR_2 = 0.2699$
Largest difference peak and hole (e $Å^{-3}$)	3.407 and -2.463	1.826 and -2.687

$R_1 = \Sigma||F_o| - |F_c|| / \Sigma|F_o|$ $\qquad$ $wR_2 = [\Sigma w(F_o^2-F_c^2)^2 / \Sigma w(F_o^2)^2]^{1/2}$

7.3. Results and discussion

7.3.1. Analytical measurements

The analytical data of all the complexes are listed in Table 7.2. The CHNS data obtained showed that all the complexes are analytically pure. The conductivity measurements were made in DMF solutions and all complexes are found to be non-electrolytes. Room temperature magnetic moments of these complexes show that all the copper(II) complexes have μ_{eff} values in the range 1.71-1.72 B.M., corresponding to the presence of one unpaired electron. These results suggest that no copper-copper interactions at room temperature are present in the complexes.

Table 7.2. Preliminary analytical data of Cu(II) bromide complexes

Compound	Observed (Calculated)%				λ_m	μ_{eff}(B.M.)
	C	H	N	S		
$[Cu(dpktsc)Br]_2 \cdot CH_3OH$ (**20**)	36.27 (36.16)	3.11 (3.27)	16.41 (16.22)	7.28 (7.43)	18	1.705
$[Cu(Hbpsc)Br_2] \cdot H_2O$ (**21**)	32.68 (32.42)	2.77 (2.93)	11.63 (11.89)	-	20	1.725
[Cu(bptsc)Br] (**22**)	38.62 (38.96)	3.42 (3.27)	13.80 (13.98)	8.22 (8.00)	11	1.743
$[Cu(bpap)Br_2] \cdot H_2O$ (**23**)	37.81 (37.93)	3.46 (3.38)	7.79 (8.29)	-	28	1.714
$[Cu(Hdbssc)Br] \cdot H_2O$ (**24**)	19.12 (19.32)	1.75 (1.62)	8.60 (8.45)		32	1.734

7.3.2. Crystal structure of complex $[Cu(dpktsc)Br]_2 \cdot CH_3OH$ (20)

This complex has a dimeric structure. The coordination geometry around each copper(II) ion is square pyramidal with a slight distortion (τ= 0.03). The S1 atom of the thiosemicarbazone moiety, the imino N3 atom, pyridine N1 atom and the Br1 atom comprise the basal plane while the apical position is occupied by the N2A atom of the symmetry related half of the dimer with a longest bond length of 2.529(3) Å to the metal atom. The thiosemicarbazone moiety of the metal free ligand shows *E* configuration about the both C12–N4 and C6–N3 bonds [15,16] whereas in the Cu(II) complex the coordinated thiosemicarbazone moiety has *E* configuration with respect to C6–N3 and *Z* configuration about C12–N4. The atoms coordinated to metal centre are found to exist in *E* configuration having N3 and N1 atoms *cis* to each other with respect to C15–N2 bond. A unique part of the Cu(II) complex and the dimeric unit generated by the association of the free pyridyl nitrogen with the Cu atom are shown along with the atom-labeling in Figs. 7.1 and 7.2 respectively.

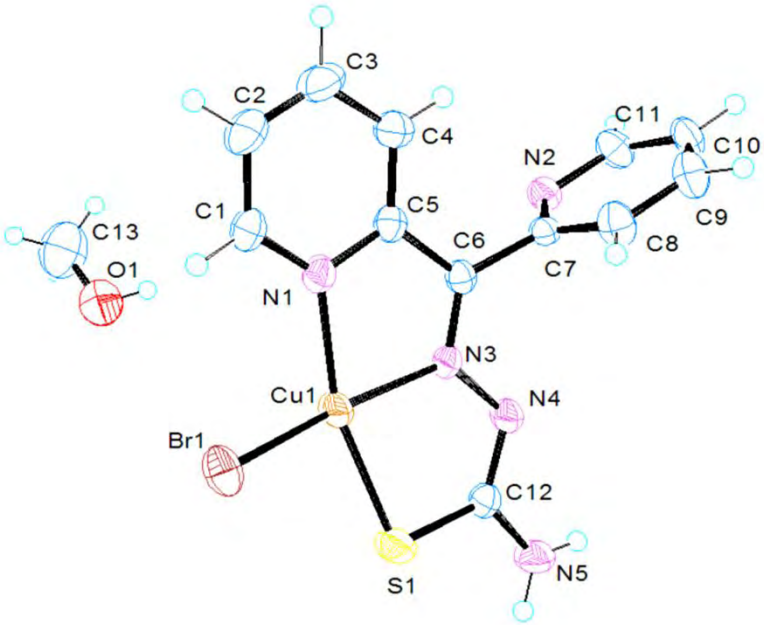

Fig. 7.1. Asymmetric unit of $[Cu(dpktsc)Br]_2 \cdot CH_3OH$ (**20**).

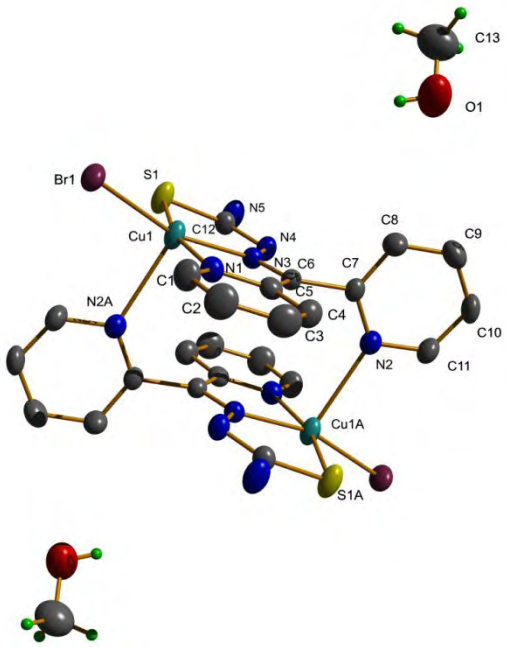

Fig. 7.2. Molecular structure of $[Cu(dpktsc)Br]_2 \cdot CH_3OH$ (**20**).

The two aromatic rings are twisted with a dihedral angle of 88.1(2)^o between the rings. Table 7.3 shows the selected bond lengths and bond angles of the compound **20**. The hydrazinecarbothioamide moiety and one of the pyridine ring comprising atoms C1–C6 and N1 are almost planar with maximum deviation of 0.052(4) Å for the atom C12 of the ring. C12–S1 bond distance (1.727(4) Å) is very

close to the single bond which suggests that the thiosemicarbazone is coordinating in protonated thiolate form. This phenomenon could also be further confirmed by the coplanar nature of the NH_2 group of the coordinated ligand with sp^2 character which facilitates an extended conjugation of the hydrazinecarbothioamide moiety with the aromatic rings.

Table 7.3. Selected bond lengths [Å] and angles [°] for the two asymmetric units of $[Cu(dpktsc)Br]_2 \cdot CH_3OH$ (**20**)

Bond lengths (Å)		Bond angles (°)	
Br1–Cu1	2.385(5)	N2–Cu1–N1	80.51(9)
Cu1–N2	1.980(2)	N2–Cu1–S1	84.35(7)
Cu1–N1	2.001(3)	N1–Cu1–S1	164.29(7)
Cu1–S1	2.215(9)	N2–Cu1–Br1	179.82(7)
N2–N3	1.367(3)	N1–Cu1–Br1	99.32(6)
S1–C13	1.725(3)	S1–Cu1–Br1	95.81(3)
N3–C13	1.325(4)		

The intramolecular non-classical hydrogen bonding interactions (C1–H1···Br1 and C11–H11···Br1) makes the complex more rigid (Table 7.4).

Table 7.4. Hydrogen-bonding interactions of $[Cu(dpktsc)Br]_2 \cdot CH_3OH$ (**20**)

D–H···A	D–H (Å)	H···A (Å)	D···A (Å)	∠D–H···A (°)
O(1)–H(1A)···Br(1)^a	0.8205	2.5761	3.396(4)	177.86
N(5)–H(5A1)···N(4)^b	0.84(4)	2.17(4)	3.006(5)	177(5)
C(4)–H(4)···O(1)^c	0.9297	2.4370	3.281(6)	150.99
C(11)–H(11)···Br(1)^d	0.9294	2.8594	3.573(4)	134.47
C(1)–H(1) .. Br(1)	0.9294	2.9066	3.450(4)	118.63

Equivalent position codes: a=x,1+y,z; b=x,y,-1+z; c=-x,1-y,1-z ; d=1-x,1-y,1-z

The intermolecular hydrogen bonding interactions (classical and non-classical) establish a supramolecular 1-D network by linking the adjacent molecules through the methanol present in the lattice and N–H···N in parallel fashion as shown in Fig. 7.3.

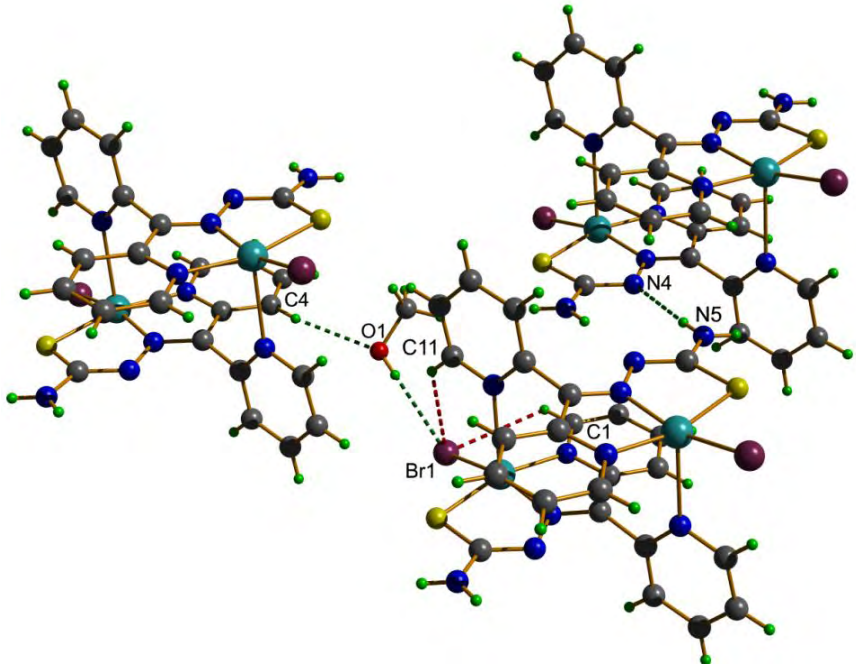

Fig. 7.3. Hydrogen-bonding interactions showing an infinite chain in the crystal structure of $[Cu(dpktsc)Br]_2 \cdot CH_3OH$..

Packing of the molecules also involves many very weak π···π interactions (Table 7.5) with centroid-centroid distances in the range 3.707(2)-5.778(2) Å. The π ···π interactions are shown in Fig. 7.4.

Table 7.5. π···π interactions of $[Cu(dpktsc)Br]_2 \cdot CH_3OH$ (**20**)

Cg(I)···Cg(J)	Cg···Cg (Å)	α (°)	β (°)	γ(°)
Cg(2)···Cg(4)^c	3.707(2)	0.00	28.03	28.03

Cg(2) = Cu(1), N(1), C(5), C(6), N(3); Cg (4) = N(2), C(7), C(8), C(9), C(10), C(11)

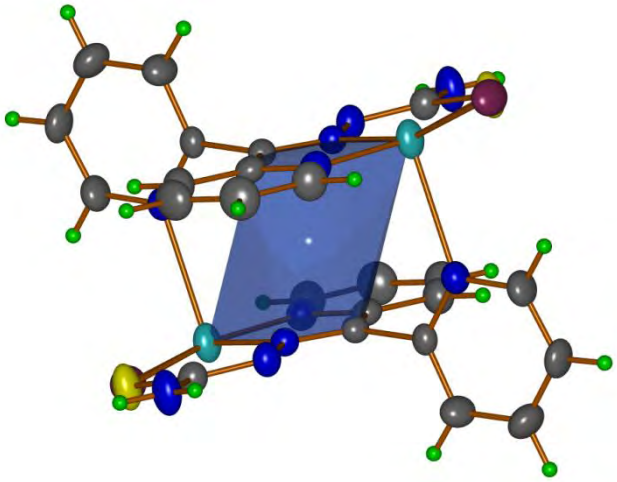

Fig. 7.4. π···π interactions of $[Cu(dpktsc)Br]_2 \cdot CH_3OH$ (**20**).

There is an N–H···π interaction (Fig. 7.5) between the hydrogen attached at N5 atom and one of the pyridyl ring comprising atoms from C7–C11 and N2 of

another molecule and also a lone-pair···π interaction between the Br1 atom and two different chelate rings comprising atoms Cu1, S1, N3, N4 and Cu1, N1, N3, C5, C6.

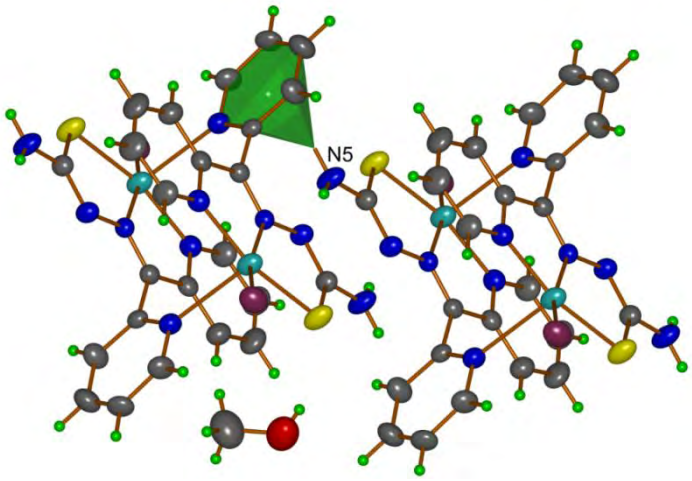

Fig. 7.5. N–H···π interactions of $[Cu(dpktsc)Br]_2 \cdot CH_3OH$ (**20**).

The diverse π···π stacking and N–H···π interactions give rise to polymeric chains in the unit cell. Table 7.6 depicts N–H···π interactions.

Table 7.6. N–H···π interactions of $[Cu(dpktsc)Br]_2 \cdot CH_3OH$

X–H(I)···Cg(J)	H···Cg (Å)	X···Cg (Å)	∠X–H···Cg (°)
N(5)–H(5B)···Cg(4)^c	2.71(4)	3.310(4)	129(3)

The unit cell packing diagram of the complex **20** is given in Fig. 7.6. It can be observed that the molecules are packed in a zig-zag manner.

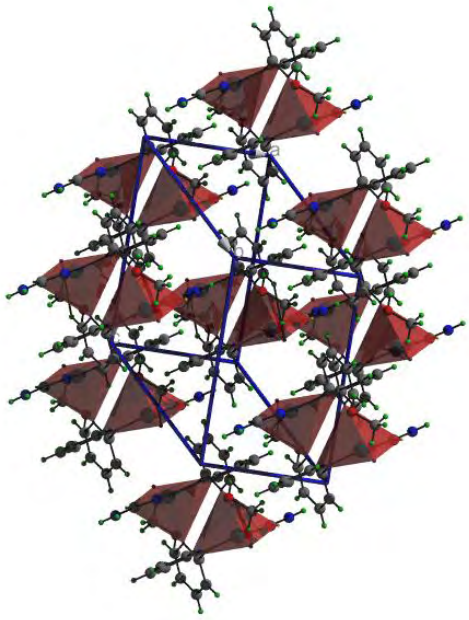

Fig. 7.6. Packing diagram of $[Cu(dpktsc)Br]_2 \cdot CH_3OH$ (**20**).

7.3.2. Crystal structure of complex $[Cu(Hbpsc)Br_2]\cdot H_2O$ (21)

The crystal structure of **21** shows two molecules per asymmetric unit and a disordered water molecule. Intra-molecular bond distances and angles around the metal in $[Cu(Hbpsc)Br_2]\cdot H_2O$ (**21**) are presented in Table 7.7. The copper(II) ion exhibits coordination number five and are attached to a neutral semicarbazone molecule acting as a tridentate ligand through the pyridine and imine nitrogens, and the carbonyl oxygen. Two bromide ions occupy the remaining coordination sites. Directional metal-ligand bonding involving the Cu(II) *d*-orbitals produces an environment around the metal that is better described as a distorted square pyramid with one bromide ion lying close to the semicarbazone ligand plane, hence completing the BrNNO pyramid basis [Cu–Br bond lengths of 2.586(17) and 2.265(2) Å], while the other one is significantly farther from the metal at the pyramid apex [Cu–Br distance of 2.725(18) and 2.275(19) Å]. The Br1–Cu1–Br2 and Br3–Cu2–Br4 bond angles are 103.04(7)^o and 108.27(7)^o. The molecular structure of the complex is as shown in Fig. 7.7. The complex is a distorted square pyramid with one bromide ion lying in the semicarbazone ligand plane completing the BrNNO pyramid base.

Table 7.7. Selected bond lengths [Å] and angles [°] for the two asymmetric units of $[Cu(Hbpsc)Br_2]\cdot H_2O$ (**21**)

Molecule 1		Molecule 2	
Bond lengths (Å)			
Cu1–N1	1.987(9)	Cu2–N5	2.035(8)
Cu1–N2	1.969(8)	Cu2–N6	1.941(8)
Cu1–O1	2.030(7)	Cu2–O2	2.025(7)
Cu1–Br1	2.586(17)	Cu2–Br4	2.725(18)
Cu1–Br2	2.265(2)	Cu2–Br3	2.275(19)
N2–N3	1.355(11)	N6–N7	1.356(11)
O1–C7	1.241(12)	O2–C20	1.249(12)
Bond angles (°)			
N1–Cu1–N2	79.4(3)	N5–Cu2–N6	78.9(3)
O1–Cu1–N2	78.4(3)	O2–Cu2–N6	79.3(3)
Br1–Cu1–Br2	103.04(7)	Br3–Cu2–Br4	108.27(7)
N1–Cu1–Br1	98.9(3)	N5–Cu2–Br3	97.3(2)
N1–Cu1–O1	156.6(3)	N5–Cu2–O2	156.7(3)
N1–Cu1–Br2	97.4(3)	N5–Cu2–Br4	98.7(2)

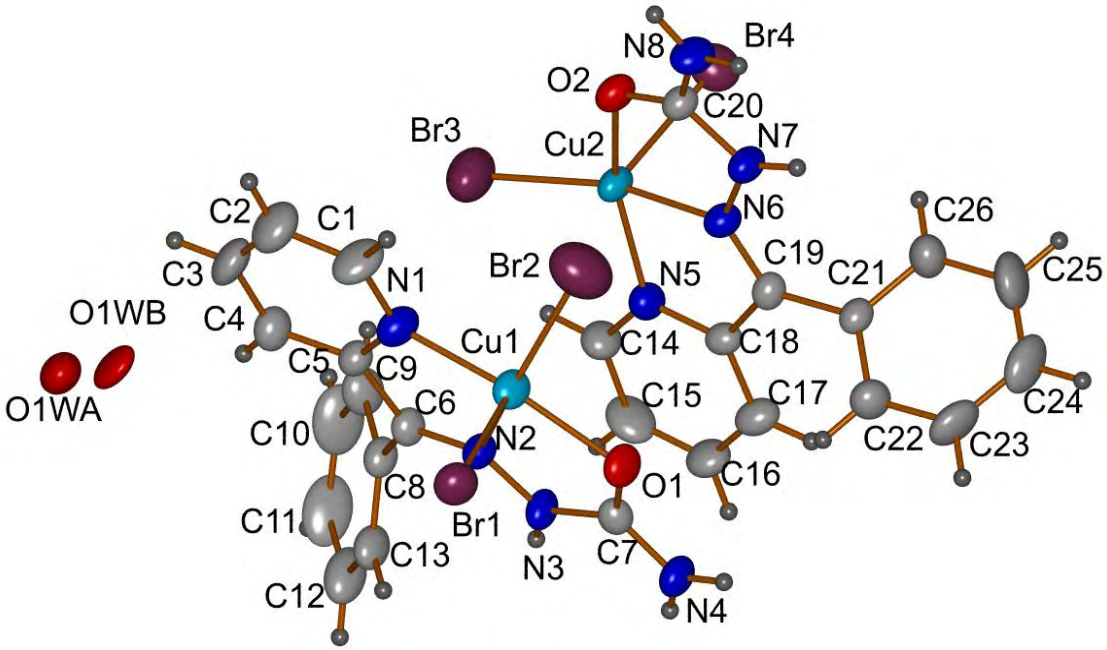

Fig. 7.7. Molecular structure of $[Cu(Hbpsc)Br_2]\cdot H_2O$ (**21**).

The crystal is stabilized by a net of intermolecular N–H···Br and C–H···Br hydrogen bonds. The hydrogen bonding interactions are shown in Table 7.8 and are pictorially represented in Fig. 7.8.

Table 7.8. Hydrogen bonding interactions of $[Cu(Hbpsc)Br_2]\cdot H_2O$ (**21**)

D–H···A	D–H (Å)	H···A (Å)	D···A (Å)	∠D–H···A (°)
N(3)–H(3')···Br(4)^{a}	0.8589	2.5854	3.338(9)	146.89
N(4)–H(4A)···Br(1)^{b}	0.8591	2.6612	3.477(8)	159.01
N(4)–H(4B)···Br(4)^{a}	0.8608	2.6087	3.398(9)	153.03
N(7)–H(7)···Br(2)^{c}	0.8595	2.5264	3.173(8)	132.74
N(8)–H(8A)···Br(1)^{d}	0.8606	2.6086	3.418(10)	157.15
N(8)–H(8B)···O(1)^{c}	0.8600	2.3465	3.079(11)	143.29
C(2)–H(2)···Br(3)^{e}	0.9306	2.7183	3.648(15)	177.01
C(11)–H(11)···Br(4)^{f}	0.9303	2.8307	3.732(14)	163.46
C(14)–H(14)···Br(3)	0.9292	2.8187	3.364(12)	118.62

Equivalent position codes: a = -1+x,y,z ; b = -x,-y,1-z; c = 1-x,-y,1-z;

d = 1+x,y,z ; e= 1-x,1-y,1-z; f= 1-x,1-y,-z

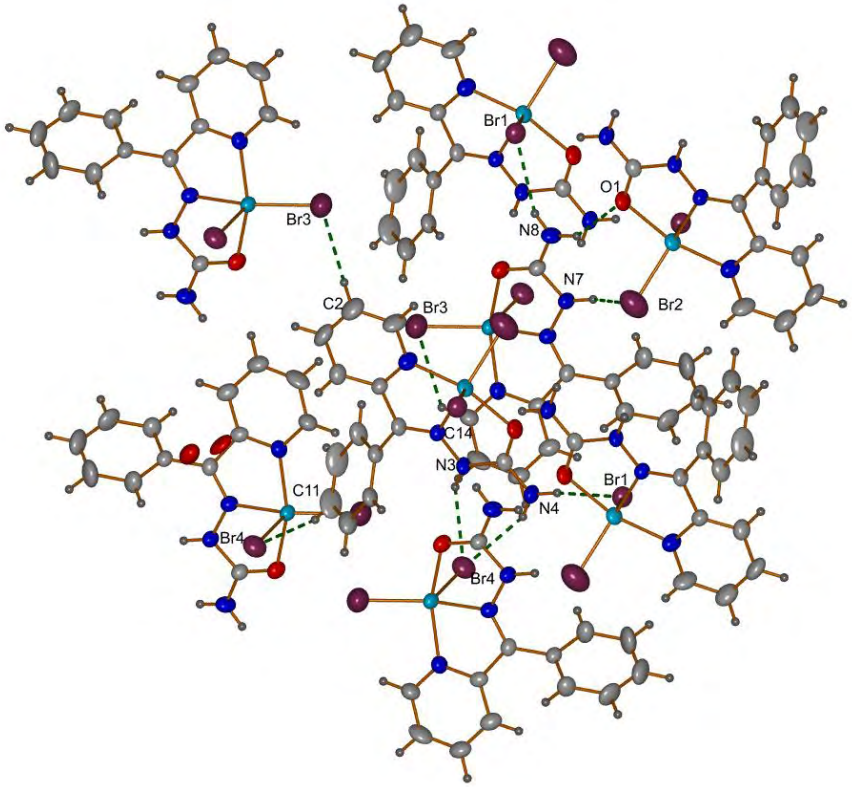

Fig. 7.8. Hydrogen bonding interactions of $[Cu(Hbpsc)Br_2]\cdot H_2O$ (**21**).

The π···π interactions are given in Table 7.9 and shown in Fig. 7.9.

Table 7.9. π···π interactions of $[Cu(Hbpsc)Br_2]\cdot H_2O$ (**21**)

Cg(I)···Cg(J)	Cg···Cg (Å)	α (°)	β (°)	γ(°)
Cg(5)···Cg(12)^g	3.800(6)	14.70	28.18	13.78

Equivalent position codes: g = x,y,z
Cg (5) = Cu1, O1 , C7 , N3, N2; Cg (12) = N5, C14, C15, C16, C17, C18

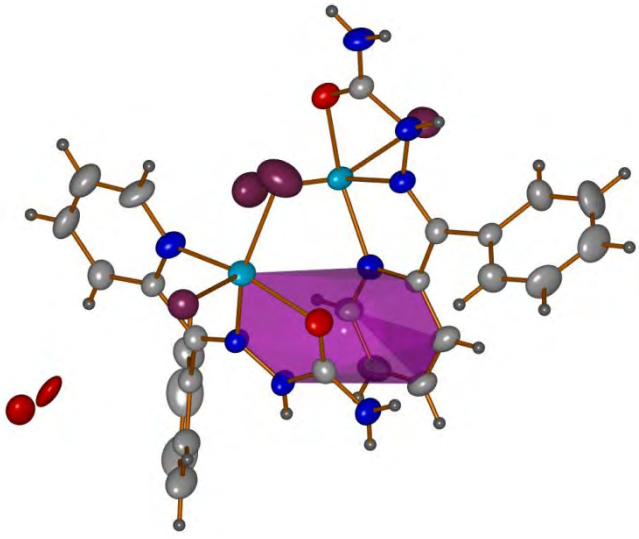

Fig. 7.9. π···π interactions of $[Cu(Hbpsc)Br_2]\cdot H_2O$ (**21**).

Various C–H and N–H···π interactions given in Table 7.10 are shown in Fig. 7.10.

Table 7.10. C–H and N–H···π interactions of $[Cu(Hbpsc)Br_2]\cdot H_2O$ (**21**)

X–H(I)···Cg(J)	H···Cg (Å)	X···Cg (Å)	∠X-H···Cg (°)
N(4)–H(4B)···Cg(7)[a]	3.2554	3.578(10)	105.14
C(16)–H(16)···Cg(14)[h]	3.2584	3.860(13)	124.28

Equivalent position codes: h= 1-x,-y,-z.
Cg (7) = Cu2, O2, C20, N7, N6; Cg (14)= C21, C22, C23, C24, C25, C26

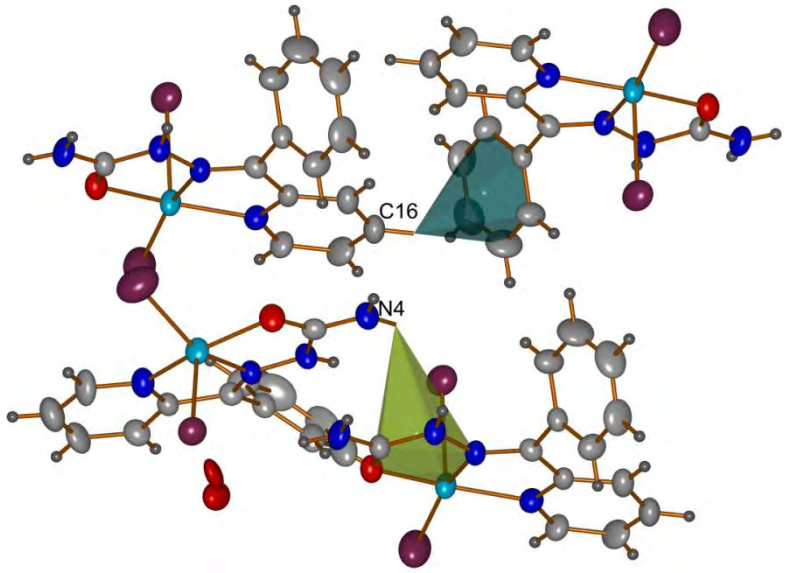

Fig. 7.10. C–H and N–H···π interactions of $[Cu(Hbpsc)Br_2]\cdot H_2O$ (**21**).

The packing diagram of the complex $[Cu(Hbpsc)Br_2]\cdot H_2O$ (**21**) along 'a' and 'b' axes are shown in Figs. 7.11 and 7.12.

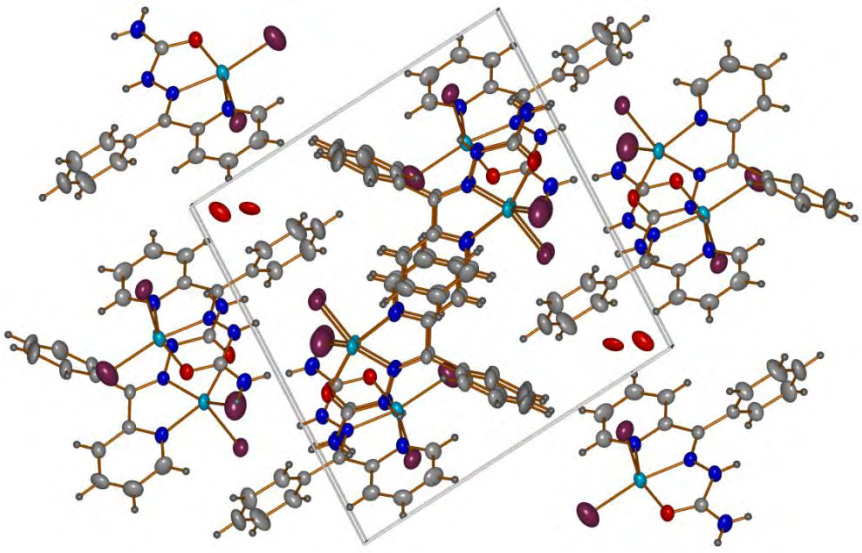

Fig. 7.11. Packing along 'a' axis.

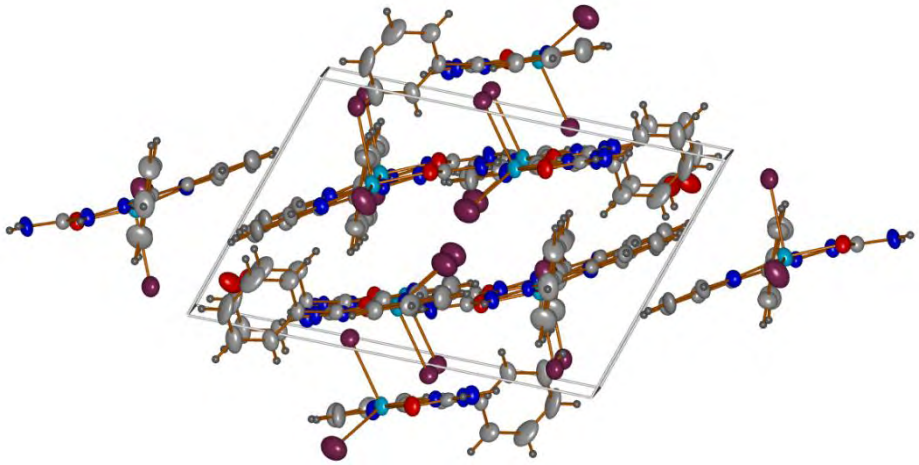

Fig. 7.12. Packing along 'b' axis.

7.3.4. Crystal structure of complex [Cu(bptsc)Br] (22)

This complex has a distorted square planar geometry around each copper(II) ion. The coordinated hydrazinecarbothioamide moiety has *E* configuration with respect to C6–N2. The molecular structure of the complex is shown along with the atom-labeling in Fig. 7.13.

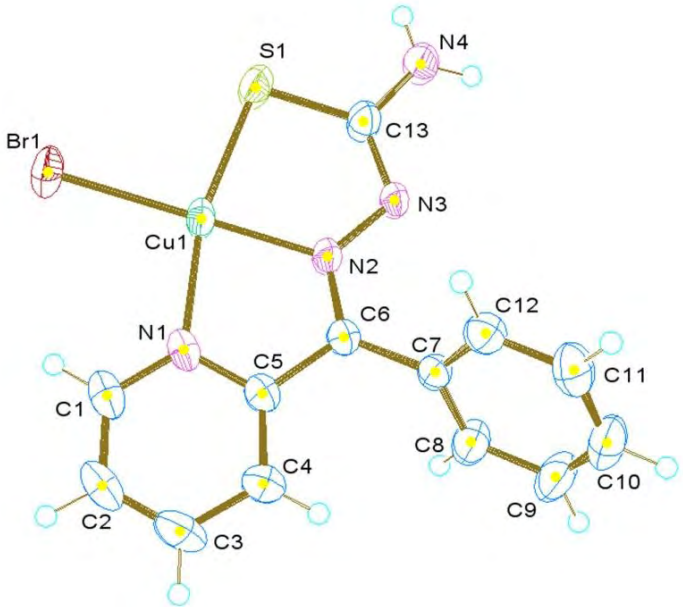

Fig. 7.13. Molecular structure of [Cu(bptsc)Br] (**22**).

The two aromatic rings are twisted with a dihedral angle of 63.79 (17)° between the rings. The hydrazinecarbothioamide moiety and the pyridine ring are almost coplanar with maximum deviation of 0.078(3) Å for the atom C13. C12–S1

bond distance (1.725 (3) Å) is very similar to the formal single bond [17] which suggests that the ligand is coordinating in deprotonated thiolate form. The coplanar nature of the NH_2 group suggests sp^2 character facilitating an extended conjugation over the entire coordination framework [18]. Whilst the intramolecular C1–H1···Br1 hydrogen bonding interactions makes the complex more rigid, the intermolecular N–H···N and C–H···S hydrogen bonding interactions (Table 7.11a) establish an infinite supramolecular 1-D sheet by connecting the adjacent molecules and propagating along 'b' axis as shown in Fig. 7.14.

Table 7.11a. Hydrogen bonding interactions of [Cu(bptsc)Br] (**22**)

D–H···A	D–H (Å)	H···A (Å)	D···A (Å)	∠D–H···A (°)
C1–H1···Br1	0.93	2.88	3.452 (4)	121
C2–H2···S1^{i}	0.93	2.73	3.531 (3)	145
N4–H1B···N3^{ii}	0.83 (2)	2.19 (2)	3.021 (4)	175 (3)
N4–H1A···Cg4^{ii}	0.80 (2)	2.79 (3)	3.256 (4)	118 (2)
C9–H9···Cg1^{iii}	0.93	2.97	3.798 (4)	149

Equivalent position codes: (i) x-1/2, -y+3/2, z+1/2; (ii) -x+2, -y+2, -z+1; (iii) -x+1/2, y+5/2, -z+1/2

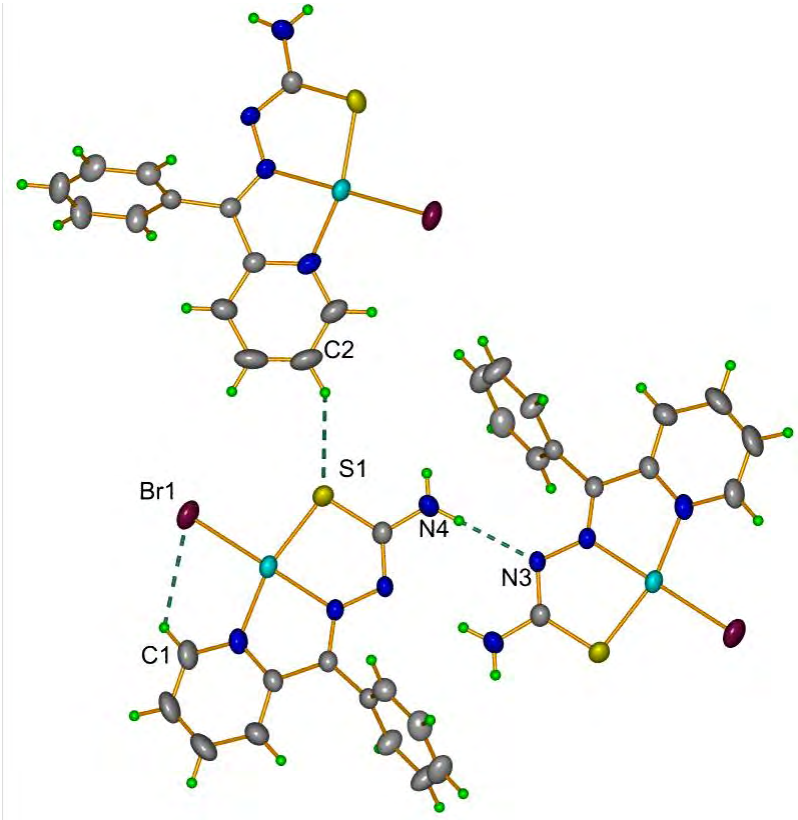

Fig. 7.14. Hydrogen bonding interactions of [Cu(bptsc)Br] (**22**).

The C–H···π and N–H···π interactions (Table 7.11b) link such infinite sheets in various directions accompanied by a weak π···π interaction with centroid-centroid distance of 3.9929 (18) Å (Fig. 7.15).

Table 7.11b. Molecular interactions of [Cu(bptsc)Br] (**22**)

π···π interactions of[Cu(bptsc)Br] (22)

Cg(I)···Cg(J)	Cg···Cg (Å)	α (°)	β (°)	γ (°)
Cg(1)···Cg(3)[a]	3.9929(18)	5.81(14)	20.95	19.90

C–H and N–H···π interactions of [Cu(bptsc)Br] (22)

X–H(I)···Cg(J)	H···Cg (Å)	X···Cg (Å)	∠X-H···Cg (°)
N(4)–H(1A)···Cg(4)[b]	2.80(3)	3.256(4)	118(2)
C(9)–H(9)···Cg(1)[c]	2.97	3.798(4)	149

Equivalent position codes: a = 2-x,y,3/2-z; b = 2-x,2-y,1-z; c = x,2-y,1/2+z

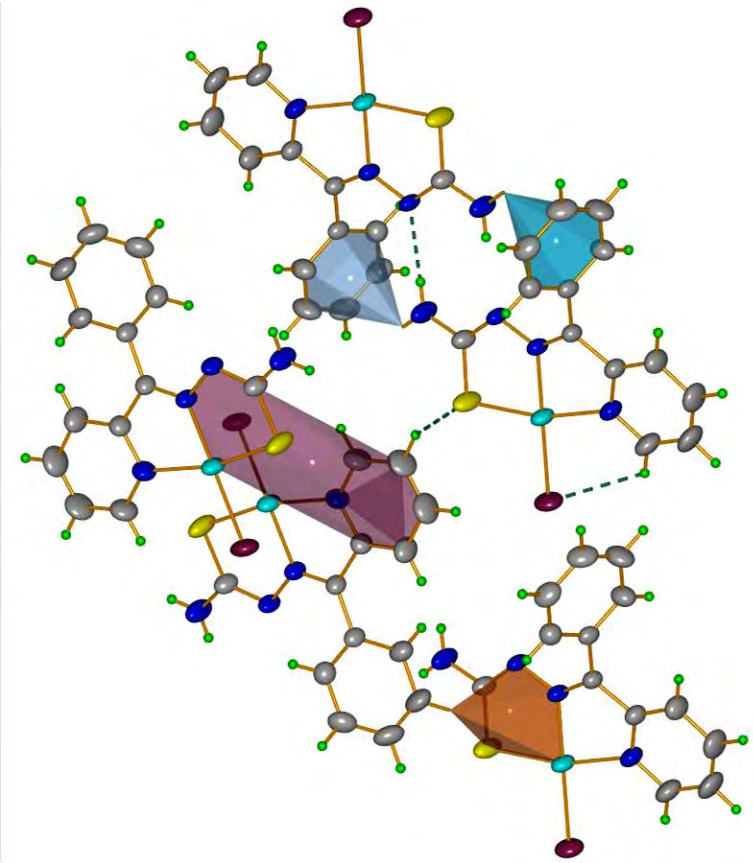

Fig. 7.15. Molecular interactions of [Cu(bptsc)Br] (**22**).

The parallel nature of arrangement of the molecules along 'c' axis is shown in Fig. 7.16.

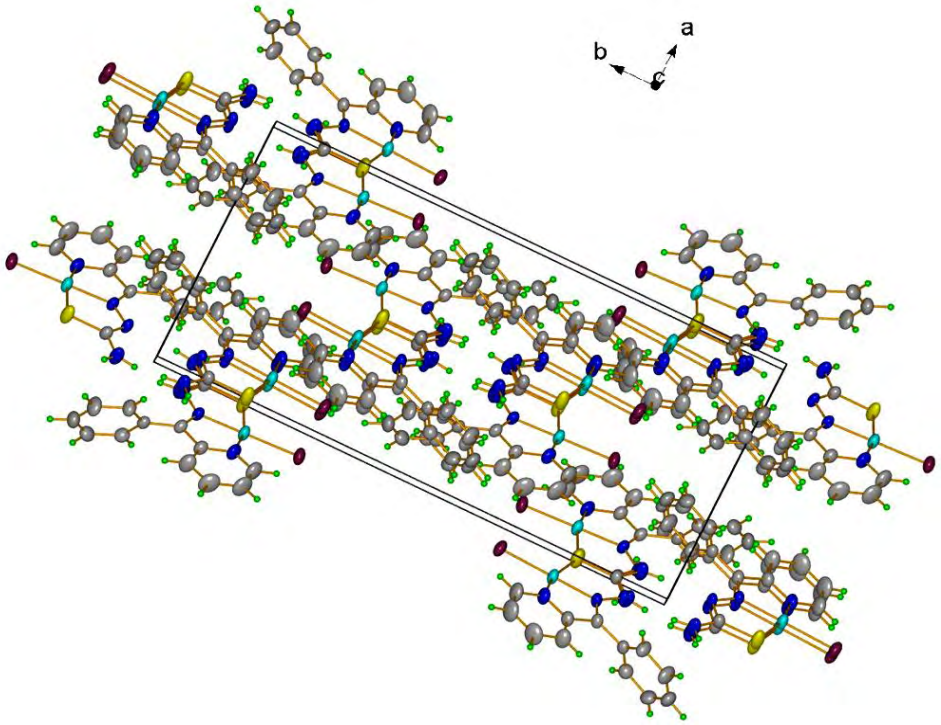

Fig. 7.16. Packing diagram of [Cu(bptsc)Br] (**22**).

7.3.5. Crystal structure of complex [Cu(bpap)Br_2]·H_2O (23)

The complex crystallizes in triclinic space group, $P\bar{1}$. The molecular structure of [Cu(bpap)Br_2]·H_2O (**23**) along with the atom numbering is given in Fig. 7.17. Selected bond lengths and angles are given in Table 7.12. The Cu(II) atom in this complex is *N*,*N*′,*O*-chelated by the neutral Schiff base ligand and has a square-pyramidal geometry.

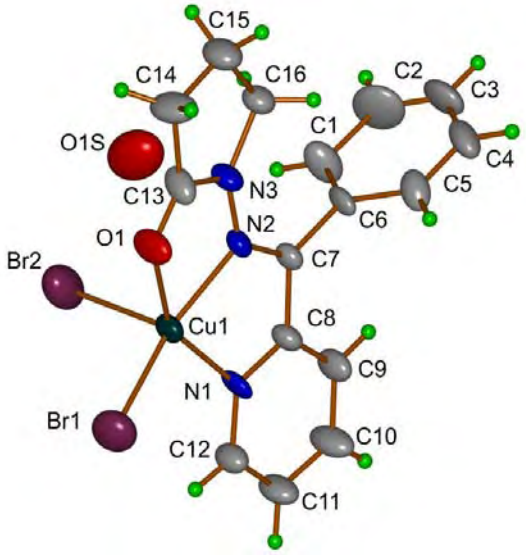

Fig. 7.17. Molecular structure of [Cu(bpap)Br_2]·H_2O (**23**).

Table 7.12. Selected bond lengths [Å] and angles [°] for $[Cu(bpap)Br_2]\cdot H_2O$ (**23**)

Bond lengths (Å)	
Cu1–N2	1.995(6)
Cu1–N1	2.025(7)
Cu1–O1	2.086(6)
Cu1–Br1	2.300(14)
Cu1–Br2	2.527(17)
O1–C13	1.208(11)
N2–N3	1.344(9)
Bond angles (°)	
N2–Cu1–N1	79.2(3)
N2–Cu1–O1	77.7(3)
N1–Cu1–O1	151.6(3)
N2–Cu1–Br1	164.1(2)
N1–Cu1–Br1	100.79(19)
O1–Cu1–Br1	97.02(18)
N2–Cu1–Br2	94.5(2)
N1–Cu1–Br2	100.0(2)
O1–Cu1–Br2	98.0(2)
Br2–Cu1–Br1	101.18(6)

The intermolecular hydrogen bonding interactions (Fig. 7.18) make the molecule more rigid and the two types of C–H···π interactions (Fig. 7.19), mainly involve in the interconnection of the neighboring molecules with H···Cg distances of 3.3071 and 2.8805 Å.

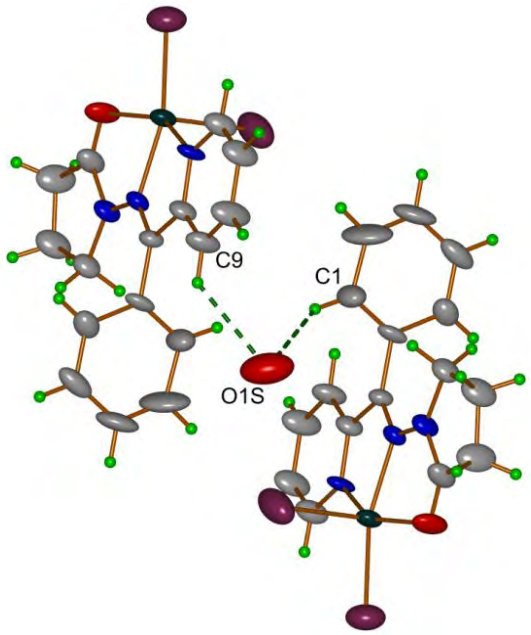

Fig. 7.18. Hydrogen bonding interactions of $[Cu(bpap)Br_2]\cdot H_2O$ (**23**).

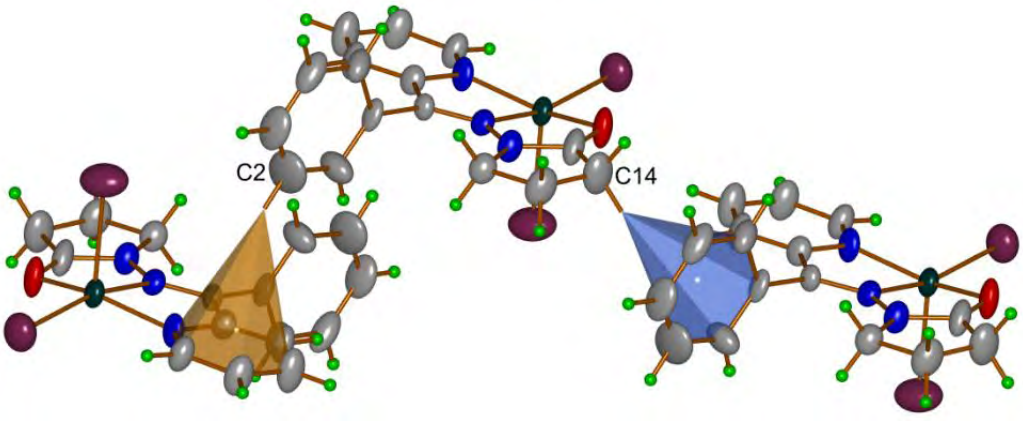

Fig. 7.19. C–H···π interactions of $[Cu(bpap)Br_2]\cdot H_2O$ (**23**).

The hydrogen bonding interactions and C–H···π interactions are shown in Tables 7.13 and 7.14.

Table 7.13. Hydrogen bonding interactions of $[Cu(bpap)Br_2]\cdot H_2O$ (**23**)

D–H···A	D–H (Å)	H···A (Å)	D···A (Å)	∠D–H···A (°)
C(1)–H(1)···O(1S)	0.9301	2.5138	3.306(17)	143.22
C(9)–H(9)···O(1S)^a	0.9302	2.5236	3.237(16)	133.72

Equivalent position codes: a= -x,1-y,1-z

Table 7.14. C–H···π interactions of $[Cu(bpap)Br_2]\cdot H_2O$ (**23**)

X–H(I)···Cg(J)	H···Cg (Å)	X···Cg (Å)	∠X-H···Cg (°)
C(2)–H(2)···Cg(7)^a	3.3071	4.130(17)	148.75
C(14)–H(14A)···Cg(8)^b	2.8805	3.671(13)	139.24

Equivalent position codes: b= 1+x,y,z; Cg (7) = N(1), C(8), C(9), C(10), C(11), C(12); Cg (8) = C(1), C(2), C(3), C(4), C(5), C(6)

The arrangement of the molecules in the unit cell along 'b' and 'c' axes are shown in Figs. 7.20 and 7.21 respectively.

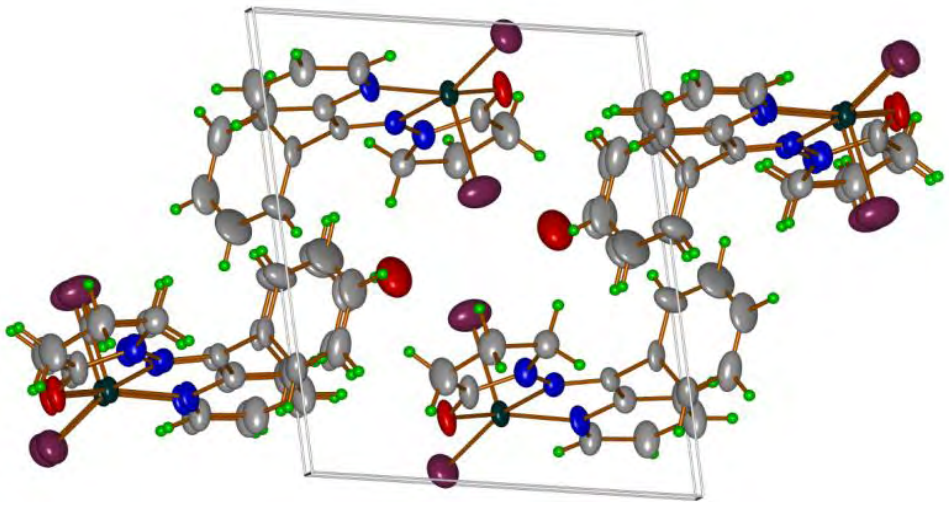

Fig. 7.20. The packing diagram of the molecule along 'b' axis.

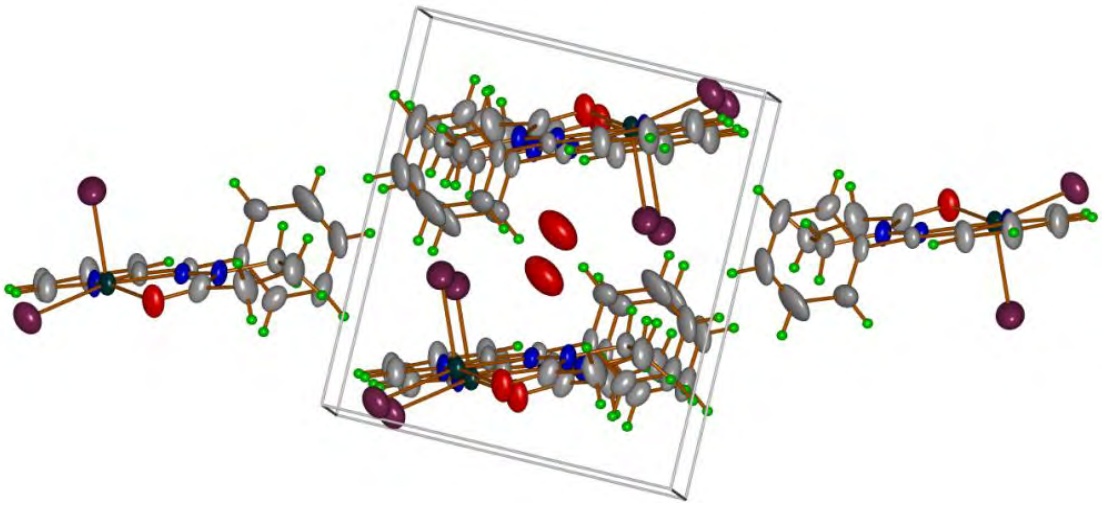

Fig. 7.21. The packing diagram of the molecule along 'c' axis.

7.3.6. Crystal structure of complex [Cu(Hdbssc)Br]·H_2O (24)

This compound crystallizes in the monoclinic space group $P2_1/n$. Fig. 7.22 shows the molecular structure of this complex with atom numbering scheme. The Cu(II) ion is *N,O,O'*-chelated by the deprotonated Schiff base ligand and is further coordinated by a Br^- anion in a distorted BrNOO square-planar geometry. Cu(II) ion in these compound is coordinated by azomethine nitrogen (N1), phenolate oxygen (O1) and amido oxygen (O2). The coordination of the semicarbazone to the Cu atom through amido oxygen is confirmed by the bond length C8–O2 [1.197(16)] Å which is very close to the reported values of semicarbazone complexes. Selected bond lengths and bond angles are shown in Table 7.15.

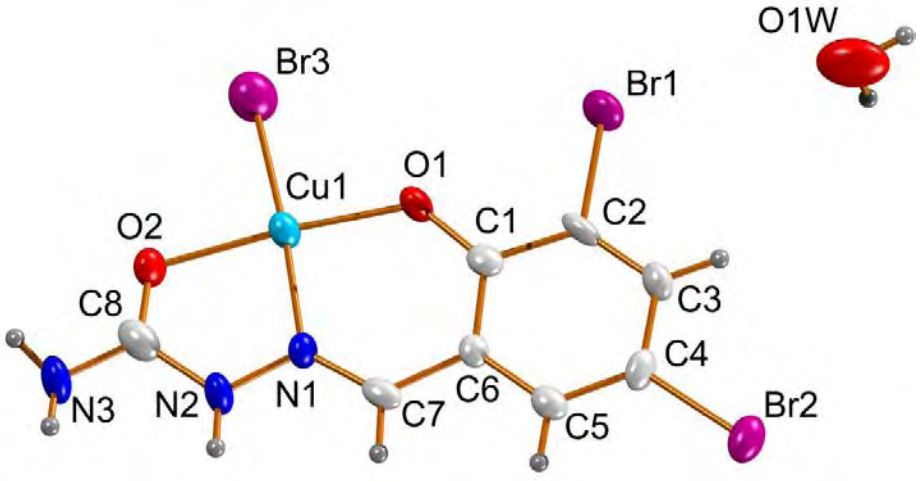

Fig. 7.22. Molecular structure of [Cu(Hdbssc)Br]·H_2O (**24**) along with atom numbering scheme.

Table 7.15. Selected bond lengths [Å] and angles [°] for [Cu(Hdbssc)Br]·H_2O (**24**)

Bond lengths (Å)	
Cu1–O2	1.982(8)
Cu1–N1	1.919(10)
Cu1–O1	1.880(8)
Cu1–Br1	2.328(2)
O2–C8	1.197(16)
N2–N1	1.374(13)
Bond angles (°)	
O1–Cu1–N1	92.0(4)
O2–Cu1–O1	170.7(4)
N1–Cu1–O2	80.5(4)
O2–Cu1–Br1	96.1(2)
N1–Cu1–Br1	172.2(3)
O1–Cu1–Br1	92.0(3)

A supramolecular hydrogen bonding network is established between the molecules as shown in the Fig. 7.23. The intermolecular hydrogen bonding interactions are shown in Table 7.16.

Table 7.16. Hydrogen bonding interactions of [Cu(Hdbssc)Br]·H_2O (**24**)

D–H···A	D–H (Å)	H···A (Å)	D···A (Å)	∠D–H···A (°)
O(1W)–H(1A)···Br(3)^a	0.86(7)	2.57(8)	3.427(15)	172(19)
N(2)–H(2)···O(1W)^b	0.8605	2.0371	2.805(18)	148.08
N(3)–H(3A)···Br(3)^c	0.86(5)	2.91(9)	3.376(12)	116(6)
N(3)–H(3A)···O(1W)^b	0.86(5)	2.34(5)	3.050(18)	140(8)
N(3)–H(3B)···Br(1)^c	0.86(7)	2.82(9)	3.564(13)	145(14)
N(3)–H(3B)···O(1)^c	0.86(7)	2.35(13)	3.090(15)	145(15)
C(3)–H(3)···Br(3)^a	0.9299	2.8865	3.789(12)	164.02
C(5)–H(5)···O(2)^d	0.9297	2.4401	3.352(15)	166.79
C(7)–H(7)···Br(3)^d	0.9294	2.8565	3.372(11)	116.26

Equivalent position codes:a = 3/2-x,1/2+y,3/2-z; c = 5/2-x,-1/2+y,3/2-z ; d = -1/2+x,1/2-y,-1/2+z; z.

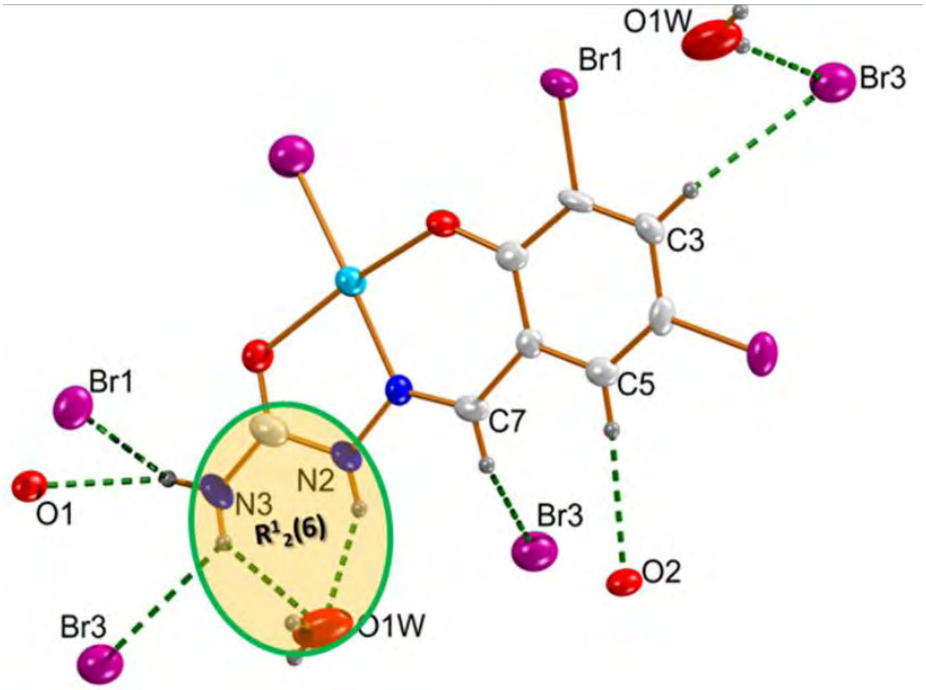

Fig. 7.23. Hydrogen bonding interactions of [Cu(Hdbssc)Br]·H_2O (**24**).

The diverse π···π stacking is present in the molecular arrangement (Fig. 7.24) with Cg···Cg distances shown in Table 7.17.

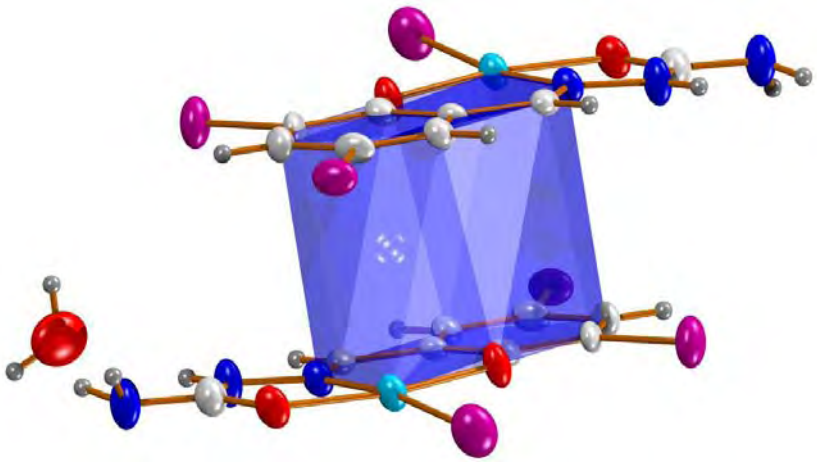

Fig. 7.24. π···π interactions of [Cu(Hdbssc)Br]·H_2O (**24**).

Table 7.17. π···π interactions of [Cu(Hdbssc)Br]·H_2O (**24**)

Cg(I)···Cg(J)	Cg···Cg (Å)	α (°)	β (°)	γ(°)
Cg(4)···Cg(5)[b]	3.591(6)	0.40	25.88	26.13

Equivalent position codes: b = 2-x,1-y,1-z

Cg (4) = Cu(1, O(1), C(1), C(6), C(7), N(1); Cg (5) = C(1), C(2), C(3), C(4), C(5), C(6).

The arrangements of the molecules along 'a' and 'c' axes are shown in Figs. 7.25 and 7.26. The packing of this molecule involves a hydrogen bonding network supported by π···π interactions throughout the entire lattice.

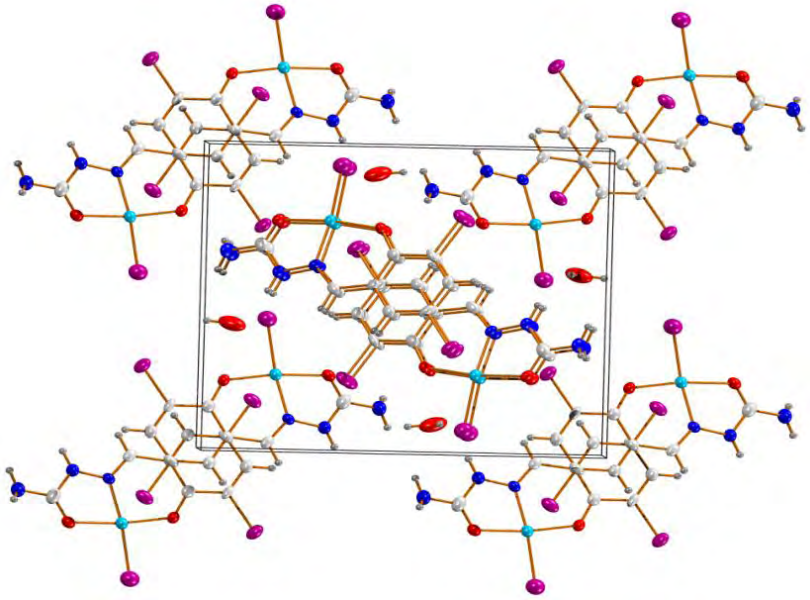

Fig. 7.25. The packing diagram of the molecule along 'a' axis.

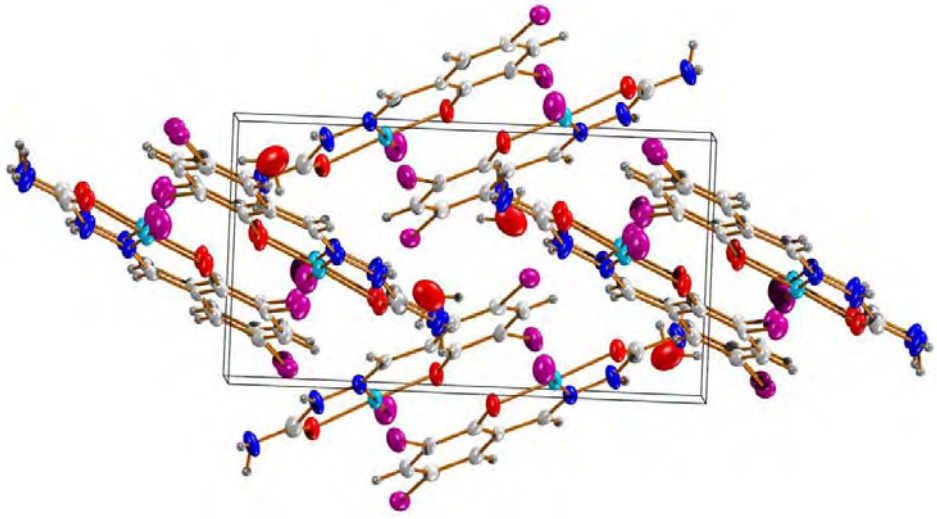

Fig. 7.26. The packing diagram of the molecule along 'c' axis.

7.3.7. Infrared spectral studies

In the infrared spectrum of the semicarbazone complex $[Cu(Hbpsc)Br_2]\cdot H_2O$ (**21**), the absorptions at 1660 cm^{-1} were attributed to the ν(C=O) stretching vibration, which can have contributions of the amide [19]. Similar variations were observed for metal complexes of N(4)-cyclohexylsemicarbazones and thiosemicarbazones derived

from 2-benzoylpyridine [20]. The in-plane deformation mode of the pyridine ring at 652 cm^{-1} in the spectrum of complex is in accordance with complexation of the hetero-aromatic nitrogen. The IR spectra of complexes **20-24** were analyzed and selected vibrational modes summarised in Table 7.18. This vibrational analysis further support the structural details unveiled by the single-crystal X-ray diffraction analysis. The strong ν(C=N) bands of semicarbazone around 1590 cm^{-1}, suggesting the coordination *via* the azomethine nitrogen [10]. The IR spectra of these complexes are shown in Figs. 7.27- 7.31.

Table 7.18. IR spectral data of the Cu(II) bromide complexes (cm^{-1})

Compound	ν(C=N)	ν(C=N)[a]	ν(N–N)	ν(C–O)	ν(C=O)	ν(C=S)
$[Cu(dpktsc)Br]_2 \cdot CH_3OH$ (**20**)	1623	1595	1151	-	-	1322
$[Cu(Hbpsc)Br_2] \cdot H_2O$ (**21**)	1590	1456	1141	-	1660	
[Cu(bptsc)Br] (**22**)	1647	1540	1160	1225		-
$[Cu(bpap)Br_2] \cdot H_2O$ (**23**)	1531	1498	1109	1230	1611	-
[Cu(Hdbssc)Br] (**24**)	1539	1424	1160	-	1650	-

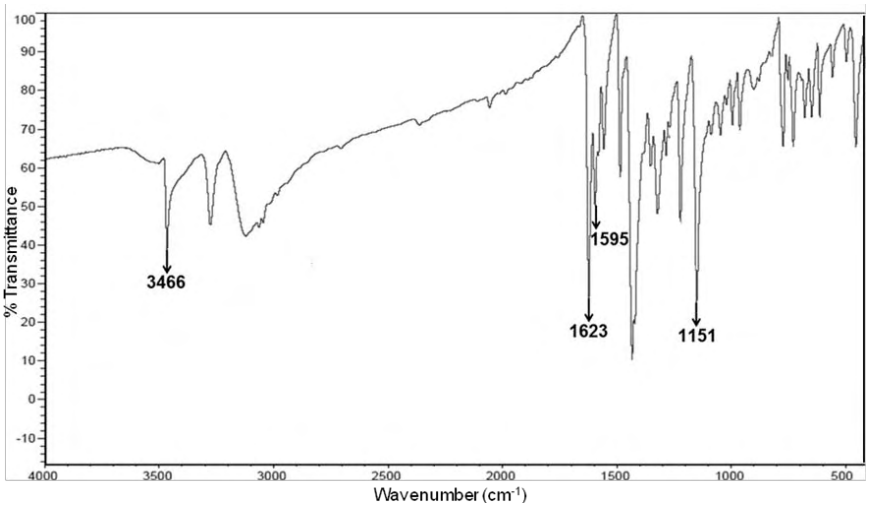

Fig. 7.27. IR spectrum of $[Cu(dpktsc)Br]_2 \cdot CH_3OH$ (**20**).

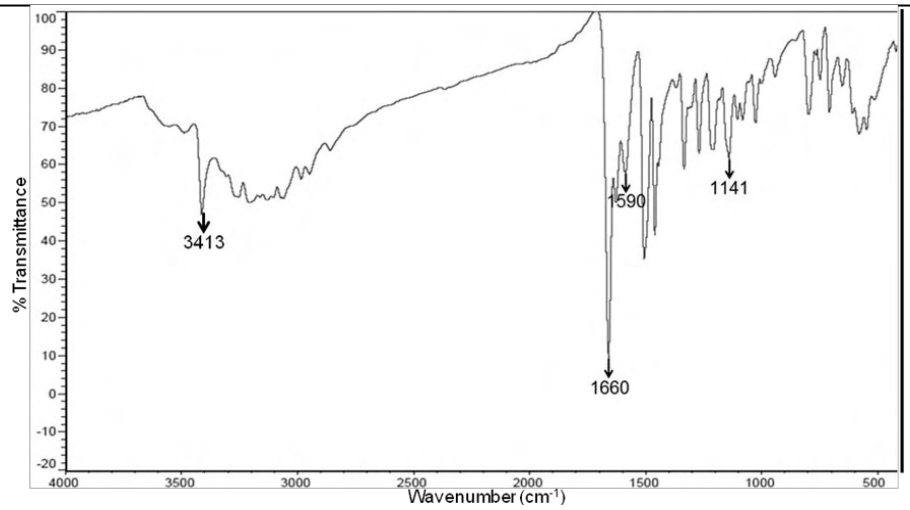

Fig. 7.28. IR spectrum of $[Cu(Hbpsc)Br_2]\cdot H_2O$ (**21**).

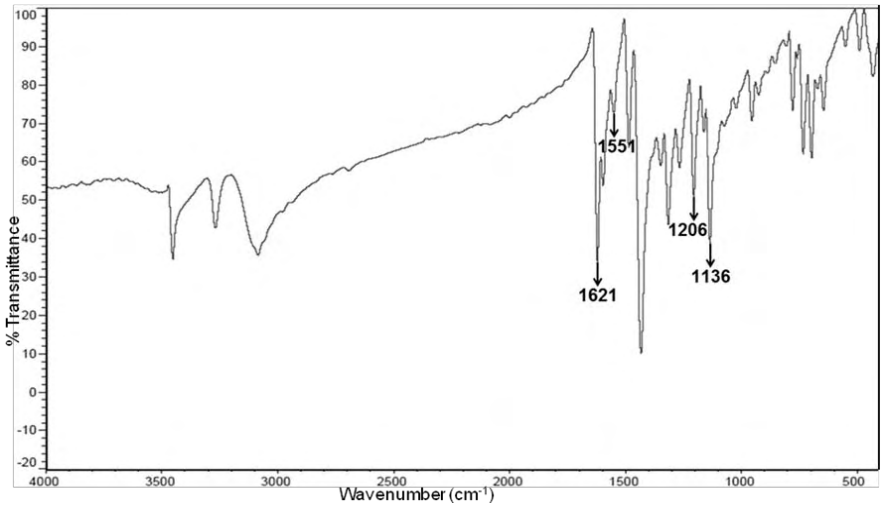

Fig. 7.29. IR spectrum of [Cu(bptsc)Br] (**22**).

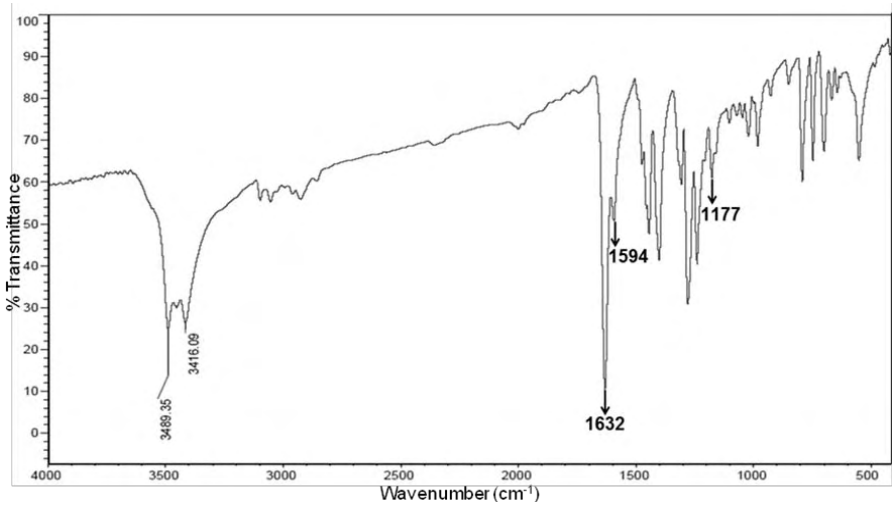

Fig. 7.30. IR spectrum of $[Cu(bpap)Br_2]\cdot H_2O$ (**23**).

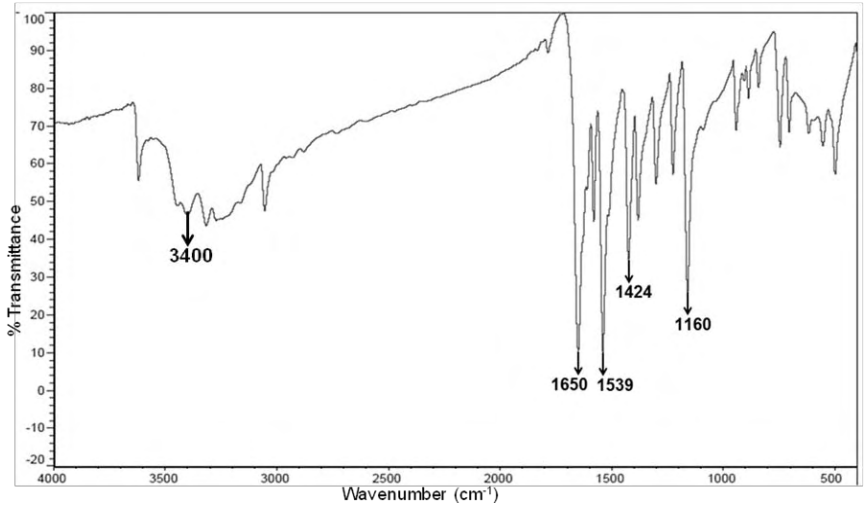

Fig. 7.31. IR spectrum of [Cu(Hdbssc)Br] (**24**).

7.3.8. Electronic spectral studies

A high energy $\pi \rightarrow \pi^*$ transition observed at ca. 43,250 cm^{-1} in the electronic spectrum of $[Cu(Hbpsc)Br_2]\cdot H_2O$ (**21**) is not significantly altered by complexation. The $n\rightarrow \pi^*$ transitions associated to the azomethine and carbonyl functions are overlapped at 31530 cm^{-1} in the spectrum of complex **21** [21]. The N→Cu(II) and O→ Cu(II) ligand-to-metal charge transfer transition bands are probably underneath the absorption at 25,930 cm^{-1} in the spectrum of complex **21**. Also, in the spectrum of complex **21** a large absorption at 12,970 cm^{-1} was attributed to a combination of *d-d* bands. The electronic spectral data of copper(II) complexes recorded in methanol solution are given in Table 7.19.

Table 7.19. Electronic spectral assignments (cm^{-1}) for copper(II) bromide complexes

Compound	*d-d*	LMCT	$n\rightarrow\pi^*/\pi\rightarrow\pi^*$
$[Cu(dpktsc)Br]_2\cdot CH_3OH$ (**20**)	16560	23890	33520, 39940, 46120
$[Cu(Hbpsc)Br_2]\cdot H_2O$ (**21**)	12970	25930	31530, 43250, 47360
[Cu(bptsc)Br] (**22**)	16670	24300	33620, 46940
$[Cu(bpap)Br_2]\cdot H_2O$ (**23**)	12440	27450	36020, 38150, 43500, 47410
$[Cu(Hdbssc)Br]\cdot H_2O$ (**24**)	14160	13370	25760, 33440, 38720, 43930,

The electronic spectra are shown in the Figs. 7.32-7.36. Bands in the region 28770-32200 cm^{-1} correspond to n-π^* transitions of the amide function [22].

The high intense ligand-to-metal charge transfer (LMCT) transitions are observed at high energy region. The intensity of these transitions reflects the overlap of the ligand and metal orbitals involved in the charge transfer. In all the complexes

20-24, LMCT transitions are observed in the region 22100-24050 cm^{-1} and which are assigned to O→ Cu and N→ Cu LMCT transitions. It is difficult to resolve them into separate bands due to the very low energy difference between these bands. All copper(II) complexes **20-24** have very broad *d-d* combination bands (Figs. 7.32-7.36) in the 14000-16000 cm^{-1} range [23,24].

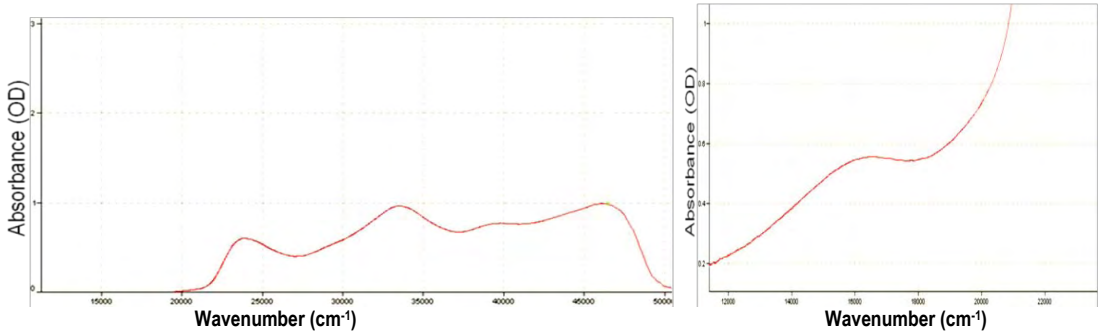

Fig. 7.32. Electronic spectra of complex $[Cu(dpktsc)Br]_2 \cdot CH_3OH$ (**20**).

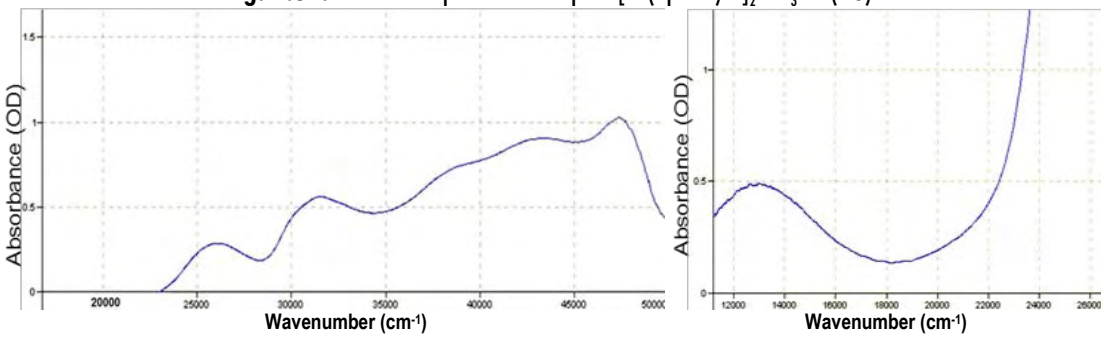

Fig. 7.33. Electronic spectra of complex $[Cu(Hbpsc)Br_2] \cdot H_2O$ (**21**).

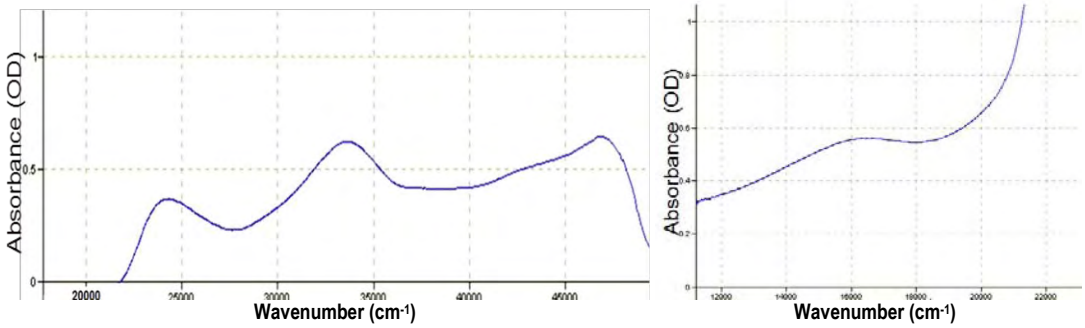

Fig. 7.34. Electronic spectra of complex [Cu(bptsc)Br] (**22**).

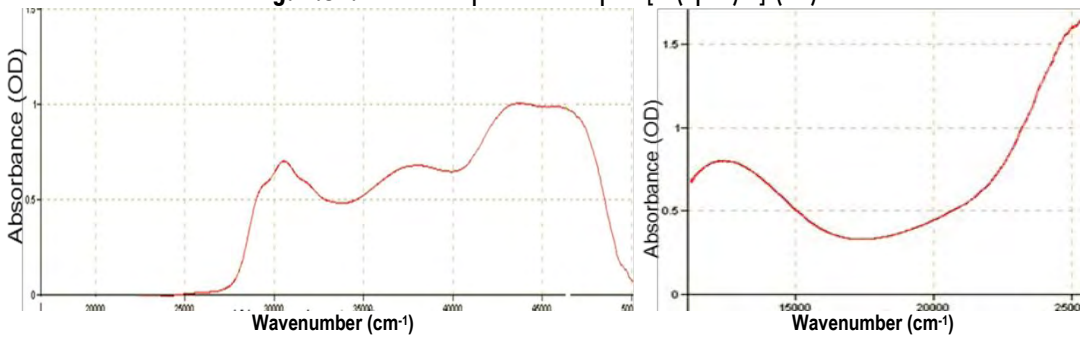

Fig. 7.35. Electronic spectra of complex $[Cu(Hdbssc)Br] \cdot H_2O$ (**24**).

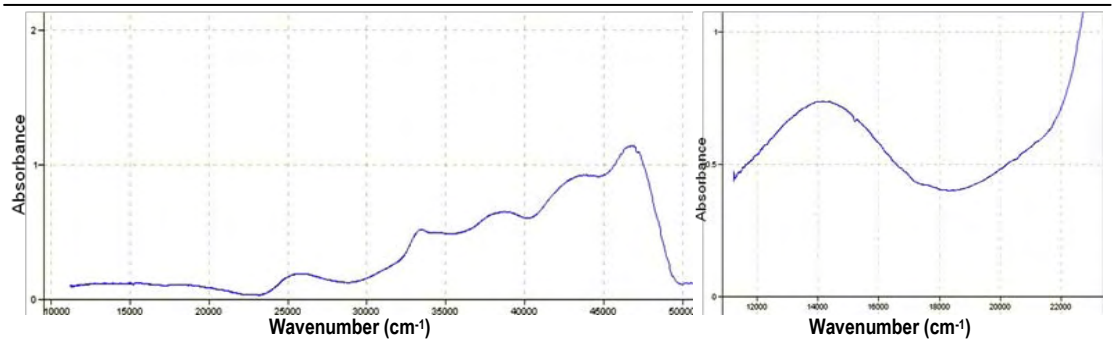

Fig. 7.36. Electronic spectra of complex $[Cu(Hdbssc)Br]\cdot H_2O$ (**24**).

7.3.9. EPR spectral studies

The EPR spectra for the complexes recorded at room temperature and liquid nitrogen temperature are as shown in Figs. 7.37 - 7.41.

For the compounds **20**, **21, 22** and **24** we got axial spectra with well defined $g_{\|}$ and $g_{\perp}$ features. The variations of $g_{\|}$ and $g_{\perp}$ values in these complexes indicate that the geometry of the compounds in the solid state is affected by the nature of the coordinating ligands. The geometric parameter G is calculated as $G = g_{\|}\text{-}2.0023/g_{\perp}\text{-}2.0023$ for axial spectra and it is a measure of exchange interaction between copper centers in the polycrystalline compound. If $G > 4.4$, exchange interaction is negligible and if it is less than 4.4, considerable exchange interaction is indicated in the solid complex [25]. The geometric parameter G for the compounds **21**, **22** and **23,** are 3.258, 2.448 and 2.441 respectively, which indicate the fact that the unit cells of the compounds contain magnetically equivalent sites. For the complexes **21**, **22** and **23**, $g_{\|} > g_{\perp} > 2$ and G values falling in the range 2-4 are consistent with a $d_{x^2-y^2}$ ground state. The solution spectra of all complexes were recorded in DMF at 77 K. It is observed that g values of this complex in the solid state at 298 K and in DMF at 77 K are not much different from each other hence the geometry around the Cu(II) ion is unaffected on cooling the solution to liquid nitrogen temperature. As $g_{\|} > g_{\perp}$, the possibility of trigonal bipyramidal geometry has been ruled out and square pyramidal structure is suggested. For the bromo complex **20,** we got a rhombic spectrum (Fig. 7.37). In the copper bromo complexes **21**, **22**, **23** and **24,** expected super hyperfine splitting due to nitrogen atoms are missing.

The spin Hamiltonian and bonding parameters of the complexes are given in Table 7.20.

Table 7.20. Spin Hamiltonian and bonding parameters of the complexes

	$[Cu(Hbpsc)Br_2]\cdot H_2O$ (**21**)	[Cu(bptsc)Br] (**22**)	$[Cu(bpap)Br_2]\cdot H_2O$ (**23**)	$[Cu(Hdbssc)Br]\cdot H_2O$ (**24**)
	Polycrystalline state at 298 K			
$g_{\|\|}$	2.243	2.097	2.219	-
$g_{\perp}$	2.087	2.041	2.128	-
g_{isc}/g_{rv}	2.139	2.060	2.158	2.127
G	2.842	2.447	1.724	-
	Solution state at 77 K			
$g_{\|\|}$	2.241	2.116	2.324	2.196
$g_{\perp}$	2.070	2.042	2.078	2.047
$A_{\|\|}$	19.660	4.160	10.028	20
α^2	0.878	0.284	0.696	0.8218
β^2	0.778	1.882	1.192	0.7832
γ^2	0.829	2.225	1.157	0.7524
$K_{\|\|}$	0.684	0.535	0.830	0.6436
$K_{\perp}$	0.728	0.632	0.805	0.6183

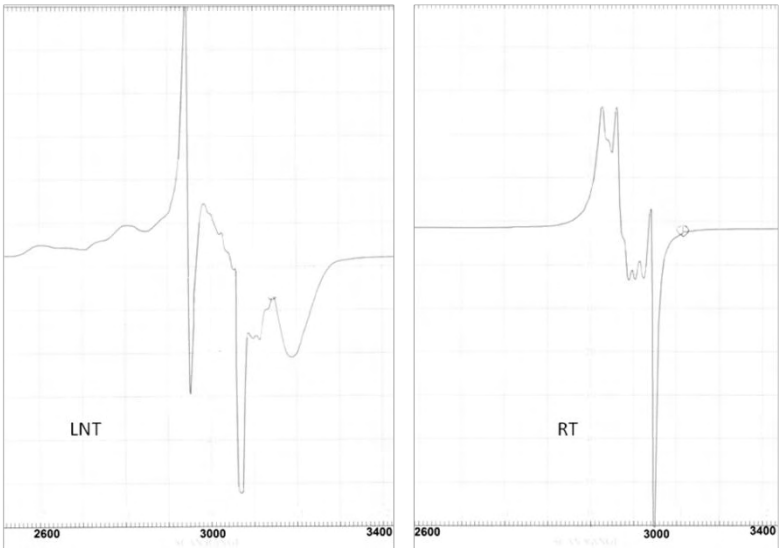

Fig. 7.37. EPR spectra of complex $[Cu(dpktsc)Br]_2\cdot CH_3OH$ (**20**).

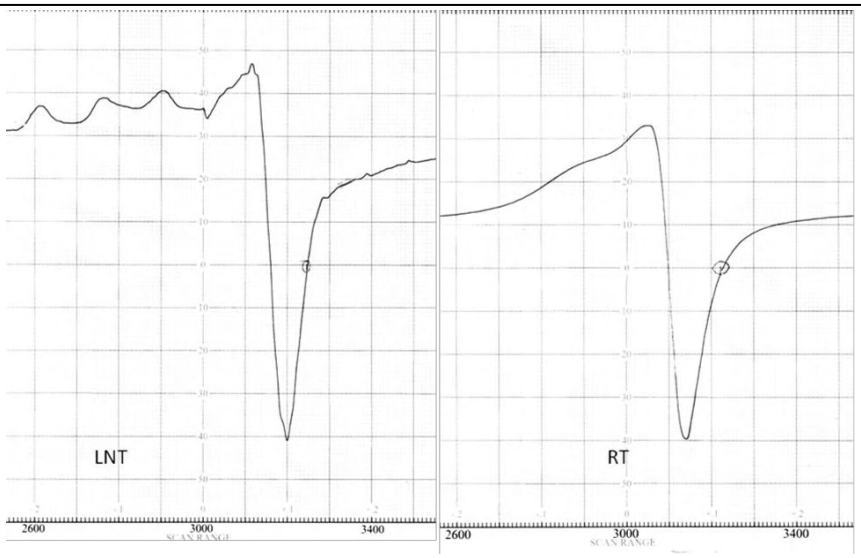

Fig. 7.38. EPR spectra of complex $[Cu(Hbpsc)Br_2]\cdot H_2O$ (**21**).

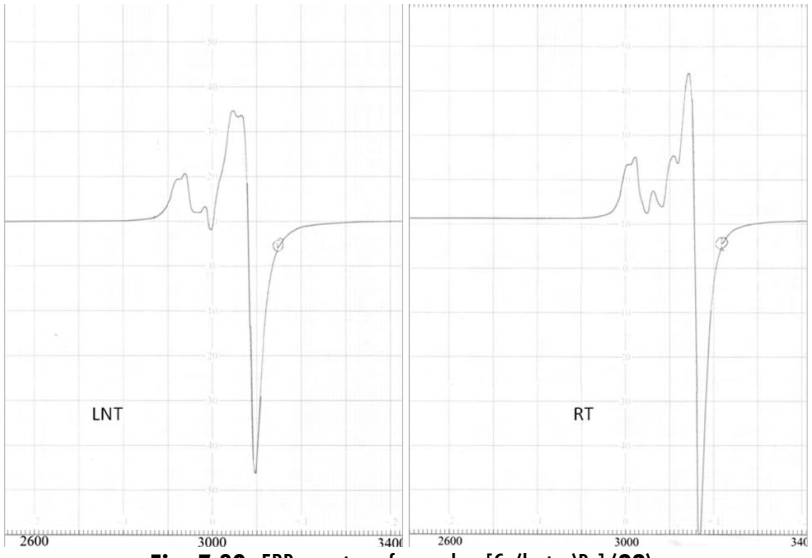

Fig. 7.39. EPR spectra of complex [Cu(bptsc)Br] (**22**).

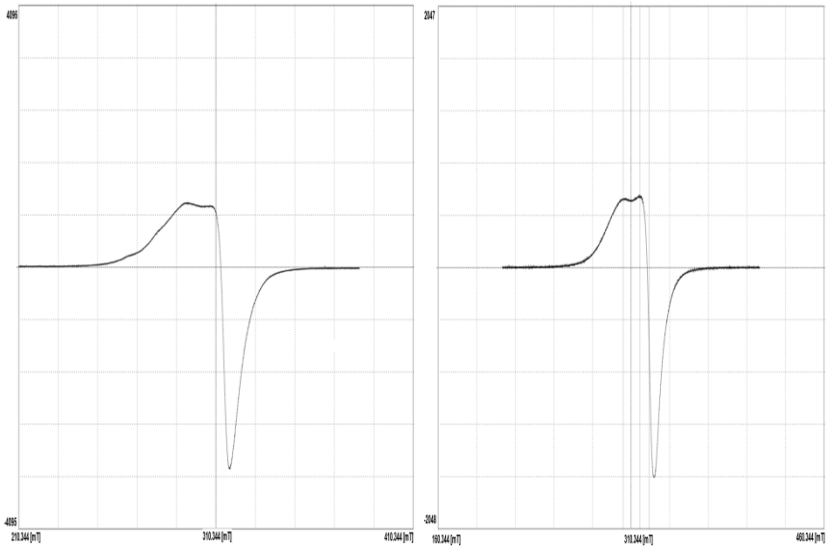

Fig. 7.40. EPR spectra of complex $[Cu(bpap)Br_2]\cdot H_2O$ (**23**).

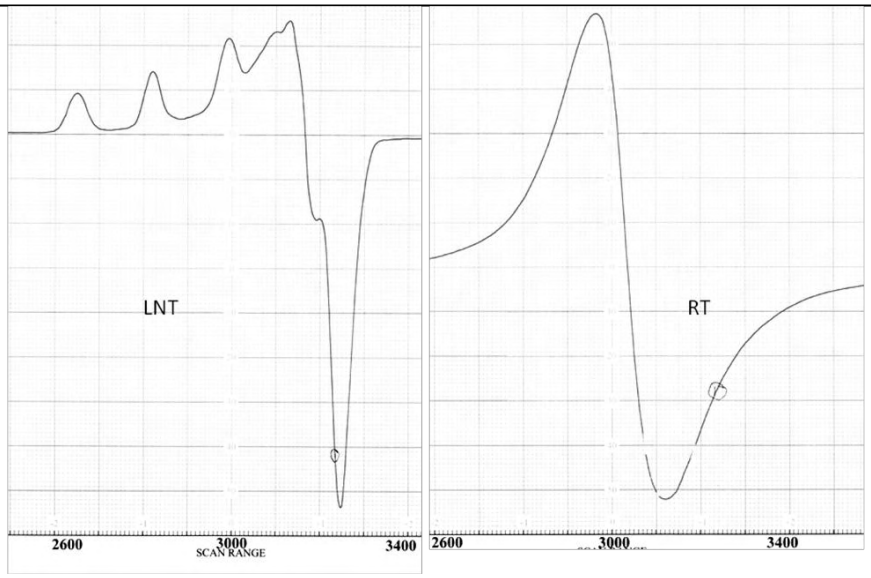

Fig. 7.41. EPR spectra of complex [Cu(Hdbssc)Br]·H_2O (**24**).

REFERENCES

1. M. Choi, N. Sukumar, A. Liu, V.L. Davidson, Biochemistry, 2009, 48, 9174.
2. C. Castelle, M. Ilbert, P. Infossi, G. Leroy, M.-T. Giudici-Orticoni, J. Biol. Chem., 2010, 285, 21519.
3. S. Tabassum, W.M. Al-Asbahy, M. Afzal, F. Arjmanda, V. Bagchib, Dalton Trans., 2012, 41, 4955.
4. R. Novotna, R. Herchel, Z. Travnic¡ek, Polyhedron, 2012, 34, 56.
5. S. Dhar, D. Senapati, P.K. Das, P. Chattopadhyay, M. Nethaji, A.R. Chakravarty, J. Am. Chem. Soc., 2003, 125, 12118.
6. (a) M.S. Ray, S. Chattopadhyay, M.G.B. Drew, A. Figuerola, J. Ribas, C. Diaz, A. Ghosh, Eur. J. Inorg. Chem., 2005, 4562. (b) P.K. Bhowmik, S. Chattopadhyay, Inorg. Chem. Commun., 2012, 22, 14.(c) A. Biswas, L.K. Das, M.G.B. Drew, C. Diaz, A. Ghosh, Inorg. Chem., 2012, 51, 10111. (d) A. Biswas, M.G.B. Drew, J. Ribas, C. Diaz, A. Ghosh, Inorg. Chim. Acta, 2011, 379, 28. (e) S. Naiya, S. Biswas, M.G.B. Drew, C.J. Gómez-García, A. Ghosh, Inorg. Chim. Acta, 2011, 377, 26. (f) A. Biswas, M.G.B. Drew, Y. Song, A. Ghosh, Inorg. Chim. Acta, 2011, 376, 422.
7. (a) A.P. Sadimenko, A.R. Katritzky (Ed.), Organometallic Complexes of Pyridyl Schiff Bases, Advances in Heterocyclic Chemistry, Academic Press, 2012, 107, 133. (b) Y.E. Alexeev, B.I. Kharisov, T.C.H. Garcia, A.D. Arnovskii, Coord.

Chem. Rev., 2010, 254, 794. (c) A.D. Garnovskii, I.S. Vasil'chenko, D.A. Garnovskii, A.S. Burlov, A.I. Uraev, Russ. J. Gen. Chem., 2009, 79, 2776. (d) A.D. Garnovskii, I.S. Vasilchenko, D.A. Garnovskii, B.I. Kharisov, J. Coord. Chem., 2009, 62, 151. (e) H. Miyasaka, A. Saitoh, S. Abe, Coord. Chem. Rev., 2007, 251, 2622. (f) W. Radecka-Paryzek, V. Patroniak, J. Lisowski, Coord. Chem. Rev., 2005, 249, 2156. (g) S. Nayak, P. Gamez, B. Kozlevcar, A. Pevec, O. Roubeau, S. Dehnen, J. Reedijk, Polyhedron, 2010, 29, 2291. (h) G.G. Mohamed, M.A. Zayed, S.M. Abdallah, J. Mol. Struct., 2010, 979, 62. (i) S. Chattopadhyay, M.G.B. Drew, A. Ghosh, Polyhedron, 2007, 26, 3513.

8. T.A. Reena, E.B. Seena, M.R.P. Kurup, Polyhedron, 2008, 27, 1825.
9. (a) S. Chandra, A. Kumar, Spectrochim. Acta, Part A, 2007, 68, 1410. (b) P.F. Rapheal, E. Manoj, M.R.P. Kurup, Polyhedron, 2007, 26, 5088. (c) S. Basak, S. Sen, S. Banerjee, S. Mitra, G. Rosair, M.T.G. Rodriguez, Polyhedron, 2007, 26, 5104.(d) M.C. Rodriguez-Arguelles, S. Mosquera-Vazquez, J. Sanmartin-Matalobos, A.M. Garcia-Deibe, C. Pelizzi, F. Zani, Polyhedron, 2010, 29, 864. (e) P.E. Aranha, M.P. dos Santos, S. Romera, E.R. Dockal, Polyhedron, 2007, 26, 1373. (f) V. Philip, V. Suni, M.R.P. Kurup, M. Nethaji, Polyhedron, 2004, 23, 1225.
10. N.C. Kasuga, K. Sekino, M. Ishikawa, A. Honda, M. Yokoyama, S. Nakano, N. Shimada, C. Koumo, K. Nomiya, J. Inorg. Biochem., 2003, 96, 298. (b) N.C. Kasuga, K. Onodera, S. Nakano, K. Hayashi, K. Nomiya, J. Inorg. Biochem., 2006, 100, 1176. (c) K. Rathore, R.K.R. Singh, H.B. Singh, J. Chem., 2010, 7, S566.
11. SMART and SAINT, Area Detector Software Package and SAX Area Detector Integration Program, Bruker Analytical X-ray; Madison, WI, USA, 1997.
12. SADABS, Area Detector Absorption Correction Program; Bruker Analytical X-ray; Madison, WI, 1997.
13. L.J. Farrugia, J. Appl. Cryst., 2012, 45, 849.
14. K. Brandenburg, Diamond Version 3.2g, Crystal Impact GbR, Bonn, Germany, 2010.

15. E.W. Ainscough, A.M. Brodie, J.D. Ranford, J.M. Waters, J. Chem. Soc. Dalton Trans., 1991, 1737.
16. V. Philip, V. Suni, M.R.P. Kurup, M. Nethaji, Polyhedron, 2005, 24, 1133.
17. C.-Y. Duan, B.-M. Wu, T. C. W. Mak, J. Chem. Soc., Dalton Trans., 1996, 3485.
18. R.J. Kunnath, M. Sithambaresan, M.R.P. Kurup, A. Natarajan, A.A. Aravindakshan, Acta Cryst., 2012, E68, m346.
19. (a) V.M. Kolb, J.W. Stupar, T.E. Janota, W.L. Duax, J. Org. Chem., 1989, 54, 2341. (b) H. Beraldo, R.D. Sinisterra, L.R. Teixeira, R.P. Vieira, M.C. Doretto, Biochem. Biophys. Res. Commun., 2002, 206, 241. (c) H. Beraldo, W. Nacif, D.X. West, Spectrochim. Acta, Part A, 2001, 57, 1847.
20. D.X. West, I.S. Billeh, J.P. Jasinski, J.M. Jasinski, R.J. Butcher, Transit. Met. Chem., 1998, 23, 209.
21. D.X. West, J.S. Ives, J. Krejci, M. Salberg, T.L. Zumbahlen, G. Bain, A. Liberta, J.V. Martinez, S.H. Ortiz, R. Toscano, Polyhedron, 1995, 14, 2189.
22. C.R.K. Rao, P.S. Zacharias, Polyhedron, 1997, 16, 1201.
23. R.P. John, A. Sreekanth, V. Rajakannan, T.A. Ajith, M.R.P. Kurup, Polyhedron, 2004, 23, 2549.
24. M. Joseph, M. Kuriakose, M.R.P. Kurup, E. Suresh, A. Kishore, G. Bhat, Polyhedron, 2006, 25, 61.
25. (a) I.M. Proctor, B.J. Hathaway, P. Nicholis, J. Chem. Soc. A, 1968, 1678. (b) S. K. Jain, B.S. Garg, Y.K. Bhoon, Spectrochim. Acta, Part A, 1986, 42, 959. (c) B.J. Hathaway, D.E. Billing, Coord. Chem. Rev., 1970, 5, 1949.

Summary and conclusion

Schiff base complexes of copper(II) are well known for the variety of the structures formed and associated magnetic properties as well as catalytic applications. Halides (Cl^-, Br^-) and pseudohalides (N_3^-, OCN^-, SCN^-, $N(CN)_2^-$ etc. are the versatile ligands which can coordinate to transition metal ions in different ways, for example as a bridging or as a terminal ligand.

Complexes with various interesting topologies have been synthesized by one-pot method using appropriate molar ratios of metal ions, organic ligands and pseudohalide ions. Pseudohalides are highly versatile ambidentate ligands with a polarizable π system and two different donor atoms, which can coordinate to metals through either the nitrogen or the S atom or both. Different bridging modes of the pseudohalide ligand can generate various types of supramolecular structures with particular properties. The thiocyanate ligand may act as an efficient mediator for the magnetic interaction between the paramagnetic transition metal centers. Most of the extended networks are related to the end-to-end coordination modes, leading either to one-dimensional, two-dimensional, or three dimensional compounds.

One of the most attractive metal ion templates in the molecular recognition process in the extended materials is copper(II). The attractiveness of copper ions in the synthesis of polymeric compounds results mainly from their attractive magnetic properties, mixed- valence oxidation-state pairs, photoluminescence, structural features.

Copper ions are biologically essential substances having important roles such as in oxygen transport and in charge transfer reactions. Copper(II) is an important and spectroscopically well investigated metal ions in the biological systems. The Jahn-Teller active ground state leads to structural properties which are not in apriori predictable by the classical molecular mechanics approach. Importantly copper is a center in the enzyme cytochrome c oxidase and superoxide dismutase. Both of these enzymes are thought to be determinants in diabetes by their roles in regulating oxidant status.

Cisplatin is a widely used and metal based drug for cancer therapy, but it possesses inherent limitations such as side effects and low administration dosage. Therefore attempts are being made to replace this drug with suitable alternatives, and numerous transition metal complexes are synthesized and screened for their anticancer activities. Next to Ru(II) complexes, Cu(II) complexes are regarded as the most promising alternatives to cisplatin as anticancer drugs. Synthetic Cu(II) complexes have been reported to act as potential anticancer and cancer inhibiting agents and a number of copper complexes have been found to be active both *in vitro* and *in vivo*. Recently it was reported that mixed ligand Cu(II) complexes of diimines could bind and cleave DNA and exhibit anticancer activity that is more efficient than that of cisplatin.

The contemporary challenge to the synthetic inorganic chemists is to produce new compounds with pre-assigned magnetic properties and, for this, the rational synthetic design for the tuning of the solid state structure is important. Thus pseudohalide bridged complexes have drawn attention of many authors because of their diverse structural types and fascinating magnetic properties. Among the larger number of bridging ligands, the azide anions are good choice because of their efficient bridging modes, especially in $\mu_{1,1}$(end-on, EO) or $\mu_{1,3}$ (end-to-end, EE). Great efforts have been devoted to the study of bridged polynuclear and dinuclear transition metal azide complexes. The literature survey indicates that a considerable number of work have been reported concerning the versatility of the azide ion. Less literature is available for magnetostructural studies on copper(II) complexes containing bridged thiocyanate groups as this coligand is less efficient as a transmitter of magnetic interactions than azide. From the magnetic point of view, the coordination modes of the azide and thiocyanate ligands greatly affect the nature and magnitude of the magnetic exchange interaction in these polynuclear pseudohalide complexes. It is well established that the complexes with symmetric EE bridges produce antiferromagnetic coupling, where as symmetric EO bridges usually exhibit ferromagnetic coupling. Furthermore, EE and EO bridging modes may simultaneously exist in the same species, leading to different topologies and magnetic properties. The studies concerning magneto-structural correlation, including the

theoretical calculations of this type of complexes have been done by several groups of researchers.

Chapter 1- Copper(II) complexes with halides and pseudohalides: A brief introduction.

A brief introduction on Schiff bases, the halides and pseudohalides and their copper metal complexes is inscribed here. The survey of the previous research works in the area of Schiff bases and their complexes with halides and pseudohalides, along with properties and applications are also included. The chapter also contains the objectives of the present study and the details of the different analytical and spectroscopic techniques used for the analysis of the Cu(II) complexes.

Chapter 2- Copper(II) complexes containing thiocyanate as coligand.

This chapter contains the discussion of the five Cu(II) complexes synthesised and characterized by various spectroscopic techniques such as IR, electronic spectral studies, EPR and single crystal XRD studies. Out of the five copper thiocyanato complexes prepared, three have square pyramidal geometry with monomeric, dimeric and polymeric structures, and all have a thiocyanate unit at the metal center; one has distorted square planar geometry with two thiocyanate units and the remaining one has distorted octahedral geometry with two thiocyanate units. In the electronic spectral studies, the broadness of the *d-d* transitions restricted the assignment of the three *d-d* bands.

Chapter 3- Copper(II) complexes containing azide as coligand.

This chapter deals with the synthesis, spectral and structural characterization of copper(II) complexes containing azide as coligand. We synthesized four azido complexes. Three of them are having distorted square pyramidal geometry, of which one is $\mu_{1,1}$ binuclear complex and the rest are $\mu_{1,1}$ coordination polymers. The fourth azido complex has distorted square planar geometry. IR spectroscopy could be used as a very valuable tool to get information regarding the coordination mode of the azides. The EPR spectra of all the Cu(II) complexes were recorded both in polycrystalline state at 298 K and in DMF at 77 K. The *g* values and the various EPR spectral parameters are calculated. The *g* values calculated indicate that in these complexes the unpaired electron of Cu(II) resides in the $d_{x^2-y^2}$ orbital.

Chapter 4- Copper(II) complexes containing cyanate as coligand.

The single crystal studies revealed that packing polymorphism is exhibited by binuclear copper cyanato $\mu_{1,1}$ semicarbazone complexes. The magnetic moments of the binuclear Cu(II) complexes were found to be in the 1.15-1.40 B.M. range. In the electronic spectral studies, the *d-d* transitions are found to be broad. So the three *d-d* transitions could not be assigned.

Chapter 5- Copper(II) complexes containing dicyanamide as coligand.

In semicarbazone dicyanamido polymer, the Cu(II) atoms are linked by bridging $\mu_{1,5}$-dicyanamide anions in an end-to-end fashion, leading to infinite meso helical chains along b axis.

Chapter 6- Copper(II) complexes containing chloride as coligand.

Among the six chloro complexes, three of them are having distorted square planar geometry. Remaining three are having square pyramidal geometry, of which two of them are chloro bridged coordination polymer and the other one, a monomer.

Chapter 7- Copper(II) complexes containing bromide as coligand.

Four monomeric bromo complexes possessing square pyramidal and square planar geometry were synthesized. A dimeric bromo complex isolated was of distorted square pyramidal geometry. In the electronic spectra of the complexes, weak *d-d* bands are observed. EPR spectra of the complexes were taken in polycrystalline state at 298 K, DMF at 298 and 77 K. The *g* value obtained from EPR spectral assignments are consistent with the single unpaired electron in the $d_{x^2-y^2}$ orbital.